University of Calgary

PRISM Repository **https://prism.ucalgary.ca**

The Vault Open Theses and Dissertations

2018-01-23

Subcellular Distribution and Function of Cardiac Ryanodine Receptor in Ventricular Myocytes and Hippocampal Neurons

Hiess, Florian

Hiess, F. (2018). Subcellular Distribution and Function of Cardiac Ryanodine Receptor in Ventricular Myocytes and Hippocampal Neurons. (Doctoral thesis, University of Calgary, Calgary, Canada). Retrieved from https://prism.ucalgary.ca. doi:10.11575/PRISM/5439 http://hdl.handle.net/1880/106358

Downloaded from PRISM Repository, University of Calgary

UNIVERSITY OF CALGARY

Subcellular Distribution and Function of Cardiac Ryanodine Receptor in Ventricular Myocytes and Hippocampal Neurons

by

Florian Hiess

A THESIS

SUBMITTED TO THE FACULTY OF GRADUATE STUDIES

IN PARTIAL FULFILMENT OF THE REQUIREMENTS FOR THE

DEGREE OF DOCTOR OF PHILOSOPHY

GRADUATE PROGRAM IN CARDIOVASCULAR AND RESPIRATORY SCIENCES

CALGARY, ALBERTA

JANUARY, 2018

© Florian Hiess 2018

ABSTRACT

Cardiac ryanodine receptors (RyR2s) are intracellular calcium (Ca2+) release channels most abundantly expressed in the heart and brain. They are clustered in the endo/sarcoplasmic reticulum (ER/SR) membrane to form elementary units for Ca2+ release. The distribution of these units determines the spatiotemporal profile and stability of ER/SR Ca2+ release. Thus, RyR2 distribution is believed to be essential in cellular processes, such as excitation-contraction coupling and learning and memory.

The distribution of RyR2s has been extensively studied in cells/tissues using anti-RyR2 antibody immunostaining. However, sample preparation required for immunostaining may affect cellular structures, besides rendering the cells/tissues non-functional. Hence, the functional relevance of the distribution of RyR2 clusters in live cells/tissue is unclear.

We have generated a knock-in mouse model that expresses green fluorescence protein (GFP)-tagged RyR2s. These mice allow us to monitor cellular/subcellular distribution of RyR2 in live cells/tissues by virtue of GFP fluorescence. To improve the detection of GFP-RyR2, we developed a novel GFP-specific probe based on anti-GFP single domain antibodies (nanobodies). Fluorescence imaging was employed to study Ca2+ release and the distribution of GFP-RyR2 in the interior and periphery of live ventricular myocytes and in intact hearts isolated from GFP-RyR2 expressing mice. We found highly-ordered arrays of stationary GFP-RyR2 clusters in the interior of cardiomyocytes in the z-line zone. In contrast, irregular and dynamic distribution of GFP-RyR2 clusters was observed in the periphery of cardiomyocytes.

Imaging of intact GFP-RyR2 brain sections revealed a widespread distribution of RyR2 in various brain regions, most prominently in regions involved in spatial learning and memory, such as the hippocampus. To investigate the functional role of RyR2 in this region, we

performed electrophysiological studies using hippocampal slices prepared from knock-in mice harboring a cardiac arrhythmia-associated human RyR2 mutation (R4496C) with enhanced channel activity. We found that enhanced RyR2 function reduces long-term potentiation (LTP) in Schaffer collateral inputs to CA1 pyramidal cells. Thus, RyR2 plays a critical role in LTP at these synapses. Behavioral studies on RyR2 mutant mice further supported the role of RyR2 in learning and memory.

Overall, these results reveal, the distribution of RyR2 clusters and its functional significance in living ventricular myocytes and hippocampal neurons.

ACKNOWLEDGEMENT

Firstly, I would like to express my gratitude to my supervisor, Dr. S.R. Wayne Chen. He realized my potential and shaped my scientific mind tremendously.

My sincere gratitude also goes Dr. Henk E.D.J terKeurs, Dr. Ray W. Turner and Dr. Jong M. Rho, the members of my committee. Their interest in my research, interdisciplinary knowledge and creativity helped me to approach my research objectives from various perspectives and sparked novel ideas to solve complications. I am grateful for their input and support throughout my time at the University of Calgary.

Also, I thank my fellow laboratory colleges and collaborators for stimulating discussions, hard work and the motivation to extend our scientific knowledge. The following institutions: a) Microscopy and Imaging Facility (MIF), b) the Live Cell Imaging (LCI) facility, c) Regeneration Unit in Neurobiology (RUN) Facility d) NIKON; and research group led by: a) Dr. Ray W. Turner, Dr. Peter Stys, Dr. Edward O`Brien, merit acknowledgment for providing state-of-the-art equipment, materials, and/or the opportunity to learn from and work with their team.

I also want to emphasize my appreciation for financial support provided by Alberta Innovates-Health Solutions, the Natural Science and Engineering Research Council of Canada, and the Canadian Institute of Health Research.

Finally, and foremost, I want to use this opportunity to thank my family and friends. Without the love from afar and true new connections in Canada I would not have been able to conduct my research. Every message, conversation and time spent together is not forgotten. You made me stronger and allowed me to overcome loneliness. You have my deepest gratitude.

TABLE OF CONTENTS

LIST OF FIGURES

LIST OF TABLES

LIST OF ABBREVIATIONS

A˚	Angstrom
AM	Acetoxymethyl ester
AMPA	alpha- amino-3-hydroxy-5-methyl-4-isoxazolepropanoicacid
AP	Action potential
ATP	Adenosine triphosphate
cAMP	Cyclic adenosine monophosphate
Ca2+	free calcium
CaM	Calmodulin
CaMKII	Ca2+/calmodulin-dependent protein kinase II
CASQ	Calsequestrin
CICR	Ca2+-induced Ca2+ release
CPVT	Catecholaminergic polymorphic ventricular tachycardia
CRU	Ca2+ release unit
DAD	Delayed afterdepolarization
DNA	Desoxyribonucleic acid
DR	divergent region
ECC	Excitation-contraction coupling
EM	electron microscopy
FWHM	full width at half maximum
GABA	gamma-aminobutyric acid
GFP	Green fluorescent protein
Gly	Glycine
GOF	gain-of-function
hcAbs	heavy chain antibodies
HEK	human embrionic kidney
ICD	implantable cardioverter defibrillator
ID	intellectual disability
Ig	Immunoglobulin
IP3(R)	inositol trisphosphate receptors
KRH	Krebs-Ringer-HEPES
K+	potassium
KI	Knock-in
KO	Knockout
LTP	Long-term potentiation
Mg2+	free magnesium
Ca2+marks	Mitochondrial Ca2+ sparks
MUP	Mitochondrial Ca2+ uniporter
Na+	sodium
NA	numerical aperture
NCX	Na+/Ca2+ exchanger
NMDA	*N*-methyl-D-aspartate
NT	neurotransmitter
PPF	paired pulse facilitation
PBS	Phosphate buffered saline
PKA	cAMP-dependent protein kinase, protein kinase A
PLB	Phospholamban
PMCA	Plasma membrane Ca2+-ATPase
PSF	point spread function
RC	RyR2-R4496C mutant
Ry	ryanodine
RyR(1)	(Skeletal) ryanodine receptor
RyR(2)	(Cardiac) ryanodine receptor
SERCA	Sarco/endoplasmic reticulum Ca2+-ATPase
Ser	Serine
SIM	structured-illumination microscopy
SOICR	Store overload-induced Ca2+ release
SR/ER	Sarcoplasmic/endoplasmic reticulum
STORM	stochastic optical reconstruction microscopy
T-tubule	Transverse tubule
TATS	transverse-axial tubular membrane system
TIRF(M)	total internal reflection fluorescence microscopy
Thr	Threonine
Tyr	Tyrosine
WT	Wild type
3D	Three-dimensional

CHAPTER 1 INTRODUCTION

1.1 Cytosolic Ca2+ signaling and homeostasis

In the human body calcium (Ca2+) is mostly present in the form of calcium phosphate as a constituent of the skeletal structure. Thus, it was first surprising that free Ca2+ (~0.007%) (1) is essential for various cellular regulatory processes and functions. Nowadays, it is believed that Ca2+ acts as pivotal secondary messenger in mechanisms underlying muscle contraction, neuronal function, and many other cellular processes (2, 3).

At a cellular level, cytosolic Ca2+ concentration is maintained at rest between 100 – 200 nM. In contrast, Ca2+ is found in milli-molar levels in the extracellular space and in the lumen of organelles, such as mitochondria and the sarco/endoplasmic reticulum (SR/ER) (1). This leads to a gradient of Ca2+ across cellular membranes that promotes ion flow in between individual compartments when movement of charged particles is permitted. Intracellular Ca2+ homeostasis is achieved via collaborative exchange in extracellular Ca2+, cytosolic Ca2+, and the intracellular Ca2+ reservoirs. Numerous Ca2+ binding proteins, a variety of channels, exchangers, and pumps are involved in the maintenance and regulation of the cell compartment specific free Ca2+ concentration (4).

In the present study, I will focus on a protein that is involved in cellular Ca2+ homeostasis via Ca2+ release from the largest intracellular Ca2+ reservoir, the sarco/endoplasmic reticulum.

1.1.1 Ca2+ release from the ER

The ER is the main intracellular Ca2+ storage organelle that is able to morphologically and functionally adapt to cellular responses. It plays a critical role in intracellular Ca2+ handling by providing a source for readily available free Ca2+, especially important in excitatory cells, such as neurons and cardiomyocytes (5).

1.1.1.1 Ca2+ release channels

Two classes of Ca2+-permeating ion channels have been found to mediate Ca2+ release from the ER: i) inositol trisphosphate receptors (IP3Rs) and ii) ryanodine receptors (RyRs). The high degree of homology, leading to a tetrameric structural arrangement and functional similarities, indicates their evolutionary relation (6). However, distinct cytosolic activation requirements lead to different functional involvement in various cellular processes. As the name indicates, the combination of inositol trisphosphate (IP3) and Ca2+ is required for the opening of IP3R. Thus, it relies on the phospholipase C pathway. In contrast, cytosolic activation of RyR is only limited to the presence of Ca2+ (7, 8). Therefore, IP3Rs have been suggested to be involved in fine-tuned Ca2+ signalling, whereas RyRs have been mostly suggested to act as Ca2+ amplifiers.

IP3Rs are found in various tissues including the heart and brain. They are involved in vital cellular processes such as neurological signal transmission (9), smooth muscle contractility (10), and apoptosis (11). The distribution and function of IP3Rs will not be discussed in the present study. This thesis will focus on the distribution and function of an isoform of RyRs, the type 2 ryanodine receptor (RyR2).

1.2 Ryanodine receptors

RyRs obtained their name from the plant alkaloid ryanodine, that was found to interfere with the cardiac system of insects (12) as a specific ligand that modulates RyR activity (13, 14). Studies of Ry binding to purified sarcoplasmic reticulum (SR) membrane vesicles first identified RyRs as SR Ca2+ release channel (15–17). Structurally, RyRs are giant homo-tetrameric Ca2+-selective trans-membrane channels (> 2 MDa) that consist of four subunits of about 5000 amino acids leading to a molecular weight of about 565 kDa. They appear as mushroom-like basic architecture in three-dimensional (3D) reconstructions. A large cytoplasmic assembly (~80% of the protein) occupies square prism-shaped space (270 x 270 x 60 A˚) in addition to a small transmembrane/luminal assembly (120 x 120 x 60 A˚) (18). The connection comprises four column elements, in a central domain. Structural characteristics lead to the definition of regions in the RyR channel, namely a "central rim" that surrounds a cavity in the core, peripheral "clamps" and connecting "handles". Each of these regions have been divided into sub-regions corresponding to globular domain appearance (19, 20).

1.2.1 Isoforms of the ryanodine receptor

Molecular cloning studies identified three isoforms of the intracellular Ca2+ release channel ryanodine receptor (RyR1, RyR2 and RyR3) that are expressed in vertebrates (21). Three separate genes on different chromosomes encode different isoforms of the RyR protein. The predominant form in skeletal muscle is RyR1 (22), whereas RyR2 is most abundantly present in cardiac and brain tissue (23–25). On the other hand, RyR3s are expressed in smooth muscle and various other tissues at relatively low levels (26). Genetic knock-out (KO) of RyR1

led to abnormalities of the skeletal muscle apparatus and perinatal death due to respiratory failure (27). RyR2 KO resulted in embryonic lethality that was caused by defects in the cardiac system correlated to deformation and overload of intracellular Ca2+ stores (28). These findings suggest that RyR1 and RyR2 play roles during development. In support of this view, the expression of RyR2 has been found to vary during development and maturation and under physiological and pathological conditions. In contrast, RyR3-deficient mice were found to be viable and fertile, without displaying gross abnormalities (29, 30).

1.2.1.1 Divergent regions in RyRs

All isoforms share an amino acid sequence homology of ≥ 65% (25). Three non-homologous regions, termed divergent regions (DR1, DR2 and DR3) have been found in the amino acid sequence of the RyR. The DR1 describes the amino acid section between residues 4254–4631 in RyR1 and residues 4210– 4562 in RyR2. Residues 1342–1403 of RyR1 and residues 1353–1397 of RyR2 are defined as DR2. Lastly, DR3 comprises residues 1872–1923 of RyR1 and residues 1852–1890 of RyR2. Major variations in these regions are thought to be largely responsible for isoform-specific expression, structural and functional features.

Differences in DR1 have been suggested to underlie distinct sensitivity of each RyR isoforms to cytosolic Ca2+ (RyR1 > RyR2 > RyR3), although Ca2+ conductance was similar (~100 pS) (31–33). Residues in DR3 have been shown to be linked to channel activity and regulation of RyR. Genetic deletion of the DR3 affected channel conductance and Ca2+/Mg2+ dependent regulation in RyR1 (34, 35). Additionally, interaction sites of RyR1 with the II–III loop of voltage-gated L-type Ca2+ channel were found to include residues 1837 and 2168 within DR3 (36).

The lowest level of homology between the RyR is found in the DR2. Sequences of RyR1 and RyR2 are mostly distinct, whereas the corresponding region in RyR3 almost completely missing (21, 37). DR2 is believed to determine distinct features that are essential for striated muscle contraction. In support of this, deletion or substitution of DR2 with the corresponding sequence of RyR3, prevented skeletal muscle contraction in RyR1 without altering caffeine-induced channel activation (38, 39). In contrast, RyR1 channels with a substitution of the DR2 with the corresponding amino acid section of RyR2 displayed functional Ca2+ release (39).

Three-dimensional mapping of residue threonine 1366 of the DR2 in RyR2 revealed its localization at domain 6. This region is constituent of the cytoplasmic multi-domain "clamp" regions of RyR2 (40). Thus, the DR2 has been suggested to be involved in conformational changes that occur during channel gating and inter-cluster interactions (40, 41).

1.2.1.2 Ultrastructure of RyR channels

Cryo-electron microscopy (EM) studies also yielded fine-structure details to understand intrinsic channel properties of RyRs (20, 42, 43). These have been crucial to this date since crystal structures of the entire RyR channel are not available. Most structural details have been derived from cyro-EM studies that focused on the skeletal RyR1 isoform. In part, this is due to the fact that these yielded data with the highest resolution. Nevertheless, all isoforms of RyRs were found to have similar overall arrangement (44, 45). Each subunit was found to possess six, or eight transmembrane segments forming a pore via the alignment of their inner helices (20, 43). Amino acid sequence of these helices resembled various tetrameric ion channels with known structure (46). Thus, similar structural arrangement has been rendered most likely.

Cryo-EM reconstruction revealed gating-associated conformational changes of RyR1. The mechanism underlying channel opening and closing remains debated (20, 42, 43). Nevertheless, it became clear that RyR1 is a bona fide allosteric protein. Substantial conformational rearrangements in cytoplasmic section results in channel opening. Interestingly, most significant movement did not only occur in proximity to the core, but also at the clamp region (42). Thus, stochastic binding of ligands or regulatory proteins to the clamp region has the potential to directly impact opening of the pore.

The central domain has been proposed to transmit conformational motion throughout the channel. However, only recently, high resolution details of the 3D ultrastructure of RyR2 were revealed that helped the understanding of conformational signal transduction (47). Each RyR2 subunit incorporated six transmembrane helices and components of a so-called cytoplasmic O-ring motif. This O-ring was found to directly interact with a part of the central domain, termed U-motif. Additionally, a direct link between the central domain and regulatory NH_2-terminal regions in the cytoplasmic segment of neighboring subunits was found (48). These observations supported the proposal that the central domain of a RyR acts as a signal transducing element (47, 49).

1.2.1.3 Microarchitecture of RyR clusters in striated muscle

RyR microarchitecture and intra- and inter-channel interactions have been extensively studied in striated muscle. Purified skeletal RyR1 channels have been found to inherently form clusters in checkerboard arrangements, even in the absence of any other protein (50). Channel-channel contacts were shown to be localized in subdomain 6 of the clamp region (51). Since this region experiences sustainable conformational rearrangements during channel activity (42),

generated motions are likely transmitted to the connected neighboring RyR1s. Thus, intra-cluster interactions of RyR1 may underlie coupled gating in skeletal muscle (52).

Cardiac RyR2 channel microorganization in fixed ventricular myocytes has been shown to be more complex and elusive. In vitro EM and cryosection data from cardiomyocytes initially suggested highly ordered cluster arrangements with lattice formations (53, 54). In contrast, recent dual-tilt electron tomography revealed not only such checkerboard organization, but also side-by-side alignment and a small portion of isolated clusters (41, 55). The functional relevance of the latter population of RyR2 for Ca2+ release remains unclear. Furthermore, the diversity in shape and size of RyR2 clusters explained the variance in estimation of the number of RyR2 channels per functional unit. These ranged from single digits to hundreds of RyR2 channels per unit (41, 53, 56–60). Cryo-EM studies of thin tissue sections from different species estimated 90–270 RyR2s per cluster. Their assessments were based on assuming a model of orderly filled, symmetric cluster architectures (53). Cluster estimates deduced from confocal images suggested typical sizes of ~100 RyR2 channels (58). In contrast, 3D electron microscopy provided a different model where approximately two thirds of the dyadic subspace contained clusters with 15 or more RyR2 channels (60). A high degree of variability was also observed with superresolution imaging. This technique yielded comparable mean estimates with ~14 RyR2 proteins per cluster (56). However, it should be noted that mean values may be misrepresenting due to the complexity of RyR2 cluster with a large population.

Importantly, coupled gating of a small group of RyR2 channels was recorded in planar lipid bilayer experiments (52). This finding led to the hypothesis that clustering of RyR2s is important for Ca2+ release. Thus, a cluster of RyR2s refers to a functional RyR2 Ca2+ release

units (CRUs), which may contain multiple smaller structural units (55). These functional units are believed to be critical for cardiac contraction.

1.2.1.4 Micro-arrangement of L-type Ca2+ channels and RyRs

In skeletal RyR1, one of the four tetramers is thought to be physically connected with the alpha-subunits of a voltage-gated L-type Ca2+ channel (61). This unique structural arrangement allows direct transmission of electrical stimuli to cause RyR1-mediated Ca2+ release (62, 63). Membrane depolarization initiates conformational changes in the L-type Ca2+ channel, which are physically transmitted to the linked RyR1, triggering opening of the Ca2+ release channel. This mechanism is unique for skeletal muscle allowing muscle contraction in the absence of external Ca2+ influx (64, 65).

In contrast, a structural link between voltage-gated L-type Ca2+ channels and RyR2 is absent in cardiac muscle. Nevertheless, voltage-gated L-type Ca2+ channel opening and RyR2-mediated Ca2+ release has been proposed to functionally couple. A highly organized cellular arrangement has been suggested to underlie this coupling in cardiac muscle. We will discuss this in more detail in a later section.

1.2.2 Regulation of RyR2

Cellular messengers, molecular regulators, and pharmacological agents have been shown to possess the ability to affect the activity of RyR2 (66). We will discuss factors that directly determine RyR-mediated Ca2+ release in the following section.

1.2.2.1 Cytosolic Ca2+ and Mg2+

The molecular mechanism underlying sensing of cytosolic Ca2+ by RyR2 has been the focus of extensive research. It has been shown that in a magnesium (Mg2+) free environment, the activity of RyR2 channels depends on the cytosolic Ca2+ concentration in a bell-shaped fashion (67). This suggests the existence of cytosolic low and high affinity Ca2+ binding sites that directly affect channel gating.

Mg2+ (> 100 µM) in the cytosol has been found to occupy low affinity Ca2+ binding sites of RyR2, thereby inhibiting the channel (68, 69). Competitive replacement by elevated Ca2+ levels in the cytosol was found to significantly alleviate the Mg2+ mediated inhibition of RyR2.

Evidence for a high-affinity Ca2+-binding site, a Ca2+ sensor, in the cytosol has been provided by lipid bilayer experiments with purified RyR2 channels. RyR2 activation was recorded in the presence of submicromolar cytosolic Ca2+ (70, 71). Ca2+ release in human embryonic kidney (HEK) cells that expressed RyR2 mutants suggested that the residue E3987 of RyR2 is critically involved in sensing of cytosolic Ca2+. Expression of RyR2-E3987A missense mutants displayed ~1000-fold less sensitivity to cytosolic Ca2+ activation (70). In support of this view, mutation of the corresponding residue in RyR3 (RyR3-E3885A) reduced also the sensitivity of RyR3 to cytosolic Ca2+ to an astounding extent (72). Furthermore, RyR1 mutation (RyR1-E4032A) diminished sensitization of the channel by caffeine and abolished Ca2+ dependent binding of radioactive ligand (73). These findings indicate that the residue E3987 is a pivotal determinant of the sensitivity of RyR2 to cytosolic Ca2+ activation.

1.2.2.2 Luminal Ca2+ in the ER/SR

Intra-luminal homeostasis of Ca2+ is maintained in the ER via the interplay of Ca2+ intake, Ca2+ release and Ca2+ buffering. The concentration of free Ca2+ within the organelle is kept at about 0.1-0.5 mM, whereas the total Ca2+ store capacity (74), including its bound form, is ~20 fold higher (3).

Compelling evidence has been provided by various research groups that revealed the role of luminal Ca2+ as a key determinant in ER/SR Ca2+ release activation. Monitoring of open probability and duration of purified RyR2 channels consistently demonstrated that luminal levels of Ca2+ directly regulate the gating of RyR2. High concentrations of Ca2+ on the luminal side led to enhanced activity of RyR2. In contrast, decreased luminal Ca2+ levels had the opposing effect (75–77). Similarly, cellular studies in cardiomyocytes showed that elevated Ca2+ level in SR caused an increase in RyR2-mediated Ca2+ release. In contrast, maintenance of low SR Ca2+ content prevented most SR Ca2+ release (78–80). Already in the 70s, it was shown that increased SR Ca2+ levels could trigger depolarization-independent spontaneous Ca2+ release events that led to contractions (80). Since then, it has been shown that when SR Ca2+ content reaches threshold levels, spontaneous SR Ca2+ release occurs in cardiac cells in the absence of depolarization (81, 82). This depolarization-independent Ca2+, overload-induced SR Ca2+ release phenomenon has been termed store-overload-induced Ca2+ release (SOICR) (83). SOICR has been shown to possess the capability to trigger cardiac arrhythmias and sudden death (84). Among other conditions, physical/emotional stress and high extracellular Ca2+ concentrations demonstrated the potential to cause SOICR in heart cells as consequence of SR Ca2+ overload (85). However, the molecular mechanism underlying SOICR remained unclear until recently.

1.2.2.2.1 RyR2 mutations that affect the sensitivity to luminal Ca2+

Multiple human catecholaminergic polymorphic ventricular tachycardia (CPVT)-linked RyR2 mutations have been found to reduce SOICR thresholds and enhance activation of RyR2 by luminal Ca2+. Such gain-of-function (GOF) RyR2 mutations promote stress-induced spontaneous RyR2-mediated Ca2+ release, delayed afterdepolarizations (DADs), cardiac arrhythmia and sudden death. We will discuss details of CPVT in another section. In the following, we will focus on the channel properties of these CPVT-associated RyR2 mutations.

Genetic analysis of CPVT patients identified the human RyR2 mutation (RyR2-R4496C) (86). Subsequent characterization of this mutant revealed its hypersensitivity to luminal Ca2+ levels. Wild-type (WT)-like Ca2+ release was observed at non-stressed low SR loads. In contrast, RyR2-R4496C showed enhanced activity after SR load had increased through exposure to elevated extracellular Ca2+ (83, 87). In vivo studies reported more frequent spontaneous Ca2+ release events in isolated cardiomyocytes from RyR2-R4496C KI mice (88, 89). In patients, the enhanced sensitivity of RyR2 to luminal Ca2+ caused stress-induced arrhythmias. These findings demonstrate that enhanced sensitivity of RyR2 to luminal Ca2+ and spontaneous RyR2 Ca2+ release due to reduced SOICR thresholds underlies the arrhythmogenic mechanism in CPVT.

Additionally, significant lesser activation of RyR2-A4860G in response to luminal Ca2+ was reported during the characterization of the idiopathic ventricular fibrillation associated mutation of RyR2 (90). Thus, pathological mechanism of multiple cardiac diseases may depend on luminal Ca2+ levels.

1.2.2.2.2 The mechanism of RyR2 regulation by luminal Ca2+

The molecular mechanism of regulation of RyR2 activity by luminal Ca2+ remains unclear. The hypothesis has been made that a “feed-through” regulation is in place. Channel gating is potentially regulated via luminal Ca2+ that passed through RyR2 in its open state to binds to cytosolic activating high affinity binding sites, or inactivating low affinity binding sites of RyR2 (91, 92). However, such a "feed-through" mechanism does not explain initial opening of the RyR2 channel. Also, evidence has been provided that the regulation of RyR2 via Ca2+ within the SR lumen does not rely on cytosol-directed flow of luminal Ca2+. Single channel recordings showed that the activity of RyR2 was directly enhanced by increased concentrations of luminal Ca2+. (76, 80, 91, 93).

Recently, the existence of a luminal Ca2+ binding site, or Ca2+ sensing element, within RyR2 channels has been proposed to directly regulate channel gating, independently from cytosolic Ca2+ regulations. Recordings in lipid bilayers allowed to distinguish RyR2 activation by cytosolic or luminal Ca2+ (75). A mutation of a cytosolic Ca2+ sensing residue in RyR2 (RyR2-E3987A) abolished RyR2 opening by cytosolic Ca2+ without affecting RyR2 luminal Ca2+ dependent activation (70). These observations suggest that the activation of RyR2 via luminal Ca2+ is different from the regulatory mechanism of RyR2 that relies on cytosolic Ca2+. In consequence, RyR2 requires a Ca2+ binding site on the luminal side that regulates the gating of a RyR2 channel.

1.2.2.2.3 Luminal Ca2+ sensor of RyR2

The exact location and nature of the putative luminal Ca2+ sensor in RyR2 channels remain to be resolved. Chen and colleagues recently demonstrated the necessity of the amino

acid residue E4872 in the helix bundle crossing region (the proposed gate) of RyR2 for its sensitivity to luminal Ca2+. In vitro studies of missense mutations at this site (RyR2-E4872A and RyR2-E4872Q) revealed complete insensitivity to luminal, but not cytosolic, Ca2+ levels of expressed RyR2 channels (93, 94). Furthermore, in vivo studies showed that hearts harboring a heterozygous suppression-of-function mutation RyR2-E4872Q were resistant to SOICR and were completely protected against Ca2+-triggered arrhythmias (93). This body of evidence suggests the residue E4872 to act as sensing element of luminal free Ca2+ in RyR2.

A recent study of the 3D ultrastructure of RyR2 provided novel details with respect to the putative luminal Ca2+ sensing element in RyR2. Importantly, residue E4872 has been shown to be located in the cytosolic part of the RyR2 channel in close proximity to the luminal side. Nevertheless, structural observations suggested that E4872 forms a salt bridge between subunits with R4874. Therewith, a binding pocket of negatively charged residues is created that is involved in the activation of RyR2 by luminal Ca2+ (48). Thus, the residue 4872 of RyR2 is a structural element that is pivotal for the formation of a luminal Ca2+ binding pocket to facilitate the regulation of RyR2 by luminal Ca2+.

1.2.2.3 Calmodulin (CaM)

CaM is a small Ca2+-binding messenger protein that directly and indirectly modulates the activity of RyR2. It is ubiquitously expressed in the cytosol of most eukaryotic cells and possesses four EF hand motifs that provide Ca2+ binding sites. The structure of CaM can be described as two globular symmetrical domains (N- and C-domain) that are linked by a flexible element (an alpha-helix). The two low affinity Ca2+ binding sites are located in the N-domain, whereas the C-domain harbors two high affinity Ca2+ binding sites (95). Upon binding of Ca2+,

conformational changes lead CaM to envelop its target.

CaM directly binds a CaM-binding site (R3581 – P3607) of RyR2 channels (96, 97) in its Ca2+ bound and Ca2+ unbound form. In a recent study of the 3D structure of RyR2, this site has been proposed to be located at the interface of multiple RyR2 domains, suggesting regulatory importance (48). The modulator to channel ratio is thereby a maximum of 4:1. At resting cytosolic Ca2+ concentration, CaM connects with RyR2 via its C-domain. At elevated Ca2+ concentrations in the cytosol, both domains of CaM, N- and C-domains, bind to RyR2 (96, 98). CaM regulates the activity of RyR2 as Ca2+-dependent inhibitor (99). Single channel recordings revealed that CaM successfully inhibits channel opening of RyR2 at submicromolar cytosolic Ca2+ levels (≤ 10 μM). However, at higher Ca2+ concentrations RyR2 gating remained mostly unaffected in the presence of CaM. Therefore, local RyR2-mediated Ca2+ release (~30-50 μM) is insignificantly affected by CaM inhibition. However, the inhibitory effect of CaM has been proposed to be essential during the termination of RyR2-mediated Ca2+ release.

Aside from direct interactions, CaM also indirectly regulates the activity of RyR2 via CaMKII activation. We will discuss this in the following section.

1.2.2.4 Phosphorylation

1.2.2.4.1 Protein Kinase A (PKA)

Phosphorylation of multiple molecular targets in the β-adrenergic signaling pathway, including the voltage gated L-type Ca2+ channel and RyR2, is mediated by PKA. Noradrenaline binding to β-adrenergic receptors in the plasma membrane initiates adenylyl cyclase activity to produce cAMP. This in turn activates PKA (100).

PKA-mediated phosphorylation of specific sites in the L-type Ca2+ channel and RyR2

have been proposed to cause conformational changes of the molecules that modulate Ca2+ signalling. In cardiac systems, an increase in Ca2+ entry via the L-type Ca2+ channel, increased Ca2+ release from the SR, elevated SR Ca2+ fill and enhanced cardiac contraction have been observed as result of PKA-mediated Ca2+ channel phosphorylation (100).

PKA phosphorylation enhanced the sensitivity of RyR2 channels to luminal Ca2+ and reduced the SOICR threshold (101). Additionally, evidence indicated that two cytosolic serine residues in the sequence of RyR2 channels, S2030 and S2808, provide PKA phosphorylation sites (101, 102). However, the physiological significance of the cytosolic PKA sites remains debated. At basal conditions S2808 has been shown to mainly occur in its phosphorylated state. Thus, phosphorylation of S2030 has been proposed to be mainly accountable for PKA-mediated enhancement of Ca2+ release via RyR2.

1.2.2.4.2 Ca2+/CaM dependent protein kinase II (CaMKII)

CaMKII has been shown to phosphorylate and therewith regulate RyR2 channel gating. As the name implies, CaMKII activation requires binding of Ca2+ bound CaM (103, 104).

CaMKII has been shown to phosphorylate the serine residues S2808 and S2814 of RyR2 (102, 105). As mentioned earlier, the significance of S2808 remains unclear, since this residue is mainly phosphorylated at basal conditions. In contrast, expression of a mutant (RyR2- S2814D) that mimics a constitutively phosphorylated state of S2814 led to an increase in propensity to ventricular tachycardia without gross structural abnormalities of the heart (105). However, the disease-associated mechanism of aberrant CaMKII phosphorylation of RyR2 remains unclear (106, 107).

1.2.2.5 Pharmacological modulators of RyRs

Unfortunately, there are currently no isoform-specific pharmacological compounds available to assess the function of RyR2. Nevertheless, dantrolene, caffeine, and ryanodine have been used to study RyR-mediated Ca2+ release.

1.2.2.5.1 Ryanodine

Ryanodine (Ry) is the name-giving chemical for RyRs. This compound is naturally occurring in *Ryania Speciosa* and has provided a specific ligand with high binding affinity for RyRs (3). Four ligand binding sites on a RyR channel were characterized with diverse affinities: one high affinity binding site (1-4 nM) and lower affinity binding sites (30-50 nM, 500-800 nM, and 2-4 μM) (108, 109). Importantly, the effect of Ry on the activity of RyR depends on the applied concentration of the chemical. Submicromolar levels of Ry maintain the channel in a sub-conducting open confirmation by binding to the high affinity binding site. In contrast, milimolar concentrations (0.3–2 mM) of Ry was found to occupy low affinity sites of RyR and thereby inhibit the channel (69, 109).

In most studies, Ry is used in concentrations with antagonizing effects (≥10 μM) that completely block the channel (110). Alternatively, Ry has been utilized to study the open state of RyRs as a probe for channel gating. The reason for such application is that Ry has been found to favor binding to the open state of the RyR2 channel suggesting that the accessibility of the binding site is increased in that confirmation. Importantly, effectiveness of binding of Ry to the high affinity site of RyRs has been shown to depend on environmental factors, such as temperature, ambient Ca2+ concentration, pH and other modulators of RyR2. For instance, caffeine enhanced Ry binding to RyR2 channels (111).

1.2.2.5.2 Caffeine

One of the most used pharmacological agonist of RyRs is caffeine. The water-soluble drug is believed to sensitize the channel to binding of cytosolic Ca2+. In support, increased open probability of RyRs was recorded as a result of the presence of caffeine at the cytosolic side in lipid bilayers (112, 113). However, Ca2+ store depletion abolished caffeine-induced Ca2+ release events from the intracellular reservoir (114, 115). This finding suggests that luminal Ca2+ is also a determinant of caffeine mediated affects. Indeed, application of caffeine sensitized RyR2 channels to luminal Ca2+. It led to increased appearance of SOICR (116) and prolonged channel opening (114, 115). In conclusion, sensitization of RyR2 channels to both, cytosolic and luminal Ca2+, underlies caffeine-induced activation of RyR2. This can be of benefit, since Ca2+ release from the intracellular store could be triggered by caffeine without alternation of the cytosolic or luminal Ca2+ level. Importantly, it should be noted that caffeine has been found to target various other molecular targets that are involved in cellular Ca2+ signaling. As such caffeine has been shown to affect phosphodiesterases, gamma-aminobutyric acid (GABA) A receptor, adenosine A_{2A} receptor and possibly A_1Rs (117). Thus, results have to be evaluated with caution.

1.2.2.5.3 Dantrolene

Dantrolene is an artificial glycolylurea that was first synthesized in 1967 as muscle relaxant (31). This pharmacological agent has been used as antagonist of RyRs. However, whether dantrolene affects the RyR2 isoforms remains unclear. In vitro studies and ligand binding assays with native and recombinant RyRs indicated that the Ca2+ channel blocker,

dantrolene, acts specifically on RyR1, but with significantly less affinitive for RyR2 (118–120). Furthermore, RyR1 and RyR3, but not the RyR2 isoform, were reported to provide in vivo targets for dantrolene inhibition (121). In contrast, dantrolene has been proposed to bind the N-terminus residues 590-609 in RyR1 and residues 601-620 in RyR2 (118, 122).

1.3 RyR2 in ventricular myocytes

Cardiac RyR2 channels have been found to arrange into collections of multiples, so called clusters, primary in the terminal cisternae membrane of the endoplasmic/sarcoplasmic reticulum (ER/SR) (45, 123, 124). Although the number of RyR2 molecules in a functional cluster and their microarchitecture remain a matter of debate, these RyR2 clusters are believed to act as elementary Ca2+ release units (125–127). Ca2+ release from one of these units has been termed Ca2+ spark (128–131). Global Ca2+ events (e.g. Ca2+ transients or Ca2+ waves) are the spatiotemporal summation of Ca2+ sparks (131). Thus, recruitment of variable numbers of RyR2 Ca2+ release units allows versatile and complexity Ca2+ release from the SR (128, 129, 132), which is believed to be pivotal for muscle contraction.

1.3.1 Cellular architecture of ventricular myocytes

A general understanding of the cellular architecture of ventricular myocytes is required to assess the role of RyR2s in the cardiac contractile machinery. Each muscle cell contains a multitude of tubular myofibrils, which consist of repeating units of so-called sarcomeres. As shown in Figure 1, each sarcomere is composed of overlapping filaments of actin (thin filament) and myosin (thick filament) that are bordered by so called Z-lines. Mitochondria are located beneath the sarcolemma in between Z-lines. Similarly, they interspace invaginations of the

sarcolemma, termed transverse tubules (t-tubules) that invade the cell along the Z-lines. Myofibrils are enveloped by an extensive network of a specialized ER, termed sarcoplasmic reticulum. This organelle can be divided into two structurally and functionally independent SR regions: longitudinal SR and terminal cisterna. RyR2s are believed to assemble in functional clusters predominantly in the terminal cisterna of the SR network, the main intracellular Ca2+ release site. It juxtapositions the t-tubule, creating a dyad in cardiomyocytes. The so-called dyadic gap (~12nm) describes the cytoplasmic space between the t-tubules and the SR (133). This microarchitecture allows rapid and precise signal transmission between the L-type Ca2+ channel and RyR2 clusters which is believed to be critical for synchronous Ca2+ release and effective, stable excitation-contraction coupling (ECC) (40, 134).

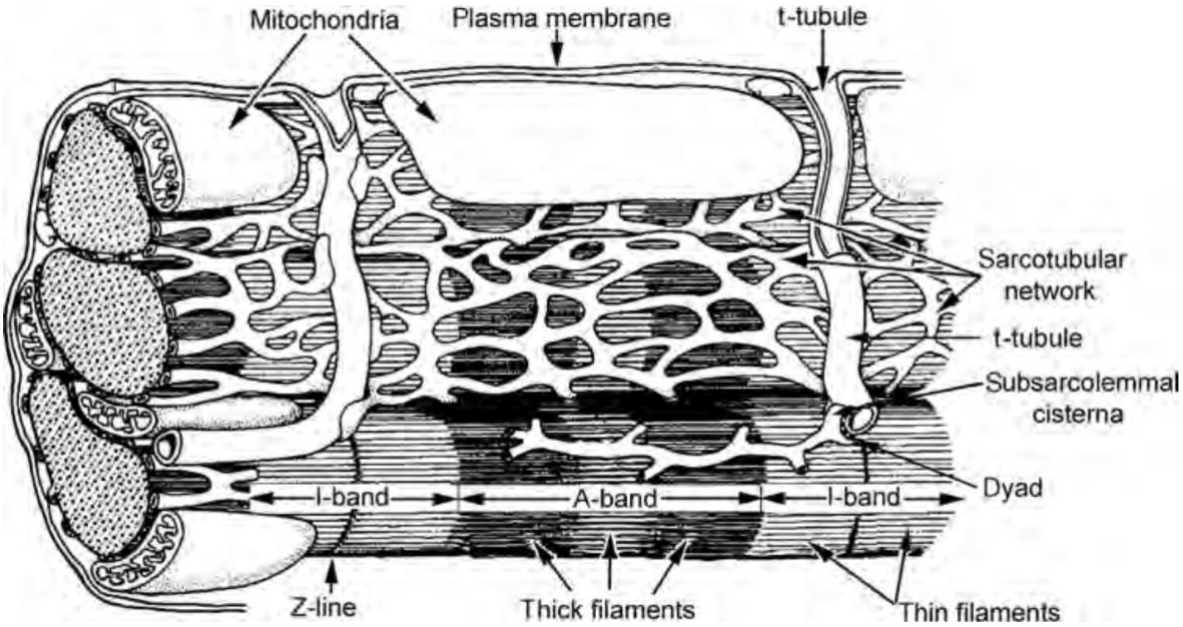

Figure 1 Cellular architecture of ventricular myocytes

A graphical depiction of a ventricular myocyte is shown. The plasma membrane of muscle cells, or sarcolemma, envelopes mitochondria and myofibrils that are enwrapped with a network of

sarcoplasmic reticulum. Invaginations of the plasma membrane, termed t-tubules, provide interfaces with the terminal cisterna of the SR, so-called dyads, at which RyR2s are believed to cluster predominantly. These run along the Z-lines, which boarder each functional muscle unit, termed sarcomere. Sarcomeres are comprised of thick (myosin) and thin (actin) filaments. Regions that contain both, thick and thin filaments, are defined as A-band. On the other hand, an I-band describes an area that only contains actin filaments. (Wolters Kluwer Health; Katz A.M.; "Physiology of the heart." Lippincott Williams & Wilkins 2010 (133)).

1.3.2 The role of RyR2 in cardiac ECC and Ca2+ homeostasis

Excitation contraction coupling describes the fundamental cellular mechanism that causally links electrical stimuli with the induction of muscle contraction via cytosolic Ca2+ elevation (3, 12). Ever since this phenomenon was reported by Alexander Sandow in 1952 (135) and put forward by Fabiato (136), many aspects of intracellular Ca2+ release during ECC have been studied. This is in part due to the fact, that abnormal cardiac Ca2+ handling has been found to underlie a variety of pathological conditions including cardiac arrhythmias, heart failure and sudden death (12, 18, 86, 137).

In ventricular myocytes, ECC relies on the transverse-axial tubular membrane system (TATS) which enables rapid signal transmission into all sarcomeres, throughout the myocyte. Electrical stimuli, in the form of action potentials (APs), invade via the sarcolemma. General membrane depolarization results from large Na+ influx (total of ~50 nA/cell) via Na+ channels at the intercalated disc and smaller Na+ conductance by related transmembrane channels at the invaginations of the membrane (138). The latter co-localize with Na+/Ca2+ exchanger NCX (12). NCX mediates Ca2+ entry in response to rising intracellular Na+ concentration (5-10 ms) in their `reverses mode`. Na+ current-mediated depolarization furthermore activates the voltage-

dependent L-type Ca2+ channels, which leads to small local influx of Ca2+ ions into the cytoplasm. The combination of both Ca2+ entries subsequently triggers a more substantial Ca2+ release from the terminal cisternae of SR via RyR2s. This process is termed Ca2+ induced Ca2+ release (CICR) (136, 139, 140), which we will discuss in more detail in a later section. The released Ca2+ (~$15x10^3$ ions per half sarcomere) diffuses passively throughout the cytosol to bind to troponin C (25,000 mol per half sarcomere). This induces structural rearrangements of the troponin-tropomyosin complex that enables the myosin motor proteins to interact with actin within the myofilaments. This so-called cross-bridge formation ($90x10^3$ per half sarcomere) facilitates sarcomere shortening through conversion of chemical energy in the form of adenosine triphosphate (ATP) to generate force (2pN per bridge). Simultaneous shortening of all units of myofibrils is ultimately observed as muscle contraction (3, 12).

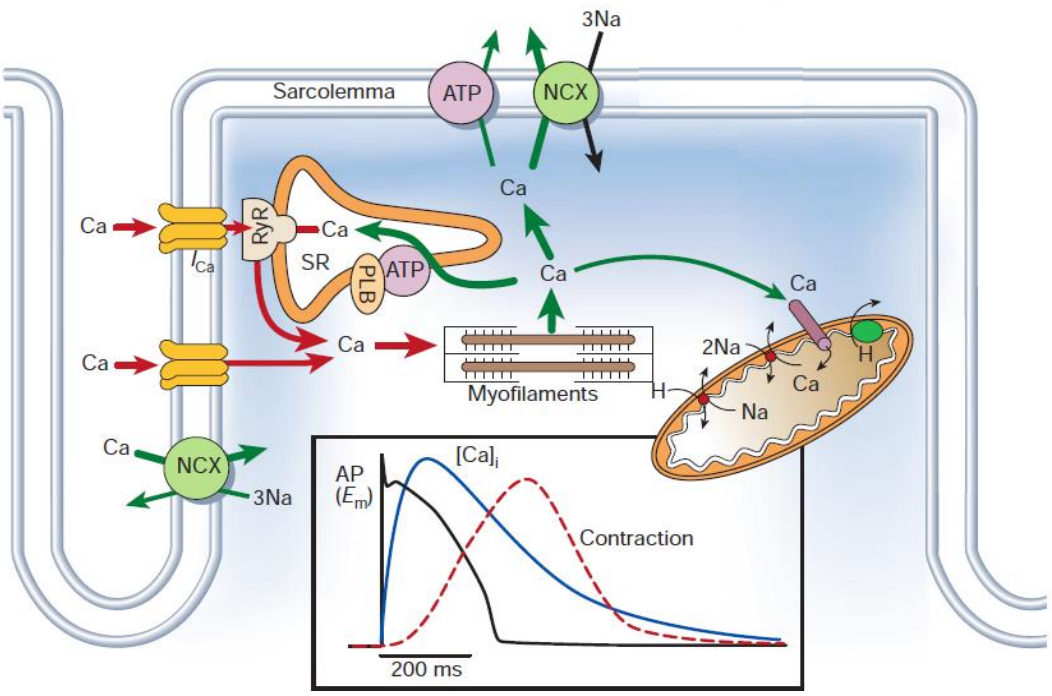

Figure 2 ECC and Ca^{2+} homeostasis in ventricular myocytes

A graphical representation of Ca2+ dynamics and the molecular apparatus underlying ECC and

cardiac Ca2+ homeostasis in ventricular myocytes is shown. An extensive sarcolemma system, with invaginations, harbors ion channels, exchangers and pumps that facilitate Ca2+ movement across the membrane. Additionally, Ca2+ release and uptake from intracellular reservoirs, namely the SR and mitochondria provide sources for fine-tuned Ca2+ signaling and ensure Ca2+ homeostasis. The inset (bottom, middle) shows the temporal translation of an action potential (AP) into a transient elevation of cytosolic Ca2+ concentration that leads to contraction during ECC in a ventricular myocyte of a rabbit at 37°C. NCX, Na+/Ca2+ exchanger; ATP, ATPase; RyR, ryanodine receptor; PLB, phospholamban; SR, sarcoplasmic reticulum. (Adapted from "Cardiac excitation-contraction coupling" by Donald M. Bers. Nature. 2002 [1])

Muscle relaxation is a result of the reduction of cytosolic Ca2+ level. This is mainly mediated by Ca2+ recycling back into the SR by the fast-acting sarco/endoplasmic reticulum Ca2+-ATPase (SERCA). To note is that the activity of SERCA is regulated by phospholamban, which acts as an inhibitor. Additionally, slower Ca2+ extrusion to the extracellular space (~30%) through the Na+/Ca2+ exchanger (NCX) and the plasma membrane Ca2+-ATPase (PMCA) re-establish resting intracellular Ca2+ levels. Furthermore, mitochondria can uptake small portions of Ca2+ via a Ca2+ uniporter. As depicted in Figure 2, The interplay of the components of this molecular apparatus allows fine-tuned spatiotemporal Ca2+ signaling while also ensuring maintenance of cytosolic Ca2+ homeostasis (3).

1.3.3 Ca2+ induced Ca2+ release

As introduced by Fabiato and Fabiato (140), CICR describes RyR2-mediated Ca2+ release from the SR in response to elevations of cytosolic Ca2+ concentration (136). Ca2+ that enters through the sarcolemma (~10µM) would not be sufficient to initiate muscle contraction. More substantial RyR2-mediated Ca2+ release from the SR (3-5 fold) is required to initiate

cross-bridge formation (12). Thus, CICR is crucial for the amplification of Ca2+ influx via the L-type Ca2+ channel and the `reverse mode` of ECC (3).

As a positive feedback mechanism, CICR has the inherent potential for unbridled self-regenerative Ca2+ release. However, cardiac SR Ca2+ release is graded and tightly controlled by the amplitude and duration of Ca2+ current though voltage gated L-type Ca2+ channels (141). This finding poses a paradox, which has been subject of extensive research. We will elaborate on this in more detail in the following section.

1.3.3.1 Coupled gating theory

The coupled gating theory suggests that adjacent RyRs are mechanically linked through physical interactions in the presence of FK506 binding proteins (FKBP) (52, 142). Thus, conformational changes during opening and closing within a channel would be transmitted to coupled RyRs. In consequence, synchronous gating of RyR clusters has been proposed to produce a CRU (52). However, complex cluster sizes and shapes in cardiac muscle cells render this model unlikely. Physical interaction between RyRs during gating remain to be confirmed in cardiomyocytes, since observations from lipid bilayer experiments are controversial.

1.3.3.2 The 'local control' theory

The 'local control' theory aims to explain the mechanism underlying stable and graded CICR (129, 143–145). In the proposed model, clusters of 10-35 L-type Ca2+ channels co-localize with ~ 10-fold more RyR2s at the interface between invaginations of the sarcolemma and the terminal cisterna of the SR to form elementary Ca2+ release units (146, 147). These units

act functionally independently from each other, which limits activation of RyR2s exclusively to Ca2+ influx through the directly associated L-type Ca2+ channels (130, 131, 146). Such a system would allow graded SR Ca2+ release that is tightly controlled by the Ca2+ entry through L-type Ca2+ channels.

Indeed, Stern (143) showed that the close proximity of voltage-dependent L-type Ca2+ channels and RyR2s permits graded coupling between Ca2+ influx and Ca2+ release. Observations of locally and temporally restricted RyR2-mediated Ca2+ release events have provided convincing evidence for the existence of individual elementary CRUs, hence the 'local control' theory (129, 131, 148). Properties of these Ca2+ sparks have been extensively studied using imaging of Ca2+- sensitive probes in the cytosol of quiescent cardiomyocytes (131). Importantly, depolarization-triggered Ca2+ sparks and spontaneous Ca2+ sparks were found to share identical characteristics. This finding suggests that both Ca2+ release events have similar structural and functional basis. Ca2+ sparks autonomy was showed as they did not interfere with each other (53, 130, 131). Additionally, simultaneous CRU-mediated Ca2+ release was observed throughout the entirety of a cardiomyocyte in response to a single AP (149).

Based on the present body of evidence, the elegant assumption has been made that a global Ca2+ wave is the spatiotemporal summation of independent Ca2+ sparks as elementary events of Ca2+ release (146). It satisfactorily explains the phenomenon of gradated SR Ca2+ release as function of the spatiotemporal membrane depolarization by recruiting various numbers of Ca2+ sparks (129, 146, 148). This model relies on the subcellular distribution of functional RyR2 clusters. The spacing of RyR2 clusters would determine the effectiveness of the recruitment of CRU in this model in which signal propagation relies on passive diffusion. Thus, understanding the distribution of RyR2 clusters is important for elucidating the fundamental

mechanism of CICR.

1.3.3.3 Termination of SR Ca^{2+} release

The stable and graded activation of Ca2+ release from the SR has been compellingly explained by the "local control" theory. However, termination of RyR2-mediated Ca^{2+} release remains controversial. The positive feedback character of CICR might lead one to believe that the Ca^{2+} release via an activated CRU is sustained until the Ca^{2+} reservoir is completely depleted. However, such all-or-none response has not been reported yet. In contrast, partial depletion of Ca2+ from the SR has been found during Ca^{2+} sparks or global Ca^{2+} events [34-37]. Hence, the termination of SR Ca^{2+} release is believed to be regulated by a robust mechanism to allow muscle relaxation, the maintenance of cardiac contractility [20].

Various theories have been suggested to explain the mechanism underlying the termination of Ca^{2+} release from the SR. An extremely low statistical probability that all RyR channels in a CRU simultaneously close renders the stochastic attrition theory unlikely [20]. Alternatively, coupled gating has been suggested to account for synchronized opening and closing of neighboring RyRs in the same CRU [38, 39]. In this model, FK506 binding proteins have been proposed to physically link RyR2s and therewith regulate not only activation, but also termination of Ca2+ release from the SR. However, such physical and functional linkage between nearby RyR2s remains highly controversial and does not explain the initiation of the closing of RyR2 channels in a CRU.

The RyR2 adaptation theory addresses the initial decrease in the open probability of RyR2. It suggests that the activity of RyR2 spontaneously and gradually decreases after opening of Ca2+ release channels [40-42]. However, the temporal scale of the proposed adaptation

process (hundreds of milliseconds up to seconds) that has been determined in artificial lipid bilayer settings does not correlate with the significantly slower termination of SR Ca^{2+} release observed in cells (within tens of milliseconds) [28]. Hence, it this theory is unlikely to explain termination of RyR2 mediated Ca2+ release from the SR.

1.3.3.3.1 Cytosolic Ca^{2+}-dependent inactivation theory

Alternatively, elevated cytosolic Ca^{2+} concentrations has been suggested to lead to the closing of RyR2 channels [43]. In support, high concentrations of cytosolic Ca^{2+} (> hundreds of μM) have been found to cause the inactivation of RyR2 channels in single channel experiments. However, evidence for cytosolic Ca^{2+}-dependent inactivation in cellular systems remains lacking. Physiological cytosolic Ca^{2+} levels (~100nM to 10μM) in intact cells may not be sufficient to cause similar effects.

Ca2+ binding proteins, such as CaM and socrin, have also been suggested to be involved in the regulation of the termination of RyR2-mediated Ca^{2+} release from the SR. On one hand, CaM has been found to inhibits RyR2 gating at submicromolar cytosolic Ca2+ levels (≤ 10 μM) [29, 44-46]. In addition, CaM mutations have been found to cause abnormal Ca^{2+} release from the SR [47]. Hence, CaM is believed to be involved in the regulation of RyR2-mediated SR Ca^{2+} release. Nevertheless, CaM is unlikely the sole determinant in the mechanism of closing of RyR2 channels Mutations of CaM lead to aberrant gating of RyR2, but did not abolish the termination of Ca2+ release [48]. On the other hand, sorcin that has been found to inhibit both, spontaneous and triggered, Ca^{2+} events [49, 50]. Thus, sorcin has been proposed to be involved in the in regulation of the termination of Ca^{2+} release from the SR. However, whether sorcin is a regulatory determinant that regulates gating of RyR2 remains unclear and needs further

evaluation in the future.

1.3.3.3.2 Luminal Ca^{2+}-dependent termination of RyR2-mediated Ca2+ release

A convincing body of evidence has indicated that the luminal Ca^{2+} level in the ER/SR directly regulates the termination of Ca^{2+} release from the intracellular store. Declining luminal Ca^{2+} concentrations, as found during CICR, have been shown to lead to RyR2 channel closing. This has been revealed by fluorescence probe-based monitoring of luminal Ca2+ dynamics that greatly aided to understand luminal Ca^{2+}-dependent termination of SR Ca^{2+} release. The use of the low affinity Ca2+ indicator Fluo-5N showed the `Ca2+ blinks, localized and rapid decrease in luminal Ca2+ concentration, as counterparts to cytosolic Ca2+ sparks [51]. The Ca2+ release profile of Ca2+ blinks showed that Ca2+ depletion from the SR is graded. Quantitative estimates suggested that less than 55% of free SR Ca2+ and a fraction of calsequestrin-bound Ca2+ (less than 30%) compose individual Ca2+ blinks [51]. In addition, SR Ca2+ release termination was found to occur at a definite luminal Ca2+ concentration of the SR, that was termed termination threshold. This threshold has been shown to be independent of Ca2+ levels in the cytosol and the Ca2+ concentration in the lumen of the SR at rest. [37]. These findings indicate that the termination threshold is an intrinsic property of the RyR2 channel. In consensus, single channels demonstrated that a reduction of luminal Ca^{2+} lead to a significant decrease in the open probability of RyR2 channels [35, 36, 52-54]. Therefore, one might suggest that the progressive depletion of Ca2+ from the lumen of the SR luminal Ca^{2+} itself leads to the termination of RyR2-mediated SR Ca^{2+} release. However, the mechanism underlying the termination of Ca^{2+} release from the SR remains unclear.

1.3.4 Distribution of functional RyR2 clusters

The distribution and organization of functional RyR2 clusters in cardiomyocytes remains controversial. It is believed to be critical for synchronous Ca2+ release and effective, stable cardiac ECC (40, 134). In support, altered arrangements of RyR2 and intracellular architectures have been implicated in the genesis of dyssynchronous Ca2+ release often observed in diseased hearts (150).

1.3.4.1 Localization of RyR2 clusters

Various approaches have been applied to localize RyR2s in cellular and subcellular context. We will discuss these in the following section to reveal potential limitations of former assessments and approaches.

1.3.4.1.1 Antibodies against RyR2

Antibodies are proteins of the immunoglobulin (Ig) family, which recognize, tag and neutralize foreign pathogens in most organisms. They identify a foreign body, the so called antigen and bind to a specific site of the target, defined as epitope (151). As key players in biological immune systems, they are derived from specifically immunized animals or genetically engineered as commonly used tool for protein targeting and linked to dyes for protein visualization in biological assays. However, the large molecular size and restricted versatility of conventional antibodies may not always lead to unambiguous localization of targets in complex cellular systems, or tissues.

RyR2 directed antibodies are commercially available. They have been extensively used for immunohistochemical examination of fixed and/or permeabilized cells or tissues (56, 59, 60). This technique relies on sample preparations with chemicals that render the tissue non-functional (152) and the use of specific anti-RyR2 antibodies (56, 58, 59, 153–155). Unfortunately, the use of antibodies for the localization of an intracellular target has several disadvantages. The large protein size of antibodies limits their access to cytosolic epitopes of the intracellular RyR2 target. Hence, permeabilization of the plasma membrane is necessary to allow the antibodies to penetrate the cell interior. This requires application of detergents (e.g.: Triton-X 100), which subjects the cell to biochemical stress and may cause cell death or protein degradation (131, 156). Thus, specimens require fixation prior to permeabilization to preserve the biological material as close to its natural state as possible. Chemical fixatives (e.g.: paraformaldehyde), terminate any biochemical functional processes via cross-linking of proteins, but prevent decay and increase physical resistance and mechanical stability (157). To note is that long term exposure with these chemicals has been shown to cause structural damage in the specimen (158). Thus, it remains unclear whether the treatment of cell or tissue with fixatives and/or permeabilization reagents alters the distribution and organization of RyR2s.

Pharmacodynamic problems may also occur with the application of antibodies. Insufficient antibody-selectivity and/or affinity to a specific epitope may lead to artificial results, or unsatisfactory visualization (159). Additionally, conformational epitopes may be masked, or altered in a dynamic biological active organism. This would lead to a total loss of reactivity with antigens (151). Thus, cells must be cautiously adjusted to optimal binding conditions. In general, these conditions are not physiological anymore and differ from the natural state of the system.

1.3.4.1.2 Genetic recombination of RyR2-reporter fusion proteins

A genetic approach can be used alternatively to visualize intracellular protein locations. Commonly the genetic code of a bioluminescent reporter is fused to the deoxyribonucleic acid (DNA) of the target protein, which is then implemented in the genome of a model organism. In consequence, the system expresses a genetic fusion protein originating from the introduced DNA (160, 161). The 4975 amino acids that comprise a subunit of a RyR2 channel are encoded on chromosome 1 (1q42-q43). The gene of RyR2 is spanning 790 kb of genomic DNA and contains 105 exons (162, 163). The size of RyR2 makes genetic modifications difficult. However, state of the technology leads to the development of recombinant RyR2 constructs that function fusion proteins with incorporated fluorescence reporter molecules (40).

Green fluorescent protein (GFP) has been used most frequently as reporter for the visualization of spatial and temporal protein localization in a wide range of biological systems (160, 161). The 27 kDa protein originates from Jellyfish *Aequorea Victoria* and emits green fluorescent light upon excitation at blue wavelengths. Fluorescence can be observed in respond to electromagnetic radiation due to autocatalytic cyclization, dehydration and oxidation of three amino acid residues within the GFP molecule (164). To note is that almost the entire protein sequence is required to generate the chromophore. However, the cyclic tripeptide serine 65-dehydroxytyrosine 66-glycine67 has been identified as light-absorbing sequence in the GFP molecule (165).

The cyclic tripeptide is the result of a nucleophilic reaction between the carboxyl carbon of serine 65 and the nitrogen atom of the amino group provided by glycine 67 leading to the formation of an imidazolin-5-one ring system. In the presence of molecular oxygen, this heterocyclic structure forms a highly conjugated π-electron resonance system with the

dehydrogenized form of the tyrosine 66 residue. This mature chromophore provides the electron orbitals to facilitate stable fluorescence of GFP (166).

On an ultrastructural level, GFP has been defined as eleven-stranded “beta-barrel” with the cyclic tripeptide chromophore at its core (see Figure 3). Tight association of amino acid residues within the beta barrel structure prevents most interactions with its interior. This compact confirmation is believed to protect the chromophore and lead to extraordinary photo-stability, robustness against environmental factors (pH, temperature, denaturation), and high quantum yields (167).

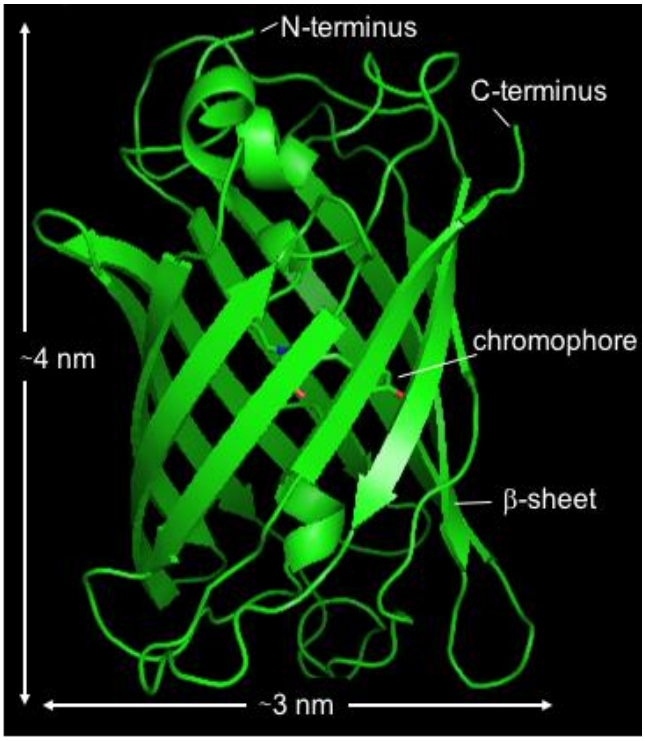

Figure 3 Three-dimensional ultrastructure of green fluorescent protein

The structural arrangement of green fluorescent protein (GFP; RSCB PDB 1EMA (168) from `Crystal structure of the Aequorea victoria green fluorescent protein.` Ormoe et al Science 1996 (169)) is graphically represented using PyMol (PyMOL Molecular Graphics System, Version 1.74 Schrödinger, LLC). A cylindrical geometry (~4x3 nm), termed `beta-barrel`, comprises

eleven beta-sheets. This cylindrical organization harbors the tripeptide chromophore at its core. Amino (N) and carboxyl (C) termini are exposed on the surface readily available.

Importantly, amino (N) and carboxyl (C) termini are exposed on the surface of the cylindrical structure (168). Thus, they are readily available for genetic modifications. This makes GFP is an ideal candidate for fusion to other proteins.

Manipulation of the genetic code of GFP led to quantum yield enhancements and stability improvements (164, 167). Such advancements facilitated high resolution monitoring of intracellular proteins in live dynamic organisms (170–172). Genetic engineering facilitates the insertion of a protein coding cDNA sequence at a particular locus in an organism's genome (173). The genetic design should consider the spatial environment and regulatory interactions. The choice of the insertion site is critical and occasionally linking segments are required to prevent the introduction of structural or functional alternations. Typically, recombinant genetic code is transfected into embryonic stem cells to generate a desired transgenic or KI model. Conventionally mice are used, since the process has been well refined (174). Several successful protein localizations in live organisms have been reported using this approach. However, the insertion of GFP into the RyR2 cDNA remains difficult, since the structural and functional protein integrity has to be maintained.

In 2004, Chen`s laboratory successfully generated a construct, encoding RyR2 protein with GFP inserted within the divergent region 2, specifically after amino acid threonine (Thr)1366 (RyR2-(Thr1366-GFP))(40). Transfected HEK293 cells expressed functional and structurally intact GFP-tagged RyR2 channels, which yielded physiological caffeine- and ryanodine-sensitive Ca2+-release and characteristic GFP fluorescence. Furthermore, in vitro

localization of GFP allowed 3D mapping of the Thr1366 to domain 6, a constituent of the cytosolic multi-domain RyR2 "clamp" regions (40).

However, the potential of the RyR2-(Thr1366-GFP) construct to develop a model organism to study RyR2 in vivo has not been explored yet. GFP-RyR2 KI mice would allow regional, cellular and subcellular localization of GFP-RyR2 protein in live cells/tissue via fluorescence-based imaging (e.g. fluorescence microscopy, super resolution imaging, etc.). This would enable us to investigate the functional relevance of subcellular RyR2 distribution for synchronous and graded intracellular Ca2+ release.

1.3.5 Imaging of cellular distribution of RyR2 clusters

Studies of the cellular expression and distribution of RyR2 have mostly depended on microscopic imaging techniques. Microscopy uses the interactions of electromagnetic waves and specimens to visualize objects that otherwise would not be within the resolution of the human eye. Technical advancements produced various specialized light and electron microscopy techniques to detect and monitor proteins in biological systems (175–177). As such, electron microscopy, confocal fluorescent microscopy, stochastic optical reconstruction microscopy (STORM), structured-illumination microscopy (SIM) and total internal reflection fluorescence microscopy (TIRFM) have been used to study the distribution of RyR2 in cells and tissue (178). Most studies focused on ventricular myocytes and heart tissue. In the following section, we will discuss and evaluate former observations and potential shortcomings.

1.3.5.1 Cellular fine-structure imaging using electron microscopy

Electron microscopy relies on the interaction of a beam of electrons and an ultra-thin specimen when passing through it. EM requires chemical fixation (e.g.: glutaraldehyde) (179), embedding of the specimen in resin and sub-micron thick samples slicing (180), and staining with toxic substances (e.g.: osmium tetroxide) to enhance contrast (181, 182). In consequence, EM cannot be used for in situ imaging. However, this technique has been applied to reveal details of various cellular fine-structures (< 50nm) (47), due to the high resolution achieved with the smaller wavelength of electrons.

Using thin-section transmission electron microscopy, Franzini-Armstrong reported in 1970 highly-ordered rows of regularly spaced electron-dense `feet-like` structures at the interface between the junctional SR and the t-tubules in the interior of skeletal myocytes (183). This study led to the subsequent identification of these feet as the cytoplasmic domains of RyRs (123, 184, 185). Additionally, it instigated efforts to further define intracellular arrangements in skeletal and cardiac cells.

1.3.5.1.1 Structural relations of L-type Ca2+ channels and RyRs

EM revealed that voltage-gated L-type Ca2+ channels clusters in invaginations of the sarcolemma interfacing arrays of RyRs in the terminal cisternae of the SR (186–188). Furthermore, it provided pivotal anatomic evidence to explain the distinct ECC mechanisms in skeletal and cardiac muscle (31). In skeletal muscle, tetramerous collectives of voltage gated L-type Ca2+ channels were found to anchor with the subunits of the homo-tetramer RyR1(189, 190). This finding significantly strengthened the credibility of the proposed molecular mechanism that relied on direct interactions of the two channels to mediate skeletal ECC (191).

In cardiac muscle, EM images showed that L-type Ca2+ channels are also localized in juxtaposition to RyR2s. However, no particular grouping of the plasma membrane channel could be determined (192, 193). Thus, physical interactions of the two components were rendered unlikely. This supported the belief that cardiac ECC relies on CICR as described by Fabiato and Fabiato (136, 140). Unfortunately, little is known about RyR2 distribution in live ventricular cardiomyocytes.

1.3.5.2 Distribution of CRU using confocal imaging

Confocal fluorescence microscopy has provided the means for reliable assessment of intracellular Ca2+ dynamics on a subcellular level. Emission light is temporally detected from a line (line scan), or xy-segment (full frame mode) of interest via optical sectioning with a resolution down to one-quarter of a micrometer (177, 194). Out-of-focus emission/excitation light is thereby physically rejected by a pinhole.

Its application extends to living organisms, and thus facilitates spatiotemporal monitoring of Ca2+-specific functional probes. Fluorescent indicators are commonly acetoxymethyl ester (AM) derivatives of chelating agents. AM conjugation with carboxylic acids produces small uncharged non-fluorescent compounds which can diffuse readily across membranes into cells. In the cytosol, nonspecific esterases hydrolyze the entered chemicals and thereby unmask charged carboxylic groups. Thus, these probes are trapped within the cell membrane and activated to yield fluorescence intensity changes in stochastic response to Ca2+ binding. Fluo3/4-AM and Rhod2-AM are high affinity BAPTA-based Ca2+indicators, that have been used extensively to study elementary RyR2-mediated Ca2+ release events in various cell types and tissues (195). They exhibit an increase of green or red fluorescence with Kd values for Ca2+ of ~335 nM and

~570 nM, respectively. Their application allowed the characterization of morphometics of Ca2+ spark (196, 197). Four main parameters which represent the amount of released Ca2+ (amplitude), the rate of release flux (rate of rise), release termination (decay time) and the spatial dimension of sparks (full width at half maximum, FWHM at peak amplitude) have been used to define Ca2+ sparks. In general, rapid onset, with limited local spread and exponential decay signify the spatiotemporal profile of Ca2+ sparks. Importantly, a high degree of variations of detected parameters indicated that Ca2+ sparks are polymorphic (128, 129, 131, 198). Variability in the recruitment of RyR2 channels within and among an individual CRU has been proposed to cause this phenomenon. Initial activation of a single RyR2 channel (199, 200), only a fraction of RyR2 within a CRU (128, 129, 201, 202), or the entire RyR2 cluster (203, 204) has been proposed to be required for the generation of a Ca2+ spark. However, the exact number of RyR2 channels remains unclear to this date. Thus, population studies of Ca2+ sparks, rather than the observation of stereotyped or all-or-none events, have been used to evaluate RyR2 mediated Ca2+ release.

1.3.5.2.1 Ca2+ spark mapping

Confocal mapping of Ca2+ sparks has been used to indirectly localize CRUs. In the interior of cardiomyocytes, RyR2 clusters at the interface between transverse tubules and SR which runs along the Z-lines of sarcomeres are believed to act as CRUs (53, 153, 154, 205). Interestingly, a recent functional investigation by Lukyanenko et al. (206) reported the detection of a significant portion of RyR2-mediated events (~20%) in between Z-lines. Thus, the existence of functional RyR2 units in the space between z-lines were proposed with an important role in the propagation of Ca2+ transients across individual sarcomeres (207). Controversy, other

studies showed that almost all RyR2 clusters are co-localized with α-actinin (59, 208), an established Z-line specific marker. The reason underlying the discrepancy between functional observations and localization studies remains unclear.

Additionally, functional studies have previously shown that CRUs are located near the membrane (209–211). However, whether all RyR2 clusters are activated by Ca2+ influx through the L-type Ca2+ channel, or similar function as previously reported in the interior is unclear.

1.3.5.3 Distribution of RyR2 clusters in cellular context using confocal imaging

Confocal microscopy has also the capability to localize structural fluorescence markers of well-established cellular structures to provide context (177, 212). Unfortunately, the resolution of confocal fluorescence microscopy is limited by the diffraction of light. Thus, it may only be used to resolve two points of not more than approximately 250nm along the x-y axes and ~500nm along the z-axis. Yet, the subcellular structure of individual RyR2 proteins in a cluster is much smaller and cannot break the diffraction barrier (213). However, confocal fluorescence microscopy has proven itself exceptionally useful to study protein expression/distribution in subcellular context. It has been employed to define the location and track organelle-specific dyes, fluorescently labeled and genetic encoded proteins to better understand their function and dynamics in live cells. The plasma membrane has been targeted with amphiphilic dyes that contain hydrocarbon chains that anchor the chemical in the membrane. Mitochondria have been visualized with dyes that selectively accumulate in this organelle due to their membrane potential gradient (178). Alternatively, antibodies against specific targets have been used to evaluate contextual protein distribution. 3D distribution of anti-RyR2s has been extensively studied in fixed and or permeabilized cells (53, 56–59, 153, 154, 205, 208, 214, 215).

Co-localization, the signal overlap/co-detection due to close spatial proximity below, or close to the resolution limit of the applied technique, has been commonly used as relative measure to describe cellular structures in microscopy. Studies confirmed tight association of RyR2s with L-type Ca2+ channels. Additionally, confocal imaging showed highly ordered arrays of RyR2 clusters in the cell interior of ventricular myocytes (53, 153, 154, 205). Intriguingly, distinct subcellular patterns of RyR2 clusters were found in the periphery of ventricular cardiomyocytes.

1.3.5.4 Distribution of RyR2 clusters in the periphery of cardiomyocytes

3D confocal imaging from independent groups showed two distinct structural features in the peripheral region of mature cardiomyocytes. On one hand, so-called `double` rows of RyR2 clusters were reported. Analysis of the inter-cluster periodicity of this RyR2 arrangement revealed bimodal distribution with peaks at ~0.7 µm and long distance peak ~1.9 µm. The latter value has been found to define transverse spacing of the rows of RyR2 arrays in the interior of cardiomyocytes and reflects sarcomere length (214). Thus, highly ordered double rows were suggested to resemble arrays of RyR2 cluster interior, but additionally harbor regularly interspaced clusters. On the other hand, an irregular pattern of RyR2 clusters was shown in the outermost optical confocal z-planes of independent studies (57, 58, 214). However, the latter observation was not further evaluated. Presumably this is due to the fact that other studies that used total internal refection microscopy, did only report `double rows` (56, 215).

1.3.5.4.1 Details of the distribution of peripheral RyR2 clusters detected via total reflection microscopy imaging

As specialized form of fluorescence microscopy, TIRFM allows spatially selective excitation of fluorophores in restricted regions of a specimen in immediate proximity to a glass/water interface (216, 217). Prisms, or the objective itself are thereby used to achieve total internal reflection. This phenomenon occurs when incident electromagnetic waves that travel through a dense medium (high refractory index) strike an interface with a less dense medium (lower refractory index) at an angle greater than the critical angle. At the critical angle refraction is 90 degrees along the medium boundary, thus no transmission of incident light. However, during total internal reflection an evanescent field is generated that is oriented along the surface of separation. Such a field provides sufficient energy to excite fluorophores in close proximity to the boundary, although it penetrates less than approximately 200nm into the medium with lower refractory index due to its exponential decay with distance from the interface (216, 218).

TIRFM has been found to be a particular useful approach to image peripheral subcellular targets in live cells. Background signals are dramatically reduced due to the lack of out-of-focus excitation/emission from other regions, such as the cell interior. Soeller`s group applied TIRFM to specifically study the relative distribution of NCX and RyR2 (56). They found highly-organized double rows of anti-RyR2 signals in the periphery of antibody-stained cardiomyocytes. Interestingly, individual RyR2 clusters appeared in a variety of sizes and shapes within this arrangement. This was further investigated in a subsequent study suggesting more complex intra-cluster organizations rather than stochastic circular close-packed arrays (155). They detected elongated clusters that were estimated to contain a number of RyR2 channels almost an order of magnitude smaller than previous studies suggested. These peripheral RyR2 clusters were localized in close proximity to one another, leading the authors to suggest intra-cluster coupling to form functional `superclusters`. However, whether all individual RyR2

clusters are functional and/or possess similar Ca2+ release properties than clusters in the interior remains unknown. Importantly, both TIRFM studies did not report irregular RyR2 patterns, thus the data are not consistent with confocal observations (57, 58, 214). To note is that both studies were carried out in fixed and permeabilized ventricular myocytes that were gently sandwiched between two coverslips to provide an interface for TIRF imaging.

1.3.5.5 Superresolution imaging -A novel approach to study the distribution of RyR2 clusters

Recently, two novel concepts have been developed to circumvent light's diffraction limitations (~250 nm) to acquire so called superresolution of biological fine-structures.

1.3.5.5.1 Light diffraction and optic resolution

Optic resolution defines the shortest distance between two radiating point sources which still allows their distinction as individuals by an imaging system (218). Conventionally, microscopic resolution is limited by the diffraction of electromagnetic waves (photons, or electrons) when they pass through a circular aperture. Emitting point sources are imaged as so called Airy disks and their lateral concentric and axial diffraction patterns (178, 219). The extent of such interference, often referred to as convolution, or `blurring`, is described by the point spread function (PSF).

The PSF is a microscope system-specific function that specifies the distribution of light near the radiating point source. The PSF depends on the illumination wavelength (λ) and the optical properties of the microscope objective (numerical aperture, NA). Commonly, it is determined empirically by imaging of spherical radiating point-like (e.g.: fluorescent) beads of known sub-resolution size (220). Advanced microscopy techniques utilize computationally

algorithms to extract information from images with known PSF and therewith overcome resolution limits.

1.3.5.5.2 Targeted and stochastic superresolution approaches

Superresolution techniques can be classified as ‘targeted’ versus ‘stochastic’ readout approaches (178, 221). Targeted readout methods (e.g.: SIM) rely on structured illumination that spatially determine where fluorophores can adopt the fluorescent state (222, 223). In contrast, stochastic readout techniques (e.g.: STORM) are based on photo-active properties of fluorescent probes that randomly switch fluorescent states (175, 194)

Superresolution microscopy has been particularly useful to study molecular details of cellular architectures. We will discuss the most common approaches and advancements in the following section.

1.3.5.5.3 Details of the distribution of RyR2 clusters revealed by stochastic optical reconstruction microscopy

As probe-based STORM relies on photo-switchable molecules. Such display fluorescence intermittency, or `photo-blinking`, the phenomenon of random switching between an emitting and a non-emitting `dark` states during continuous excitation, in a reducing/oxidizing environment. Thiol-containing agents (e.g.: glutathione) stabilize stochastically entered non-radiating triplet, or other dark states, which revive spontaneously or light-induced via oxidation with molecular oxygen (175, 177).

Time-elapsed recording of transiently emitting molecules facilitates spatial separation of such light sources from constant radiating, otherwise indistinguishable, background. Mathematical

computation further allows the determination of the exact pixel light originated from. A collective merging of all blinking molecule-positions leads to a superresolution image. The resolution of such depends on labeling density and fluorophore properties, in particular, the stability of their non-radiating state. STORM utilizes cyanine based synthetic fluorophores (175) to facilitate fine-structure analysis with nanometer spatial resolution even in dense background systems. Not limited by the diffraction of light, this method has provided details of 3D cellular fine-structure (e.g.: microtubules, etc.) and features of organelles (e.g.: mitochondria, etc) at the molecular level (176, 224). STORM reconstruction of photo-active membrane and organelle marker signals allowed super-resolved imaging (~30–60 nm spatial and 1–10 sec temporal resolution) even in live cells (225).

Stochastic superresolution imaging has further defined the distribution of antibody-labeled targets. As such as RyR2, structural protein junctophilin-2, Ca2+ buffer protein calsequestrin and microtubule protein caveolin-3 were localized in the periphery of fixed and permeabilized cardiac tissue and cells (56, 57, 226). A tight association of RyR2 with junctophilin-2 was showed in the periphery of cardiomyocytes (57). In contrast, superresolution revealed minimal (4.9%) co-localization of caveolin-3 and RyR2s (227). This is 23.7 % less than estimations of diffraction limited confocal images suggested (178). To note is that stochastic readout techniques that investigated RyR2s in cardiomyocytes exclusively focused on the periphery of fixed and permeabilized cardiomyocytes (56, 57, 227). Studies acquired images with ~30 nm lateral resolution via an approach the authors have described as reversible photo-bleaching (RPM). Conceptually, this technique is the same as dSTORM (228, 229).

Similarly, application of STORM may provide novel details of the distribution of RyR2 clusters. However, the development of selective antibodies conjugated to a fluorophore with a stable dark state is required to utilize such a superresolution technique.

1.3.5.5.4 Details of the distribution of RyR2 clusters observed with structured-Illumination microscopy

As illumination-based method, SIM utilizes spatially structured excitation to generate moiré fringes (219). The latter describes interference patterns that appear in the product of two superimposed non-identical opaque ruled patterns with transient gaps. Their coarse character contrasts either of the original fine patterns and contains normally inaccessible high-resolution information in the Fourier transform (219, 230).

For conventional microscopy, the diffraction of light limits detectable frequencies as a circular ‘observable region’ in reciprocal space. Within low resolution information is found at the origin and higher frequencies distant from the source center. The radius of the ‘observable region’ depends on the objective lens aperture. Commonly microscopic imaging is performed with illumination frequencies only at the center of the `observable region`. In contrast, SIM utilizes sinusoidally striped structured-illumination to excite with a total of three diffraction frequencies. In consequence, emission light from the sample contains the convolution of three superimposed components in reciprocal space. Thus, images gained information that originate in offset regions and was moved into the observable region, without physically altering the latter. Arithmetic de-convolution facilitates extraction of such information. In consequence, recording of image series illuminated at different pattern orientation (rotations) and phase allows computational reconstruction with improved resolution (231, 232).

Superresolution microscopy has extended our knowledge about the organization of CRUs (56, 57, 226). Hitherto, the molecular organization of functional units of RyR2 receptors has remained unresolved. Furthermore, functional correlations of Ca2+ release and RyR2 localization is desired to gain new insight about the architecture of CRUs and changes in health and disease.

Application of targeted readout methods allowed super-resolved localization of the t-tubule membrane system, even in living cardiomyocytes (233). Thus, it is promising to facilitate in situ localization of RyR2 in live tissue and cells in the near future. To note is that the quality of SIM imaging has been reported to depend on optimal illumination parameters used for acquisition (231). These are specific for different wavelengths. Thus, potential benefit could result from the development of probes that facilitate signal localization at distinct illumination parameters. As such, our study is aimed to develop anti-GFP probes that yield distinct signals additional to GFP-fluorescence.

1.3.5.6 Nanobodies – A novel tool to study the distribution of RyR2s

Immunoglobulin G proteins that are found in all vertebrates have been extensively used for the localization of targets, such as peptides or proteins, in biological materials. These monomer structure comprises two heavy and two light chains. Thus, they conventionally assemble in an Y-structure. In detail, the light chain is composed of two domains, whereas the heavy chain with four segments. Each domain, consists of ~110 amino acids and is classified by their variability in sequence. Mostly conserved regions in light and heavy chain were termed constant (CL; CH1, CH2, CH3 respectively). In contrast, domains at the N-terminal of both, heavy and light chains (VH and VL), exhibited a high degree in variation of amino acid composition. Their assembly is believed to provide hydrophobic interaction interfaces that

facilitate adaptive epitope-specific binding at the exposed tips of the 'Y'. As shown in Figure 4, antigen-binding depends on the combination of both chains to form two identical flat or concave interaction sites. The complex structure of IgG makes them large-sized molecules (~ 150 kDa; 90 nm) (234), which limits their flexibility, transportation and activity range.

Recently, a new type of antibody was discovered in llamas, other camelids and sharks (235, 236). Classified as heavy chain antibodies (hcAbs), they derived their name from their unusual composure of only heavy chains. Interestingly, antigen binding requires only a structural fragment of these unique antibodies, so-called nanobodies. As depicted in Figure 4, These nanobodies have been found to be the smallest intact antigen recognizing protein (~ 13 kDa) reported yet (237, 238). Their small size and high affinity makes them an ideal research tool. Furthermore, their unusual shape and flexibility enables them to reach and bind cavities of antigens, which conventionally flat or concave antigen-binding sites could not interact with. Their simplicity leads also to high refolding capacities, high solubility and thermal stability. Additionally, they can be directly linked to commercial dyes. Also, to note is that nanobodies have been found to provide hydrophilic interaction sites for antigens contrasting hydrophobic binding interfaces in conventional antibodies. With all these advantages, they are an ideal tool as targeting and delivery systems for protein visualization in tissue and cellular organisms (235, 236)

Ries et al. (239) employed this new approach to target GFP in a vast spectrum of biological materials: I) yeast, II) a cell line and III) cultured hippocampal rat neurons. Thereby, they coupled anti-GFP nanobodies to fluorescence dyes (i.a.: Alexa Fluor 647) - fluorophores switchable between a non-fluorescent and a fluorescent state upon the exposure with light – to allow single-molecule localization super resolution imaging. They provided a convincing body

of evidence that the use of nanobodies facilitated an efficient delivery of bright organic fluorophores to GFP in all tested organisms. Thereby, the linkage error to the target generated by the small anti-GFP nanobodies (~13kDa; 1.5nm x 2.5nm) could be minimized to ~5-10 nanometers (238, 239). This novel improvement, compared to conventional large-size AB labeling, allows accurate nanometric spatial resolution in almost any GFP model to withdraw information on a molecular level. More importantly, the unique specificity of anti-GFP nanobodies permits unambiguous targeting of epitopes in complex systems, even when genetically fused to other proteins. Thus, application of such anti-GFP probes in GFP-RyR2 KI mice may yield novel detail of the distribution of RyR2.

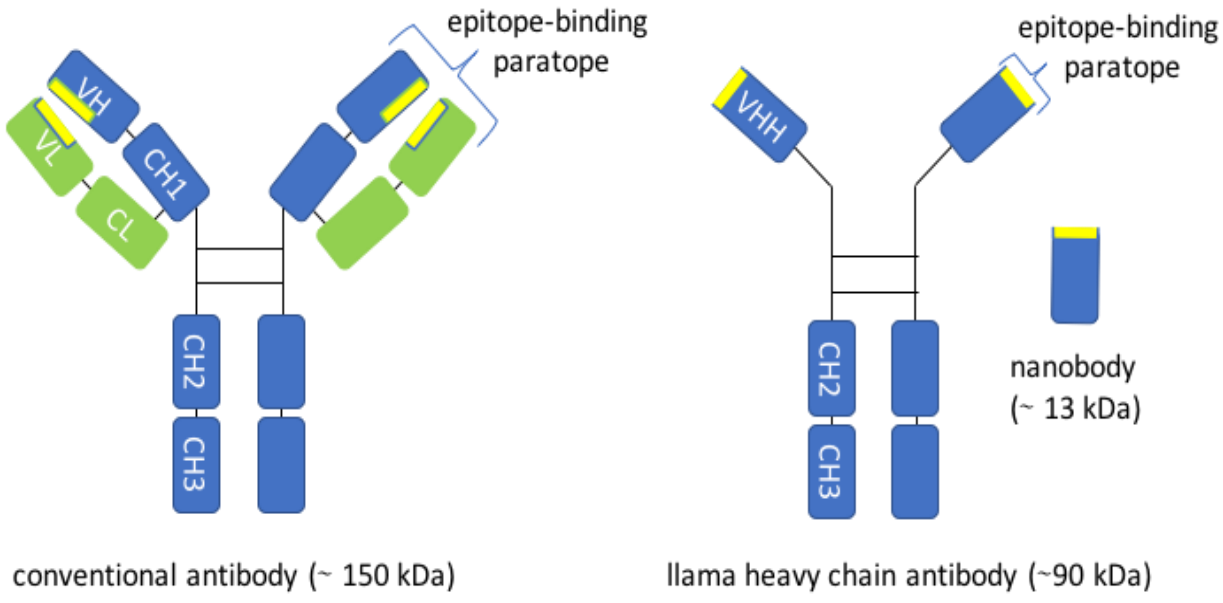

Figure 4 Structural features of conventional and llama heavy chain antibody

A structural comparison of a conventional immunoglobulin (Ig) G antibody and heavy chain antibody (hcAbs) that is found in llama is graphically depicted. A monomer of IgG is composed of two heavy (chain of blue ellipsoids) and light (chain of green ellipsoids) chains. The antigen-

binding paratope (yellow box) of conventional IgG is formed by the variable domains of heavy and light chains (VH and VL). In contrast, only a fragment of the heavy chain antibody, termed nanobody, or VHH domain in camelid hcAbs, is required for specific epitope targeting (adapted from `Nanobodies as modulators of inflammation: potential applications for acute brain injury.` Rissiek et al. 2014 (240)).

1.4 Functional coupling of ER/SR Ca2+ release and mitochondrial Ca2+ homeostasis

Aside from the ER/SR, mitochondria provide intracellular Ca2+ stores. Due to their tremendous capacity for Ca2+ uptake, they have also been described as Ca2+ sink (241). Ca2+ uptake is mediated by mitochondrial Ca2+ uniporter (MUP), a transmembrane protein in the inner membrane of the organelle. Ligand (Ca2+) binding facilitates ion transport, which relies on the large electrochemical gradient for Ca2+ across the inner mitochondrial membrane. MUP has been described with very low affinity for Ca2+ that would require cytosolic Ca2+ levels to elevate to ~5-10 µM to activate mitochondrial Ca2+ uptake. However, such cytosolic conditions have never been reported in healthy cardiomyocytes. Thus, Rizzuto et al (242) suggested functional coupling of mitochondria and juxta-positioned ER/SR in so called microdomains to facilitate slow uptake of high Ca2+ concentrations (≥ 10 µM) that can occur spatiotemporally restricted under physiological conditions. However, whether such microdomains also allow Ca2+ uptake via MUP at lower Ca2+ levels remains controversial.

1.4.1 The role of mitochondrial Ca2+ transport in cardiac ECC

One of the most heated debates in the field of muscle physiology has focused on the question whether spatiotemporal cytosolic Ca2+ elevation during cardiac ECC is affected by

mitochondrial Ca2+ buffering on a beat-to-beat basis, or not. To this date, it remains unclear. A large body of evidence has provided support for either fast mitochondrial Ca2+ uptake, or slow Ca2+ accumulation and buffering of mitochondria in cardiomyocytes.

In consensus, it has been demonstrated that MUP has the kinetic ability to react to rapid fluctuations in cytosolic Ca2+ levels on an instantaneously, near beat-to-beat, temporal scale. In support, a high affinity binding side for Ca2+ in concentrations as low as 2nM was identified in electrophysiological studies (241). However, whether such rapid alternations of mitochondrial Ca2+ are necessary and/or even beneficial during ECC in cardiac cells has divided the field.

Dynamic mitochondrial Ca2+ uptake and efflux on beat-to-beat basis would require substantial Ca2+ release and recycling from the SR. The amount of released Ca2+ would have to exceed the buffer capacity of both, the cytosolic and mitochondrial matrix, to facilitate Ca2+ flux. At the same time, enough Ca2+ would have to be provided to cause cardiac contraction. Additionally, ATP-dependent shuttling of Ca2+ into the SR would not be favorable from an energetic point of view for the cells (241).

1.4.1.1 Mitochondrial Ca2+ Sparks, or Marks

Information have been gained from various approaches, spanning from assessments in isolated mitochondria to intact heart (243, 244). Interestingly, multiple studies in permeabilized cardiomyocytes (primary rat cells and cultures) reported caffeine and ryanodine sensitive changes of mitochondrial Ca2+ levels. Therein, authors argued for rapid Ca2+ uptake by mitochondria of local RyR2-mediated Ca2+ release from the SR (245, 246).

Hajnóczky`s group reported the existence of Ca2+ marks (mitochondrial Ca2+ sparks), a term the authors created to describe transient Ca2+ elevations in the mitochondrial matrix that

are elicited by Ca2+ sparks (245). Their observation was made in Rhod-2 loaded mitochondria in permeabilized H9C2 cell cultures. In this set up, they detected transient elevations of local Ca2+ within a single mitochondrion in response to caffeine-triggered Ca2+ sparks. Spatiotemporal features of Ca2+ marks were described with fast initiation phase (rate of rise ≤ 50ms) and much slower decay (full duration at half maximum ~215ms) than Ca2+ sparks. Interestingly, this study showed also an increase in Ca2+ spark frequency and duration after the application of antimycin A and carbonilcyanide p-triflouromethoxyphenylhydrazone. These drugs were used to inhibit mitochondrial Ca2+ uptake. Thus, it was suggested that mitochondrial Ca2+ is directly influenced by elementary RyR2-mediated Ca2+ release and vice versa (245).

However, evidence of the existence of Ca2+ marks, thus whether RyR2-mediated Ca2+ release directly influences mitochondrial Ca2+ levels, remains lacking in cardiomyocytes with intact plasma membranes.

1.4.1.2 Species selectivity in Ca2+ dynamics between ER/SR and mitochondria

It should be noted that rapid intra-organelle Ca2+ dynamics between SR and mitochondria during ECC have been indicated to be species selective. Using different approaches, cardiomyocytes that were isolated from guinea-pig and rabbit yielded mitochondrial Ca2+ transients on a beat-to-beat level, whereas rat, cat, ferret and hamster cells, or hearts, did not (245). However, whether this phenomenon is the result of distinct intrinsic mechanisms of mitochondrial Ca2+ uptake, or the presence of different regulatory elements remains unknown.

1.5 Catecholaminergic polymorphic ventricular tachycardia (CPVT)

Catecholaminergic polymorphic ventricular tachycardia is a rare arrhythmogenic disorder that presents with adrenergic induced bidirectional or polymorphic ventricular tachycardia (86, 137, 240). The disease manifests with physical exercise or emotional stress induced syncope and sudden cardiac death early in life, without structural abnormalities of the heart and coronary arteries. CPVT patients display normal electrocardiogram recordings at rest. Stressed individuals experience an increase in monomorphic premature ventricular contractions (PVCs).These can ultimately lead to bidirectional or polymorphic VT and cardiac arrest (33-38% of patients) (247, 248). Additionally, physical strain induced atrial arrhythmias have been also found in CPVT diagnosed patients (247).

Untreated CPVT causes extremely high mortality (up to 50% by the age of 35) (86, 249, 250). Thus, CPVT has been suggested to be the underlying reason for ~ 12% of autopsy-negative unanticipated deaths and more than 1% of unexpected death in infants (251, 252). In most cases, first symptoms are observed already as toddlers and adolescents, although occasionally CPVT does not occur until adulthood. The age of onset (first syncope) has been shown to be correlated with the seriousness of the disease. Only 60% of patients survive longer than 10 years after a CPVT diagnosis (253). Beta-blockers, such as flecainide and carvedilol, were found to reduce syncope in CPVT patients, thus have therapeutically effects (254). Sever cases however required the implantation of an automatic internal defibrillator (255). However, even with treatment, lethal incidences occurred in up to 13% of CPVT patients (247, 256).

The analysis of genomic DNA from CPVT patients linked the disease with the chromosomal locus 1q42-43 (257). Since then, multiple subtypes of CPVT have been identified.

The arrythmogenic mechanism of all CPVT classes share one key element, abnormality of RyR2-mediated Ca2+ release (258).

The most common form of CPVT (CPVT1) is caused by autosomal dominant genetic variation in the gene of RyR2 itself. Over 50 different missense mutations of RYR2 have been directly linked to CPVT (86, 254), mainly accumulation in exon 16 of RYR2 (259, 260). Up to 79% of a cohort of CPVT patients were found to harbor mutations of RYR2, leading ~ 10% of this population to pass away as a result of sudden death (258).

1.5.1 Mechanism underlying cardiac symptoms of CPVT

The mechanism that underlies CPVT has been extensively studied. In general, CPVT-linked RyR2 mutations are believed to sensitize the channel to activation by Ca2+ and thus increase the propensity of spontaneous Ca2+ release (86). NCX-mediated inward currents can occur in response to a cytoplasmic Ca2+ overload. The excess Ca2+ is extruded by the forward mode of NCX, leading to an unbalanced net exchange of charge. This can lead to delayed after-depolarization (DADs), arrhythmias and sudden death (12). Three distinct models have been developed to explain altered RyR2-mediated Ca2+ release in CPVT.

1.5.1.1 FKBP12.6 dissociation leads to `leaky` RyR2 channels

The role of FKBP12.6 in the regulation of RyR2 remains controversial. Marks and associates generated the hypothesis that dissociation of the FKBP12.6 enhances the activity of RyR2 channels, which in turn lead to cardiac arrhythmias. A series of studies from them reported evidence indicated that FKBP12.6 binds the cytosolic portion of RyR2 as `stabilizing` element to maintain the channel closed during diastole (66). They proposed that CPVT-associated mutations

of RyR2 possess decreased binding affinity to FKBP12.6 already at basal conditions. Thus, stress-induced PKA phosphorylation of RyR2 leads to loss of FKBP12.6 association, resulting in`leaky` RyR2 channels with increased probability of Ca2+ release and prolonged opening. In addition, Marks' group applied 1,4-benzothiazepine derivatives, namely S107, and K201 (alias JTV519) which restored the activity of RyR2 mutants. Authors attributed this phenomenon to enhancement of the binding of FKBP12.6 to RyR2 (250, 261). The same group developed FKBP12.6 KO and RyR2 R2474S knock-in mice that showed stress-induced cardiac arrhythmias which could be prevented by the use of K201(262) and S107 (263), respectively.

Albeit all this evidence by one group, other groups challenged this hypothesis on various levels. Lipid bilayer recordings of two independent groups showed that FKBP12.6 did not altered RyR2 gating, neither at basal conditions nor after application of catecholamines (264, 265). Investigation of the mode of action of K201 revealed that suppression of RyR2-mediated spontaneous Ca2+ release and reduced binding of radioactive labeled ryanodine occurred independent of FKBP12.6 (266). This suggests a distinct mechanism underlying the antiarrhythmic effects of this drug. In addition, in vivo and in vitro characterization of RyR2-R4496C in mice demonstrated that K201 failed to prevent catecholamine-induced arrhythmias and interactions of FKBP12.6 and RyR2 were not affected (267). This was surprising, since Marks and colleagues have reported that the corresponding human RyR2 mutation (RyR2-R4497C) impaired FKBP12.6 binding to RyR2 thus causing the cardiac disease linked symptoms (262). Taken together, the role of FKBP12.6 in the arrhythmogenic mechanism of CPVT remains unresolved.

1.5.1.2 Stress-induced Store overload induced Ca2+ release

As graphically depicted in Figure 5, a second model has introduced the principle of store overload-induced Ca2+ release (268). It relies on the regulation of the activity of RyR2 by the luminal Ca2+ level. At rest, the concentration of free Ca2+ in the SR lumen remains below a threshold that would cause spontaneous channel opening of RyR2s. However, during stress, Ca2+ levels within the intracellular store increase in response to stress leading to SOICR when a critical threshold of luminal Ca2+ is reached. CPVT-associated modifications of RyR2 are believed to reduce the SOICR threshold below luminal Ca2+ concentrations observed during stress and diastole. Thus, they cause spontaneous diastolic and stress-induced Ca2+ release. In support of this theory, CPVT-linked mutations of RyR2 have been shown to increase the sensitivity of RyR2 to luminal Ca2+, but not cytosolic Ca2+, in lipid bilayers, HEK293 cells, cardiomyocyte and intact hearts (L433P; RR176Q/T2504M; S2246L; R2474S; N4104K; Q4201R; R4496C; and I4867M;and N4895D) (83, 87, 89, 264, 267). Additionally, Chen and colleagues demonstrated that the RyR2 A4860G mutation displays a loss of luminal Ca2+ activation (90). The recent finding of residues of RyR2 in the pore that act as luminal Ca2+ sensor provided compelling evidence for this model underlying CPVT (269). Nevertheless, it should be noted that distinct CPVT-linked mutations (R176Q/T2504M and L433P) attenuated Ca2+ dependent inhibition, thus affect the sensitivity of RyR2 to both, cytosolic and luminal Ca2+ (264, 270).

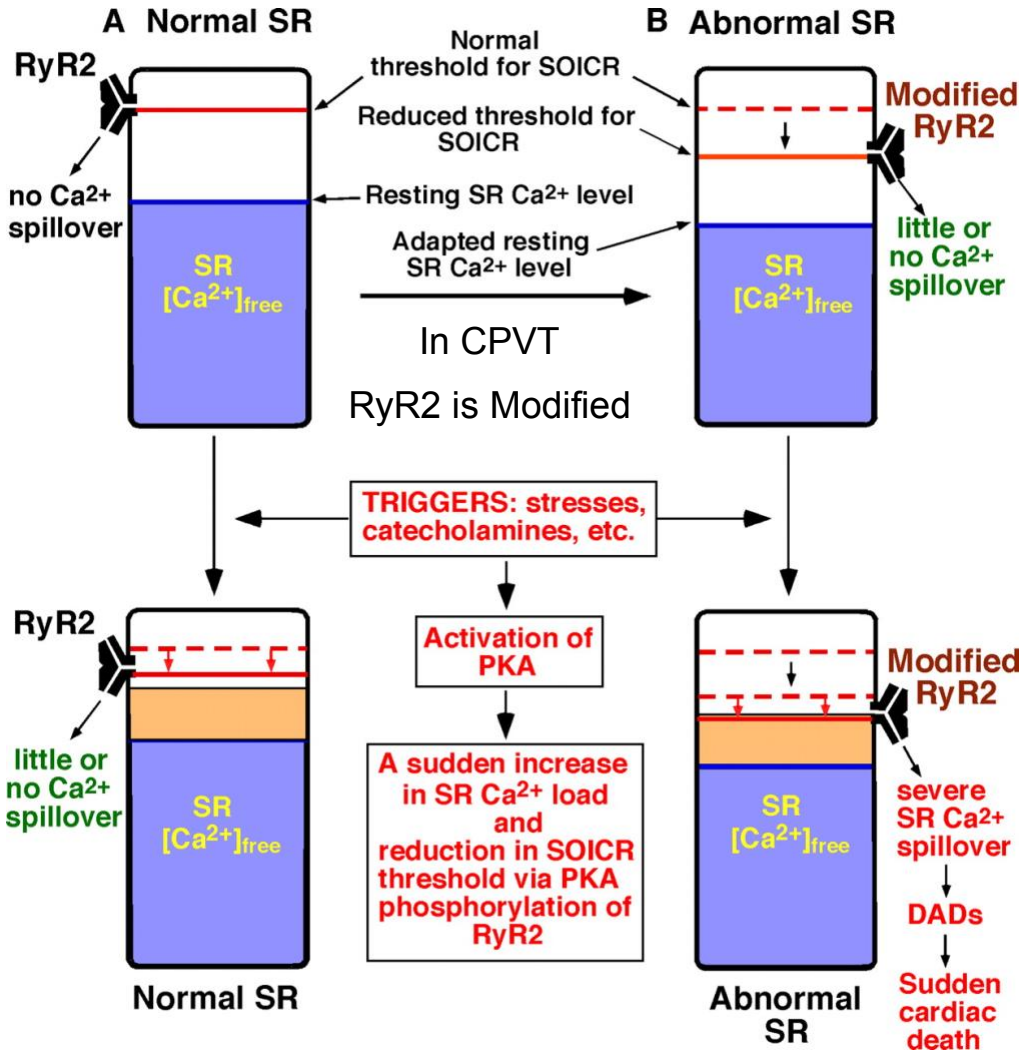

Figure 5 A model of stress-induced store overload induced Ca2+ release underlying CPVT

A graphic representation of Ca2+ release from the sarcoplasmic reticulum mediated by normal RyR2 channels (A) and abnormal CPVT associated RyR2 mutations (B) in correlation to free Ca2+ levels in the lumen of the SR. The concentration of free Ca2+ is schematically shown at rest (blue fields) and when a rapid increase occurs as consequence of stimulation (orange areas) by catecholamines or stress, that induces PKA mediated phosphorylation of RyR2. To note is that differences in the resting level of free Ca2+ in normal (A) and abnormal CPVT SR (B) have been suggested to be the result of SR autoregulation/adaptation (271). As intrinsic property of RyR2, the threshold for SOICR is illustrated as red line. It has been indicated that the threshold for SOICR is reduced in the CPVT SR as a result of the expression of RyR2 mutations. Thus, severe Ca2+ spillover that can cause delayed after depolarization and cardiac arrhythmias has

been proposed to happen when the free luminal Ca2+ concentration reaches the reduced SOICR threshold in the from CPVT SR. (Adapted from "Functional consequences of protein kinase A-dependent phosphorylation of the cardiac ryanodine receptor: sensitization of store-overload-induced Ca2+ release." by Xiao B. et al. The Journal of Biol. Chem. 2007 (101))

1.5.1.3 `Leaky` RyR2 channels result from abnormal intra-molecular interactions

The third theory suggests that destabilized intra-molecular interactions of domains of RyR2 underlie CPVT (137). The N-terminal domain and the central domain of RyR2 are associated via a tight zipping motif. CPVT-linked mutations of RyR2 have been proposed to weaken inter-domain interactions and cause folding abnormalities, thus `unzipping` the channel structure. This interference with autoregulation leads to `leaky` RyR2 channels with abnormal Ca2+ release properties (272). Those have been proposed to lead ultimately to dysfunctional RyR2-mediated Ca2+ release. In support, Matzusaki`s group observed that synthetic peptides that mimic sequences of CPVT mutant channels destabilize intra-domain interactions in RyR2 and lead to more frequent spontaneous Ca2+ release events (273, 274). Interestingly, different CPVT mutations lead to distinct conformational folding patterns of RyR2 with abnormal intramolecular interactions (273, 275).

Overall a combination of these three models possibly to underlie RyR2-associated CPVT. However, further research is required to understand the molecular mechanism of CPVT. Current diagnosis of CPVT relies mainly on family-histories and targeted DNA sequencing. However, in the future whole genomic sequencing at birth might identify CPVT-mutation carriers before they become symptomatic.

1.5.2 Treatments of cardiac symptoms in CPVT patients

Pharmacological prevention of cardiac events in RyR2-assosiated CPVT-patients involves mainly beta-blockers such as carvedilol and flecainide. These drugs are believed to directly suppress the activity of RyR2. In support, among various tested beta blockers, only carvedilol has been shown to inhibit SOICR in CPVT models (89, 90, 269). The mode of action of flecainide that leads to its effective application as medication for CPVT remains debated (272, 273, 275). On one hand, flecainide was shown to reduce opening probability and mean open time of RyR2 channels. On the other hand, flecainide was suggested to inhibit the Na channel to prevent DADs, but not act on RyR2 directly (276).

Alternatively, more invasive surgical approaches have been shown to improve conditions for humans with CPVT phenotypes. Left cardiac sympathetic denervation has been shown to prevent individuals from ventricular tachyarrhythmias (277). Alternatively, the use of an implantable cardioverter defibrillator (ICD) had beneficial effects on CPVT patients. However, considering the age of most CPVT patients, surgical implementations are risky. Shock or pain may cause stress and trigger ventricular arrhythmias, and sudden death.

1.5.3 CPVT-patients display intellectual disability

Aside from the arrhythmogenic symptoms, a significant portion of patients expressing CPVT-associated RyR2 mutations also displayed intellectual disability (ID), cognitive deficits, and other neurodevelopmental disorders (278–280). An adolescent girl carrying a missense mutation of RYR2 (L4188P) represented with cognitive dysfunction, seizures and ventricular tachycardia (280). Additionally, de novo missense mutations of RYR2 (G4955E) in a 9-year-old boy caused ID, seizures and atrial arrhythmias (279). Although an increased body of evidence

supports the link between RyR2 dysfunction and intellectual disability, the mechanism by which CPVT-associated RyR2 mutations affect cognitive function is unknown.

A key step towards understanding the physiological and pathological roles of RyR2 in intellectual abilities is the determination of the exact subcellular location of RyR2 clusters.

1.6 Neuronal Ca2+ signaling: ER as neuron-within-a-neuron

Neuronal Ca2+ signaling relies on a binary membrane system. On one hand, the plasma membrane incorporates external input (e.g., excitatory and inhibitory stimuli) to produce action potentials. On the other hand, a continuous ER system that spans throughout the entire cell, even extending into dendritic spines and axonal terminals, facilitates responses to internal signals (e.g., Ca2+, signaling molecules, etc.) via nonlinear Ca2+ release (2).

The ER has been described as neuron-within-a-neuron since it has many characteristics that are normally affiliated with the plasma membrane (see Figure 6). Both are systems that have integrative and regenerative properties. Furthermore, they possess a `memory` of preceding events as a result of activity-dependent phosphorylation of ion channels in the plasma membrane and accumulation of Ca2+ in the ER. Reciprocal interaction among these membrane systems relies on cytosolic Ca2+ to regulate specific processes in neurons, including gene transcription, excitability, synaptic transmission and plasticity.

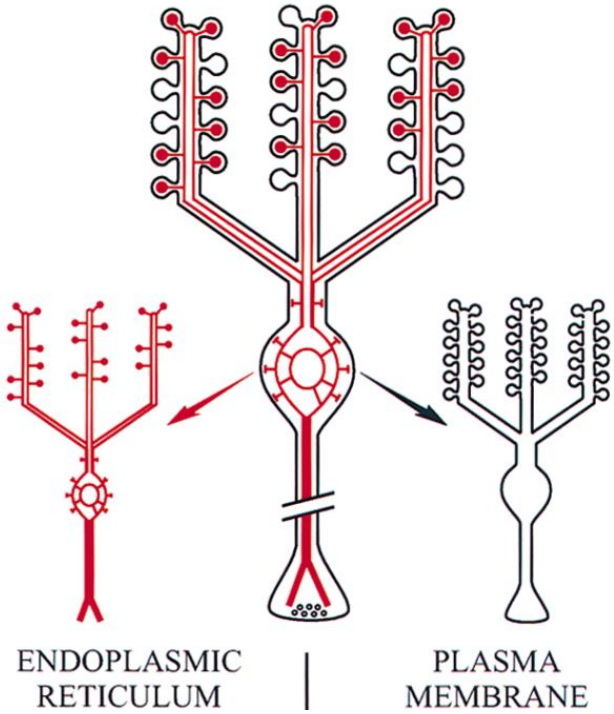

Figure 6 Neuron-within-a-neuron

The binary membrane system that is involved in neuronal Ca2+ signalling is graphically depicted. The extensive ER system extends even into dendritic shafts and axonal terminals (adapted from Berridge M. J. "Neuronal Calcium Signalling." 1998 (2)).

1.6.1 Compartmentalized Ca2+ homeostasis in neurons

Spatial segregation of neurons into compartments allow subcellular-specific Ca2+ signaling (281, 282). Thus, molecular components that are involved in cytosolic Ca2+ homeostasis could be involved in distinct functions depending on their subcellular localization in pre/post-synaptic terminals, axons, dendritic shafts and spines, or the soma.

As such, RyRs have become of great interest since it mediates Ca2+ release from the ER which is present throughout neurons.

1.6.2 Synaptic Ca2+ signaling in neurons

Elevation of cytosolic Ca2+ is an essential step in synaptic transmission. Both Ca2+ influx from the extracellular space and Ca2+ release from the intracellular stores contribute to the cytosolic Ca2+ increase that drives many neuronal processes (2, 283, 284). In neurons, Ca2+ influx is mediated by various plasma membrane receptors and channels, including voltage-dependent Ca2+ channels, *N*-methyl-D-aspartate (NMDA) receptors, alpha - amino-3-hydroxy-5-methyl-4-isoxazolepropanoicacid (AMPA) receptors, whereas intracellular Ca2+ release is governed by RyRs and IP3Rs (2, 283).

1.6.2.1 Role of RyRs in synaptic transmission

Although the significance of intracellular Ca2+ release is becoming increasingly appreciated, it has been insufficiently explored yet. RyR-mediated Ca2+ release has been suggested to be involved in synaptic transmission and signal propagation.

An increasing body of evidence indicates that an analogous CICR mechanism operates in neurons. Thereby, Ca2+ influx signals are amplified upon neuronal activation by RyR-mediated Ca2+ release (285, 286). This intracellular Ca2+ release has been proposed to contribute to a major portion of cytosolic Ca2+ elevation that governs transmitter release, postsynaptic signaling, gene transcription, pre and post-synaptic plasticity, learning and memory (2, 283, 284). However, the molecular basis and the exact roles of the specific RyR2 isoform in neuronal Ca2+ signaling are poorly understood. Knowing the precise subcellular expression and distribution of RyR2 is fundamental to the understanding their functional roles in neurons.

1.6.2.2 Expression and distribution of RyRs in the brain

Misleadingly, RyR3 has been described as the `brain RyR isoform` in literature. This semantic misconception was introduced since RyR3 was first identified by sequence analysis from cDNA isolated from rabbit brain (21). Nevertheless, all three RyR isoforms are expressed in the brain.

1.6.2.2.1 Isoform specific distribution of RyR2 in the brain

RyRs have been extensively studied in striated muscle. However, little is known about isoform-specific subcellular distribution and neuronal function of RyR2 proteins. Already in 1990, radioactive binding assays showed that RyR2 is most abundantly expressed throughout the brain (287). Subsequent [^{3}H]-ryanodine binding experiments, mRNA and antibody localization studies showed similar results and further defined the regional and cellular expression of RyR2. Most extensive levels of RyR2 directed probes were found in the hippocampus and cortex (287–292). These brain regions are important for spatial learning, memory and cognition.

At a subcellular level, RyRs were found to be expressed in different compartments of hippocampal neurons, including presynaptic terminals, dendritic spines, dendritic shafts, and the soma (286, 288, 290, 293, 294). Consistent with these localizations of RyRs, functional studies have implicated an important role of RyRs in synaptic transmission, long-term potentiation (LTP), synaptic plasticity, and gene expression (285, 293, 295–301).

However, the precise subcellular localization and specific roles of the RyR2 isoform in hippocampal neurons are largely undefined. This is due, in part, to the presence of all 3 RyR isoforms in hippocampal neurons, the uncertain antibody specificity in the context of the whole brain tissue, and the lack of isoform-specific functional probes for RyR2.

Intriguingly, training in a water-maze that is specifically designed to stimulate spatial learning and memory led to an increase in the level of RyR2 mRNA and protein in hippocampus (302–305). This observation suggests that RyR2 plays an important role in hippocampal cognition. However, the role of RyR2-mediated Ca2+ release in the molecular mechanisms that underlie such abilities remains unclear.

1.6.3 RyRs in LTP

A number of functional studies have demonstrated that RyRs are critically involved in the induction of long-term potentiation (LTP), a major component of synaptic plasticity, learning and memory (306, 307). LTP describes persistent (≥ 30min) strengthening of chemical synapses in response to neuronal activity. Synaptic strength is defined as the product of three factors: presynaptic release probability; number of neurotransmitter (NT) release sites and postsynaptic response to a singular NT input (308). It is reflected by the amplitude of postsynaptic potentials, which is increased during LTP in an input dependent fashion.

RyR modulator-sensitive Ca2+ release at pre- and post-synapse was reported to be involved in LTP in various neurons. Enhanced activity of RyRs by caffeine or inhibiting of RyRs by ryanodine or dantrolene has a marked effect on the capability of LTP, learning and memory (309–311). However, these pharmacological studies do not distinguish the specific roles of each RyR isoform. Antisense oligonucleotides have been used to selectively knockdown the expression of RyR isoforms(292), but the effectiveness of this knockdown approach in intact animals is not clear. Genetic knockout of RyR3 has been shown to affect learning and memory(312), but this knockout approach is not feasible for RyR1 and RyR2, as RyR1 or RyR2

deficient mice die early during embryonic development(28, 313). Altogether, assessment of the functional roles of the specific RyR2 isoform in neurons has remained challenging.

1.6.3.1.1 RyR2 in LTP and cognition

Only recently, RyR2 was directly linked to LTP and cognition by Marks and colleagues (314, 315). They used knock-in mice that harbored RyR2 mutants with an altered phosphorylation side at residue S2808. Expression of RyR2-S2808A prevented from stress-induced learning disabilities and had beneficial effects in Alzheimer`s disease crossbreeds. In contrast, RyR2-S2808D mice showed defective LTP and cognitive dysfunction. Furthermore, they showed that their RyR2 directed benzodiazepine derivate, S107, rescued cognitive impairment and the capability to produce LTP. As in the striated muscle field, Marks` group proposed that phosphorylation-dependent FKBP12.6 dissociation from RyR2 underlies the neuro-pathogenic mechanism. However, the regulatory role of FKBP12.6 of the activity of RyR2 remains controversial (please see 1.5.1.1 FKBP12.6 dissociation leads to `leaky` RyR2 channels). Thus, other possible regulatory mechanisms should be explored to understand the roles of RyR2 in neuronal function.

For instance, a knock-in mouse model that harbors a CPVT-linked RyR2 mutation (RyR2-R4496C) would be an ideal candidate to evaluate the impact of the effects of enhanced sensitivity to luminal Ca2+. Marks and colleagues suggested that K201 re-establishes the binding of RyR2 by FKBP12. However, cardiac symptoms in RyR2-R4496C mice were not affected by K201, indicating that the equivalent to the human RyR2-R4497C mutation does not lead to FKBP12.6 dissociation (267).

1.6.4 Non-linear Ca2+ release from ER in neurons

Intracellular Ca2+ events in neurons rely on the progressive loading of the ER. As continuous network it provides both, a source and a reservoir for Ca2+. Despite its significance, little is known about the factors that determine Ca2+ release from the ER in neurons.

Intriguingly, Ca2+ release in hippocampal neurons has been shown to be non-linear and graded. A global intracellular Ca2+ event transiently prevented further stimulations. In addition, Ca2+ influx in response to single plasma membrane depolarization was not sufficient to trigger Ca2+ release from the ER. Nevertheless, trains of action potentials triggered Ca2+ release from the ER in hippocampal neurons (316). In support, Ca2+ Sparks were found in hippocampal neurons (297, 317–319). However, the impact of enhanced sensitivity of RyR2 to luminal Ca2+ remains to be elucidated in neurons.

1.7 Research objective and specific aims

Recently, Chen's group created a RyR2-(T1366-GFP) knock-in mouse model that expresses a green fluorescence protein - tagged RyR2. Therewith, I can investigate the expression/distribution of RyR2 in live cardiomyocytes. Additionally, Chen and associates generated KI mice expressing a CPVT-linked RyR2-R4496C mutation (83, 87, 89, 269), with enhanced sensitivity to luminal Ca2+. With these novel KI mice, I am in the unique position to study RyR2 expression/distribution and function in various tissues.

The objective of this study is to define the functional significance of the subcellular distribution of RyR2 in ventricular myocytes and hippocampal neurons. The **working hypotheses** are that (1) highly ordered arrays of RyR2 clusters are the exclusive Ca2+ release sites in the interior of ventricular myocytes; (2) the distribution of functional RyR2 CRUs at the periphery of the cell is distinct from arrangements in the interior of ventricular cardiomyocytes and (3) expression of CPVT-linked RyR2 mutation impairs hippocampus Ca2+ signalling, LTP formation and cognitive abilities in knock-in mice. To test these hypotheses, three specific aims are outlined as follows.

1.7.1 Define the subcellular distribution of RyR2 clusters and Ca2+ release sites in ventricular myocytes

Highly ordered arrays of functional RyR2 clusters are believed to be critical for synchronous Ca2+ release during stable graded ECC in ventricular myocytes. The subcellular distribution of RyR2 has been extensively studied using anti-RyR2 antibodies. However, the use of antibodies

requires fixation and/or permeabilization that renders the sample non-functional. Thus, little is known about the subcellular distribution of functional RyR2 clusters in live cardiomyocytes.

Interestingly, a recent functional study by Lukyanenko et al. (206) reported the detection of a significant portion of RyR2-mediated events (~20%) in between Z-lines. Thus, the existence of functional RyR2 units in the space between z-lines were proposed with an important role in the propagation of Ca2+ transients across individual sarcomeres (207). Controversially, other studies showed that almost all RyR2 clusters are co-localized with α-actinin (59, 208), an established Z-line specific marker. The reason underlying the discrepancy between functional observations and localization studies remains unclear.

To investigate the surprising lack of compatibility I took advantage of the novel knock-in mouse model that expresses GFP-tagged RyR2. I aim to correlate the RyR2 clusters and Ca2+ release sites in live ventricular myocytes. To achieve this goal, I first plan to define the exact subcellular distribution of RyR2 clusters in ventricular myocytes. Therefore, I determined the subcellular distribution of GFP-RyR2 clusters in live and fixed cells isolated from our KI mice using confocal imaging. This will show whether fixation affects the distribution of RyR2 clusters in cardiomyocytes. I further co-localized GFP-RyR2 signals with intracellular landmarks, namely i) mitochondria; ii) transverse-axial-tubular system and iii) the Z-line residual protein alpha-actinin. This will provide information to define the exact location of GFP-RyR2 clusters in subcellular context. Secondly, I synchronously recorded Ca2+ sparks and GFP-RyR2 clusters in live ventricular myocytes. This will reveal the position of CRUs in correlation with the location of RyR2 clusters and help to explain discrepancy in former functional and localization studies.

1.7.2 Determine the distribution of functional RyR2 units at the periphery of live ventricular myocytes

The distribution of functional RyR2 units at the periphery of ventricular myocytes remains unknown. Localization studies in fixed and permeabilized cardiomyocytes suggested different patterns of RyR2 clusters at the periphery and the interior. Three different distributions of RyR2 arrangements have been observed: (i) irregular/disordered, (ii) double rows, and (iii) single rows. Evidence has suggested that functional RyR2 clusters are present near the membrane (209–211). However, whether all RyR2 clusters in these distinct patterns function similarly to those in the interior is unclear.

To address this issue, I used the GFP-RyR2 KI mouse model to study the distribution and function of RyR2 clusters near the sarcolemma in living ventricular myocytes. Using confocal and TIRF imaging, I aim to determine the exact localization of GFP-RyR2 nearest to the sarcolemma. To explore the possibility that the observations of different patterns of RyR2 occurs due to protein trafficking effects, I will further record time series to evaluate the dynamics of RyR2 clusters. Additionally, functional correlation of Ca2+ release events and the observed RyR2 clusters will be provided via fluorescence monitoring of Ca2+ indicator loading ventricular myocytes. This will reveal whether all RyR2 clusters in the patterns nearest to the sarcolemma operate with similarly Ca2+ release properties to those in the interior.

1.7.3 Investigate the mechanism of cognitive disability associated with CPVT – linked RyR2 mutations

A number of studies suggested a link between CPVT RyR2 mutations and cognitive disability. However, the mechanism by which CPVT RyR2 mutations affect learning and

memory is unknown. To address this question, I aim to determine the precise subcellular localization and specific roles of the RyR2 isoform in different compartments (presynaptic terminals, dendritic spines, dendritic shafts, and the soma) in neurons in regions associated with cognitive functions, such as the hippocampus. I will use brain slices from the GFP-RyR2 knock-in mice and an anti-GFP probe that I specifically generated to unambiguously localize GFP-RyR2 in hippocampal neurons. This will allow us to reveal the exact subcellular location of RyR2 clusters via confocal and SIM imaging. I further co-localized GFP-RyR2 signals with neuronal markers for presynaptic terminals, dendritic spines and dendritic shafts. This will provide context to define the exact location of GFP-RyR2 clusters at a subcellular level.

With this information, I further aim to assess the impact of a CPVT-linked RyR2 mutation R4496C on presynaptic and postsynaptic function in hippocampal CA1 neurons in brain slices from the RyR2 R4496C mutant mice. I will compare the capability to produce paired pulse facilitation and long-term potentiation, the molecular mechanism underlying learning and memory. Additionally, I will assess Ca2+ signaling in hippocampal neurons in intact brain slices. I will further evaluate whether the behavior of RyR2 R4496C mutant mice is different from WT littermates. Lastly, I aim to determine neuronal activity in hippocampal neurons to see whether there are differences.

Overall, this will reveal novel insights into the impact of CPVT-associated RyR2-R4496C mutation on cognitive function.

CHAPTER 2 DISTRIBUTION AND FUNCTION OF CARDIAC RYANODINE RECEPTOR CLUSTERS IN LIVE VENTRICULAR MYOCYTES

2.1 INTRODUCTION

Excitation-contraction coupling in cardiac muscle cells occurs via a mechanism known as Ca2+-induced Ca2+ release (84, 320). In this process, depolarization of the transverse tubular membrane activates the voltage-dependent L-type Ca2+ channel, resulting in a small influx of Ca2+ into the cytosol. This Ca2+ entry then triggers a large Ca2+release from the sarcoplasmic reticulum (SR)2 by opening the cardiac ryanodine receptor (RyR2) channel located in the SR membrane and, subsequently, muscle contraction (84, 320). Hence, RyR2 acts as a Ca2+ amplifier during Ca2+-induced Ca2+release. A potential problem with this Ca2+ amplification process is that Ca2+ efflux from the SR could further activate RyR2 and Ca2+ release. Such positive feedback would lead to regenerative Ca2+ release. However, Ca2+ release from the SR in normal heart cells is graded and tightly controlled (128, 143, 144, 148, 203, 321, 322). How heart cells are able to achieve graded and stable amplification of Ca2+ influx via the positive feedback process of Ca2+-induced Ca2+ release is not completely understood.

The distribution of RyR2 in cardiomyocytes is believed to play a critical role in achieving the gradation and stability of Ca2+-induced Ca2+ release. RyR2 proteins are organized in the form of clusters in cardiomyocytes. These RyR2 clusters represent the elementary Ca2+ release units (53, 129, 143–145, 321, 323, 324). Activation of these elementary Ca2+release units (RyR2 clusters) produces elementary Ca2+ release events, known as Ca2+ sparks (128–131, 146). The spatiotemporal summation of these Ca2+ sparks is thought to underlie the global Ca2+ transients

(131). The gradation of SR Ca2+ release in response to Ca2+ influx could then be achieved by recruiting various numbers of Ca2+ release units (128–130, 146, 325).

The distribution and organization of RyR2s in cardiomyocytes have been extensively investigated (58, 153, 211, 214, 326). It has been shown that RyR2 clusters are associated with transverse tubular membranes located along z-lines (53, 153, 154, 205). Interestingly, a significant portion of RyR2 clusters (~20%) was found to be located between z-lines (206). These RyR2 clusters located in the middle of the sarcomere are thought to play an important role in the propagation of Ca2+ transients (207). However, other studies showed that nearly all RyR2 clusters are co-localized with α-actinin (59, 208), a marker of the z-line. The reason for this discrepancy is unclear. It is important to note that nearly all studies on RyR2 distribution in cardiomyocytes were carried out in fixed and/or permeabilized cells or tissues using immunostaining with anti-RyR2 antibodies. It is unclear whether cell or tissue fixation and/or permeabilization would alter the distribution and organization of RyR2. It is also uncertain whether the anti-RyR2 antibodies used recognize RyR2 unrelated epitopes. These concerns warrant the need to study the distribution of RyR2 directly in a more physiological setting.

Information on the distribution of functional groups of RyR2s is also lacking. It is unclear whether the distribution of functional groups of RyR2s correlates with that of RyR2 clusters detected in fixed, permeabilized cardiac cells. Using mitochondria as markers, Lukyanenko *et al.* (206) showed that most of the Ca2+ sparks (functional groups of RyR2s) were detected in regions between mitochondria, where z-lines are thought to be located. However, a significant portion of Ca2+ sparks was also detected in regions near the middle of mitochondria. These indirect studies suggest that functional groups of RyR2s may exist between z-lines in the middle

of sarcomere. However, a direct correlation between Ca2+ sparks and RyR2 clusters has yet to be demonstrated.

To circumvent these potential problems with respect to antibody specificities or sample handling, we generated a knock-in mouse model expressing a GFP-tagged RyR2. Using confocal fluorescence imaging, we directly determined the distribution of RyR2 clusters in live cardiomyocytes isolated from the GFP-RyR2 mice. We found that nearly all GFP-RyR2 clusters were localized to the z-line zone and associated with transverse, but not longitudinal, tubules. On the other hand, GFP-RyR2 clusters were not co-localized with mitochondria, although they are in close proximity. Co-detection of GFP-RyR2 clusters and Ca2+ sparks revealed that Ca2+ sparks originate exclusively from RyR2 clusters. These studies shed novel insights into the distribution of RyR2 clusters and its functional correlation in living cardiomyocytes.

2.2 EXPERIMENTAL PROCEDURE

2.2.1 Generation of a knock-in mouse model expressing a GFP-tagged RyR2

A genomic DNA phage clone containing part of the mouse cardiac ryanodine receptor gene was isolated from the lambda mouse 129-SV/J genomic DNA library (Stratagene) and used to construct the RyR2 GFP knock-in targeting vector. This genomic DNA fragment (~15 kb) was released from the lambda vector by NotI and subcloned into pBluescript to form the RyR2 genomic DNA plasmid. PCR-based site-directed mutagenesis was performed to generate a 660-bp DNA fragment containing the AscI site inserted after residue Thr-1366 using the RyR2 genomic DNA plasmid as a template. The GFP flanked by glycine-rich linkers was inserted into this fragment via the AscI site. A 5.7-kb NotI-BamHI fragment was then subcloned into the targeting vector that contains a neomycin selection cassette flanked by FRT sites using NotI and BamHI to form the 5′ arm. A 5.4-kb SalI-XhoI fragment was inserted into the targeting vector to form the 3′ arm. All PCR fragments used for constructing the targeting vector were confirmed by DNA sequencing. The targeting vector was linearized with NotI and subsequently electroporated into R1 embryonic stem (ES) cells. G418-resistant ES clones were screened for homologous recombination by Southern blotting using an external probe. Briefly, genomic DNA was extracted from G418-resistant ES cell clones. ES cell DNA was digested using NcoI, separated on a 0.8% (w/v) agarose gel, and subsequently blotted onto a nitrocellulose membrane. A DNA probe (~700 bp) was generated by PCR from mouse genomic DNA using the specific primers 5′-GAGGAAGTACAGATCAGTTCTTA-3′ (forward) and 5′-AGCCTAGAGA CTTTCCCTTTCAC-3′ (reverse). The PCR product was subsequently radiolabeled using [^{32}P]dCTP by random priming (Invitrogen). DNA blots were hybridized with the radiolabeled

probe and visualized by autoradiography. Eight positive homologous recombinants were detected of 780 ES cell clones, two of which were microinjected into blastocysts from C57BL/6J mice to generate male chimeras. Male chimeras were bred with female 129sve mice to generate germ line-transmitted heterozygous GFP-RyR2-neo knock-in mice. GFP-RyR2-neo male mice were bred with female mice that express Flp recombinase to remove the selectable marker (the neomycin-resistant gene, neo). The genotypes from F1 generation without neo were determined by PCR using DNA from tail biopsy specimens using the DNeasy tissue kit from Qiagen and the DNA primers PRIMER1 (5′-ATATCACTCCTAGACATACCCTCA-3′, forward), PRIMER2 (5′-CTTCAGCTCGATGCGGTTCAC-3′, forward) and PRIMER3 (5′-AGACCAGACAAGCCATCACACTA-3′, reverse).

2.2.2 Isolation and fixation of ventricular myocytes

Ventricular myocytes were isolated using retrograde aortic perfusion as described previously (266). Isolated cells were kept at room temperature in Krebs-Ringers-HEPES (KRH) buffer (125 mM NaCl, 12.5 mM KCl, 25 mM HEPES, 6 mM glucose, and 1.2 mMMgCl2, pH 7.4) containing 20 mM taurine, 20 mM 2,3-butanedione monoxime, 5 mg/ml albumin, and 0.5–1 mM free Ca2+ until use. A portion of the isolated cells from the same mouse heart was fixed by 4% (w/v) paraformaldehyde in Ca2+ free KRH solution for 10 min at room temperature. Excess paraformaldehyde was removed by washing with KRH containing glycine (0.5 M). The fixed cells were kept in KRH buffer and stored at 4 °C until use.

2.2.3 Staining of live cardiomyocytes

Live ventricular myocytes were stained with 3 μM di-8-ANEPPS (Invitrogen) or 2 μM MitoTracker Red-FM (Invitrogen) in KRH buffer containing 0.5–1 mM Ca2+ for 5–20 min at room temperature. The stained cells were washed three times for 5 min each with KRH solution containing 0.5–1 mM Ca2+ and kept at room temperature until use.

2.2.4 Cell permeabilization

Fixed ventricular myocytes were permeabilized with 1% (v/v) Triton (EMD Millipore) in KRH solution for 1 h. The permeabilized cells were washed three times and blocked with BlockAid blocking solution (Molecular Probes) overnight at 4 °C. Myocytes were washed again and incubated with primary monoclonal anti-α-actinin antibody (A7811; Sigma) diluted to 250 ng/ml in blocking solution for 1 h at room temperature. Cells were then washed three times for 10 min each in blocking solution before incubated with a secondary antibody (4 ng/ml), Alexa Fluor 633-conjugated anti-mouse goat IgG (H+L) (Molecular Probes), for 45 min at room temperature. After further washes with KRH buffer three times for 10 min each, cells were kept in Ca2+ free KRH at 4 °C until imaging.

2.2.5 Single cell imaging of GFP-RyR2 clusters, mitochondria, transverse/longitudinal tubules, and α-actinin in isolated ventricular myocytes

All imaging of live isolated ventricular myocytes was performed within 4–6 h after cell isolation. Isolated myocytes were placed onto laminin-coated micro glass coverslips (VWR, no.

1). After 5–10 min, unattached myocytes were gently removed via KRH buffer exchange (0.5–1 mM Ca2+). Cells were then staged onto the microscope for confocal imaging. Cell integrity was tested by pacing at 2–3 Hz. Only cardiomyocytes that followed electrical pacing were selected for subsequent live cell imaging. Fixed and permeabilized cardiomyocytes were transferred onto non-coated micro glass coverslips (VWR, no. 1) and allowed to settle to the coverslip for at least 10 min before imaging. Images were acquired with an inverted Nikon A1R scanning confocal microscope system equipped with a Nikon 60×/numerical aperture 1.2 Plan-Apochromat water immersion objective and selective excitation and emission filters. Excitation light was provided by argon (488 nm; Coherent Sapphire), yellow diode (561 nm; Coherent Sapphire), and red diode (635 nm; Coherent Sapphire) lasers to detect GFP (maximum excitation of 488 nm and maximum emission of 510 nm), di-8-ANEPPS (maximum excitation of 488 nm and maximum emission of 630 nm), MitoTracker Red-FM (maximum excitation of 581 nm and maximum emission of 644 nm), and Alexa Fluor 633-conjugated secondary antibody (maximum excitation of 630 nm and maximum emission of 650 nm). Basic image processing and spectral fluorescence unmixing for co-detection and analysis of GFP and di-8-ANEPPS fluorescence signals were performed using the NIS Elements AR 4.13 software (Nikon).

2.2.6 Line scanning confocal imaging of individual Ca2+ sparks in GFP-RyR2 ventricular myocytes

Ventricular myocytes isolated from GFP-RyR2 mice were loaded with Rhod-2 AM (5 μM; Invitrogen) for 20 min at room temperature. The cells were then washed with KRH buffer three times and transferred onto laminin-coated cover glasses (VWR, no. 1). After mounted onto the detection stage, they were superfused with KRH solution containing 1.8–2 mM free Ca2+ at

35–37 ℃. Confocal line scan Ca2+ imaging was performed to record individual Ca2+ release events using the Nikon A1R confocal microscope system equipped with a Nikon 60×/numerical aperture 1.2 Plan-Apochromat water immersion objective. Images of Ca2+ release events were acquired at a sampling rate of 1.8–1.9 ms/line along the longitudinal axis of the myocytes in the line scan mode.

2.2.7 Monitoring mitochondrial and cytosolic Ca2+ in ventricular myocytes isolated from GFP-RyR2 knock-in mice

Ventricular myocytes were loaded with Rhod-2 AM (2.5–5.0 μM) at 4 °C for 75 min to facilitate loading of Rhod-2 AM to mitochondria as previously described (327–329). Cytosolic Rhod-2 dye was removed through incubation at 37 °C for 3–4 h until a clear mitochondrial pattern of Rhod-2 labeling was observed. The cells were then superfused with KRH buffer containing 3 mM extracellular Ca2+ and paced at 3 Hz for 30–60 s. The fluorescence signals of GFP and Rhod-2 were co-detected using confocal fluorescence microscopy. For monitoring cytosolic Ca2+ level, the Rhod-2-loaded cells were incubated with Fluo-4 AM (2.5–5 μM) in KRH buffer containing 0.5 mM Ca2+ for 25 min at room temperature. The Fluo-4/Rhod-2-loaded cells were then washed and superfused with KRH containing 3 mM extracellular Ca2+ and paced again at 3 Hz for 30–60 s. The fluorescence signals of Fluo-4, GFP, and Rhod-2 were co-detected using confocal fluorescence microscopy.

2.2.8 Computer analysis

All image processing and detection methods were implemented using MATLAB (The Mathworks Inc., Boston, MA).

2.2.8.1 RyR2- segmentation

GFP-RyR2 *x-y* images were processed as follows. First, a histogram-based normalization procedure was applied to the images to adjust the range to the background fluorescence level. The normalization ensured that the resulting images were not affected by outlier pixels in the image. Noise filtering and GFP-RyR2 enhancement was performed by applying a two-dimensional convolution using a Gaussian template with a σ value of ~1 μm (twice the diameter of the microscope's point spread function). The resulting convolved image was rescaled to the interval [0.1], and all regions above 0.5 were marked as candidates for GFP-RyR2. Regions smaller than 0.1 μm2 were discarded, and regions containing more than one local maxima (because of noise) were smoothed by means of a median filter until left with a single central maxima. Spatial resolution ranged from 0.03 to 0.1 μm.

2.2.8.2 Cluster size measurement

For each detected GFP-RyR2 cluster, cluster size was defined as the distance at which the intensity decays to 80% of its maximum, measured by Gaussian fits to eight cross-sections of the cluster taken in angular increments of 45°.

2.2.8.3 Automated spark detection and localization

Line scan images were normalized using a time-dependent basal fluorescence level to correct for temporal drifts in the basal fluorescence. Sparks were detected from the normalized images by using a custom watershed segmentation method with a size-dependent stopping rule. Background noise was estimated to filter sparks using amplitude thresholding. Sparks producing

a goodness of fit in the exponential decay fit $\hat{R}2 < 0.85$ were excluded from the analysis. All detected sparks were validated manually. The distance from the spark initiation focus to the nearest RyR2 cluster was measured.

2.2.9 Statistical analysis

All values shown are means ± S.E. unless indicated otherwise. To test for differences between groups, we used unpaired Student's *t* tests (two-tailed). A *p* value of <0.05 was considered to be statistically significant.

2.3 RESULTS

2.3.1 Generation of a knock-in mouse model expressing a GFP-tagged RyR2

To study the distribution of RyR2 clusters and the correlation of their distribution to function in living cells, we generated a knock-in mouse model expressing a GFP-tagged RyR2 (Figure 7*A*). The GFP was inserted into RyR2 after residue Thr-1366 (Figure 7*B*). To minimize potential steric hindrance, the GFP sequence was flanked by 10-residue Gly-rich linkers on both sides of the GFP (Figure 7*B*). The three-dimensional location of the inserted GFP was mapped previously to subdomain 6 in the "clamp" region of the three-dimensional structure of RyR2 (Figure 7*C*) (40). The GFP-tagged RyR2 formed caffeine- and ryanodine-sensitive functional Ca2+ release channel (40), indicating that the insertion of GFP did not grossly alter the structure and function of the RyR2 channel. We also did not observe gross defects in the GFP-tagged RyR2 mice.

2.3.1.1 Distribution of RyR2 clusters in live and fixed ventricular myocytes

To determine the distribution of RyR2 in living cells, we isolated ventricular myocytes from GFP-RyR2 mouse hearts in the presence of low concentrations of Ca2+ (0.5–1.5 mM) to minimize spontaneous contraction. The GFP fluorescence signal was then detected using a confocal microscope in a line scan mode. As shown in Figure 8, GFP-RyR2s were clearly detected as highly organized discrete clusters in the interior and at the periphery of the cell (Figure 8). A majority of these clusters were distributed in highly ordered transverse rows with an average spacing of 1.88 μm (Figure 8*a* and Table 1). Some of the GFP-RyR2 clusters were dislocated, particularly within or near the perinuclear region (Figure 8*b*) or in other regions of the cell (Figure 8*c*). These observations are consistent with those reported previously (58, 153, 211, 214, 326). We also detected intercalated GFP-RyR2 clusters at the periphery of isolated live

ventricular myocytes (Figure 8*d*), similar to those described previously in fixed cardiac cells (58, 214).

To ascertain whether the fixation procedure commonly used in immunostaining studies of RyR2 distribution in cardiac cells would alter the distribution of RyR2 clusters, we repeated the confocal imaging studies on isolated, fixed ventricular myocytes from the GFP-RyR2 mouse heart (Figure 9). The overall distribution, distance between rows of GFP-RyR2 clusters, the nearest distance, and the GFP-RyR2 cluster size in live and fixed ventricular myocytes were found to be similar (Table 1). Thus, fixation does not significantly alter the distribution of RyR2 clusters in ventricular myocytes. It should be noted that no green clusters were detected in wild type ventricular myocytes (not shown).

Table 1 GFP-Ryr2 cluster distribution in live and fixed ventricular myocytes

The properties of GFP-RyR2 cluster distribution were determined from confocal fluorescence images of live and fixed ventricular cardiomyocytes isolated from the same GFP-tagged RyR2 knock-in mice. The data shown are means ± S.E.

	Longitudinal distance between GFP-RyR2 cluster rows	**Mean nearest neighbor**	**Mean cluster radius**	**Cluster density**	**No. of cells**
	μ*m*	μ*m*	μ*m*	*No. per* μ*m2*	
Live cells	1.880 ± 0.172	0.759 ± 0.029	0.383 ± 0.049	0.294 ± 0.054	10
Fixed cells	1.855 ± 0.096	0.771 ± 0.023	0.394 ± 0.052	0.314 ± 0.063	11

2.3.1.2 Location of RyR2 clusters in the z-line zone in ventricular myocytes

It has been proposed that a significant portion (~20%) of RyR2 clusters is associated with the network SR and that these network SR-associated RyR2 clusters are located between z-lines (206). To directly determine the distribution of RyR2 clusters in relation to the z-line, we marked the z-line zone in fixed ventricular myocytes isolated from the GFP-RyR2 mouse heart by using an anti-α-actinin antibody, a commonly used marker for z-lines. Staining with the anti-α-actinin antibody revealed the z-line zone in a typical striated pattern (Figure 10, *A* and *a*). Interestingly, regions with dislocated or coiled z-lines were frequently detected (Figure 10, *A* and *b*), similar to those reported previously (59, 208). The distribution of GFP-RyR2 clusters in the same cell is shown in Figure 10*B*. The merged image of α-actinin staining and GFP-RyR2 signals is shown in Figure 10*C*. Remarkably, nearly all GFP-RyR2 clusters are localized within the z-line bands of α-actinin staining (Figure 10, *C* and *a*), even in regions with dislocated or coiled z-lines (Figure 10 *C* and *b*). There are only a few GFP-RyR2 clusters (~0.6%) that were detected between z-lines. Therefore, these observations suggest that RyR2 clusters nearly strictly follow the z-lines.

2.3.1.3 Co-localization of RyR2 clusters with tubular system in ventricular myocytes

Previous immunostaining studies showed that RyR2 clusters were co-localized with both transverse and longitudinal tubules in fixed cardiomyocytes (154, 206, 215). To determine whether GFP-RyR2 clusters are co-localized with transverse and/or longitudinal tubules in living cells, we labeled the tubular-system in ventricular myocytes isolated from the GFP-RyR2 mouse heart with the di-8-ANEPPS dye. We then simultaneously detected the GFP and di-8-ANEPPS signals using confocal spectral imaging. As shown in Figure 11*A*, the di-8-ANEPPS dye labeled

the sarcolemma, and the transverse (Figure 11*A*, *panel a*) and longitudinal tubules (Figure 11*A*, *boxes b* and *c*), similar to those reported previously (154, 208, 215, 330). Figure 11*B* shows the distribution of GFP-RyR2 clusters. Merging the GFP signals with those of di-8-ANEPPS revealed that nearly all the GFP-RyR2 clusters were co-localized with the transverse tubules (Figure 11C, *boxes a* and *b*). Only few GFP-RyR2 clusters (<0.1%) were associated with the longitudinal tubules in a given confocal image of an entire cell (Figure 11*C, box c*), similar to that described previously (208, 215). Therefore, RyR2 clusters are primarily co-localized with transverse, but not longitudinal tubules.

2.3.1.4 Relative distribution of RyR2 clusters and mitochondria in ventricular myocytes

It has been suggested that there is a tight Ca2+ transmission between mitochondria and SR via RyR2s (331). It is of interest then to examine the relative distribution of RyR2 clusters and mitochondria. To this end, we labeled the mitochondria using the MitoTracker Red dye in isolated ventricular myocytes from the GFP-RyR2 mutant heart. The GFP and MitoTracker Red signals were then simultaneously detected using confocal line scan imaging. The distribution of mitochondria and GFP-RyR2 clusters is shown in Figure 12 (*A* and *B*, respectively). Interestingly, GFP-RyR2 clusters were located in regions between mitochondria (Figure 12*C*, *box a*). Some GFP clusters were located in regions without mitochondria (Figure 12*C*, *boxes b* and *c*). These results suggest that RyR2 clusters are not co-localized with mitochondria, although they are in close proximity with each other.

2.3.1.5 Co-localization of GFP-RyR2 clusters and Ca2+ sparks in ventricular myocytes

Previous studies showed that Ca2+ sparks primarily occurred along z-lines where RyR2 clusters

were thought to be located (205, 332), suggesting that Ca2+ sparks originate from RyR2 clusters. To directly correlate the occurrence of Ca2+ sparks and the location of RyR2 clusters, we simultaneously recorded GFP and Ca2+ spark signals in ventricular myocytes isolated from GFP-RyR2 mouse hearts using confocal line scan imaging. As shown in Figure 13, GFP-RyR2 clusters were depicted as *green bands* in the line scan images (*middle green panel*). Spontaneous Ca2+ sparks were clearly detected as brief, localized small Ca2+ transients (*top panel*). Close examination of the line scan image showed that all Ca2+ sparks were initiated within the *green bands* (*bottom panel*).

To quantify the distribution of Ca2+ sparks (n = 447) in relation to GFP-RyR2 clusters, we measured the distance from spark initiation sites to the center of the nearest GFP-RyR2 cluster (Figure 14, A and B). We found that 99.6% of Ca2+ sparks were initiated within the mean GFP-RyR2 cluster size. Only 0.4% of Ca2+ sparks (2 of 447) were initiated outside the mean GFP-RyR2 cluster size (Figure 14C). One off center Ca2+ spark was located very close to the boundary of the GFP-RyR2 cluster (Figure 14D, panel a). The other off center Ca2+ spark was detected in a region with an irregular distribution of GFP-RyR2 clusters (Figure 14D, panel b). Hence, it is possible that this single off center Ca2+ spark may come from an out of focus, misregistered GFP-RyR2 cluster. Therefore, simultaneous detection of GFP-RyR2 clusters and Ca2+ sparks reveals that Ca2+ sparks exclusively originate from the RyR2 clusters. Because nearly all GFP-RyR2 clusters are localized along z-lines (Figure 10), the lack of Ca2+ sparks between GFP-RyR2 clusters indicates that Ca2+ sparks are unlikely to occur between z-lines.

2.3.1.6 Influence of Ca2+ release from GFP-RyR2 clusters on mitochondrial Ca2+ level in ventricular myocytes

Considering that GFP-RyR2 clusters are not co-localized with mitochondria (Figure 12), it is of interest to determine whether Ca2+ release from GFP-RyR2 clusters could influence the Ca2+ level in mitochondria. To monitor mitochondrial Ca2+ level, we loaded the GFP-RyR2 ventricular myocytes with Rhod-2 AM using the protocol of Trollinger *et al.*(328) with cold loading followed by warm incubation. As shown in Figure 15*A*, we observed a pattern of Rhod-2 loading similar to that of MitoTracker Red staining (Figure 12), suggesting Rhod-2 loading to mitochondria as reported previously (327–329). Like the relative distribution of GFP-RyR2 clusters and MitoTracker Red staining (Figure 12), GFP-RyR2 clusters are also not co-localized with Rhod-2 labeling (Figure 15, *B* and *C*). To promote the occurrence of Ca2+ sparks, we electrically stimulated the GFP-RyR2 ventricular myocytes at 3 Hz in the presence of elevated extracellular Ca2+ (3 mM) and monitored mitochondrial Ca2+ level during and after the cessation of stimulation. We observed beat to beat mitochondrial Ca2+ transients during stimulation (Figure 15*D–F*). However, after cessation of stimulation, we could not detect significant local, transient elevations of Ca2+ or Ca2+ sparks in regions corresponding to either mitochondria or GFP-RyR2 clusters (Figure 15*D*). On the other hand, Ca2+ sparks were readily detected after loading the cells with Fluo-4 AM (Figure 15*G*). These observations suggest that Ca2+ release from GFP-RyR2 clusters in the form of Ca2+ sparks does not seem to substantially influence mitochondrial Ca2+ level.

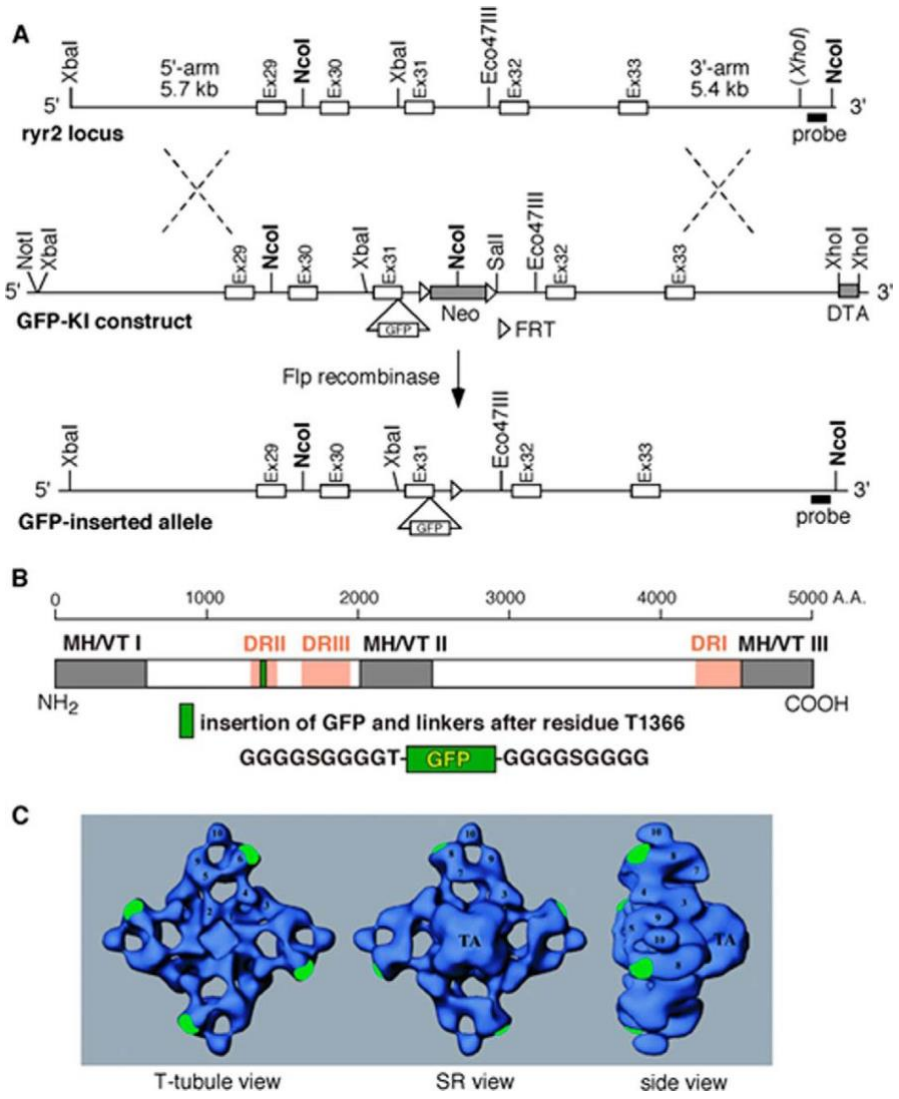

Figure 7 Generation of GFP-tagged RyR2 knock-in mice.

A, in-frame insertion of GFP into exon 31 of RyR2 was achieved via homologous recombination as illustrated. B, a linear structure of RyR2 showing disease hot spot regions (gray boxes; MH/VT I–III) harboring mutations associated with malignant hypothermia (MH) or ventricular tachyarrhythmias (VT). Divergent regions in RyR (pink boxes; DR I-III) are also indicated. GFP flanked by glycine-rich linkers was inserted into RyR2 after residue Thr-1366. C, localization of the inserted GFP to the "clamp region" in the cytosolic assembly of the three-dimensional structure of RyR, viewing from the T-tubule (left), SR (center), and the side of the channel (right) (used with permission from Hiess et al, ***J Biol Chem*****,** 2015 (333)).

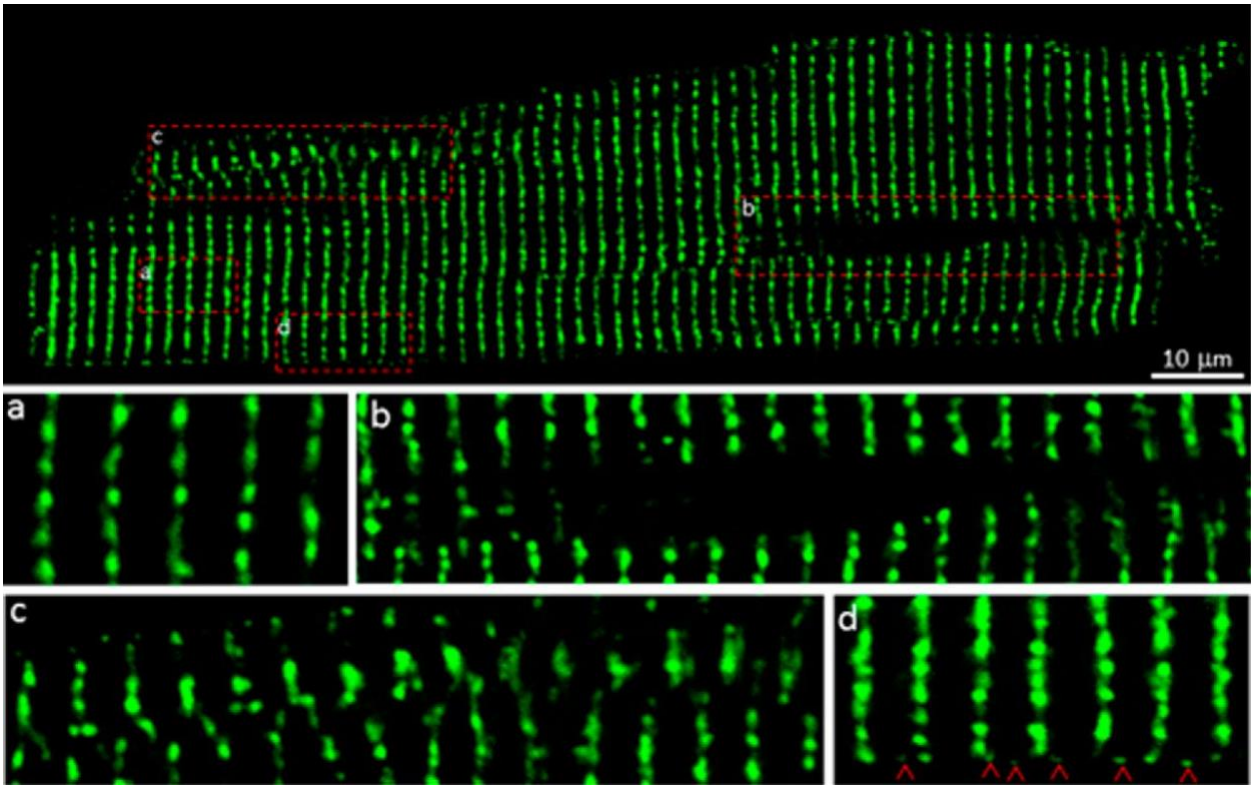

Figure 8 Distribution of GFP-RyR2 clusters in live ventricular myocytes.

A representative confocal fluorescence image of a live ventricular myocyte (*n* = 109) isolated from GFP-RyR2 knock-in mice (*top panel*) shows the distribution of GFP-RyR2 clusters. *Panels a–d* show organization details in different regions: the cell interior (*panel a*), the perinuclear region (*panel b*), regions with disordered cluster distributions (*panel c*), and the subsarcolemmal region (*panel d*). *Red arrowheads* indicate intercalated GFP-RyR2 clusters at the periphery of the cell (used with permission from Hiess et al, ***J Biol Chem***, 2015 (333)).

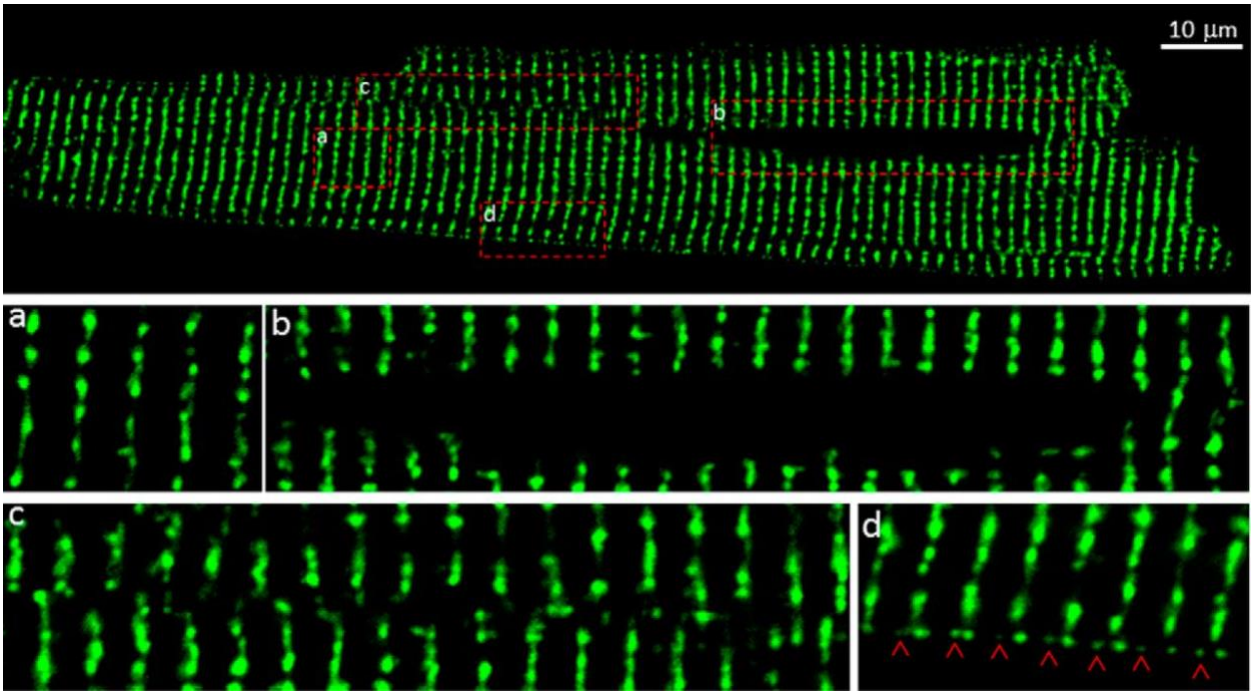

Figure 9 Distribution of GFP-RyR2 clusters in fixed ventricular myocytes.

A representative confocal fluorescence image of a fixed ventricular myocyte (*n* = 84) isolated from GFP-RyR2 mice (*top panel*) shows the distribution of GFP-RyR2 clusters. *Panels a–d* show GFP-RyR2 cluster distribution in the cell interior (*panel a*), the perinuclear region (*panel b*), regions with disordered clusters (*panel c*), and the subsarcolemmal region (*panel d*). *Red arrowheads* indicate intercalated GFP-RyR2 clusters at the periphery of the cell (used with permission from Hiess et al, ***J Biol Chem***, 2015 (333)).

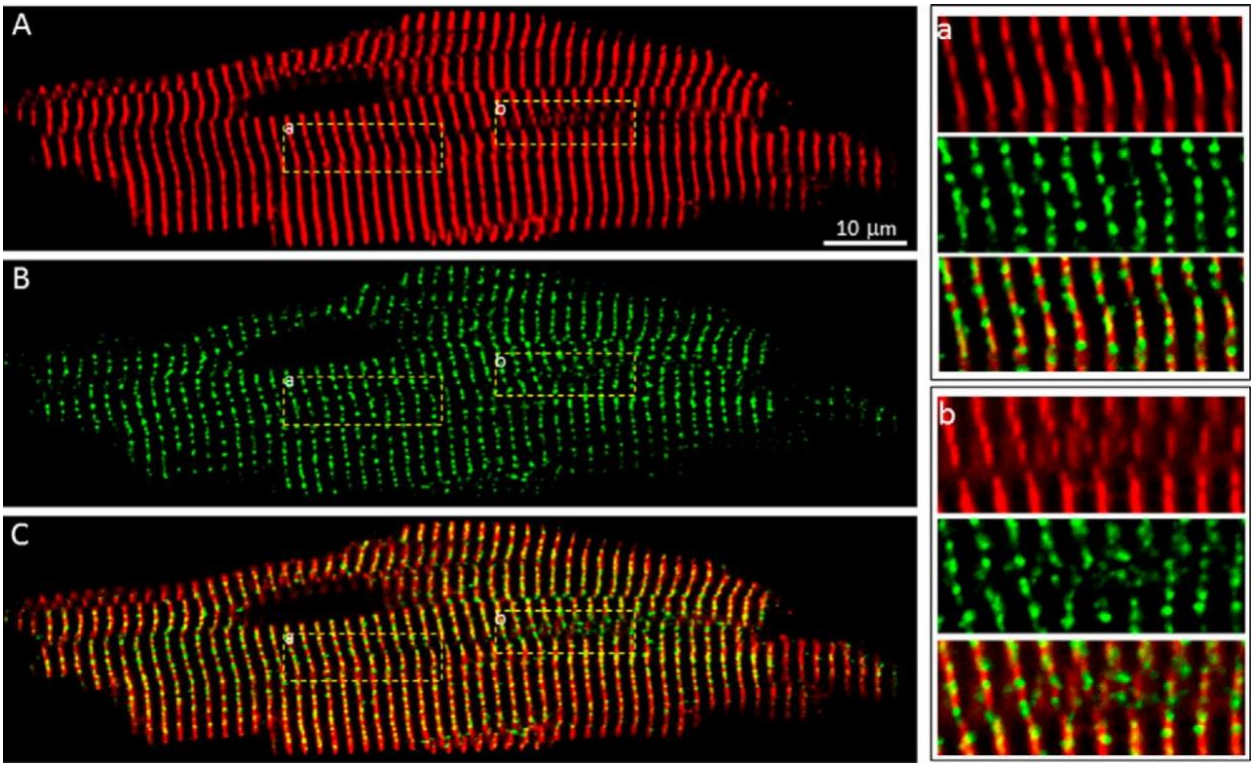

Figure 10 Co-localization of GFP-RyR2 clusters with the z-line zone.

A, a representative confocal fluorescence image of a fixed, permeabilized GFP-RyR2 ventricular myocyte (*n* = 39) stained with anti-α-actinin antibody. *B*, GFP-RyR2 cluster fluorescence signals of the same cell. *C*, merged image of the α-actinin and GFP-RyR2 signals. The panels at the *right* show ordered (*panel a*) and disordered (*panel b*) co-distributions of α-actinin and GFP-RyR2 clusters. (used with permission from Hiess et al, ***J Biol Chem***, 2015 (333)).

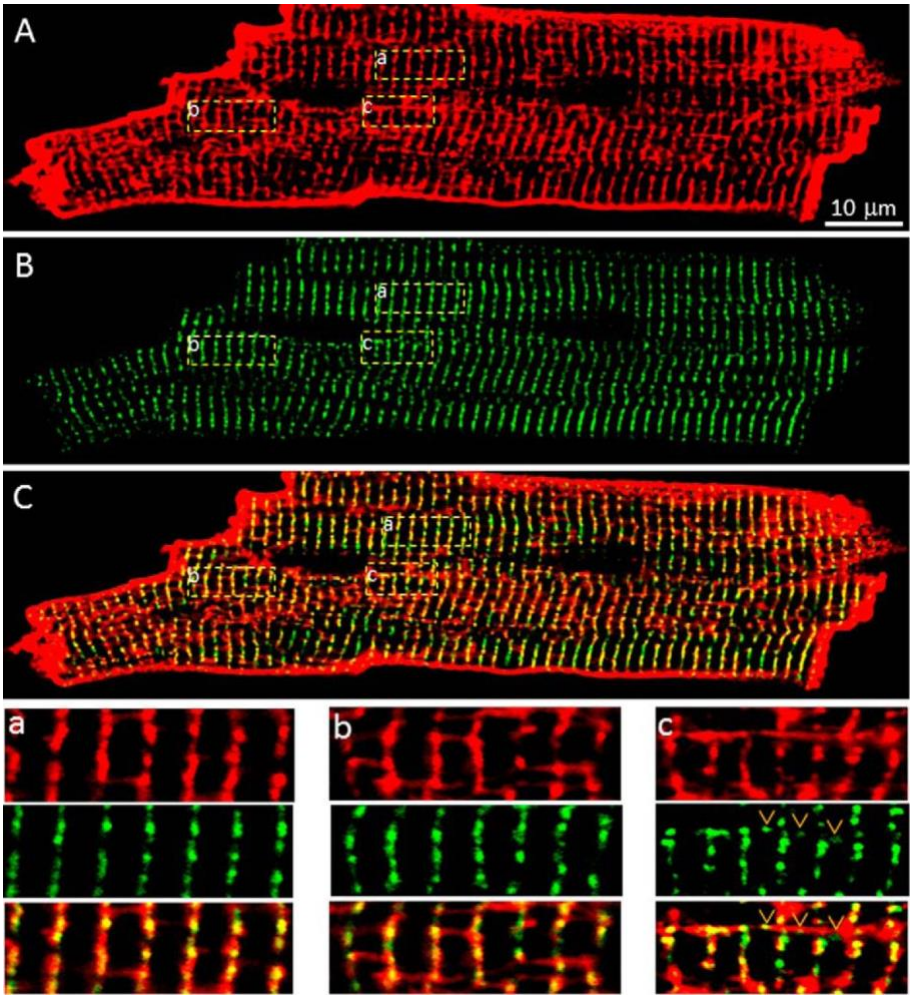

Figure 11 Relative distribution of GFP-RyR2 clusters and the tubular system.

A, the tubular membrane system in live GFP-RyR2 ventricular myocytes (*n* = 27) was labeled with di-8-ANEPPS and visualized with confocal fluorescence imaging. *B*, GFP-RyR2 cluster fluorescence signals of the same cell. *C*, merged image of the di-8-ANEPPS and GFP-RyR2 signals. The panels at the *bottom* show co-localization of GFP-RyR2 clusters with transverse tubules (*panel a*), no co-localization of GFP-RyR2 clusters with longitudinal tubules (*panel b*), and co-localization of a few GFP-RyR2 clusters with longitudinal tubules located near the perinuclear region (*panel c*) (used with permission from Hiess et al, ***J Biol Chem***, 2015 (333)).

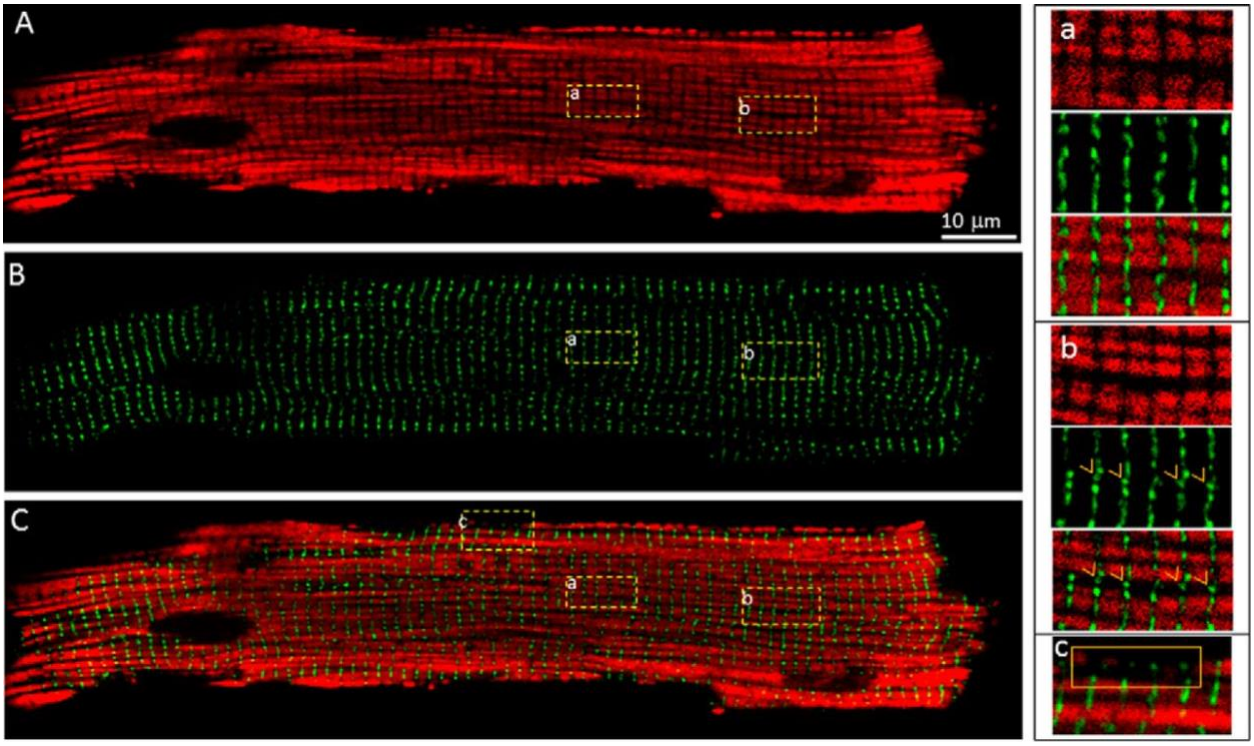

Figure 12 Relative distribution of GFP-RyR2 clusters and mitochondria.

A, mitochondria in live GFP-RyR2 ventricular myocytes (*n* = 24) were labeled with MitoTracker Red-FM and visualized with confocal fluorescence imaging. *B*, GFP-RyR2 cluster fluorescence signals of the same cell. *C*, merged image of the MitoTracker Red-FM and GFP-RyR2 signals. The panels at the *bottom* show GFP-RyR2 clusters located between mitochondria (*panel a*) or in areas that are devoid of mitochondria in the interior (*panel b*) or at the periphery (*panel c*) of the cell (used with permission from Hiess et al, ***J Biol Chem***, 2015 (333)).

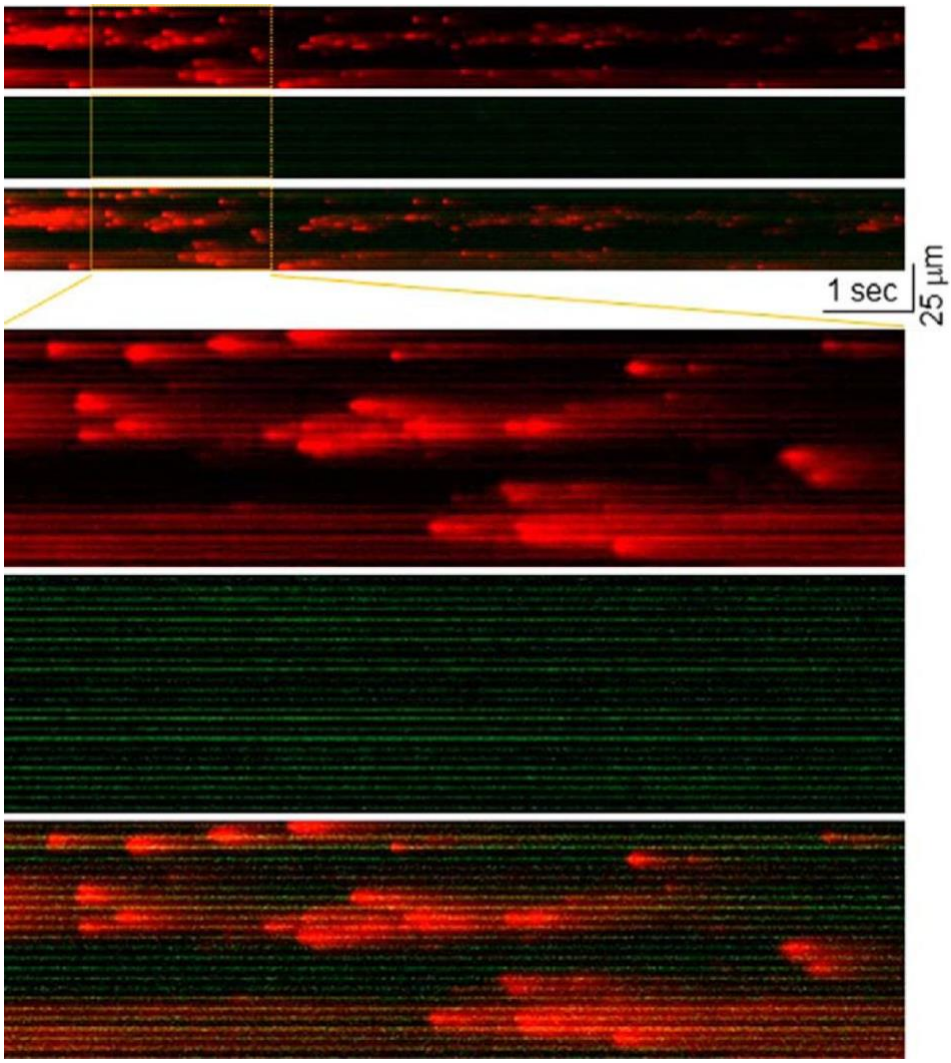

Figure 13 Co-localization of Ca2+ sparks and GFP-RyR2 clusters in live ventricular myocytes.

A, mitochondria in live GFP-RyR2 ventricular myocytes (*n* = 24) were labeled with MitoTracker Red-FM and visualized with confocal fluorescence imaging. *B*, GFP-RyR2 cluster fluorescence signals of the same cell. *C*, merged image of the MitoTracker Red-FM and GFP-RyR2 signals. The panels at the *bottom* show GFP-RyR2 clusters located between mitochondria (*panel a*) or in areas that are devoid of mitochondria in the interior (*panel b*) or at the periphery (*panel c*) of the cell (used with permission from Hiess et al, ***J Biol Chem***, 2015 (333)).

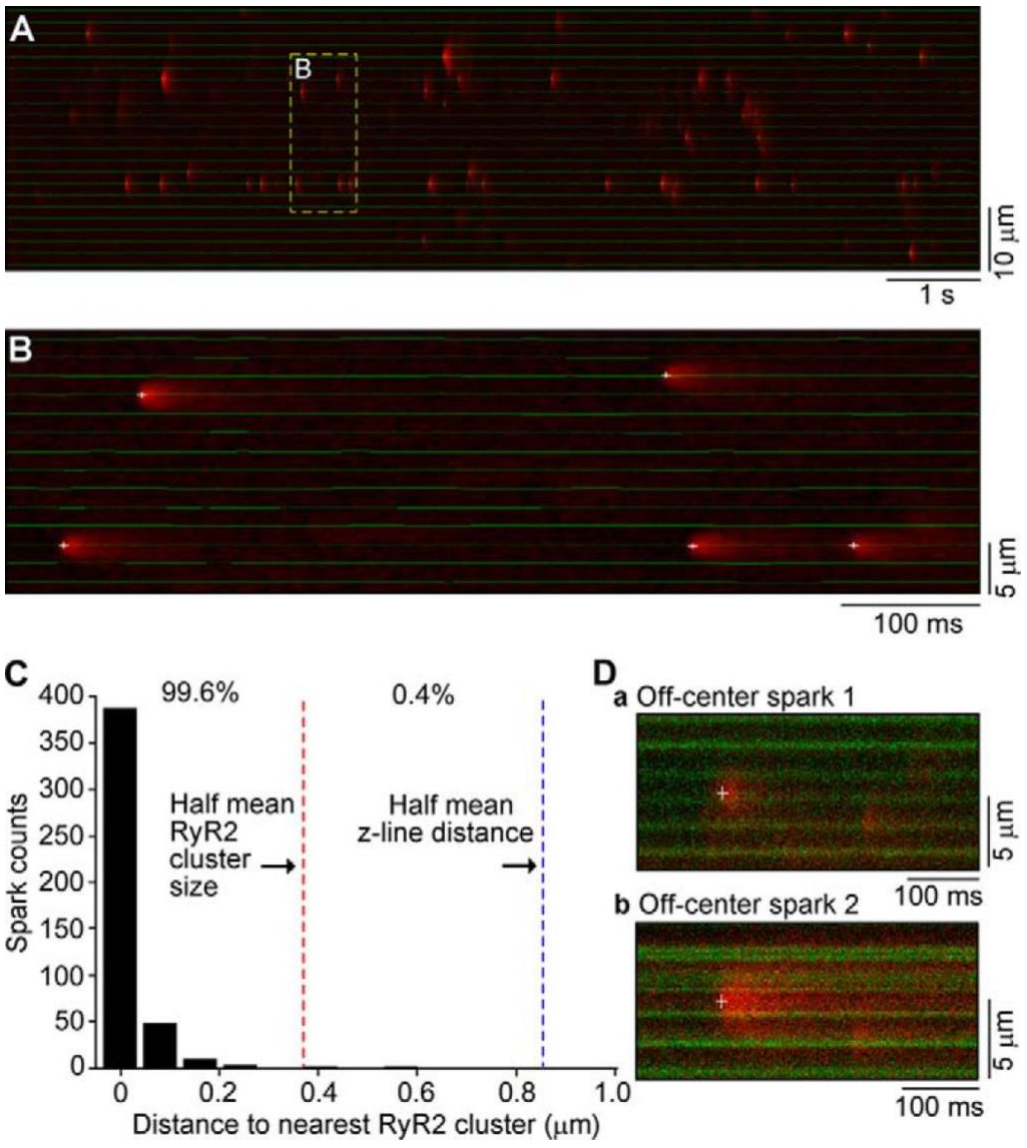

Figure 14 Distribution of Ca2+ sparks in relation to GFP-RyR2 clusters in live ventricular myocytes.

A, a representative image of Ca2+ sparks and GFP-RyR2 clusters recorded simultaneously using confocal line scanning as described in the legend to Figure 13. *B*, automated detection and localization of Ca2+ spark initiation sites (marked by *white crosses*) and centers of GFP-RyR2 clusters (indicated by a *green line*). *C*, distribution of the distance from spark initiation sites to the center of nearest GFP-RyR2 clusters. *D*, line scan images of off-center Ca2+ sparks and GFP-RyR2 clusters shown as *green bands. Crosses* mark the spark initiation sites (used with permission from Hiess et al, ***J Biol Chem***, 2015 (333)).

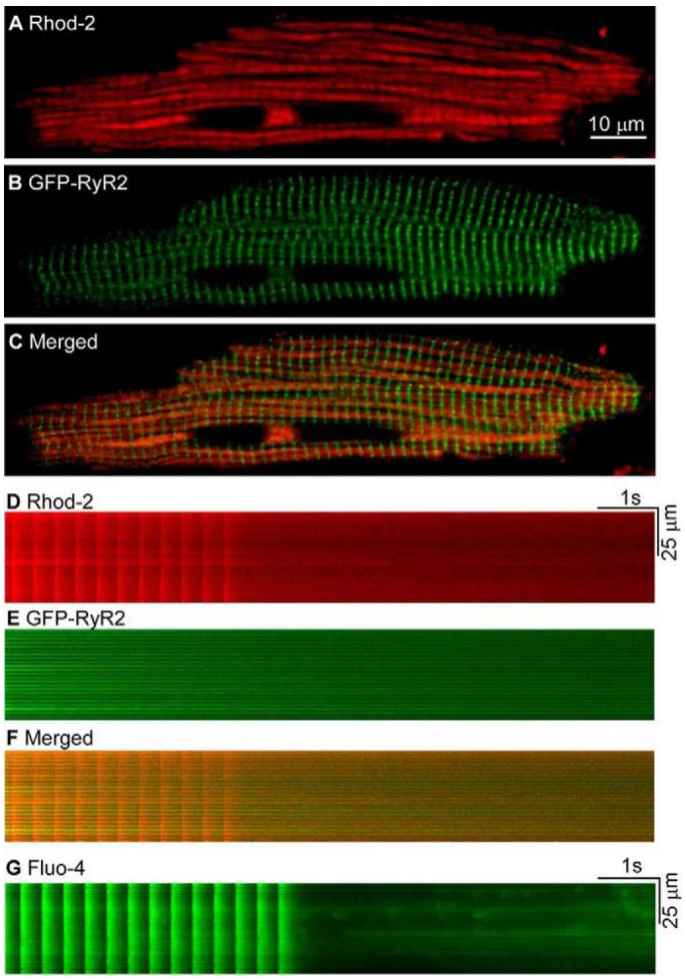

Figure 15 Influence of depolarization-induced Ca2+ release and Ca2+ sparks on mitochondrial Ca2+ level in GFP-RyR2 ventricular myocytes.

A, mitochondria in live GFP-RyR2 ventricular myocytes (*n* = 16) were loaded with Rhod-2 AM and visualized with confocal fluorescence imaging. *B*, GFP-RyR2 cluster fluorescence signals of the same cell as in *A*. *C*, merged image of the Rhod-2 labeling and GFP-RyR2 signals. *D*, fluorescence signals of Rhod-2 loaded GFP-RyR2 ventricular myocytes (*n* = 28) during and after termination of pacing at 3 Hz in the presence of 3 mM extracellular Ca2+. *E*, GFP-RyR2 cluster fluorescence signals of the same cell as in *D*. *F*, merged image of the Rhod-2 and GFP-RyR2 signals. *G*, cytosolic Ca2+ transients and Ca2+ sparks revealed by Fluo-4 in GFP-RyR2 ventricular myocytes (*n* = 16) during and after termination of pacing at 3 Hz in the presence of 3 mM extracellular Ca2+ (used with permission from Hiess et al, ***J Biol Chem***, 2015 (333)).

2.4 DISCUSSION AND CONCLUSION

The present study investigates the distribution of RyR2 clusters and its function correlation in live ventricular myocytes using knock-in mice expressing a GFP-tagged RyR2. Nearly all studies on RyR2 distribution in cardiac cells have been carried out in fixed/permeabilized cells. It is unclear whether fixation and permeabilization could alter the distribution and organization of RyR2. To address this potential concern, we determined and compared the distribution of RyR2 clusters in live and fixed/permeabilized cardiomyocytes from GFP-tagged RyR2 mice. No differences in RyR2 distribution were detected between live and fixed cardiomyocytes. Furthermore, the distribution and organization of GFP-RyR2 clusters in live cardiomyocytes are very similar to those revealed by immunofluorescence labeling using anti-RyR2 antibodies. Thus, the fixation and permeation procedure is unlikely to grossly affect the distribution and organization of RyR2.

Our co-detection of GFP-RyR2 clusters and α-actinin, a commonly used marker for z-lines, revealed that virtually all GFP-RyR2 clusters are localized in the z-line zone. This strict co-localization of RyR2 clusters and the z-line zones has also been observed using fluorescent anti-RyR2 antibodies (59, 208). Different from these observations, Lukyanenko *et al.* (206) reported that a significant portion of RyR2 clusters (~20%) were located between z-lines in the middle of the sarcomere, although no direct co-localization of RyR2 clusters and z-lines was shown in their study. These RyR2 clusters located at sites away from the z-lines were thought to play an important role in the spread of Ca2+ transients along the myofilaments (207). Chen-Izu *et al.* (58) did find some RyR2 clusters located between two rows of RyR2 clusters at the periphery, but not in the interior, of isolated, fixed cardiomyocytes. Similarly, we also observed these intercalated GFP-RyR2 clusters at the periphery of isolated live cardiomyocytes. However, very few GFP-RyR2

clusters were detected between z-lines in the interior of the cell. The reason for this potential discrepancy is unclear. It is interesting to note that the distribution and organization of RyR2 clusters and z-lines are not always in a regular striated pattern in cardiomyocytes. There are regions in which both the RyR2 clusters and z-lines are dislocated. Some of the dislocated RyR2 clusters in one area of the cell appeared to be located between the z-lines of the adjacent area, but they were in fact strictly co-localized with the z-line bands of α-actinin despite their irregular patterns of distribution. Thus, some of the RyR2 clusters that appear to be located in the middle of the sarcomere may have resulted from dislocated or misregistered RyR2 clusters/z-lines.

Ca2+ sparks have been detected mainly along z-lines in cardiomyocytes (205, 332). This is consistent with the distribution of RyR2 clusters along z-lines. However, Lukyanenko *et al.* (206) showed that a significant portion of Ca2+ sparks occurred between z-lines, suggesting that functional groups of RyR2s may exist between z-lines or in the middle of the sarcomere. It is important to point out that in the study of Lukyanenko *et al.*, mitochondria were used as an indirect structural marker for localizing the site of Ca2+ sparks in relation to z-lines. Given the existence of dislocated RyR2 clusters/z-lines, it is unclear whether Ca2+ sparks detected in the middle of the sarcomere truly originated from functional groups of RyR2 resided between z-lines. To determine whether Ca2+ sparks occur between z-lines, we co-detected GFP-RyR2 clusters and Ca2+ sparks simultaneously in GFP-RyR2 cardiomyocytes. We found no Ca2+ sparks occurring between GFP-RyR2 clusters. Ca2+ sparks originated exclusively from GFP-RyR2 clusters. Because nearly all GFP-RyR2 clusters are localized in the z-line zones, it follows that Ca2+ sparks originated from GFP clusters would also be localized in the z-line zones. Thus, our data are inconsistent with the proposition that Ca2+ sparks occur between z-lines.

Ventricular myocytes contain transverse and longitudinal tubules. RyR2 clusters were primarily co-localized with transverse tubules in fixed cardiac cells (208, 215). Consistent with this, we also found that GFP-RyR2 clusters were mainly co-localized with the transverse tubules in live cardiomyocytes. Only a few GFP-RyR2 clusters were co-localized with the longitudinal tubules. There is also no close co-localization between RyR2 clusters and mitochondria in live cardiomyocytes. GFP-RyR2 clusters were detected in areas without mitochondria or were absent in a zone with mitochondria. Nearly all GFP-RyR2 clusters were located in regions that are devoid of mitochondria. In line with the lack of co-localization of GFP-RyR2 clusters and mitochondria, we could not detect significant local, transient elevations of mitochondrial Ca2+ level as a result of Ca2+ sparks from GFP-RyR2 clusters. Taken together, RyR2 clusters appear to follow the z-lines, but not the tubular system or the mitochondria.

In summary, in the present study, we employed a novel GFP-tagged RyR2 mouse model to directly visualize RyR2 clusters in live and fixed ventricular myocytes. The distribution of GFP-RyR2 clusters was similar in live and fixed cardiomyocytes. GFP-RyR2 clusters nearly strictly follow the z-lines and are closely associated with the transverse, but not longitudinal tubules. GFP-RyR2 clusters are located in areas that are devoid of mitochondria. Co-detection of GFP-RyR2 clusters and Ca2+ sparks reveals that Ca2+ sparks exclusively originate from RyR2 clusters. The GFP-RyR2 mice represent a useful model for studying the distribution, dynamics, and structure-function correlation of RyR2 clusters in the heart and other tissues *in vivo*.

CHAPTER 3 DYNAMIC AND IRREGULAR DISTRIBUTION OF CARDIAC RYANODINE RECEPTOR IN THE PERIPHERY OF LIVE VENTRICULAR MYOCYTES

3.1 INTRODUCTION

Cardiac Ryanodine receptors (RyR2s) are intracellular Ca2+ release channels. They reside in the sarcoplasmic reticulum (SR) membrane of myocytes and are crucial for excitation-contraction coupling (ECC)(3, 320). In this process, membrane depolarization leads to a small Ca2+ influx into the cytosol via the voltage-dependent L-type Ca2+ channel. This subsequently triggers a more substantial Ca2+ release from the SR via RyR2s, leading to muscle contraction (3, 320). This RyR2-mediated Ca2+ amplification is known as Ca2+-induced Ca2+ release (CICR). As a positive feedback mechanism, CICR has the inherent potential for unwanted self-regenerative Ca2+ release. However, despite potential regeneration, cardiac ECC is graded and tightly controlled (128, 143, 144, 148, 203, 321, 322). The distribution and function of RyR2s are believed to be crucial for graded CICR during ECC. Stern (143) showed that close proximity of voltage-dependent L-type Ca2+ channels and RyR2s permit graded coupling between Ca2+ influx and Ca2+ release.

RyR2s themselves have been found to arrange into clusters, which are thought to be the elementary functional units (53, 129, 143–145, 321, 323, 324). Ca2+ release from one of these elementary units has been termed Ca2+ spark (128–131, 146). Global Ca2+ events are the spatiotemporal summation of Ca2+ sparks (131). Hence, graded SR Ca2+ release is explicable via the recruitment of variable numbers of RyR2 Ca2+ release units (128–130, 132, 146, 325). The effectiveness of such recruitment would depend on the distribution of the RyR2 Ca2+

release units or RyR2 clusters. The spacing of these RyR2 clusters has also been suggested to be an important determinant of the initiation of spontaneous propagating Ca2+ events (150). Thus, understanding the distribution of RyR2 clusters is important for elucidating the fundamental mechanism of CICR.

The distribution of RyR2s has been extensively studied (53, 56–59, 153, 154, 205, 208, 214, 215). Tightly-organized arrays of RyR2 clusters with single transverse rows have been found in the interior of ventricular myocytes. In contrast, different patterns of RyR2 distribution were observed in the peripheral region. On the one hand, three-dimensional (3D) confocal imaging studies showed an irregular pattern of distribution of RyR2 clusters in the outermost optical confocal z-planes (57, 58, 214). On the other hand, total internal reflection fluorescence (TIRF) imaging (56, 215) reported a `double row` pattern of distribution of RyR2 clusters near the sarcolemmal membrane. The exact reason for this discrepancy is unclear. Confocal imaging collects light from optical segments greater than 500nm (217, 218). Hence, disordered distribution observed by confocal imaging could be due to the capture of signals from multiple layers near, but not only from, the periphery. In contrast, TIRF imaging is used to capture signals close to the cell surface (217, 218). Thus, one would propose that double-rows of RyR2 clusters observed using TIRF may reflect RyR2 distribution in the periphery.

Nearly all studies of the distribution of RyR2 clusters have been carried out in fixed and permeabilized cells/tissues using RyR2 antibody immunostaining (53, 56–59, 153, 154, 205, 208, 214, 215, 326, 334). Hence, sample preparation (fixation and permeabilization) required for immunostaining may change cellular structures, besides rendering the cells/tissues non-functional (152). Furthermore, the specificity and accessibility of the antibodies may be of concern under some experimental conditions. Moreover, it appears that there are 3 patterns of

distribution of RyR2 clusters located near the sarcolemmal membrane of cardiomyocytes: (i) irregular/disordered, (ii) double rows, and (iii) single rows. Although, it is well known that there are functional RyR2 clusters located near the membrane (209–211), whether all these RyR2 clusters with different patterns of distribution are activated by Ca2+ influx through the L-type Ca2+ channel or function similarly to those in the interior is unclear. These issues make the need to study the in situ distribution and function of RyR2 clusters in living cells without tissue fixation and permeabilization for the use of antibodies clearly evident.

We recently generated a knock-in mouse model expressing a GFP-tagged RyR2 (333). This model provides a tool to study the distribution and function of RyR2 clusters in intact live cells without the need for immunostaining, thus avoiding aforementioned concerns. In a previous study (333), we revealed highly-organized arrays of GFP-RyR2 clusters that correlate with the Ca2+ release sites in the interior of ventricular myocytes. In the present study, we employed 3D confocal imaging and TIRF microscopy to determine and compare the distribution of GFP-RyR2 in the interior and periphery in isolated ventricular myocytes and in intact hearts from the GFP-RyR2 mice. We confirmed the existence of tightly-ordered arrays of GFP-RyR2 clusters in the cell interior. In contrast, an irregular pattern of distribution of GFP-RyR2 clusters was observed in the periphery using both imaging techniques. Moreover, unlike interior RyR2 clusters that showed litter detectable movement, irregularly distributed peripheral RyR2 clusters displayed dynamic movements that are modulated by RyR2 modulators. Furthermore, we found that peripheral RyR2 clusters with an irregular distribution pattern function with a Ca2+ release profile similar to that of RyR2 clusters in the interior. These observations shed novel insights into the distribution and function of RyR2 clusters in the periphery of living cardiomyocytes.

3.2 EXPERIMENTAL PROCEDURES

3.2.1 Animal studies

All animal studies were approved by the Institutional Animal Care and Use Committees at the University of Calgary and were performed in accordance with US National Institutes of Health guidelines. Adult knock-in mice expressing a GFP-tagged RyR2 (333) and wild type (WT) control littermates (8–16 weeks of age) of both sexes were used.

3.2.2 Isolation of intact hearts

A Langendorff apparatus (93) was employed to perfuse excised hearts from GFP-RyR2 knock-in mice with Krebs-Ringers-HEPES (KRH) buffer (NaCl, 125 mM; KCl, 12.5 mM; HEPES, 25 mM; glucose, 6 mM; $MgCl_2$, 1.2 mM; taurine, 20 mM; 2,3-butandion-monoxim, 20 mM; albumin, 5 mg/ml; $CaCl_2$, 0 – 1 mM; pH 7.4; oxygenated with 95% O_2 and 5% CO_2) at room temperature. Hearts were then placed onto a recording chamber for 3D confocal live cell imaging of GFP fluorescence signals in epicardial ventricular myocytes.

3.2.3 Single mouse ventricular myocyte preparation for confocal GFP-RyR2 imaging

Single ventricular myocytes were isolated from GFP-RyR2 knock-in mouse hearts using collagenase type II (Worthington Biochem) and protease digestion. Isolated cells were placed onto laminin-coated glass coverslips in the presence of KRH buffer. After up to 2 hours of settling, unattached myocytes were gently removed via KRH buffer exchange and remaining myocytes transferred onto a recording chamber. Cell integrity was tested via pacing at 2Hz. Only cardiomyocytes that followed electrical pacing were selected for subsequent 3D confocal live cell imaging of GFP-RyR2, as previously described (333).

3.2.4 3D confocal live cell imaging

A Confocal (xy galvano/resonant) imaging was performed with an inverted Nikon A1R, or A1Rplus microscope system equipped with a Plan-Apochromat 60×/1.2-NA water immersion objective, or Plan-Apochromat 60×/1.27-NA oil immersion objective and selective excitation and emission filters. 3D confocal z-stacks of GFP-RyR2 (Ex/Em 488/510nm) were acquired in 0.2-0.3 µm z-increments from a region of interest with a vertical/axial thickness of 25-40µm. All imaging of live cells and tissue was performed no longer than 8 hours after their isolation.

3.2.5 Confocal single-cell Ca2+ imaging

Ventricular myocytes isolated from GFP-RyR2 mice were loaded with Rhod-2 AM Ca2+ indicator (2.5-5 µM; Invitrogen) in KRH buffer for 20 minutes at room temperature (93). After 20 minutes de-esterification of Rhod-2 AM, the cells were washed, transferred onto laminin-coated cover glasses and permitted to adhere for up to 2 hours. The myocytes were then placed in a recording chamber and exposed to KRH solution containing 2-3 mM free Ca2+ at which spontaneous Ca2+ release events could be detected.

High-speed confocal xy resonant imaging was employed at interior and outermost peripheral xy-planes within the same cell to simultaneously record individual Ca2+ release events and GFP-RyR2 fluorescence signals. Excitation light was provided by argon (488 nm) and diode (561nm) lasers to detect GFP-RyR2 (Ex/Em 488/510 nm) and Rhod-2 AM Ca2+ indicator signals (Ex/Em 550/580 nm). Image series of Ca2+ release events were acquired in 25.5µm optical sections at a sampling rate of 50-60 frames per second (FPS).

3.2.6 GFP-RyR2 cluster imaging in ventricular myocytes using a TIRF microscope

Isolated ventricular myocytes from GFP-RyR2 mice and wild-type littermates were transferred onto 35 mm glass-bottomed micro-dishes with or without laminin-coating (Ibidi, Minitube, Canada). Cell adhesion was permitted for up to 2 hours in KRH buffer (0.5–1 mM Ca2+), before staging the dishes onto the microscope. Data were acquired with an inverted Carl Zeiss Elyra LSM780 microscope equipped with an alpha Plan-Apochromat 100×/1.46-NA oil immersion objective and excitation and emission filters. Excitation light was provided by HRdiode488-100 laser (488 nm) to detect GFP. Images of the periphery (TIRF mirror angle >64°) and the interior (angle 0) of the same cell. Layers in between were recorded in stacks with 0.25-0.3 µm z-steps (mirror angle 59-62°) with highly-inclined and laminated optical sheet (HILO) illumination (152) for molecular imaging. Whole image intensity profiles for Fourier transforms were obtained with Fiji (ImageJ). The intensity profiles were Gaussian fitted and relative intensity was used for pattern analysis. Time-lapse series were recorded at rates of 1-6 frames per minute for at least 12 minutes with exposure times less than 100 ms per image. TrackMate (335) ImageJ plugin was used for advanced cluster dynamic analysis.

3.2.7 Ca2+ imaging in live GFP-RyR2 expressing cells via a TIRF microscope

Ventricular myocytes isolated from GFP-RyR2 mice were loaded with Fluo-4 AM Ca2+ indicator (2.5-5 µM; Invitrogen) plus 0.02% Pluronic F-127 in KRH buffer for 20 minutes at room temperature. The cells were then washed, and transferred onto 35mm glass-bottomed micro-dishes (Ibidi; Minitube Canada). Cell adhesion was permitted for up to 2 hours. Spontaneous Ca2+ release events were recorded in KRH solution containing 2-3 mM free Ca2+. Time series were acquired with the same TIRF microscope as described above. Excitation light

was provided by HRdiode488-100 laser (488 nm) to detect GFP and simultaneously Fluo-4 Ca2+ indicator signals (maximum emission of 506 nm). Images of the periphery and interior of the same cell were obtained. Ca2+ dynamics were recorded at 50-60 FPS in multiples of 10 seconds.

3.2.8 Computational image analysis

Ventricular myocytes isolated from GFP-RyR2 mice were loaded with Fluo-4 AM Ca2+ Basic image processing of fluorescence signals was performed using the NIS Elements AR 4.13 software (Nikon); ZEN Black (Zeiss) and Fiji (ImageJhttps://imagej.nih.gov/ij/). Spark detection and characterization system was implemented and performed using MATLAB (The Mathworks Inc., Boston).

3.2.9 Automated spark detection and analysis

Ventricular myocytes isolated from GFP-RyR2 mice were loaded with Fluo-4 AM Ca2+ GFP-RyR2 cluster signals were revealed via average projection from temporal fluorescence image sequences. The brightest GFP-RyR2 cluster sites from each cell were determined semi-automated after application of an intensity threshold.

Ca2+ release images were partitioned using a regular square lattice of size 0.5 μm. In each image of a sequence, the mean fluorescence value was extracted for each grid site to obtain a temporal fluorescence signal for each grid site. Ca2+ indicator fluorescence signals (f) corresponding to grid sites that coincided with GFP-RyR2 clusters were used for subsequent analysis. Signal at each site was normalized using the baseline value (f0) defined as the lower 1% of the fluorescence signal. The continuous wavelet transform was calculated using a gauss2 wavelet family function, with two scales, one corresponding to short/spark-like events (~150ms)

and one associated to long events (~450ms). Ca2+ release event candidates were detected by wavelet thresholding using two sets of heuristic threshold values specific to confocal and TIRF microscopy images.

For the present study, only non-propagating spark-like release events were considered. Thus, events that appeared in both temporal scales and events in the longer temporal scale were discarded. Such events were assumed to correspond to propagating Ca2+ release (e.g. mini-waves and waves). For each of them, the following features were determined: absolute peak amplitude, local baseline, amplitude relative to the local baseline, rate of rise, time to peak, full duration at half maximum and exponential decay time. This set of features was used to further filter events satisfying pre-established criteria to exclude false positives.

3.2.10 Statistical analysis

All values shown are means ± SEM unless indicated otherwise. To test for differences between groups, we used unpaired Student's t-tests (two-tailed). p values smaller than 0.05 were considered to be statistically significant.

3.3 RESULTS

3.3.1 Confocal imaging of interior and peripheral distribution of RyR2 clusters

To study the distribution of RyR2 in different subcellular regions of live ventricular myocytes, we employed our recently generated knock-in mouse model expressing a GFP-tagged RyR2 (333). Using 3D confocal imaging, we detected GFP fluorescence in ventricular myocytes isolated from adult GFP-RyR2 mouse hearts. As shown in Figure 16Aa, GFP-RyR2s in the interior were organized as arrays of tightly ordered clusters. In contrast, imaging focusing near the periphery showed irregular distribution and appearance of RyR2 clusters (Figure 16Ab). To exclude the possibility that the irregular distribution of RyR2 clusters in the periphery was artificially introduced by cell isolation, we imaged intact hearts from GFP-RyR2 mice. As shown in Figure 16Ba, optical confocal z-stack planes of the left ventricle showed highly organized arrangements of GFP-RyR2 clusters in the cell interior. In contrast, the distribution of GFP-RyR2 clusters in the periphery of the same area was disordered (Figure 16Bb). These data indicate that the observation of different distribution patterns of GFP-RyR2 clusters in the interior and periphery was not the result of cell isolation. Thus, RyR2 clusters are organized in a highly-ordered manner in the interior, but in an irregular pattern in the periphery of live ventricular myocytes.

3.3.2 Distribution of RyR2 clusters in the interior and periphery assessed using a TIRF microscope

Previous TIRF studies reported organized arrangements of RyR2 clusters as double rows in the cell periphery of fixed and permeabilized ventricular myocytes (56, 215), which is different from that observed in GFP-RyR2 expressing cells (Figure 16). To compare the imaging data, we

also employed a TIRF microscope to determine the distribution of GFP-RyR2s in different subcellular layers within the same live ventricular myocyte. As shown in Figure 17Aa and Figure 22A& Figure 23A, imaging with epi-fluorescent illumination that was focused on the interior showed highly-ordered, single-row arrays of GFP-RyR2 clusters. Highly inclined and laminated optical sheet (HILO) illumination (angle < critical angle) showed arrays of GFP-RyR2 clusters in intermediate layers (Figure 17Ab, Figure 23B). TIRF imaging of the same cell showed irregular distribution of GFP-RyR2 clusters in the periphery (Figure 17Ac and Figure 22A & Figure 23A). As a control, ventricular myocytes isolated from wild-type littermate mouse hearts, yielded no detectable fluorescence signal under the identical imaging conditions (Figure 22B). As shown in Figure 17B, two-dimensional Fourier transformations were derived from the respective fluorescence images. Distinct maxima were observed in the transforms in the interior (Figure 17Ba, Figure 24) and intermediate layers (Figure 17Bb). In contrast, peripheral GFP-RyR2 clusters did not show intensity peaks in Fourier space (Figure 17Bc, Figure 24). Quantitative comparison of image sets from 13 cells is shown in Figure 17C. These data indicate the absence of patterns/regularity of GFP-RyR2 clusters in the periphery and the presence of ordered GFP-RyR2 distribution in the intermediate layers and interior of the same ventricular myocyte. Note that irregularly distributed peripheral RyR2 clusters were observed in the presence or absence of laminin used for coating the glass-coverslips to facilitate cell attachment (Figure 24G, H). Also note that although our TIRF imaging did not detect the double-row pattern of distribution of RyR2 clusters, HILO illumination did reveal the presence of RyR2 clusters with the double-row pattern of distribution (Figure 23B). These observations suggest that RyR2 clusters with the double-row pattern of distribution are located more interior than the irregularly distributed RyR2 clusters.

3.3.3 Dynamics of RyR2 clusters in the periphery and interior of live ventricular myocytes

To determine whether there are dynamic changes in RyR2 cluster distribution, we recorded time-lapse image series of interior and peripheral GFP-RyR2 clusters using a TIRF microscope. As shown in Figure 18A, nearly all GFP-RyR2 clusters in the interior appeared to be stationary under our imaging conditions. Similarly, the majority of peripheral GFP-RyR2 clusters appeared to remain at stable positions (Figure 18B a-e; f/g blue tracks). However, movements were observed with some RyR2 clusters in the periphery. As indicated in Figure 18B, translocation of GFP-RyR2 clusters along the z-axis was observed as dis/re-appearance of GFP-RyR2 signals (Figure 18B a-c zoom: z-Translocation – pink dashed circle). GFP-RyR2 cluster fusion (Figure 18B d-e zoom: Fusion -turquois dashed circle) and unit separation (Figure 18B b-e zoom: purple dashed circle) were also detected as GFP fluorescence signal merging/splitting. Additionally, considerable xy movements were observed (Figure 18B f: red track). These observations indicate that, unlike interior RyR2 clusters, peripheral RyR2 clusters display dynamic movements that are readily detectable under our imaging conditions.

To determine whether the movements of these peripheral RyR2 clusters are regulatable, we assessed the impact of reduced extracellular Ca2+, caffeine (a RyR2 agonist), and tetracaine (a RyR2 inhibitor) on the movements of peripheral RyR2 clusters using time-lapse TIRF imaging (Figure 19). We found that tetracaine (2 mM) dramatically diminished the fraction of cells that displayed cluster movements (Figure 19A,B). Furthermore, reducing the extracellular Ca2+ concentration from 2 to 0.5 mM markedly decreased the fraction of cells that showed cluster movements (Figure 19C). Interestingly, the effect of reduced extracellular Ca2+ on cluster movements could be reversed by the addition of caffeine (1 mM) (Figure 19D). These data indicate that the movements of these irregularly distributed peripheral RyR2 clusters are affected

by Ca2+ and other RyR2 modulators, suggesting that the movement of these peripheral RyR2 clusters may be regulated by their own activities.

3.3.4 Confocal imaging of Ca2+ release at the interior and peripheral RyR2 clusters

Our recent studies showed the distribution and function of RyR2 clusters in the interior of ventricular myocytes (333). However, whether peripheral RyR2 clusters with an irregular pattern of distribution function with Ca2+ release properties similar to those of interior RyR2 clusters is unclear. To address this question, we determined and compared local non-propagating spontaneous Ca2+ release events at the peripheral and interior GFP-RyR2 clusters within the same cells. We employed high-speed confocal imaging to simultaneously record GFP-RyR2 locations and Rhod 2-AM signals in the interior and peripheral focal planes of the same myocytes. As shown in Figure 20A, highly ordered arrays of GFP-RyR2 clusters were found in the interior. In contrast, peripheral focus showed irregular distribution of GFP-RyR2 clusters. Spontaneous elementary release events, Ca2+ sparks, were clearly detected at the GFP-RyR2 cluster locations as small spatiotemporally restricted small increases in Rhod 2 fluorescence intensity (Figure 20A - dashed orange circles). Figure 20B shows quantitative comparison of elementary Ca2+ release characteristics, including (a) amplitude; (b) rate-of-rise; (c) duration at half maximum; and (d) decay time; observed in the periphery and interior of the same cells. These data demonstrate that peripheral RyR2 clusters with an irregular pattern of distribution are functional with a Ca2+ release profile similar to that of interior RyR2 clusters.

3.3.5 Ca2+ release at the interior and peripheral RyR2 clusters assessed by a TIRF microscope

Confocal imaging allows only diffraction-limited optical sectioning (217, 218). To overcome this limitation, we employed a TIRF microscope in the TIRF mode. We recorded spontaneous Ca2+ release events at GFP-RyR2 clusters in the interior and periphery of the same ventricular myocytes. As shown in Figure 21A, image series of the interior and periphery showed GFP-RyR2 clusters as stationary fluorescence peaks throughout the recording. In contrast, Ca2+ release events were detected as temporally and spatially restricted intensity fluctuations of the cytosolic Ca2+ indicator (Fluo4-AM) fluorescence. Ca2+ sparks appeared clearly at GFP-RyR2 clusters (Figure 21A - dashed red circles). Analysis of Ca2+ release characteristics, including (a) amplitude; (b) rate-of-rise; (c) duration at half maximum; and (d) decay time; observed in the periphery and interior of the same cells are summarized in Figure 21B. These data further support the notion that the irregularly distributed RyR2 clusters in the periphery function with a Ca2+ release profile similar to that of RyR2 clusters in the interior of live ventricular myocytes. Thus, both the confocal and TIRF imaging studies demonstrate that the characteristics of Ca2+ sparks detected in the interior and periphery are similar. This similarity suggests that a major portion of the Ca2+ signals detected in the periphery are unlikely to be due to the diffusion of Ca2+ from Ca2+ sparks originated from the interior.

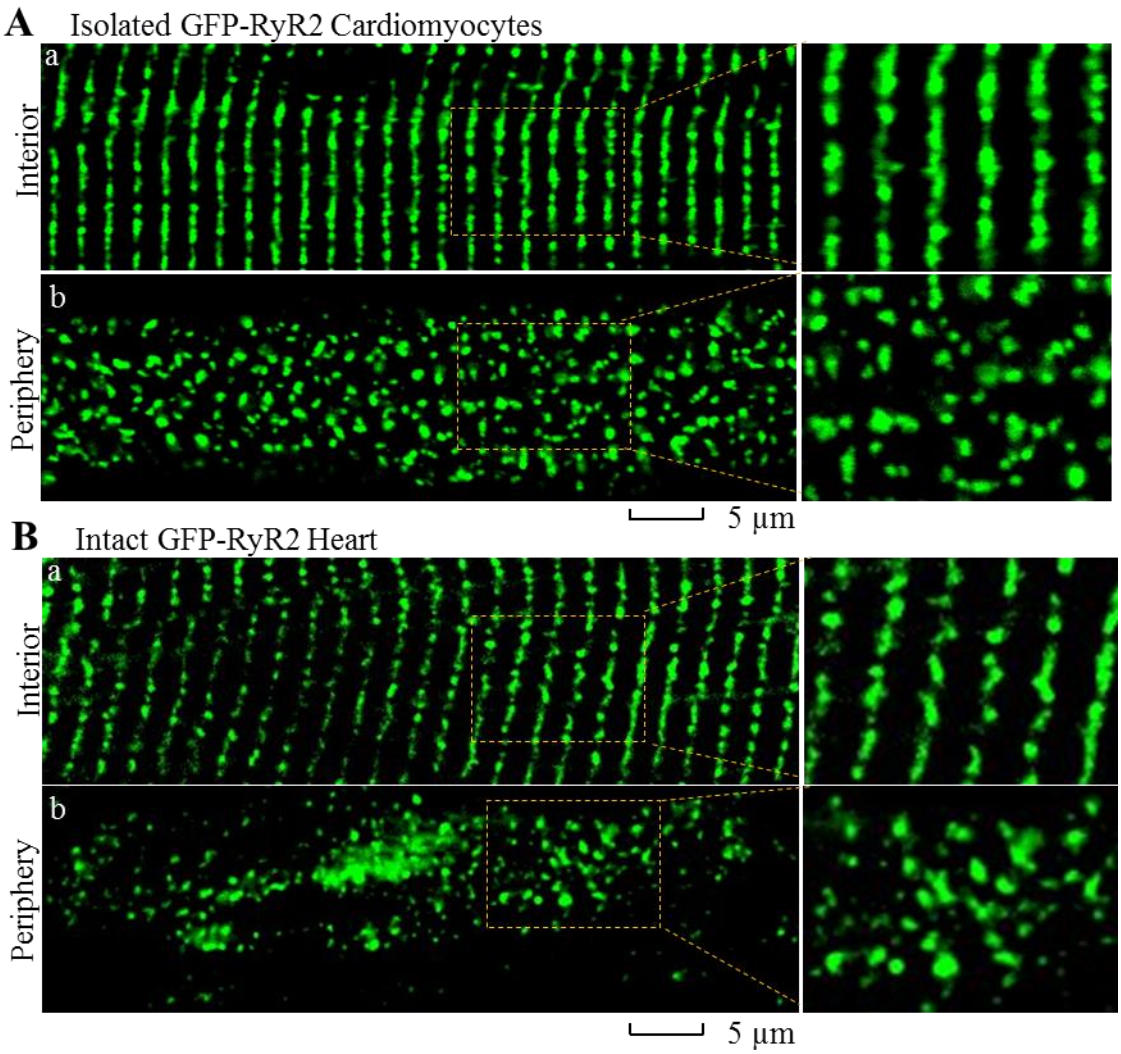

Figure 16 Different distribution of GFP-RyR2 clusters in the periphery and interior of live isolated ventricular myocytes and intact heart

Representative confocal images from z-stack of (A) live ventricular myocytes (n = 10) and (B) intact hearts (n = 14 scans from 3 hearts) isolated from mice expressing a GFP-tagged RyR2 are shown. Imaging focusing on the interior showed highly ordered arrays of GFP-RyR2 clusters (green puncta) with clear single transverse rows in both, live isolated cells and tissue (Aa and Ba). In contrast, optical confocal z-planes near the periphery showed irregular distribution of RyR2 clusters within the same cell/tissue (Ab and Bb). Enlarged images of selected areas are shown on the right. (used from accepted manuscript 2017BIOPHYSJ307979R)

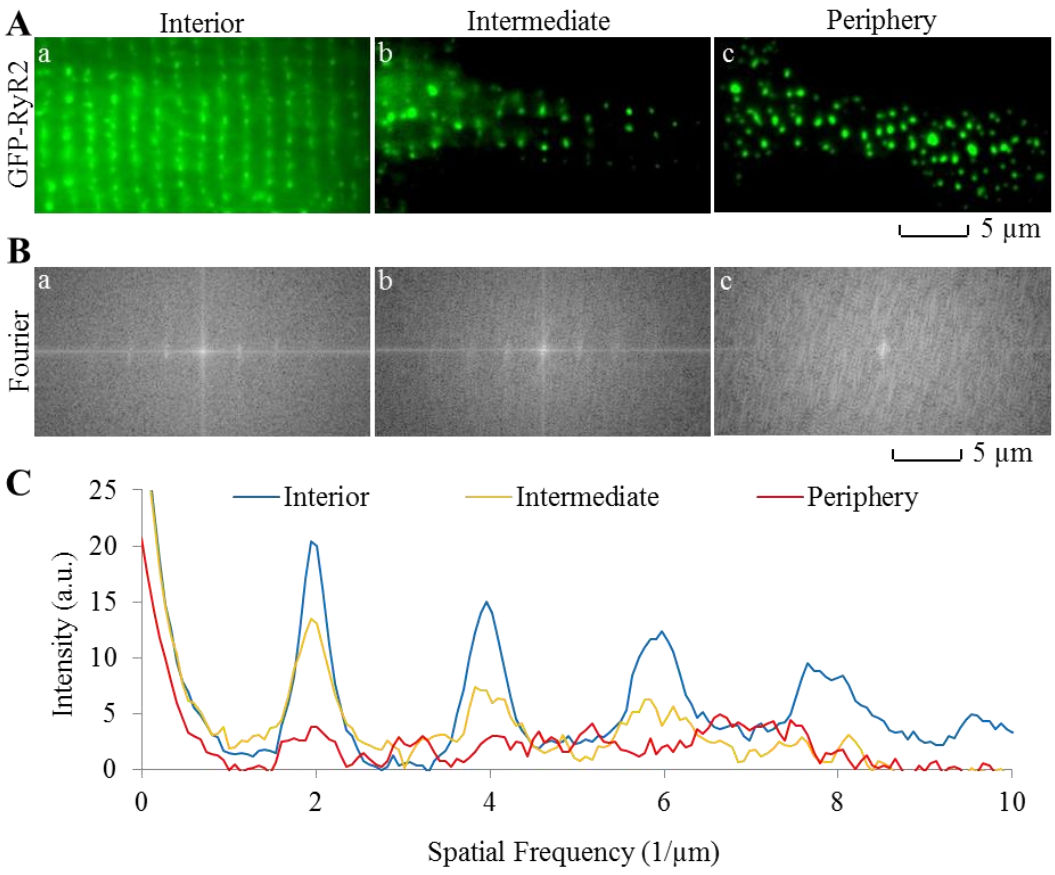

Figure 17 TIRF imaging of the distribution of GFP-RyR2 clusters in different layers within the same ventricular myocytes

Fluorescence images (A) and corresponding 2D Fourier transforms (B) of different layers within the same ventricular myocytes isolated from GFP-RyR2 mice are represented. Imaging of epi-fluorescent illuminated (angle = 0) interior showed highly-ordered, single-row arrays of GFP-RyR2 clusters (Aa). Highly inclined and laminated optical sheet illumination (angle < critical angle) of the same cell displayed arrays of GFP-RyR2 clusters with intercalated units in intermediate layers (Ab). Irregular distribution of GFP-RyR2 clusters was found in the periphery through TIRF imaging (Ac). Distinct maxima were observed in representative Fourier space of the interior (Ba) and intermediate layers (Bb). In contrast, Fourier transform of the TIRF image of peripheral GFP-RyR2 clusters did not reveal intensity peaks (Bc). Quantitative pattern comparison of different layers within the same cell (n = 13 cells) is shown in panel C. (used from accepted manuscript 2017BIOPHYSJ307979R).

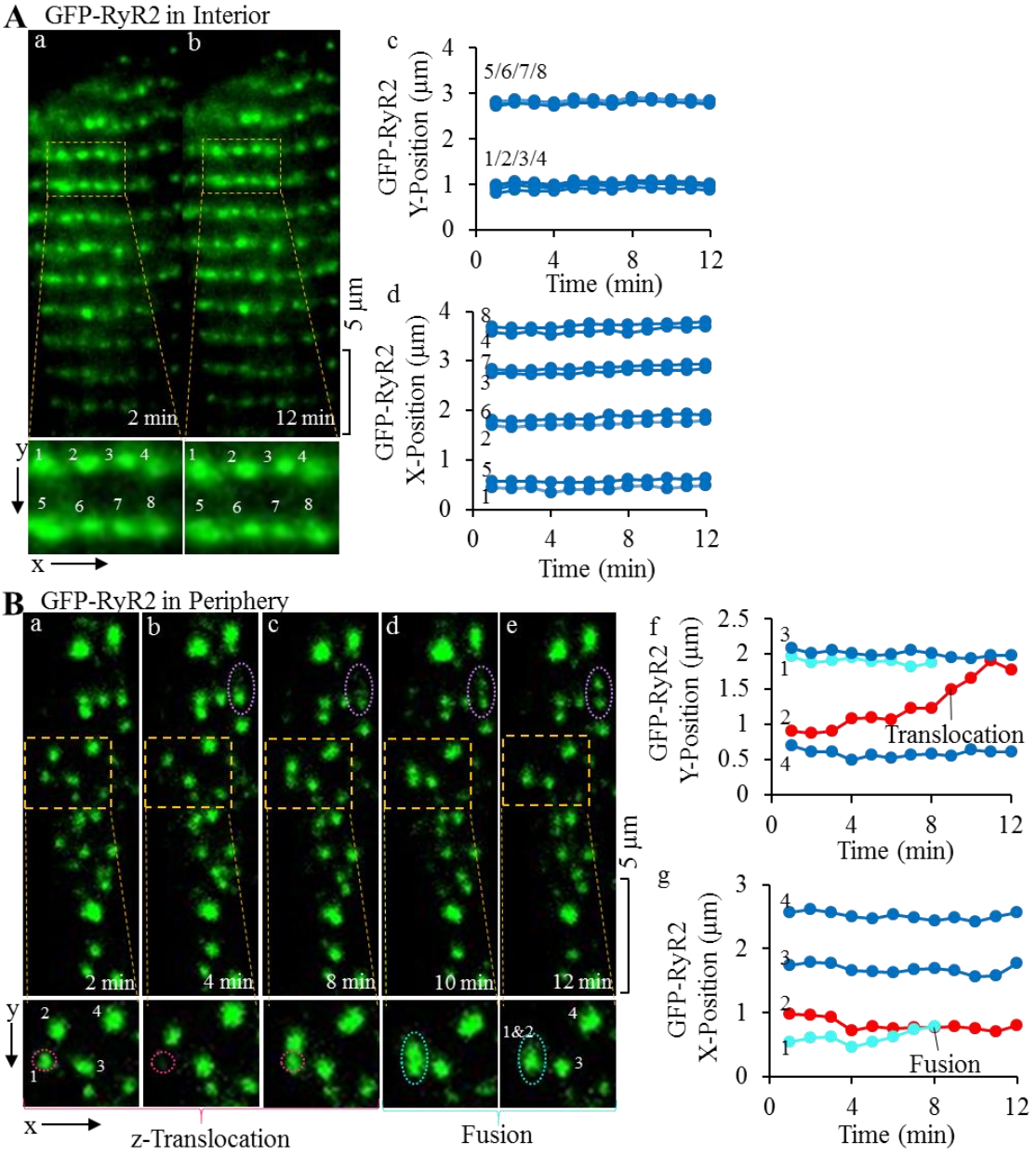

Figure 18 Time-lapse TIRF Imaging of Dynamics of GFP-RyR2 Clusters in the Periphery and Interior of Live Ventricular Myocytes

Representative images from time-lapse series of interior and peripheral GFP-RyR2 clusters, recorded using a TIRF microscope, are shown. Arrays of ordered GFP-RyR2 clusters were found in the interior. All GFP-RyR2 fluorescence signals (*clusters 1-8*) in the interior remained stationary (A a/b). TrackMate advanced cluster dynamic analysis showed only minimal x-, y-

signal movements (A c/d *blue tracks)*. In contrast, distribution of signals appeared disordered in the periphery (b a-e). The majority of peripheral GFP-RyR2 signals remained at same positions (B a-e; f/g *blue tracks*). However, multiple clusters displayed dynamic movements: (i) Translocation along the z-axis (B a-c zoom – *pink dashed circle*); (ii) GFP-RyR2 cluster fusion (B d-e zoom: *turquois dashed circle*); and (iii) unit separation (B b-e zoom: *purple dashed circle*). Additionally, TrackMate analysis showed major xy movement (B f: red track). (n = 5 cells) (used from accepted manuscript 2017BIOPHYSJ307979R)

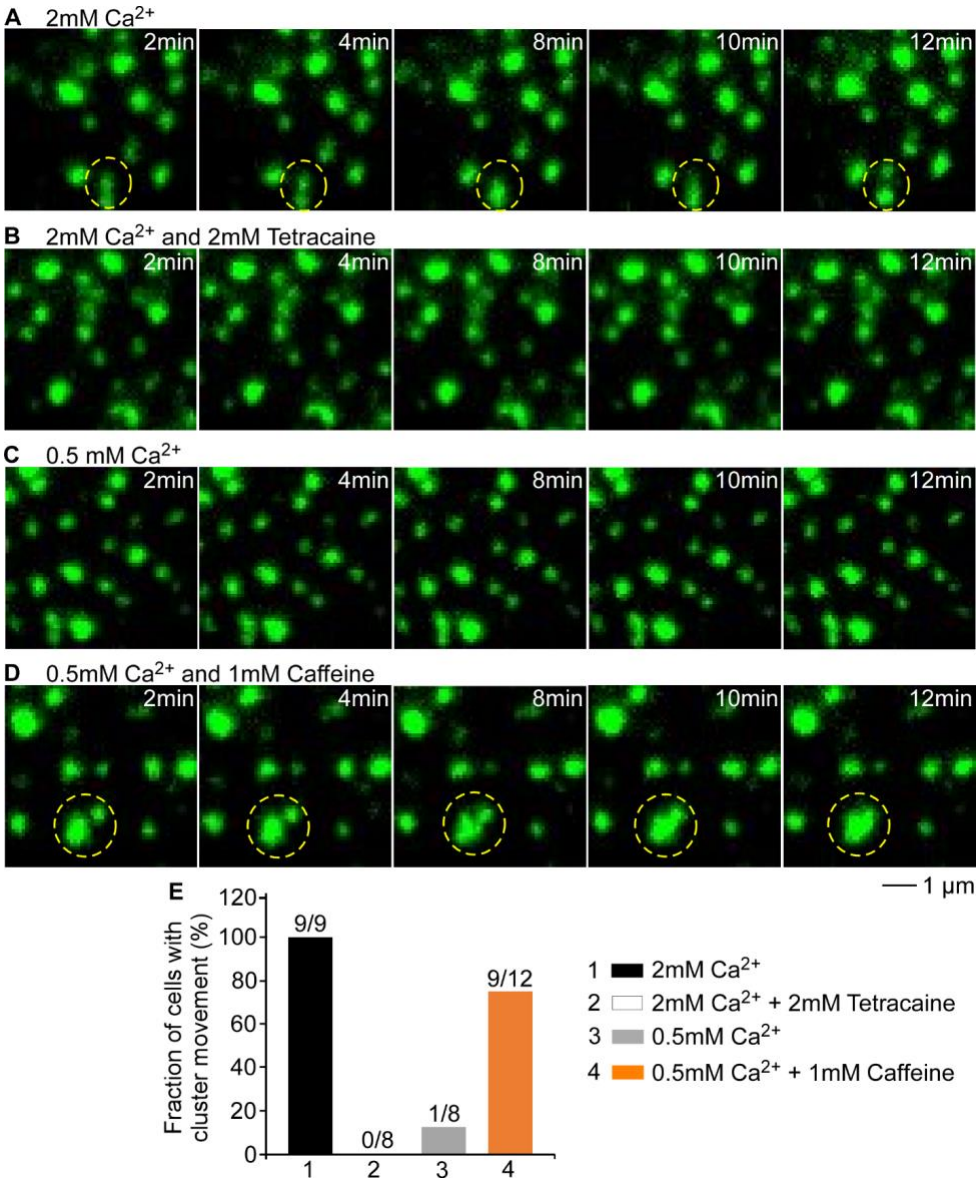

Figure 19 Movements of GFP-RyR2 clusters in the periphery of live ventricular myocytes are affected by RyR2 modulators

Representative images from time-lapse TIRF series of peripheral GFP-RyR2 clusters were recorded in the presence of (A) 2 mM extracellular Ca2+, (B) 2 mM extracellular Ca2+ plus 2 mM tetracaine, (C) 0.5 mM extracellular Ca2+, and (D) 2 mM extracellular Ca2+ plus 1 mM caffeine. Representative GFP-RyR2 cluster separation/fusion is highlighted by yellow dashed circles. (E) Fraction of cells that showed GFP-RyR2 cluster movement (n = 8-9 cells) (used from accepted manuscript 2017BIOPHYSJ307979R)

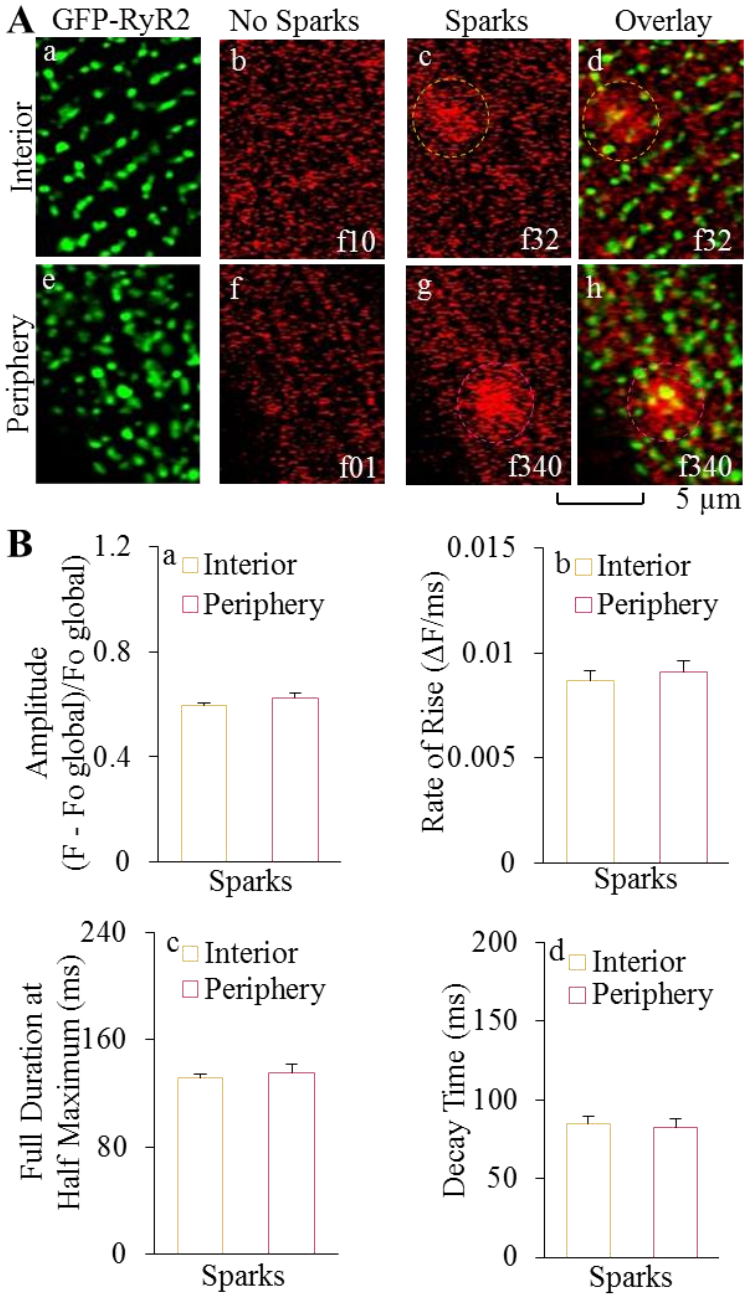

Figure 20 Confocal imaging of spontaneous Ca2+ release events at GFP-RyR2 clusters in the interior and periphery within the same ventricular myocytes

High-speed confocal imaging of spontaneous Ca2+ release (red fluorescence) at GFP-RyR2 clusters (green puncta) at the interior and peripheral confocal focus planes of the same ventricular myocyte is shown. Distribution of GFP-RyR2 clusters in the interior was found

highly-ordered, contrasting irregular patterns at the periphery (GFP-RyR2). Ca2+ sparks were detected at GFP-RyR2 locations as spatiotemporally restricted small increases in Rhod-2 fluorescence intensity (A). Quantitative comparison of characteristics of elementary Ca2+ release at RyR2 clusters (a) amplitude; (b) rate-of-rise; (c) duration at half maximum; and (d) decay time; (n = 16 cells; 927 Ca2+ spark events in interior and 774 Ca2+ spark events in the periphery; f, frame) (used from accepted manuscript 2017BIOPHYSJ307979R).

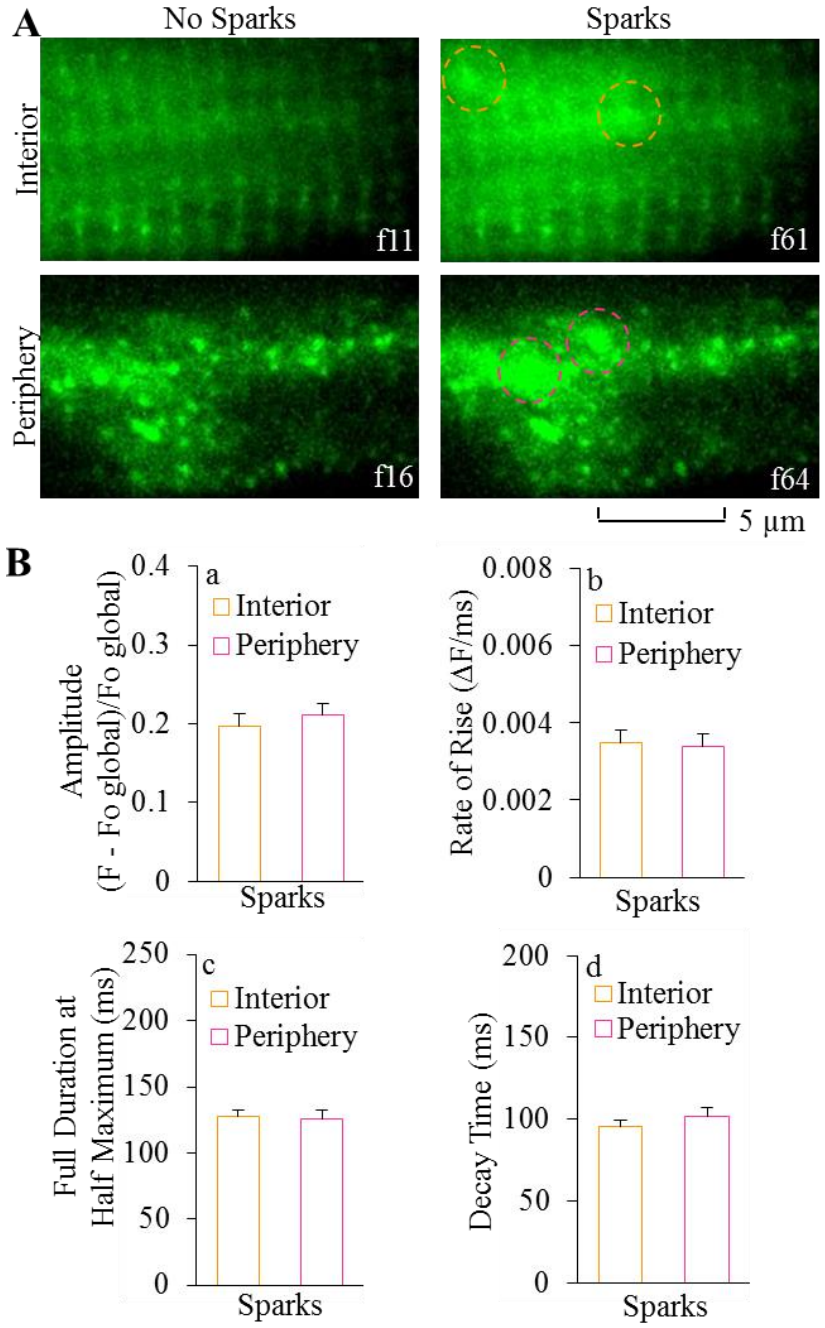

Figure 21 TIRF imaging of spontaneous Ca2+ release events at GFP-RyR2 clusters in the interior and periphery within the same ventricular myocytes

Spontaneous Ca2+ release at GFP-RyR2 clusters was recorded in the interior and periphery of the same ventricular myocyte with a TIRF microscope. Images from the time series (50-60 FPS) of GFP-RyR2 clusters were observed as stationary fluorescence peaks throughout the recording,

as displayed. Their distribution appeared highly-ordered in the interior and disordered in the periphery of the same cell (A). Ca2+ sparks appeared clearly at GFP-RyR2 clusters as transient and spatially restricted elevations in fluorescence signals (A). Quantitative comparison of characteristics of elementary Ca2+ release at RyR2 clusters (a) amplitude; (b) rate-of-rise; (c) duration at half maximum; and (d) decay time are shown (n = 10 cells; 1872 Ca2+ sparks in interior and 4153 Ca2+ sparks in periphery; f, frame). (used from accepted manuscript 2017BIOPHYSJ307979R)

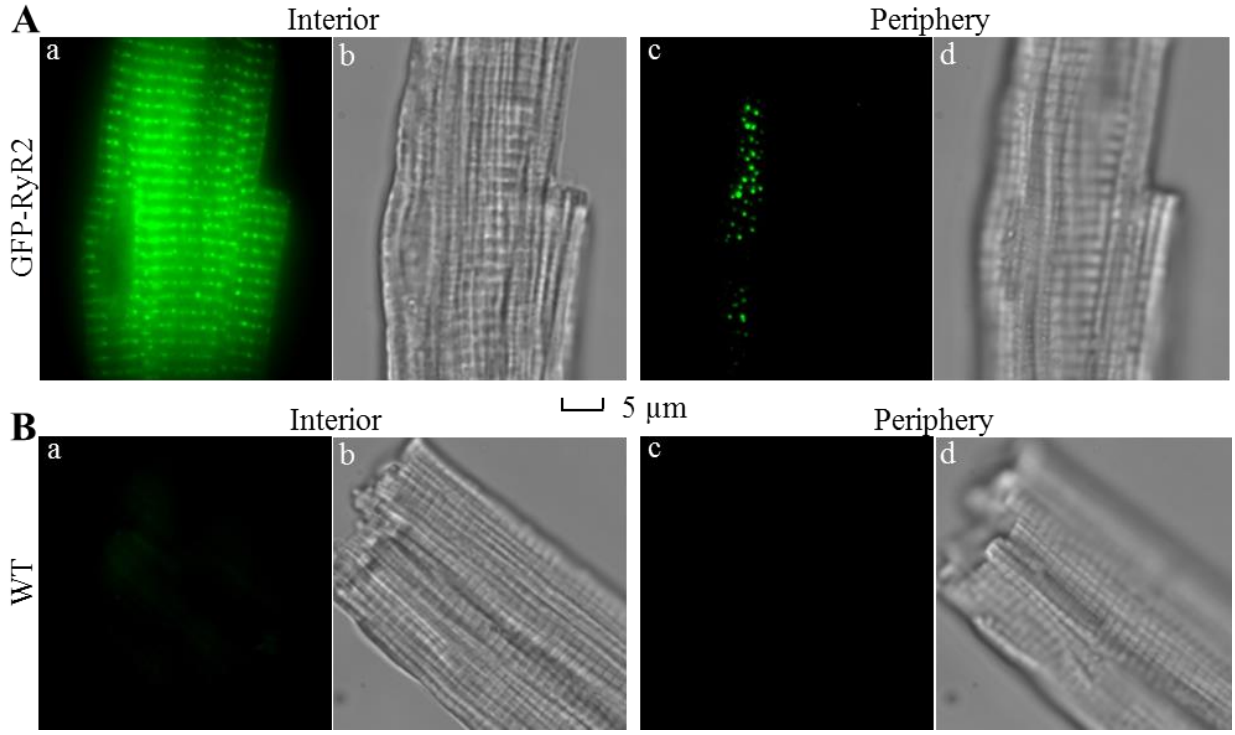

Figure 22 Fluorescence Signal Detection with a TIRF Microscope in the Interior and Periphery of Ventricular Myocytes Isolated from GFP-RyR2 Mice and WT Littermates

Representative confocal images from z-stack of (A) live ventricular myocytes (n = 10) and (B) intact hearts (n = 14 scans from 3 hearts) isolated from mice expressing a GFP-tagged RyR2 are shown. Imaging focusing on the interior showed highly ordered arrays of GFP-RyR2 clusters (green puncta) with clear single transverse rows in both, live isolated cells and tissue (Aa and Ba). In contrast, optical confocal z-planes near the periphery showed irregular distribution of RyR2 clusters within the same cell/tissue (Ab and Bb). Enlarged images of selected areas are shown on the right. (used from accepted manuscript 2017BIOPHYSJ307979R).

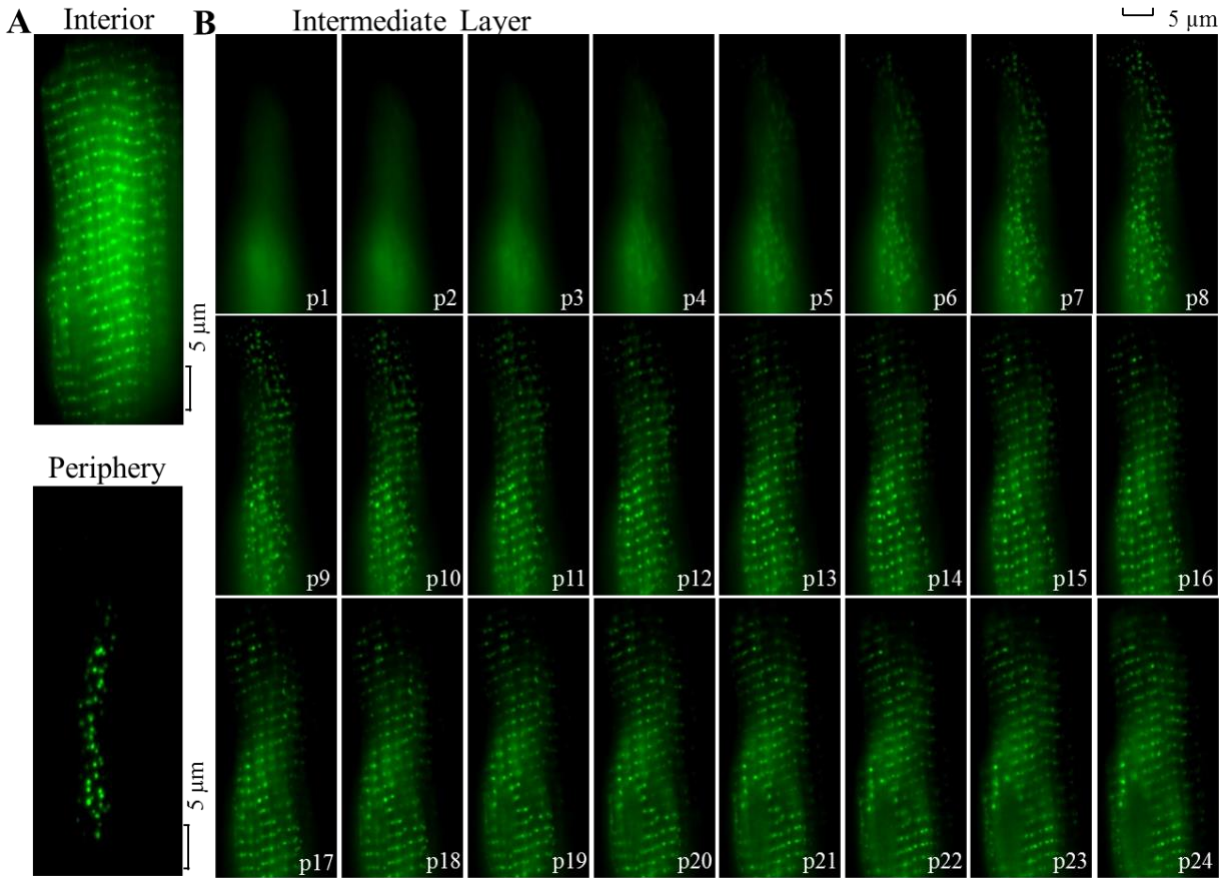

Figure 23 Imaging of Layers between the Interior and Periphery within the Same Ventricular Myocytes Detected using a TIRF Microscope

A. Representative images of periphery and interior in the same ventricular myocytes isolated from GFP-RyR2 mice were taken with a TIRF microscope. B, Optical z-stack planes (z stack distance 0.25um; plane p1-24) of layers with HILO illumination of the same cell. (n = 14 cells). (used from accepted manuscript 2017BIOPHYSJ307979R).

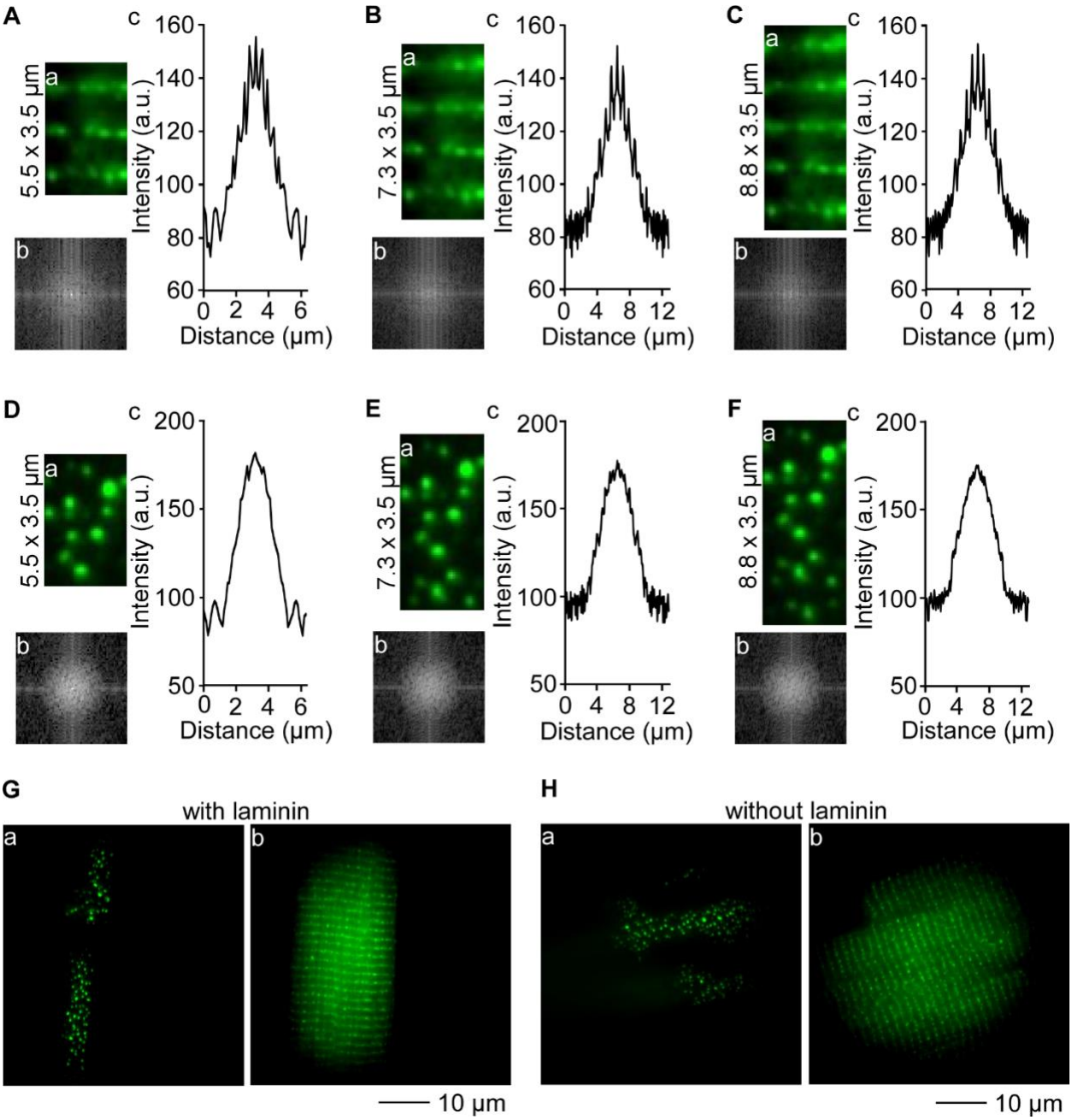

Figure 24 Fourier Transformation of Interior and Peripheral GFP-RyR2 Cluster Images with Different Area Sizes and Effects of Laminin on the Distribution of GFP-RyR2 Clusters in the Periphery and Interior of live Ventricular Myocytes

Fluorescence image areas with different sizes (A-F, panel a), corresponding 2D Fourier transforms (A-F, panel b), and intensity profiles derived from the Fourier transforms (A-F, panel c) of the interior (A-C) and the periphery (D-F) of live ventricular myocytes isolated from GFP-

RyR2 mice are represented. Imaging of epi-fluorescent illuminated (angle = 0) interior showed highly-ordered, single-row arrays of GFP-RyR2 clusters (A-C, a). Irregular distribution of GFP-RyR2 clusters was found in the periphery through TIRF imaging (D-F, a). Distinct maxima were observed in all representative Fourier space of the interior (A-C, c), even in pattern analysis of areas as small as 5.5x3.5μm (A, c). In contrast, Fourier transform intensity profiles of the TIRF image of peripheral GFP-RyR2 clusters did not reveal intensity peaks in images with identical areas (D-F, c). Panels G and H shows TIRF images (a) and epi-fluorescence images (b) obtained from isolated GFP-RyR2 ventricular myocytes attached to glass coverslips with (G) and without (H) laminin coating. (used from accepted manuscript 2017BIOPHYSJ307979R)

3.4 DISCUSSION AND CONCLUSION

The distribution of RyR2 clusters (the Ca2+ release units) is believed to be a critical determinant of controlled Ca2+ release and thus the stability of ECC in the heart. Although the distribution and function of RyR2 clusters in the interior of cardiomyocytes have been extensively studied, the distribution and function of RyR2 clusters in the periphery is poorly understood. This is in part due to the difficulty in imaging the distribution and function of peripheral RyR2 clusters. In the present study, we employed a unique knock-in mouse model expressing a GFP-tagged RyR2 to determine the distribution and function of GFP-RyR2 clusters in the periphery of live ventricular myocytes using confocal and TIRF microscopy. We found RyR2 clusters in the interior are organized in a highly-ordered striated pattern with little detectable movement. In contrast, peripheral RyR2 clusters are arranged in an irregular pattern with dynamic movements that are affected by RyR2 modulators. Importantly, the irregularly distributed peripheral RyR2 clusters are functional with a Ca2+ release profile similar to that in the interior. However, the physiological significance of these irregularly distributed peripheral RyR2 clusters has yet to be defined.

3.4.1 Discrepancies regarding the distribution of peripheral RyR2 clusters

Previous studies have shown two different patterns of distribution of RyR2 clusters in the peripheral region of ventricular myocytes. 3D confocal microscopy showed disordered distribution of RyR2 clusters in the outermost optical confocal z-planes (57, 58, 214). In contrast, RyR2 clusters displayed a `double row` feature in images obtained by TIRF microscopy (56, 215). The exact reasons for this discrepancy are unclear. Differences in sample preparation and/or antibody binding conditions may account for these different observations. Furthermore,

the optical sectioning capability of the imaging techniques used differs. On the one hand, employment of pinholes in confocal microscopy can only restrict light collection to optical segments greater than 500nm in thickness (217, 218).Thus, the observed irregular pattern of RyR2 clusters may reflect combined signals from multiple layers near, but not exclusively from, the periphery. On the other hand, evanescent fields generated during TIRF imaging illuminate only the near field (≈100 nm)(217, 218). Thus, only fluorophores in close proximity to the cell surface at the cell-glass coverslip interface are excited and imaged. Therefore, one would expect that the periphery just beneath the plasma membrane is occupied by double-rows of RyR2 clusters. However, we found an irregular pattern of distribution of GFP-RyR2 clusters using both the confocal and TIRF imaging in the periphery of live ventricular myocytes. On the other hand, we observed double rows of RyR2 clusters using HILO illumination. Together, these observations suggest that double rows of RyR2 clusters are located more interior than the irregularly distributed RyR2 clusters.

A possible reason for the differences between our study and former TIRF studies (56, 215) may be due to the use of fixed and permeabilized cardiomyocytes versus live ventricular myocytes in the present study. In our experience, we found that live ventricular myocytes adhere readily to the glass coverslips, forming multiple contacts with the surface of the coverslips, whereas, fixed and permeabilized cells did not adhere to the glass coverslips. The lack of contact of fixed and permeabilized cells to the surface of coverslips would make TIRF imaging of the cell periphery difficult. To circumvent this problem, Jayasinghe et al.(215) embedded fixed myocytes in agarose blocks. These blocks were permeabilized, stained with anti-RyR2 antibody, and mounted for TIRF imaging. Another TIRF study (56) used antibody-labeled, fixed and permeabilized cells in suspension. It is important to note that in both studies, the fixed,

permeabilized cells were stacked between two coverslips. However, whether agarose embedding and/or application of mechanical forces affects the distribution of peripheral RyR2 clusters is unclear. The peripheral layers could have been altered and/or shifted out of the TIRF detection range by these mechanical stresses. In this regard, our live cell imaging approach revealed in situ distribution of RyR2 clusters in the periphery of living and excitable cardiomyocytes.

It should be noted that the areas detected by TIRF imaging are much smaller than the areas of the cells, and the shapes of the illuminated areas are always irregular. This is expected if the areas detected by TIRF reflect the areas of the live cells contacting the glass-coverslip. The small size and irregularity of the contact areas would make the detection of long-range orderliness/patterns difficult, if not impossible. This also raises an important question of whether the contact areas detected by TIRF are large enough to determine the relative orderliness of the distribution of RyR2 clusters located in different regions of the cell. To address this question, we performed Fourier transformation of fluorescence images obtained from the interior and peripheral areas with different sizes. We found that an epi-fluorescent image from the interior with an area as small as 5.5 x 3.5 μm is sufficient to reveal intensity peaks (orderliness). On the other hand, a TIRF image from the periphery with the same area showed no intensity peaks (Figure 24 A-F). Note that the TIRF images yield brighter signals and more detailed Fourier transforms than epi-fluorescent images. Thus, the absence of peaks in the Fourier space of TIRF images is unlikely due to optical differences in the detection techniques. Therefore, although it may not be large enough to detect long-rang orderliness/patterns, the peripheral contact area detected by TIRF (>5.5 x 3.5 μm) is large enough to assess the orderliness of peripheral RyR2 clusters relative to that in the interior.

There are also other factors that may potentially affect the distribution of RyR2 clusters in

the periphery. For instance, the use of laminin may affect the adhesion of live cardiomyocytes to the glass-coverslip and hence the pattern of distribution of RyR2 clusters in the periphery. To test this possibility, we compared the patterns of distribution of peripheral GFP-RyR2 clusters in the presence and absence of laminin. We found an irregular pattern of distribution of GFP-RyR2 clusters in the periphery in the presence or absence of laminin (Figure 24G, H), different from that in the interior. Therefore, it is unlikely that the irregular pattern of distribution of RyR2 clusters observed in the periphery is due to the use of laminin. In addition, it is possible that the pattern of distribution of RyR2 clusters in the periphery may vary from species to species. In the present study, we employed cardiomyocytes isolated from the GFP-RyR2 knock-in mice, whereas, rat or rabbit cardiomyocytes were used in other studies (56–58, 214, 215). However, it is important to note that the irregularly distributed RyR2 clusters were also observed in the peripheral region of rat and rabbit cardiomyocytes in other studies (58, 214). Hence, mouse, rat, and rabbit cardiomyocytes express these irregularly distributed RyR2 clusters in the peripheral region of the cell. It is also possible that the insertion of GFP into the RyR2 sequence may affect the distribution of peripheral RyR2 clusters. However, the insertion of GFP does not seem to significantly alter the distribution of RyR2 clusters in the interior. Furthermore, as mentioned above, irregularly distributed non-GFP-labelled, native RyR2 clusters have also been detected in the periphery of rat and rabbit cardiomyocytes (58, 214). Hence, the irregular pattern of distribution of GFP-tagged RyR2 clusters observed in our GFP-RyR2 mouse cardiomyocytes is unlikely to be a region-specific artifact resulted from the insertion of GFP.

3.4.2 Movements of RyR2 clusters

Chen-Izu et al.(58) and Jayasinghe et al.(215) suggested that RyR2 trafficking and protein turnover potentially have led to the different peripheral patterns of distribution of RyR2 clusters in antibody-stained ventricular myocytes. Cell fixation might have captured a snapshot of the migration of RyR2 clusters from the interior towards the surface along the SR membrane system (and vice versa). However, our time-lapse TIRF imaging revealed that the majority of irregularly distributed GFP-RyR2 clusters were stationary in the periphery of live ventricular myocytes. Also, all GFP-RyR2 clusters in the interior of these cells showed little detectable movements during the entire recording period (>20 minutes). Thus, the irregular distribution of peripheral RyR2 clusters is unlikely to be the consequence of trafficking of all superficial clusters. Furthermore, the peripheral RyR2 clusters that underwent dynamic movements were closely-localized with those stationary RyR2 clusters. Thus, it is unlikely that the movement of these RyR2 clusters resulted from movement induced by a patch of cell membrane. Such membrane movements would be expected to affect a large membrane area, which would simultaneously affect the movement of many closely juxtaposed RyR2 clusters. However, this is clearly not the case. We observed x-, y- and z-directed translocation of GFP-RyR2 clusters. We also observed fusion, or separation of GFP-RyR2 clusters in the periphery. Importantly, we found that these movements are affected by extracellular Ca2+ concentrations and the RyR2 activator (caffeine) and inhibitor (tetracaine). These observations suggest that the movement of irregularly distributed RyR2 clusters in the periphery is a regulated process. The detailed mechanism underlying these complex dynamic movements of peripheral RyR2 clusters has yet to be defined.

It is important to point out that it is much more difficult to detect movements of RyR2 clusters located in the cell interior. The interior RyR2 clusters are likely to be confined to the

small area of the narrow t-tubules. It is also hard to resolve RyR2 clusters located deeper into the myocytes due to lower z-resolution and optical aberrations. Therefore, under our imaging conditions, we cannot rule out that interior RyR2 clusters may also undergo dynamic movements. In this regard, it is of interest to note that RyR2 tetramers within a cluster are mobile (55). It is also important to know that each RyR2 cluster may contain multiple smaller clusters (56). Thus, each of the GFP fluorescent spots observed in our study could be composed of multiple clusters of RyR2, which is consistent with our observations that GFP-RyR2 clusters detected in the periphery can undergo fusion into a big cluster or separation into smaller clusters.

3.4.3 Function and relevance of peripheral RyR2 clusters

The distribution of RyR2 clusters is believed to be an important determinant of normal Ca2+ release in the heart. Highly ordered arrays of RyR2s in the interior are proposed to underlie stable, graded CICR during ECC. However, little is known about the functional relevance of peripheral RyR2 clusters. On the one hand, Dan et al. (214) showed that during cardiomyocyte maturation the distribution of RyR2 clusters in the periphery changed dramatically. Local non-uniformities in the growth of sarcomeres has been proposed to underlie the appearance of dislocated RyR2s (58, 336). Thus, one might speculate that these irregularly distributed RyR2 clusters in the periphery reflect those observed in early development. On the other hand, peripheral RyR2 clusters have been suggested to be involved in centripetally propagating Ca2+ release (214). Spacing between functional RyR2 units in the periphery of cardiomyocytes has also been suggested to be a determinant of the probability of initiation of global Ca2+ waves (150). However, despite these functional implications, it has remained unclear whether peripheral RyR2 clusters with an irregular pattern of distribution are functional and have Ca2+

release properties similar to those of interior RyR2 clusters. Our confocal and TIRF recordings of Ca2+ release at RyR2 clusters in the periphery demonstrated that irregularly distributed peripheral RyR2 clusters are indeed functional. Furthermore, we showed that peripheral RyR2 clusters possess the same Ca2+ release profile as clusters in the interior. Therefore, peripheral RyR2 clusters may play a role in determining the Ca2+ release profiles in the region just beneath the cell surface of ventricular myocytes.

Irregular distribution of RyR2 clusters has been observed in the setting of cardiac hypertrophy and heart failure (337). This irregular distribution of RyR2 clusters has been implicated in the generation of Ca2+ waves and triggered arrhythmias. However, we found irregular distribution of functional RyR2 Ca2+ release units in the periphery of live, presumably healthy, cardiomyocytes. Thus, by itself, irregular sub-membrane distribution of RyR2 clusters does not necessarily associate with cardiac pathology. It may have potentially unique physiological roles in Ca2+ signaling in cardiac cells, which remain to be investigated.

3.4.4 Conclusion

In the present study, we employed a GFP-tagged RyR2 mouse model to compare the distribution and function of RyR2 clusters in the periphery and interior of live ventricular myocytes. We found that the distribution of RyR2 clusters in the periphery is irregular and dynamic, different from those in the interior. We also demonstrated that peripheral RyR2 clusters form functional Ca2+ release units with a similar Ca2+ release profile as that in the interior. Our results shed novel insights into the distribution and function of RyR2 clusters in the periphery of intact cardiomyocytes.

CHAPTER 4 The Arrhythmogenic RyR2 Mutation R4496C Enhances Neuronal Excitability and Impairs Hippocampal Long-term Potentiation, Learning, and Memory

4.1 INTRODUCTION

Ryanodine receptor type 2 (RyR2) is an intracellular Ca^{2+} channel that plays an essential role in excitation-contraction coupling in cardiac muscle by governing the release of Ca^{2+} from the sarcoplasmic reticulum (3). RyR2 is also a critical player in the pathogenesis of cardiac arrhythmias. A large number of naturally occurring RyR2 mutations have been associated with catecholaminergic polymorphic ventricular tachycardia (CPVT) (86). The arrhythmogenic mechanism of RyR2-associated CPVT has been extensively investigated. It is generally believed that CPVT-linked RyR2 mutations sensitize the channel to activation by Ca^{2+}, which increases the propensity for spontaneous Ca^{2+} release, delayed afterdepolarization, and triggered arrhythmias (86). In addition to the heart, RyR2 is the most abundantly expressed RyR isoform in the brain, especially in the hippocampus and cortex, regions that are important for learning/memory and cognition (287–292, 338, 339) Interestingly, the level of RyR2 mRNA and protein in hippocampus was markedly increased following intensive training in a water-maze task (302–305). These observations suggest that RyR2 plays an important role in hippocampal synaptic plasticity and learning/memory. As such, altered RyR2 function is expected to have pathological impact on cognitive function. Indeed, apart from the arrhythmogenic phenotypes, a significant portion of patients harboring CPVT-linked RyR2 mutations also displayed intellectual disability, cognitive deficits, and other neurodevelopmental disorders (278–280). Although an increased body of evidence demonstrates the link between CPVT RyR2 mutations and

intellectual disability, the mechanism by which CPVT RyR2 mutations affect cognitive function is unknown.

To gain insights into the roles of RyRs in neuronal function, numerous studies have investigated the cellular and subcellular localizations of RyRs in the brain. It has been shown that RyRs are expressed in different compartments in hippocampal neurons, including presynaptic terminals, dendritic spines, dendritic shafts, and the soma (286, 288, 290, 293, 294). Therein, they have been suggested to be involved in various neuronal functions. Consistent with these subcellular localizations of RyRs, functional studies have implicated an important role of RyRs in synaptic transmission, long-term potentiation (LTP), synaptic plasticity, and gene expression (285, 293, 295–301). However, the precise subcellular localization and specific roles of the RyR2 isoform in different compartments (presynaptic terminals, dendritic spines, dendritic shafts, and the soma) in hippocampal neurons are largely undefined. This is due, in part, to the presence of all 3 RyR isoforms in hippocampal neurons, the uncertain antibody specificity in the context of whole brain tissue, and the lack of isoform-specific functional probes for RyR2.

To be able to specifically define the subcellular localization of the RyR2 isoform in the brain, in the present study, we used a knock-in (KI) mouse model that expresses a green fluorescence protein (GFP)-tagged RyR2. To increase the specificity and sensitivity of GFP detection, we generated a GFP-specific probe. Using these new reagents, we unambiguously localized RyR2 in the dendritic shafts and soma, but not in the presynaptic terminals or dendritic spines, in hippocampal neurons. Furthermore, to specifically assess the impact of CPVT RyR2 mutations, we employed a KI mouse model expressing a CPVT-linked human RyR2 mutation R4496C that enhances channel function (83, 86, 87, 267, 269). We found that the CPVT RyR2-R4496C mutation had no effect on presynaptic short-term facilitation. On the other hand, we

showed that the R4496C mutation impaired hippocampal LTP, learning and memory. We also showed that a CPVT RyR2 mutation increased the occurrence of spontaneous Ca2+ transients and action potential firing, suggesting RyR2 as an important determinant of neuronal excitability. Therefore, our data reveal the precise subcellular localization of RyR2 in hippocampal neurons and the functional consequences of a CPVT RyR2 mutation for neuronal excitability and cognitive function. Our results provide novel insights into the mechanisms of intellectual disability associated with RyR2 mutations.

4.2 EXPERIMENTAL PROCEDURE

4.2.1 Animal studies

All animal studies were approved by the Institutional Animal Care and Use Committees at the University of Calgary and were performed in accordance with US National Institutes of Health guidelines. Adult knock-in mice expressing a GFP-tagged RyR2 (GFP-RyR2) (333), heterozygous RyR2-R4496C (RC) (269) and wild type (WT) control littermates (3-4 month of age) of both sexes were used.

4.2.2 Generation and labeling of GFP-specific probe

The cDNA encoding the GFP binding protein cAbGFP4 (237, 340) was amplified by PCR using a forward primer: GCACAGGTTCAACTGGTGGAAAGC and a reverse primer: TTATTATTTAGAGCTCACCGTCACCTG. The PCR fragment was then subcloned into the pET28HMT expression vector using the SspI restriction enzyme. The sequence of the PCR fragment was confirmed by DNA sequencing. The GFP binding protein fused to the C-terminus of the polyhistidine-tagged maltose-binding-protein was overexpressed in DH5a E. coli cells and purified using the HisPur™ Ni-NTA Resin (Thermo Fisher; 8821). The recombinant fusion protein (the GFP-probe) was diluted in PBS (NaCl, 137 mM; KCl, 2.7 mM; Na2HPO4, 10 mM; and KH2PO4, 1.8 mM; pH 7.4) and conjugated with the succinimidyl – ester of Alexa Fluor 647 (Thermo Fisher; A20106) for at least 1 hr at room temperature. Excess dye was removed using the Zeba™ Spin Desalting Columns (Thermo Fisher; 89882) and the fluorescently labelled GFP-probe (30 µg/ml) was stored at 4 degree until use.

4.2.3 Preparation of brain slices for imaging

GFP-RyR2 mice and WT littermates (3-4 month old) were anesthetized and transcardially perfused with pre-chilled carbogen-bubbled artificial cerebrospinal fluid (aCSF) (NaCl, 125 mM; KCl, 3.25 mM; MgCl2, 1.5 mM; and CaCl2, 1.5 mM; D-glucose, 25 mM; and NaHCO3, 25 mM; pH 7.4 adjusted with NaOH) or with the slicing solution (N- methyl D-glucamine 119.9 mM, KCl 2.5 mM, NaHCO3 25 mM, CaCl2 1.0 mM, MgCl2 6.9 mM, NaH2PO4 1.4 mM, glucose 20 mM, pH 7.4). They were then sacrificed by decapitation and whole brains were submerged rapidly into ice cold aCSF or slicing solution, bubbled with 95% O2 and 5% CO2. For confocal and structured illumination microscopy (SIM), coronal sections (150 μm) were collected and fixed with paraformaldehyde (4%) in aCSF for ≤ 5 min at room temperature (RT). The reaction was stopped using aCSF containing glycine (0.5 M). Free floating sections were then blocked with a mixture (v/v = 50%) of BlockAid™ Blocking Solution (Molecular Probes; B10710) and Image-iT™ FX Signal Enhancer (Molecular Probes; I36933) for 1-2 hr at RT. Blocked brain slices were labeled with the GFP-probe for 30-45 min at RT, washed, mounted and imaged. For co-localization studies, the GFP-probe stained slices were permeabilized for 15 min with Triton X-100 (0.1%) and stained with Rhodamine Phalloidin (Thermo Fisher; R415) for 1 hr at RT or overnight at 4 ^{o}C with primary antibodies against synaptophysin (Millipore; MAB5258 - SY38 clone), syntaxin (Enzo Life Sciences; ADI-VAM-SV013 – SP6 clone) or microtubule-associated protein 2 (MAP2)(Sigma; M1406 AP-20 clone). Brain slices that were treated with primary antibodies were further incubated for 1-2 hr at RT with rhodamine-conjugated secondary antibody (rhodamine (TRITC) AffiniPure™ goat anti-mouse IgG (H+L)) (JacksonImmuno Research Laboratories Inc.; 115-025-003) before they were embedded in Prolong™ Gold Antifade Mountant (Thermo Fisher; P36930) for subsequent

imaging.

4.2.4 Confocal and structured illumination microscopy (SIM) imaging

High resolution confocal xy imaging was performed with an inverted Nikon A1Rplus microscope system equipped with a Plan Fluor DIX H N2 40x/1.3-NA oil immersion objective or Plan-Apochromat alpha 60x/1.27-NA oil immersion objective and selective excitation and emission filters. Large image acquisition was performed through automated fluorescence-based image stitching (50% image overlay). The fluorescence signals of GFP-RyR2 (Ex/Em 488/510 nm), rhodamine-conjugated phalloidin, anti-mouse (Ex/Em 561/594 nm), and the GFP-probe (Ex/Em 638/665 nm) were acquired at the indicated excitation and emission wave lengths. SIM superresolution was performed on an inverted Carl Zeiss ELYRA LSM 780 microscope PS1 system equipped with an Plan-Apochromat DIC M27 63x/1.4 oil immersion objective and excitation and emission filters. For each color, raw image z-stacks were acquired in 0.1 µm z-increments from a region of interest with a vertical/axial thickness of 5 µm using 5 rotations, 5 phases. Zeiss ZEN 2012 black software (Zeiss,Germany) was used for channel alignment and SIM image reconstruction.

4.2.5 Confocal Ca2+ imaging of hippocampal neurons in brain slices

Coronal brain slices (300 µm) from RyR2 WT and RyR2-R4496C mutant mice (3-4 months old) expressing the GCaMP6f Ca2+ sensing probe driven by the *Thy1* promotor were mounted onto an inverted Nikon A1 microscope system, equipped with a Plan-Apochromat 1-WI 60×/1.2-NA water immersion objective and selective excitation and emission filters. High-speed confocal xy microscopy was employed to acquire image series of Ca2+ transients in 150 µm

optical sections at a sampling rate of 1.1 frames per second (FPS). GCaMP6f fluorescence signals (Ex/Em 488/510 nm) from hippocampal cells in the CA1 region were continuously recorded at the resting condition (spontaneous Ca2+ transients) for 15 min, followed by the addition of KCl (50 mM) (KCl-induced Ca2+ transients).

4.2.6 Single cell patch-clamp recording

Action potentials were measured in pyramidal CA1 neurons of transverse dorsal hippocampal slices (260 µm) from RyR2 WT and RC mutant mice (3-4 months old) using whole-cell patch clamp with an Axopatch 700B amplifier (Axon Instruments). AP firing was recorded utilizing external solution (NaCl 124 mM, KCl 2.5 mM, HEPES 5 mM, glucose 12.5 mM, MgCl2 2 mM, CaCl2 2 mM, pH, 7.4) and soft-glass recording pipettes (Sutter Instruments; Novato CA) filled with an internal solution (potassium gluconate 135 mM, KCl 10 mM, HEPES 10 mM, CaCl2 1 mM, MgCl2 1 mM, EGTA10 mM, ATP1 mM, GTP 0.1 mM, and pH 7.4 adjusted with KOH). The pipette resistance was 4–6 MΩ after filling with internal solution. Spontaneous AP firing by pyramidal cells in the CA1 region was recorded at RT in whole cell current clamp mode. For the measurement of current triggered APs, APs were initiated by injecting current from 0 to 300 pA for 1 s in 10 pA steps at 10 s intervals (341). Data were acquired and analyzed using pCLAMP 10.4 (Molecular Devices; Sunnyvale CA).

4.2.7 Electrophysiological recording of short-term plasticity and long-term potentiation in hippocampal Schaffer collaterals

Schaffer collateral fibers were stimulated in stratum radiatum at the CA3 – CA2 boundary to record field excitatory postsynaptic potentials (fEPSPs) in the CA1 stratum radiatum

(in ~220-280 µm distance from stratum pyramidale) of transverse dorsal slices (300 µm) from RyR2 WT and R4496C mutant mice (3-4 months old). The slope of fEPSPs were determined from peaks that occurred ~2-6 ms after the stimulation to avoid potential interference from cell body population spikes as described by Low et al.(342) and Turner et al. (343). Paired pulse facilitation was assessed via current stimulation (60 µA) with inter-stimulus intervals of 20-300 ms. The baseline was established for at least 20 min before a series of 15 sets of two consecutive pulses was applied. fEPSP slopes of the initial pulse (P1) was set in relation to the fEPSP slope recorded in response to a secondary pulse (P2) yielding the paired pulse ratio (P2/P1) for comparison. Long-term potentiation (LTP) was induced using a tetanic high-frequency stimulation (HFS; 4 trains of 100 pulses at 100 Hz, with 20 s intervals). Synaptic responses were recorded for at least 30 min after tetanization and quantified as the slope of the evoked fEPSP as percentage of the baseline. The baseline was recorded for at least 20 min. Basal excitatory synaptic transmission was assessed via comparison of input-output relations: current input versus (i) slopes of fEPSP and (ii) Schaffer fiber volley amplitude

4.2.8 Spatial learning and memory test

Spatial learning and memory were evaluated using the Morris water maze (MWM) task (344). Experiments were carried out blindly. RyR2-R4496C mutant mice and RyR2 WT littermates were trained to localize a hidden escape platform (10 x 10 cm) in a circular pool (116.84 cm in diameter, 50 cm in depth) (San Diego Instruments, CA) via distal visual cues. The platform was submerged 1-2 cm beneath the surface in water (22-24˚C) which was rendered opaque by addition of milk powder. The localization of the pool in relation to visual cues was maintained constant during the entire task. The cues were distinct in color and size. Digital

division of the tracking area (pool) into four quadrants was performed by the SMART video tracking system, Smart 3.0 (Panlab Harvard Apparatus; Barcelona Spain). The escape platform was placed in the centre of the south-west quadrant for the entirety of the learning phase (4 training days) and digitally defined as target. Spatial training consisted of 4 days with 1 session comprising 5 trials per mouse. Mice were released with their heads facing the pool wall at one of four entry locations (north, east, south and west) in non-repetitive random order. Swimming was automated video-tracked until the subject found the escape platform and remained on it (≥ 5 s), or until a maximum of 1 minute. Mice that did not locate the hidden platform within the time limit of 60 seconds were guided to the escape platform until they spent ≥10 seconds on it. In between trials (inter-trial interval ≥ 10 min), mice were housed in heated cages to avoid performance deficits due to exhaustion, or hypothermia. The latency and swimming speed to reach the escape platform were recorded for comparison. After the learning phase, memory retention was evaluated by one probe trial 24 hours after the last training session. The escape platform was removed before mice were released from the north entry point into the pool. Their swimming was video-tracked for 60 seconds. The area at the location of the removed hidden platform was defined as target and the south-west quadrant the target quadrant. The percentage of time mice spent in the target quadrant (including the target) were measured for comparison. The mean swim speed was also determined to evaluate potential differences caused by performance dysfunction due to physical disabilities.

4.2.9 Novel object recognition

RyR2-R4496C mutant mice and RyR2 WT littermates were habituated for 10 min per mouse in an equally illuminated, odor-free, white, plastic box (40x40x50 cm^3) embedded with

fresh aspen shavings and shreds. In between each mouse trial the box was wiped with ethanol to avoid odor-induced stress. 24 hours after habituation, two identical objects ware placed at equal distance to each other and the corners into the box. Each mouse was placed into the center, and allowed to move freely for 10 min. Mice were video recorded during this familiarizing phase. Side preferences was evaluated by dividing the time a mouse spent exploring one object by the time they spent at the other object. Twenty-four hours later, one of the objects was replaced by a novel object. The other object remained constant. The selection of a familiar object to be replaced was random. Each mouse was again placed into the center of the box and allowed to move freely for another 10 min while videotaped. General exploration was evaluated by determining the time exploring at the objects. The discrimination ratio describes the time a mouse explored the novel object divided by the total time it spent exploring (novel and familiar objects). The above experiments were carried out blindly.

4.2.10 Computational image analysis

Basic image processing of fluorescence signals was performed using the NIS Elements AR 4.13 software (Nikon); ZEN 2012 black software (Zeiss, Germany) and Fiji (ImageJ https://imagej.nih.gov/ij/; NIH). Colocalization analysis was processed with the customized program ImageTrak (345) written by PKS. Electrophysiological recordings were acquired and analyzed using pCLAMP 10.4 (Molecular Devices; Sunnyvale CA). Behavioral video tracking was performed using SMART 3.0 (Panlab Harvard Apparatus; Barcelona Spain).

4.2.11 Statistical Analysis

All values shown are means ± standard error of means (SEM) unless indicated otherwise.

To test for differences between groups, we used unpaired Student's *t*-tests (two-tailed). P values smaller than 0.05 were considered to be statistically significant.

4.3 RESULTS

4.3.1 Specific localization of RyR2 in the brain using GFP-RyR2 knock-in mice and a novel GFP probe

Given the presence of all 3 RyR isoforms in the brain, it is difficult to specifically localize the RyR2 isoform in brain tissue. To circumvent these problems, we have generated a knock-in mouse model in which the RyR2 isoform is tagged by the green fluorescent protein (GFP). We performed confocal imaging of brain slices from the GFP-tagged RyR2 mice to directly visualize the location of the GFP-RyR2 isoform in hippocampus, a region known to be important for learning, memory, and cognition. As shown in Figure 25, strong green fluorescence signals were detected in the hippocampus in GFP-RyR2 brain slices (Figure 25Aa). In contrast, only weak auto-fluorescence green signals were detected in similar areas of brain slices from wild-type (WT) littermates (i.e. without GFP) (Figure 25Ad). Confocal imaging with higher magnification further revealed the location of GFP-RyR2s in the soma and dendrites of pyramidal shaped cells in the CA1 region (Figure 25Ba), and of granule cells in the dentate gyrus region (Figure 35A) in hippocampus. Again, only weak auto-fluorescence green signals were detected in the CA1 and dentate gyrus regions in WT brain slices (Figure 25Bd and Figure 35D).

To further minimize auto-fluorescence green signals and to increase the sensitivity and specificity of GFP detection, we generated a red fluorescent, GFP-specific probe in which a GFP-binding protein (GBP) (or GFP-nanobody) was fused to the C-terminus of the maltose-binding protein (MBP). This MBP-GBP fusion protein was expressed, purified, and labelled with Alexa Fluor 647 (AF647) dye. To test the specificity of this novel GFP probe, we incubated the GFP probe with fixed ventricular myocytes isolated from the GFP-RyR2 mouse hearts. As shown in Figure 34, GFP-RyR2s in ventricular myocytes form clusters that are organized in a

highly ordered striated pattern. Importantly, the signals of the red GFP probe detected in ventricular myocytes are superimposed with those of the GFP (Figure 34). Similarly, we found that the red GFP probe signals detected in the CA1 and dentate gyrus regions in the GFP-RyR2 brain slices are also superimposed with those of the GFP (Figure 25Ba, b, c and Figure 35A, B, C). On the other hand, little or no red GFP probe signals were detected in the same areas of WT (no-GFP) brain slices (Figure 25Bd, e, f and Figure 35D, E, F). Taken together, these data indicate that the AF647-labelled MBP-GBP fusion protein is a highly specific probe for GFP-RyR2 in brain slices. These results also demonstrate that RyR2s are highly expressed in cells in the areas of CA1 and dentate gyrus of the hippocampus.

4.3.2 Subcellular localization of RyR2 in hippocampal neurons using confocal imaging

Functional studies have suggested that RyRs play an important role in Ca2+ handling in various compartments in hippocampal neurons (285, 295, 317). However, it is unclear whether the RyR2 isoform is involved in Ca2+ handling in all or only some specific neuronal compartments. To address this question, we first determined the subcellular localization of GFP-RyR2 in hippocampal neurons by performing co-localization analysis of GFP-RyR2 with well-established markers for different neuronal compartments. Using our novel and specific GFP probe, we found that there is little or no co-localization of GFP-RyR2 signals with synaptophysin or syntaxin staining, both of which are well-established markers for presynaptic terminals, in hippocampal CA1 neurons (Figure 26A, Figure 37A) and in granule cells of dentate gyrus (Figure 36A; Figure 37B). We also found only minimal/partial co-localization of GFP-RyR2 signals with phalloidin staining, a well-established marker for dendritic spines, in the hippocampal CA1 (Figure 26B) and dentate gyrus (Figure 36B) regions. In contrast, we found

that the GFP-RyR2 signals were extensively co-localized with the staining of the microtubule 2 associated protein 2 (MAP2), a well-established marker for postsynaptic sites (dendrites and soma), in the hippocampal CA1 (Figure 26C) and dentate gyrus (Figure 36C) regions. Clearly, the GFP-RyR2 signals were detected throughout dendritic shafts of CA1 pyramidal neurons and granule cells of dentate gyrus (Figure 26C, Figure 36C). These data indicate that the RyR2 isoform is specifically localized throughout the dendritic shaft and soma, but not at the presynaptic terminals or the dendritic spines of CA1 pyramidal neurons and dentate gyrus granule neurons in hippocampus.

4.3.3 Subcellular localization of RyR2 in hippocampal neurons using superresolution imaging

To further define the subcellular localization of RyR2, we performed co-localization studies of GFP-RyR2 and well-established neuronal markers using structured illumination microscopy (SIM)-based super-resolution imaging. As shown in Figure 27 and Figure 38, SIM superresolution imaging revealed fine details of staining of synaptophysin, phalloidin, MAP2, and GFP-RyR2 in hippocampal CA1 (Figure 27) and dentate gyrus (Figure 38) regions with staining patterns very similar to those observed using confocal imaging. Consistent with our findings using confocal imaging, SIM super-resolution imaging also showed that there is a minimal/partial overlap between the GFP-RyR2 signals and the synaptophysin or phalloidin staining signals in hippocampal CA1 (Figure 27A) or dentate gyrus (Figure 38A) regions. In contrast, there is an extensive overlap of signals of GFP-RyR2 and MAP2 staining in hippocampal CA1 (Figure 27A) and dentate gyrus (Figure 38A) regions. Quantitative analysis of colour overlap in SIM images showed that there is ~50% overlap between GFP-RyR2 and MAP2

signals, whereas, there is <5% overlap between GFP-RyR2 and synaptophysin or phalloidin signals in CA1 and dentate gyrus regions (Figure 27B, Figure 38B). Taken together, our confocal and super-resolution imaging studies clearly demonstrate that RyR2 is localized throughout the dendritic shaft and soma, but not at the presynaptic terminals or the dendritic spines in hippocampal CA1 neurons and in the granule cells of dentate gyrus.

4.3.4 The CPVT RyR2 mutation R4496C has no significant impact on presynaptic short-term facilitation

We next investigated how arrhythmogenic RyR2 mutations affect synaptic transmission. We first determined the impact of a CPVT-causing RyR2 mutation R4496C on presynaptic short term plasticity. The RyR2 R4496C mutation was identified in patients with CPVT and has been shown to enhance the sensitivity of RyR2 to Ca2+ activation (83, 86, 87, 267, 269). We performed the paired-pulse stimulation protocol to assess presynaptic short-term facilitation in hippocampal Schaffer collaterals in brain slices from RyR2 R4496C mutant and WT mice. As shown in Figure 28, there was no significant difference in paired pulse facilitation between the RyR2 R4496C mutant Schaffer collaterals and those of the WT (Figure 28A, B) with a paired pulse facilitation profile similar to that reported previously (346). Maximal facilitation (~160%) was observed at secondary pulses (P2) 40-60 ms after the initial pulse (P1) in both the WT and RyR2-R4496C mutant (Figure 28B). There were also no significant differences in the amplitude of Schaffer fiber volleys nor in the field excitatory postsynaptic potential (EPSP) slopes in relation to the current input between the WT and RyR2 R4496C mutant (Figure 28C, D), indicating that the WT and R4496C mutant hippocampal Schaffer collaterals exhibited similar basal synaptic activity. Thus, these observations demonstrate that the CPVT R4496C mutation

does not significantly affect presynaptic short-term plasticity, consistent with the absence of RyR2 expression at the presynaptic terminals.

4.3.5 The CPVT RyR2 R4496C mutation impairs long-term potentiation (LTP) in hippocampal Schaffer collaterals

Although RyR2s are absent at presynaptic terminals, they are highly expressed at postsynaptic sites. It is then possible that CPVT RyR2 mutations may affect postsynaptic plasticity. To test this possibility, we measured LTP at Schaffer collateral – CA1 synapses in brain slices from the CPVT RyR2 R4496C mutant mice and WT littermates. As shown in Figure 29, fEPSP slopes in response to stimulation of Schaffer collaterals in both the WT and R4496C mutant brain slices remained increased (≥ 130%) for at least 30 min after a train of high frequency stimulation (HFS), indicating the presence of long-term potentiation (LTP) (Figure 29A,B). However, the extent of LTP was significantly reduced in R4496C mutant compared to that in WT (Figure 29C). Again, there were no significant differences in the amplitudes of fiber volleys or fEPSP slopes in relation to the current input between WT and R4496C mutant brain slices. Therefore, these data support the notion that the CPVT RyR2 mutation impairs hippocampal LTP.

4.3.6 The CPVT RyR2 R4496C mutation impairs learning and memory

Given the link between hippocampal LTP and learning/memory, it is possible that CPVT-causing RyR2 R4496C mutation, which impairs hippocampal LTP, may also affect learning and memory. To test this possibility, we performed Morris water maze (MWM) tests on the mutant mice and their WT littermates (3-4 months) to evaluate their spatial learning and memory. As

shown in Figure 30, the RyR2 R4496C mice required significantly longer time than WT mice to find the submerged platform in the MWM task (Figure 30A) and spent significantly less time in the target quadrant in the probe test 24 hrs after the last training session (Figure 30B,C). It should be noted that there is no difference in the mean swim speed between the WT and RyR2 R4496C mutant mice (Figure 39), indicating similar locomotion performance in WT and R4496C mice. We also carried out novel object recognition (NOR) tests to evaluate their capability in object recognition and memory. We found that the RyR2 R4496C mutant mice spent significant less time exploring the novel object than WT mice (Figure 30D). Note that both WT and R4496C mutant mice showed no side preference in the NOR tests (Figure 39B), and that there is no significant difference in the exploration time between WT and R4496C mutant mice (Figure 39C). Collectively, these results indicate that the CPVT RyR2 R4496C mutation impairs both hippocampal LTP, learning, and memory.

4.3.7 The CPVT RyR2 R4496C mutation increases spontaneous Ca2+ transients in hippocampal CA1 neurons.

Neuronal excitability is believed to be a critical determinant of LTP, learning, and memory (2, 347, 348). It is thus reasonable to propose that impairment in LTP, learning, and memory observed in the R4496C mutant mice may result from altered neuronal excitability. To test this hypothesis, we crossed the RyR2 R4496C mutant mice with *Thy1* GCaMP6f transgenic mice that express a genetically encoded fluorescence Ca2+ indicator GCaMP6f (349). Under the control of the *Thy1* promoter, the GCaMP6f protein is highly expressed in neurons in the hippocampus and cortex, and is capable of reporting both spontaneous and evoked Ca2+ transients (350–352). We then assessed the neuronal excitability of hippocampal CA1 neurons in

brain slices from RyR2 WT/GCaMP6f and RyR2-R4496C/GCaMP6f mice by monitoring spontaneous Ca^{2+} transients that are known to result from the firing of action potentials (APs) in neurons (353–355). As shown in Figure 31, among the hippocampal CA1 neurons that responded to KCl depolarization, only a small fraction of these KCl responsive neurons in WT brain slices showed spontaneous Ca^{2+} transients at rest (Figure 31A, C, D). Note that here KCl depolarization was used to localize active neurons. On the other hand, the fraction of KCl-sensitive hippocampal CA1 neurons that exhibited spontaneous Ca^{2+} transients in RyR2-R4496C mutant brain slices at rest was markedly increased (Figure 31B, D, E) compared to that in WT (54.7±5.9% in R4496C vs 22.1±4.6% in WT, $P<0.01$). The average cumulative duration of spontaneous Ca^{2+} transients in R4496C hippocampal CA1 neurons was also significantly longer than that in WT (Figure 31F). These results indicate that CPVT RyR2 R4496C mutation increases the occurrence of spontaneous Ca^{2+} transients, suggesting increased neuronal excitability.

4.3.8 The CPVT RyR2 R4496C mutation increases spontaneous and triggered action potential (AP) firing in hippocampal CA1 neurons

To directly assess the impact of CPVT RyR2 R4496C mutation on neuronal excitability, we performed single cell patch clamp recordings in hippocampal CA1 pyramidal neurons in brain slices from the WT and RyR2 R4496C mutant mice. As shown in Figure 32, spontaneously firing APs were detected in both WT and R4496C mutant hippocampal CA1 pyramidal neurons. However, the fraction of CA1 pyramidal neurons that displayed spontaneous AP firing was substantially higher in R4496C brain slices than in WT (Figure 32A, B) ($P <0.05$). Furthermore, the current threshold required to trigger AP firing in R4496C mutant CA1 pyramidal neurons by

current injection was significantly lower than that needed to trigger AP firing in WT neurons (Figure 32C, D, E) ($P<0.05$). The frequency of current-triggered APs in R4496C mutant CA1 pyramidal neurons was markedly increased compared to that in WT neurons (Figure 32C, D, F) ($P<0.05$). These data demonstrate that the CPVT R4496C mutation increases neuronal excitability of hippocampal CA1 pyramidal neurons.

4.3.9 Basal activity-dependent LTP induction in RyR2 R4496C mutant hippocampal CA1 neurons

The CPVT RyR2 R4496C mutation resulted in impaired hippocampal LTP and increased neuronal excitability in hippocampal CA1 neurons. This suggests a potential link between enhanced neuronal excitability and impaired LTP. To test this potential link, we measured LTP in hippocampal Schaffer collaterals in brain slices from the RyR2 R4496C mutant and WT mice with low and high basal stimulation current before high frequency stimulation (HFS). As shown in Figure 33, when a small basal stimulation current (20 μA) was used, significant LTP (>130%) could be induced by HFS in RyR2 R4496C mutant hippocampal Schaffer collaterals, although it was much smaller than that in WT (Figure 33A). However, no LTP in R4496C mutant hippocampal Schaffer collaterals could be induced by HFS when a larger basal stimulation current (100 μA) was applied, whereas, significant LTP could still be induced in WT hippocampal Schaffer collaterals under the same conditions (Figure 33B). These data indicate that LTP induction in RyR2 R4496C mutant hippocampal Schaffer collaterals is highly sensitive to the strength of basal stimulation. These results also suggest that the impaired hippocampal LTP, learning, and memory observed in RyR2 R4496C mutant mice may result from the increased neuronal excitability.

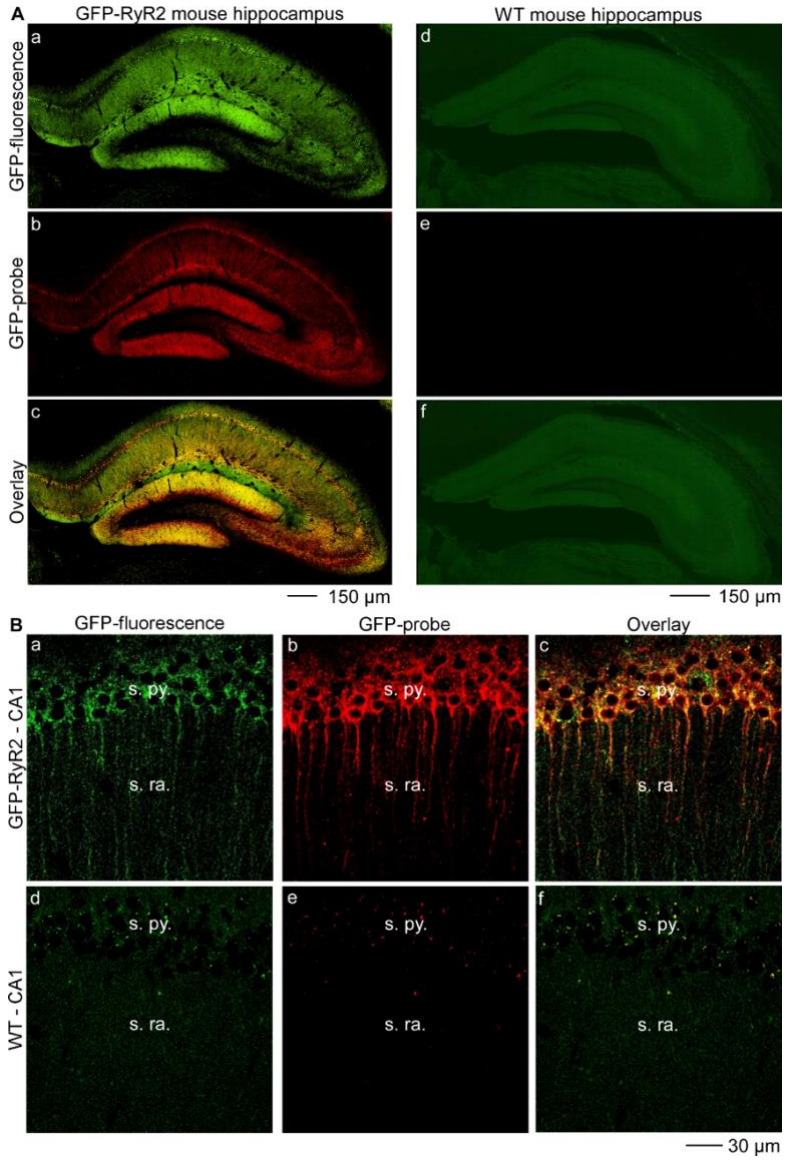

Figure 25 Subcellular localization of GFP-RyR2 in hippocampus

Representative confocal fluorescence images of hippocampus in brain slices (150 µm) from mice expressing the GFP-tagged RyR2 (Aa-c) and WT littermate (Ad-f) are shown (n = 16 from 8 brains). GFP-fluorescence (Aa,d), GFP-probe staining (Ab,e), and overlay of the GFP and GFP-probe signals (Ac,f) are depicted. GFP-fluorescence (Ba,d), GFP-probe staining (Bb,e), and overlay of the GFP and GFP-probe signals (Bc,f) in the stratum pyramidale (s.py) and stratum radiatum (s.ra.) areas in the hippocampal CA1 region in brain slices from mice expressing the GFP-tagged RyR2 (Ba-c) and WT littermate (Bd-f) are shown (n = 25 from 8 brains) (unpublished manuscript).

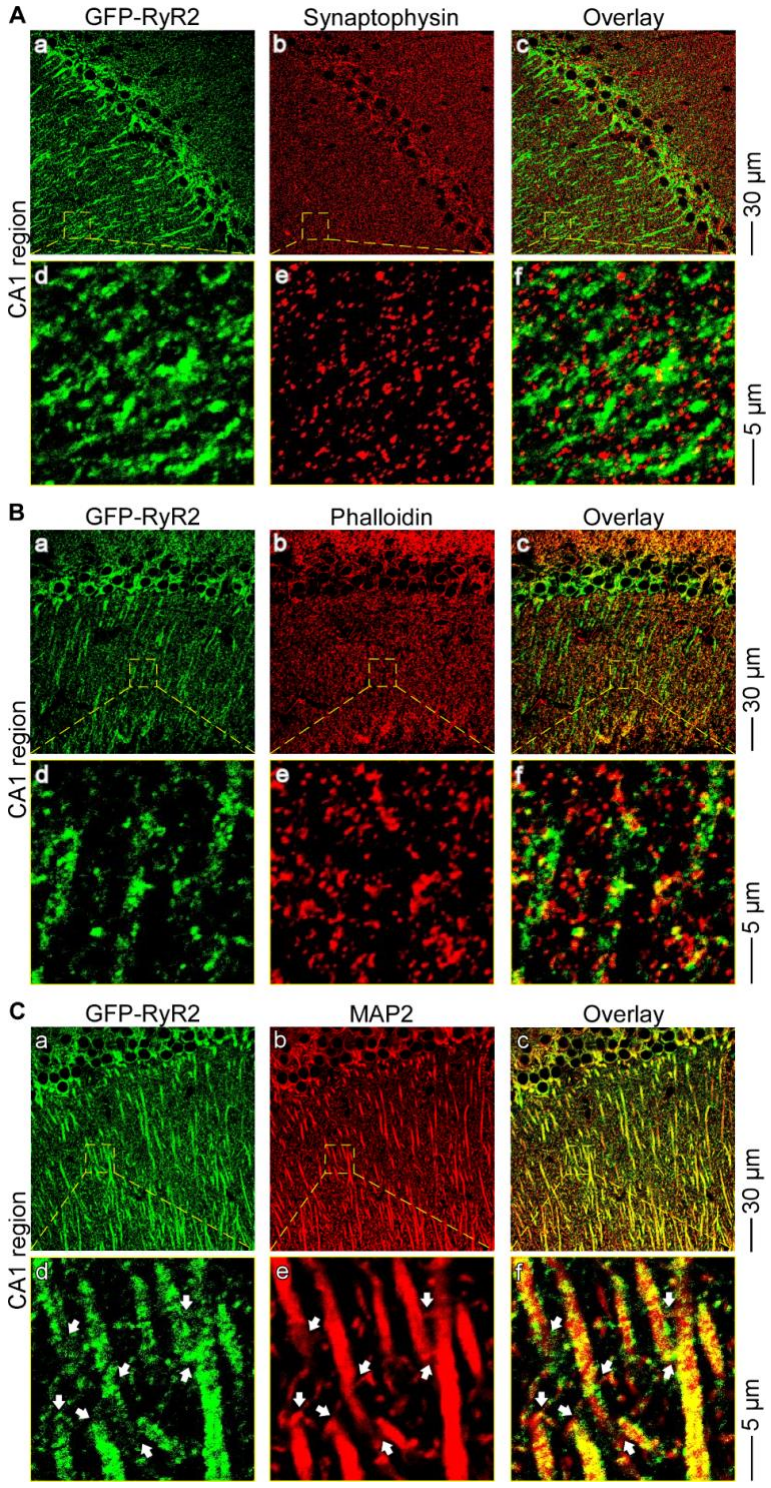

Figure 26 Co-localization of GFP-RyR2 with synaptic markers in hippocampal CA1 region using confocal imaging

Representative high-resolution confocal fluorescence images of hippocampal CA1 region in

brain slices from mice expressing a GFP-tagged RyR2 that were co-stained with the GFP-probe (displayed in green) and the presynaptic major vesicle protein synaptophysin (A); the F-actin targeting phalloidin (B); or the microtubule-associated protein 2 (MAP2) (C) are shown (n = 30 from 8 brains). GFP-probe staining (a,d), synaptic marker staining (b,e) and overlay of the GFP-probe and synaptic marker signals (c,f) are depicted. Dendritic branch points are indicated by white arrows (Cd-f). (unpublished manuscript).

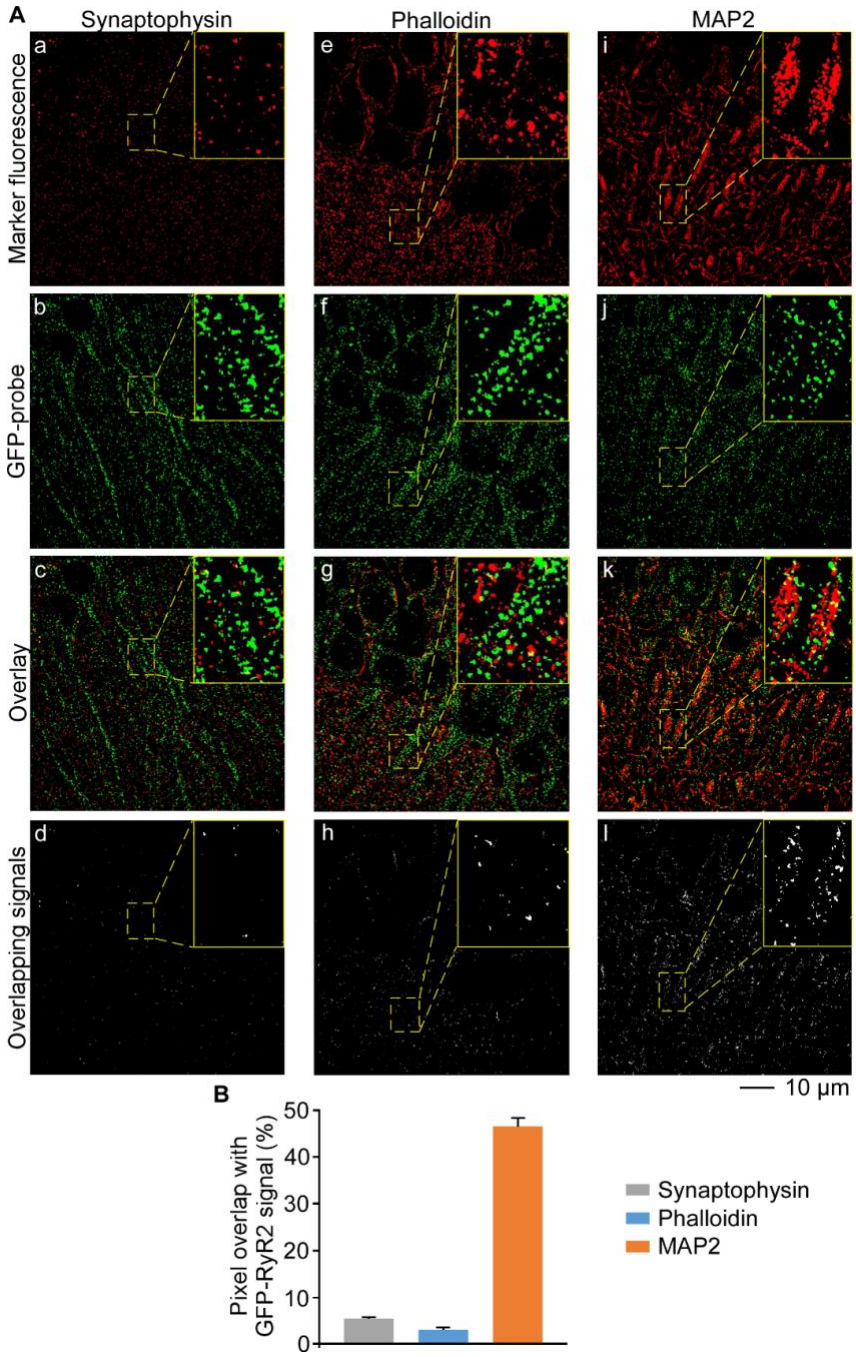

Figure 27 Co-localization of GFP-RyR2 with synaptic markers in hippocampal CA1 region using super-resolution imaging

The co-localization of GFP-RyR2 and synaptic markers was determined using structured-illumination microscopic (SIM) imaging of the hippocampal CA1 region. Brain slices were prepared from GFP-RyR2 mice and co-stained with the presynaptic major vesicle protein

synaptophysin (Aa-d), the F-actin targeting phalloidin (Ae-h), or the microtubule-associated protein 2 (MAP2; Ai-l). The synaptic marker fluorescence (Aa,e,i), GFP-probe staining (Ab,f,j), overlay of the GFP-probe and synaptic marker signals (Ac,g,k), and the extent of overlapping signals between the GFP-probe and synaptic markers (Ad,h,l) are shown. Overlapping signals between GFP-RyR2 and synaptophysin, phalloidin or MAP2 were quantified in panel B. Data shown are mean ± SEM (n = 6 images from 3 brains). (unpublished manuscript).

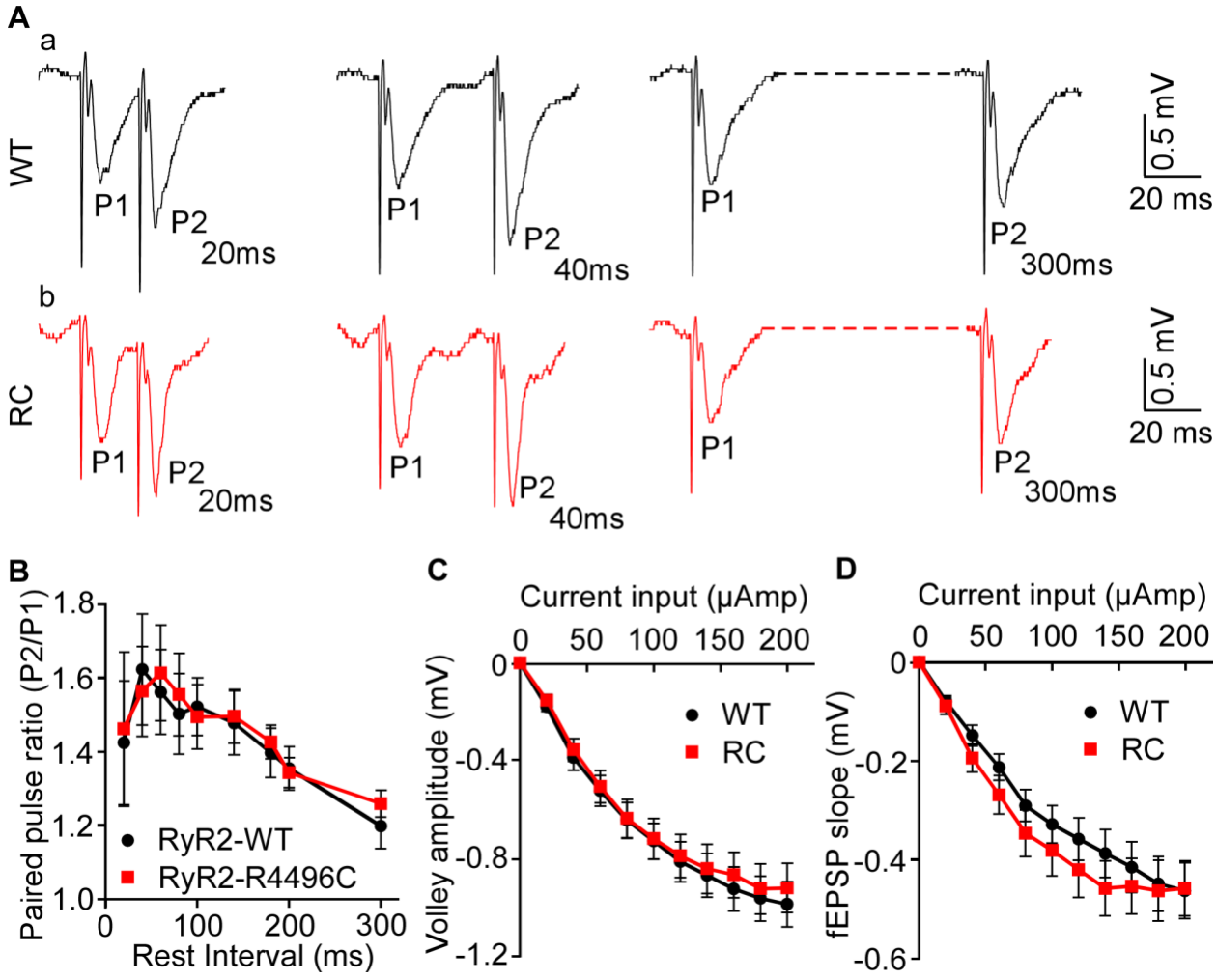

Figure 28 CPVT RyR2 Mutation R4496C has no significant effect on presynaptic short-term facilitation

Representative traces of paired pulse recordings in Schaffer collaterals in dorsal hippocampal slices from RyR2 WT (Aa) and RyR2-R4496C (RC) mutant (Ab) mice (3-4 months old) are shown. Stimulus input current for Schaffer collaterals was 60 µA. The relationship between paired pulse ratio and rest interval in WT and R4496C mutant brain slices is shown in panel B. Note that there are no significant differences in the amplitude of fiber volleys (C) or in the fEPSP slopes (D) in relation to the current input between the WT and RyR2 R4496C mutant brain slices. Data shown are mean ± SEM (n = 10 slices from 8 WT and 7 RC brains)

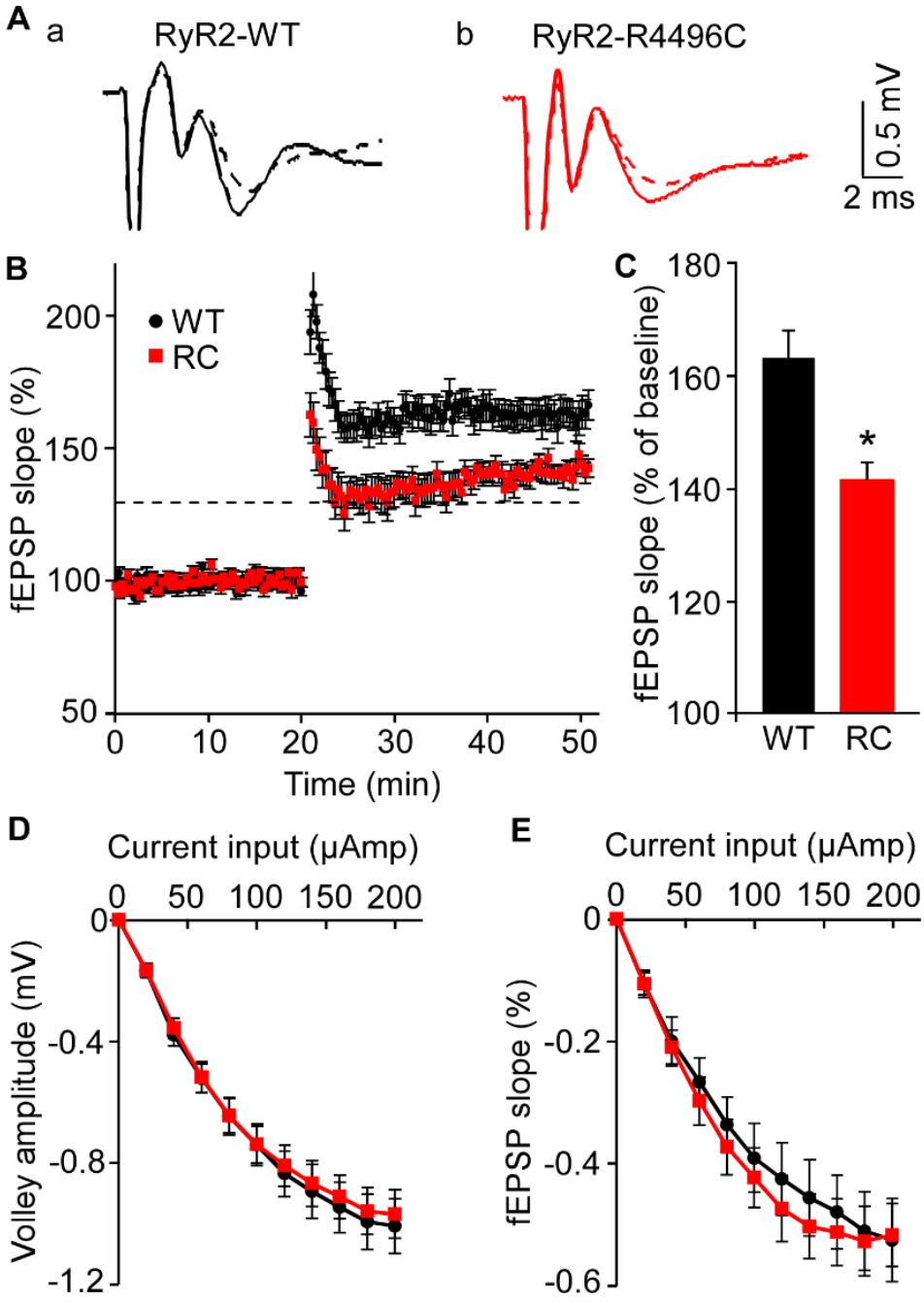

Figure 29 Impairment of long-term potentiation in the Schaffer Collaterals of CPVT RyR2 R4496C mutant brain

Synaptic response to tetanic high-frequency stimulation (HFS, 4 trains of 100 pulses at 100 Hz with 20s intervals) was assessed using field excitatory postsynaptic potential (fEPSP) recordings in the CA3-CA1 neuronal connections of RyR2 WT and R4496C mutant mouse brain slices (3-4

months old). The baseline was recorded for at least 20 min. Synaptic potentiation was determined by measuring the slope of the evoked fEPSP as percentage of the baseline before and 30 min after a HFS. (A) Representative fEPSP traces under basal conditions (dashed lines) and after HFS (solid lines) in WT (Aa) and R4496C mutant (Ab) brain slices. (B) fEPSP slopes in Schaffer collaterals in both the WT and R4496C mutant brain slices remained increased (≥ 130% indicated by the dashed line in Ba) for at least 30 min after HFS. (C) Average fEPSP slopes in WT and R4496C mutant brain slices (at 40-50 min). Note that there are no significant differences in the amplitude of fiber volleys (D) and fEPSP slopes (E) in relation to the current input between WT and R4496C mutant brain slices. Data shown are mean ± SEM (n = 14 brain slices from 7 WT, and 15 brain slices from 8 R4496C) (*P<0.01). (unpublished manuscript).

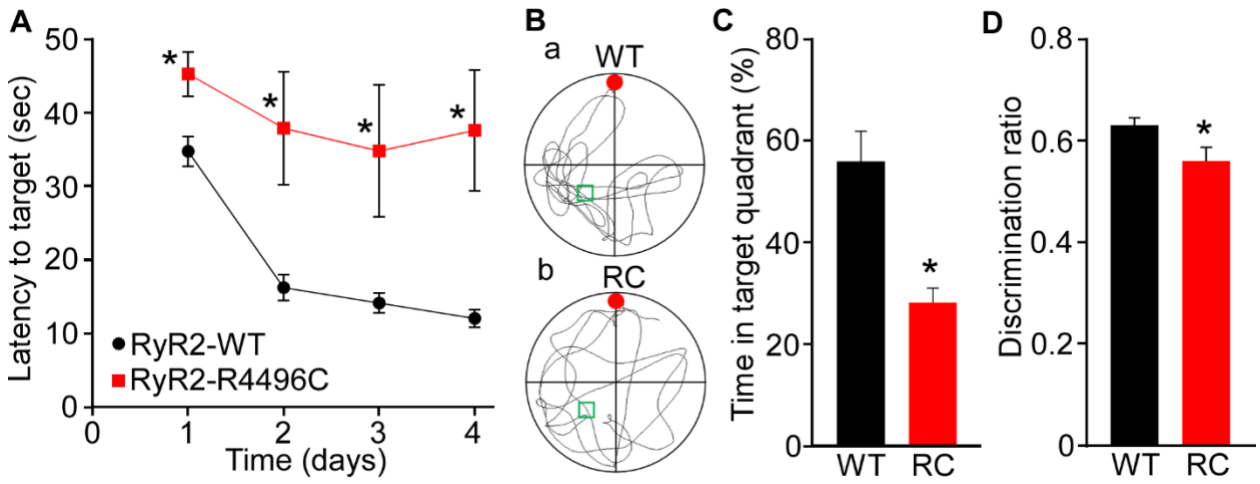

Figure 30 Cognitive Deficits in mice harboring CPVT RyR2 Mutation R4496C

Spatial learning was assessed in mice harboring the CPVT-linked RyR2 R4496C mutation (RC) and WT littermates using the Morris water maze (MWM) test. (A) The latency to reach the target escape platform during the training period (days 1-4) of RyR2-WT and RyR2-R4496C mice. (B) Representative swimming traces in MWM test of the WT (Ba) and RyR2-R4496C mutant (Bb) mice. Red sphere indicates entry point. Green square indicates the position of the platform. (C) Time spent in the target quadrant (bottom left quadrant) after removing the platform (green square) in the probe test 24-hr after the last training session. (D) The percentage of time spent in the novel object during the Novel Object Recognition (NOR) test in WT and R4496C mutant mice. Data shown are mean ± SEM (n = 8 for WT and 8 for R4496C) (*P<0.05). (unpublished manuscript).

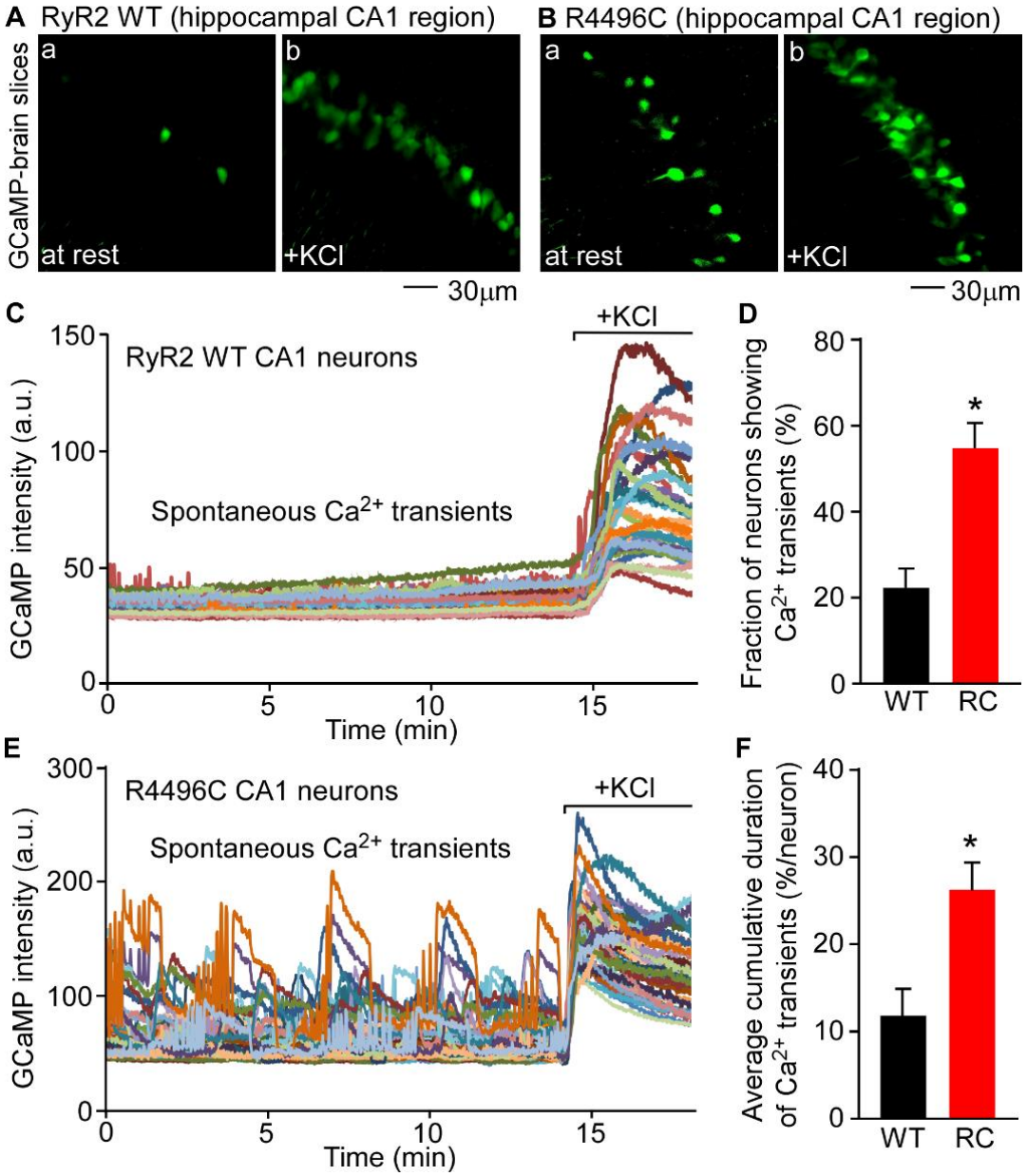

Figure 31 CPVT RyR2 mutation R4496C enhances spontaneous Ca2+ transients in hippocampal CA1 neurons.

Hippocampal brain slices (300 μm thick) were prepared from RyR2 WT and R4496C mutant mice (3-4 months old) expressing the GCaMP6f Ca2+ sensing probe. GCaMP6f fluorescence signals from individual hippocampal CA1 neurons were continuously recorded at the resting condition (spontaneous Ca2+ transients) for 15 min, followed by the addition of KCl (50 mM) (KCl-induced Ca2+ transients) using the Nikon A1R laser confocal microscope in the XY-scan

mode. (A, B) GCaMP fluorescence images of hippocampal CA1 neurons in RyR2 WT (A) and R4496C mutant (B) mouse brain slices at rest (a) and after KCl perfusion (b). Fluorescence traces of spontaneous and KCl-induced Ca2+ transients in individual RyR2 WT (C) and R4496C (E) CA1 neurons are shown. (D) The fraction (%) of neurons showing spontaneous Ca2+ transients under the resting condition (i.e. the percentage of neurons showing spontaneous Ca2+ transients among all neurons responded to KCl). (F) Total duration of spontaneous Ca2+ transients (%) was defined as the percentage of total duration of spontaneous Ca2+ transients over the period of 15 min recording at rest (%, total Ca2+ transient duration/neurons/15min-recording period). Data shown are mean ± SEM (n = 13 slices from 3 WT brains with 431 neurons, and n = 13 slices from 4 R4496C brains with 392 neurons) (*P<0.01). (experiment conducted by Dr. Sun; unpublished manuscript).

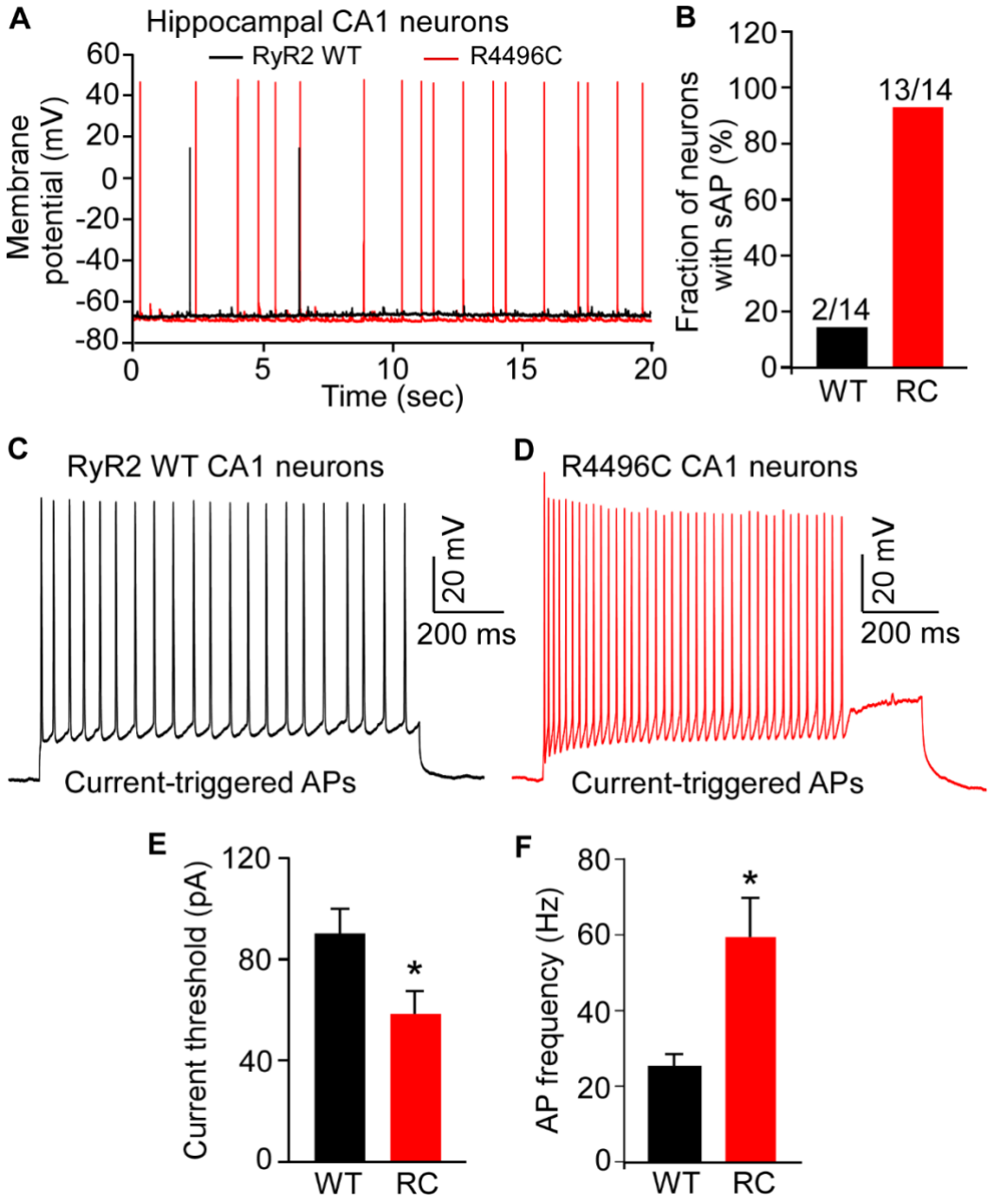

Figure 32 CPVT RyR2 mutation R4496C enhances spontaneous and triggered action potential firing in hippocampal CA1 neurons.

Hippocampal brain slices (260 µm thick) were prepared from RyR2 WT and R4496C mutant mice (3-4 months old). Action potential firing was recoded using whole-cell patch clamp with an Axopatch 200B amplifier. (A) Representative traces of membrane potential recordings showing spontaneous action potential (sAP) firing in RyR2 WT (black trace) and R4496C mutant (red trace) mouse hippocampal CA1 neurons. (B) Fraction (%) of RyR2 WT and R4496C (RC) CA1

neurons displaying sAP firing. Note that the GOF RyR2 mutation R4496C markedly increases the percentage of CA1 neurons showing sAP firing. (C, D) Representative traces of membrane potential recordings showing AP firing after current injection of 150 pA into the RyR2 WT (C) and R4496C mutant (D) hippocampal CA1 neurons. (E) Current threshold (pA) was defined as the minimum current injection required to trigger the first AP firing in WT and R4496C (RC) mouse hippocampal CA1 neurons. Note that the R4496C mutation reduces the current threshold for triggering AP firing. (F) The frequency of current injection-triggered APs. Not that the R4496C mutation increases the AP firing frequency in hippocampal CA1 neurons. Data shown are mean ± SEM (n = 14 neurons in slices from 3 WT brains, and n = 14 neurons in slices from 3 R4496C brains) (*$P<0.05$). (experiment conducted by Dr. Yao; unpublished manuscript).

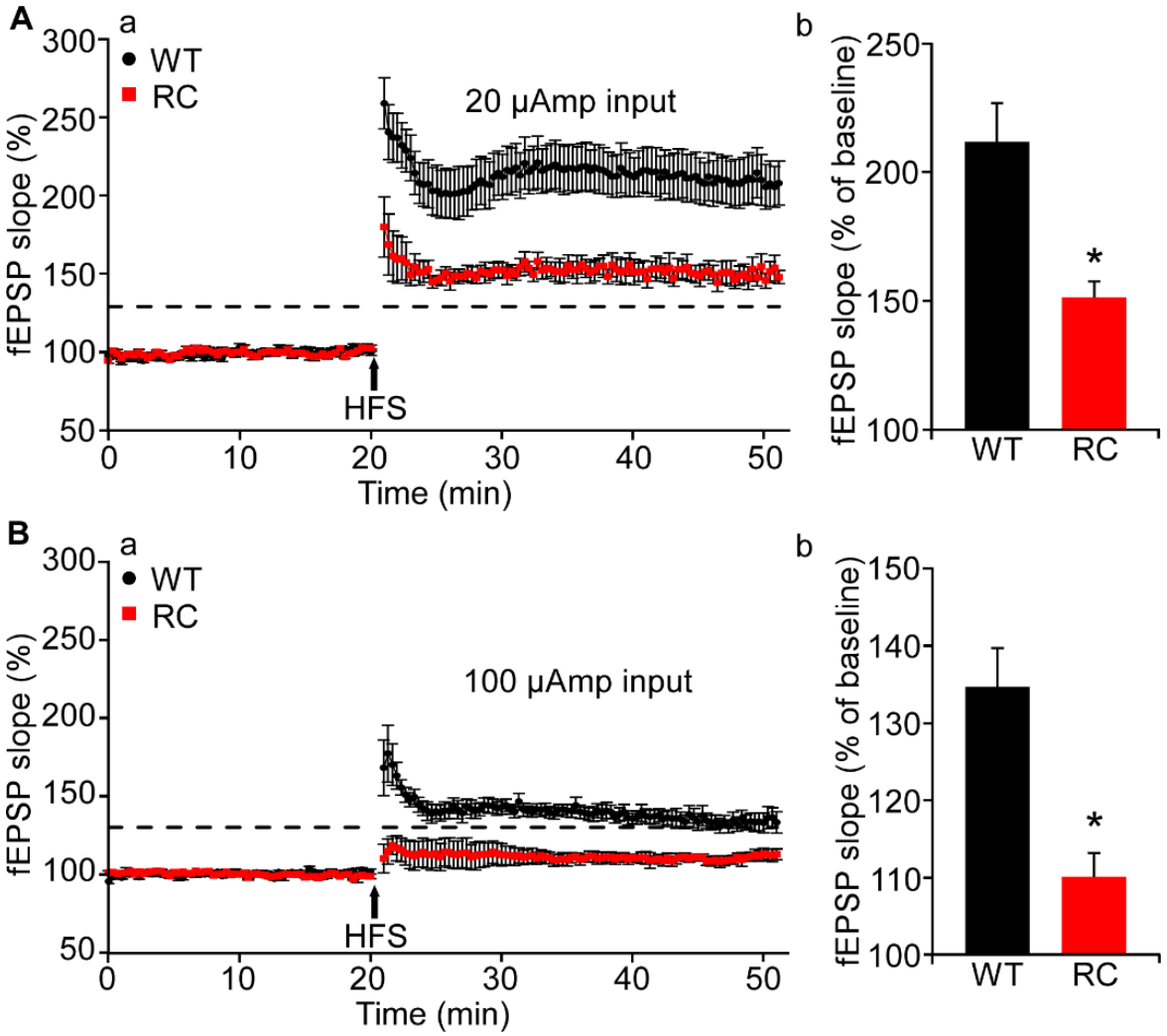

Figure 33 Effect of basal stimulation on LTP induction in RyR2 WT and R4496C mutant hippocampal CA3-CA1 pathway

Synaptic transmission in response to tetanic high-frequency stimulation (HFS; 4 trains of 100 pulses at 100 Hz, with 20-sec intervals) was assessed in Schaffer collaterals of RyR2 WT and R4496C (RC) mutant brain slices (300 µm; 3-4 months) after conditioning with 20 µAmp (A) (n = 7 brain slices from 4 WT mice, and n = 6 brain slices from 3 R4496C mice) and 100 µAmp (B) (n = 5 brain slices from 3 WT mice, and n = 6 brain slices from 4 R4496C mice) current input. Average slopes (20min) of baseline field excitatory postsynaptic potentials (fEPSP) were compared to average slopes of the fEPSP recorded 20 to 30 min after HFS as percentage of the baseline (Ab and Bb). Dashed lines indicate 130% LTP. Data shown are mean ± SEM (*P<0.01). (unpublished manuscript).

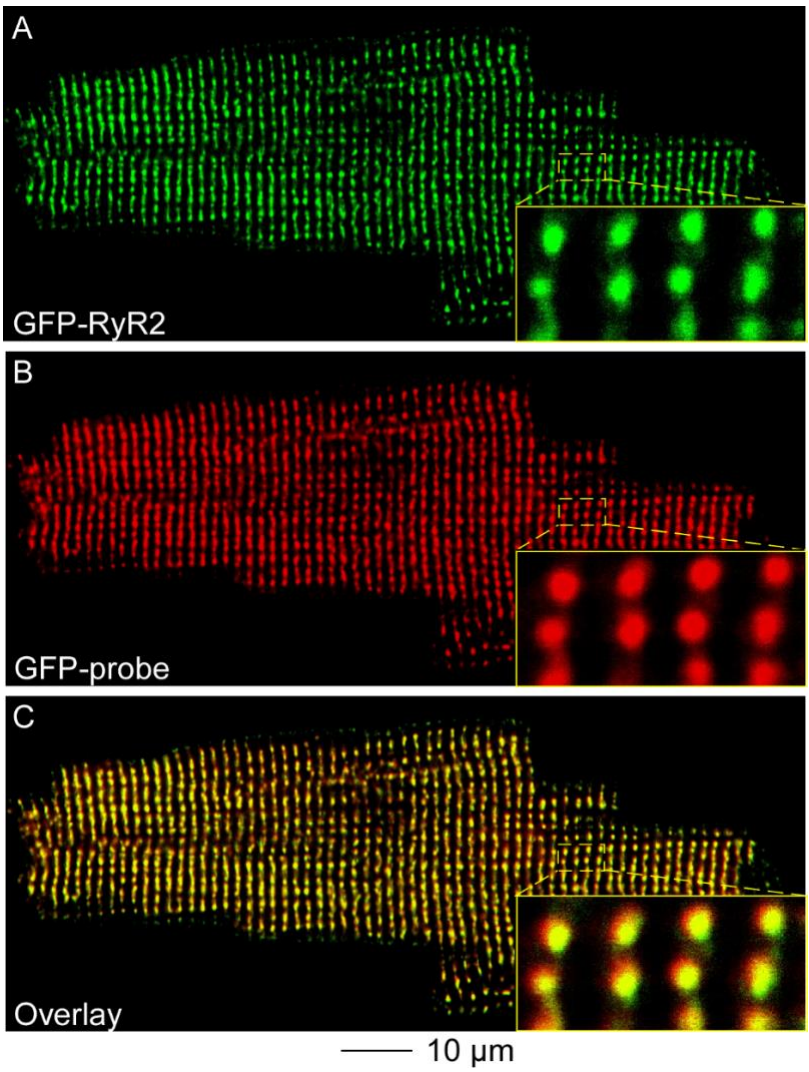

Figure 34 Co-detection of GFP fluorescence and GFP-probe staining in ventricular myocytes isolated from the GFP-RyR2 mice

Representative confocal images of ventricular myocytes isolated from GFP-RyR2 expressing mice are displayed. Localization of GFP-RyR2 by virtue of the GFP fluorescence (A) and signals of AF647 conjugated GFP-probe (B) showed typical single-rowed arrays of RyR2 clusters in the interior of ventricular myocytes. (C) Signal overlap between GFP-RyR2 and GFP-probe fluorescence. (unpublished manuscript).

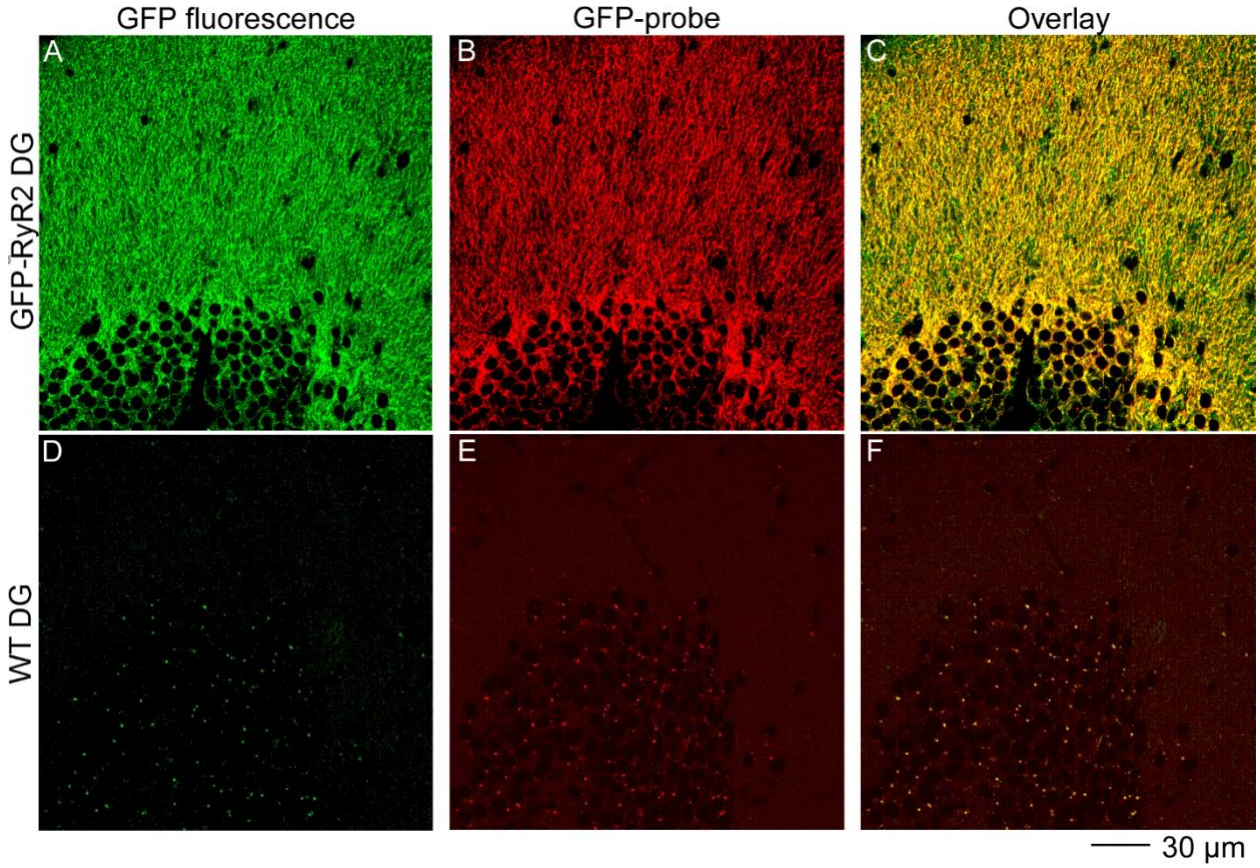

Figure 35 Subcellular localization of GFP-RyR2 in hippocampal dentate gyrus granule neurons in brain slice

Representative high-resolution confocal images of the dentate gyrus (DG) in GFP-probe labelled brain slices (150 µm) are shown. GFP-RyR2 fluorescence (A) and GFP-probe signals (B) overlap in the dendrites and soma of granule-shaped cells in DG (C). There are little GFP-RyR2 fluorescence (D), GFP-probe signals (E), or overlay of these signals (F) in DG in WT brain slices (n = 25 from 8 brains). (unpublished manuscript).

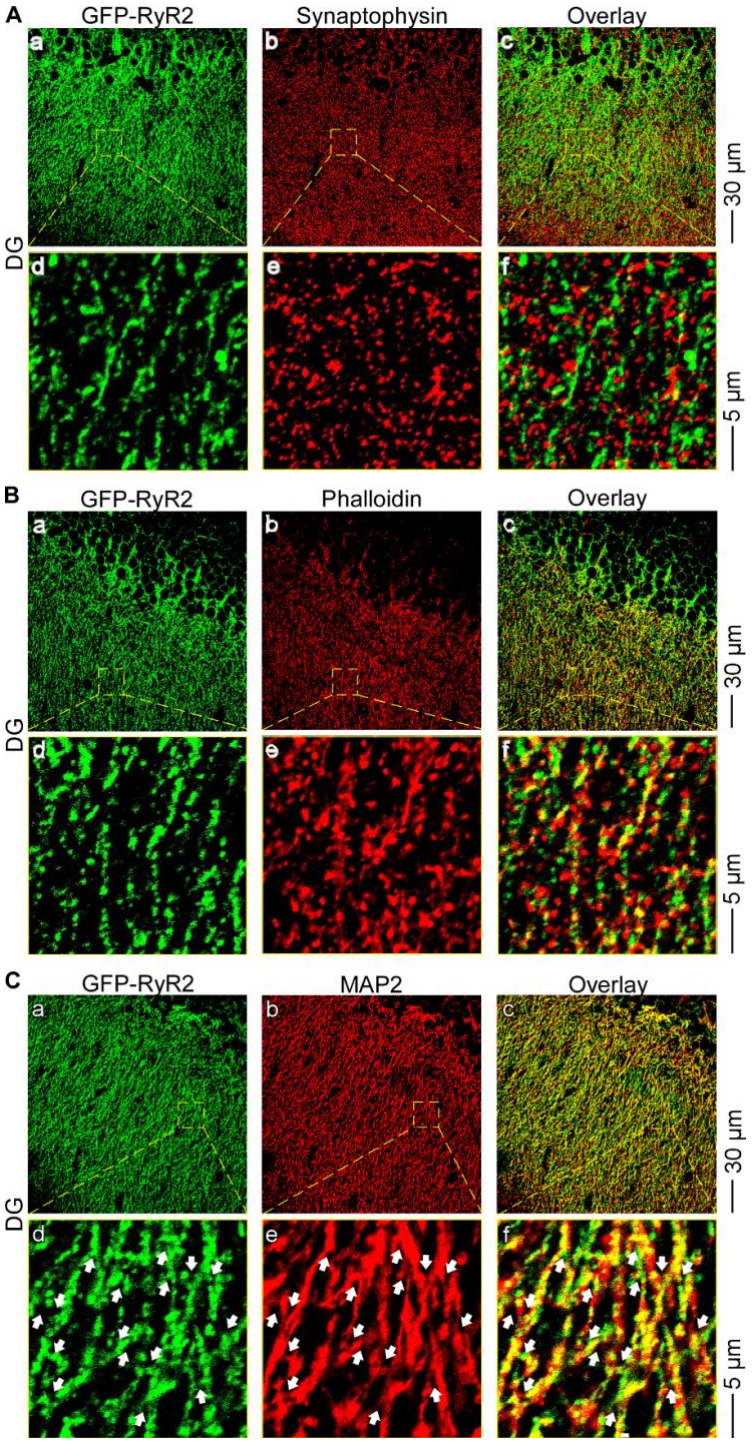

Figure 36 Co-localization of GFP-RyR2 with synaptic markers in hippocampal dentate gyrus region using confocal imaging

Representative high-resolution confocal fluorescence images of hippocampal dentate gyrus region in brain slices from mice expressing a GFP-tagged RyR2 that were co-stained with the

GFP-probe (displayed in green) and the presynaptic major vesicle protein synaptophysin (A); the F-actin targeting phalloidin (B); or the microtubule-associated protein 2 (MAP2) (C) are shown (n = 35 from 8 brains). GFP-probe staining (a,d), synaptic marker staining (b,e) and overlay of the GFP-probe and synaptic marker signals (c,f) are depicted. Dendritic branch points are indicated by white arrows (Cd-f). (unpublished manuscript).

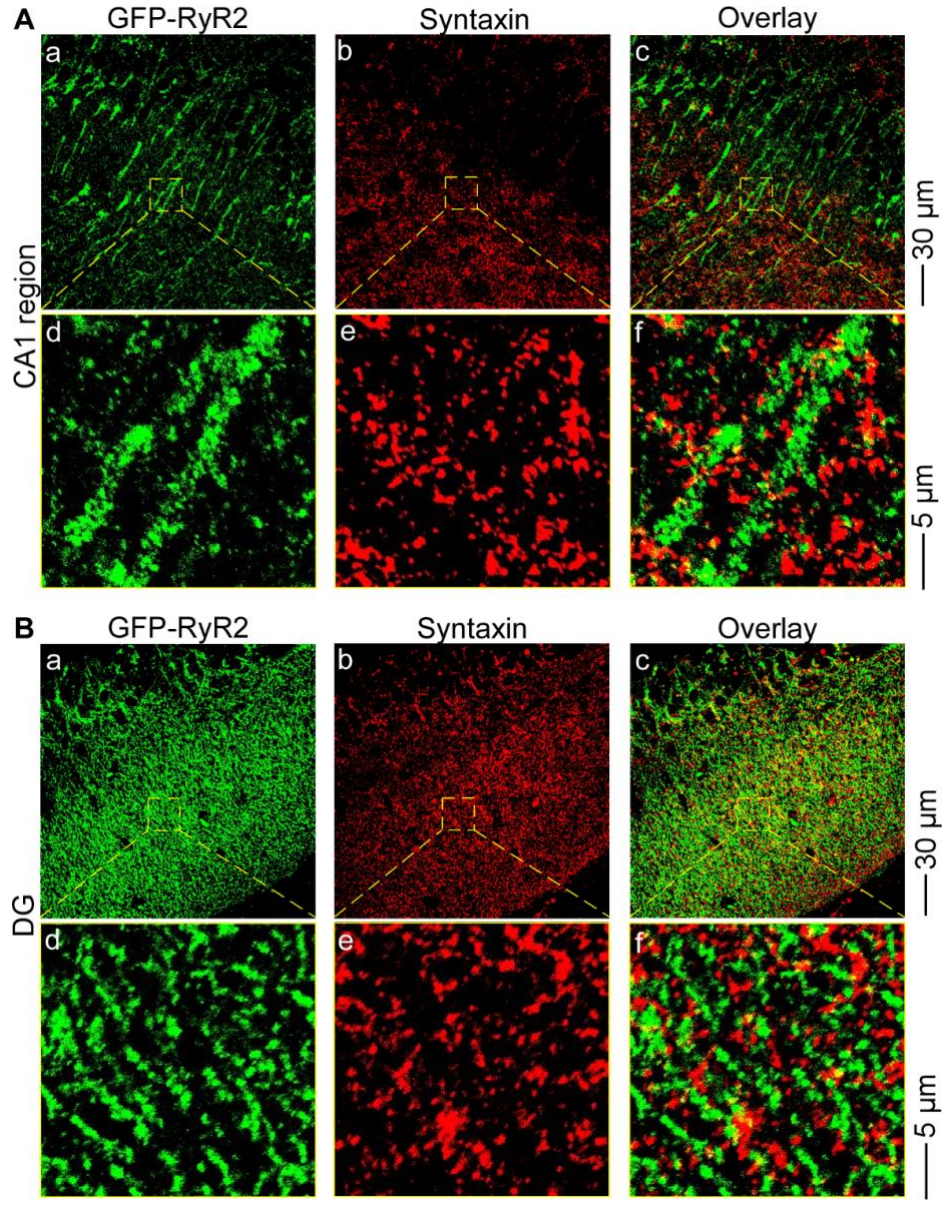

Figure 37 Localization of GFP-RyR2 and presynaptic vesicle fusion protein syntaxin in CA1 and dentate gyrus regions using confocal imaging

Representative high-resolution confocal fluorescence images of hippocampal CA1 (A) and dentate gyrus (B) regions in brain slices from mice expressing a GFP-tagged RyR2 that were co-stained with the GFP-probe (displayed in green) and the presynaptic vesicle fusion protein syntaxin are shown (n = 8 from 3 brains). GFP-probe staining (a,d), syntaxin staining (b,e) and overlay of the GFP-probe and syntaxin signals (c,f) are depicted. Not that there is only marginal

signal overlap between GFP-RyR2 and syntaxin signals in CA1 region (Ac,f) or in the DG region (Bc,f). (unpublished manuscript).

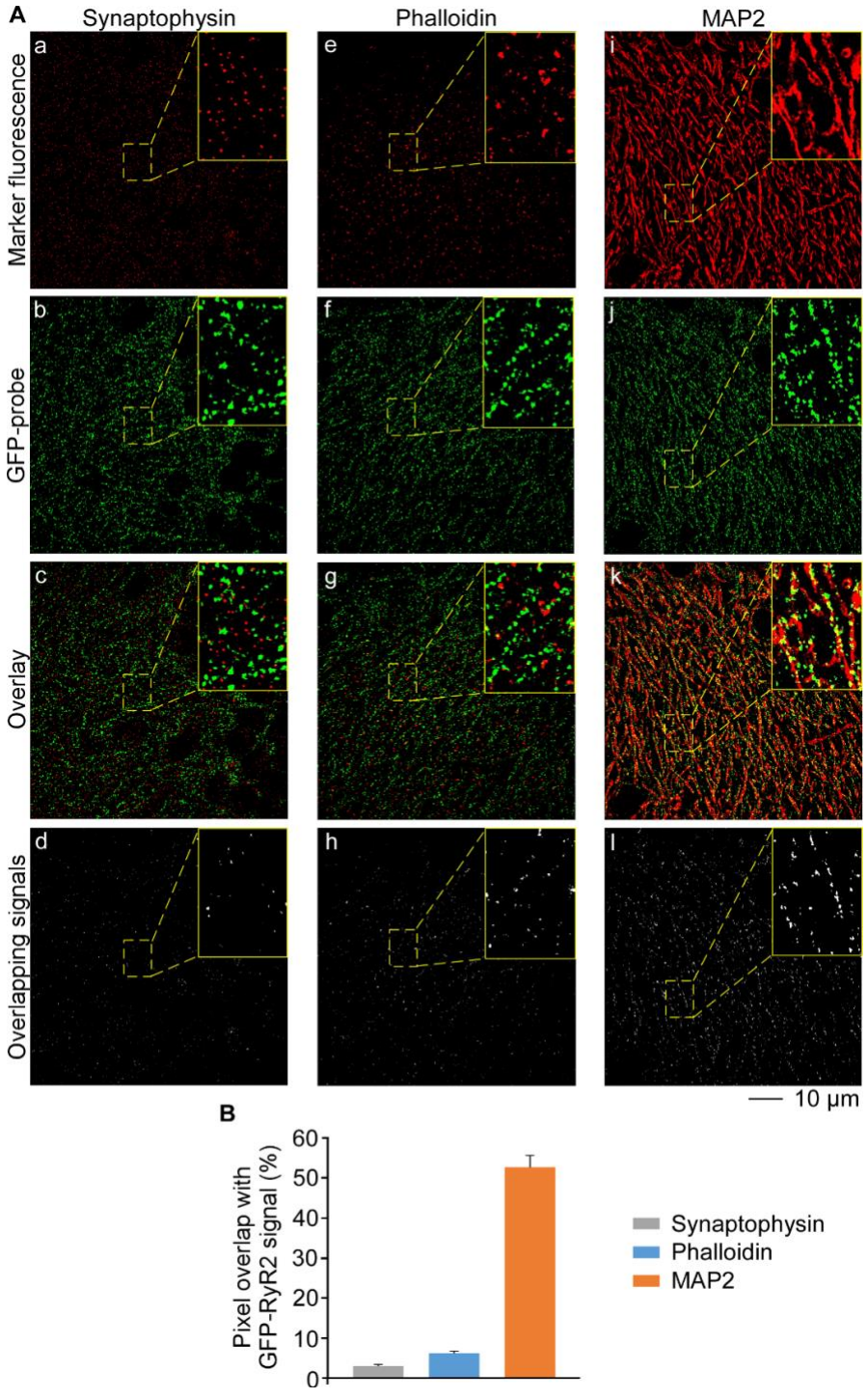

Figure 38 Co-localization of GFP-RyR2 with synaptic markers in hippocampal dentate gyrus region using super-resolution imaging

The co-localization of GFP-RyR2 and synaptic markers was determined using structured-illumination microscopic (SIM) imaging of the hippocampal dentate gyrus region. Brain slices

were prepared from GFP-RyR2 mice and co-stained with presynaptic major vesicle protein synaptophysin (Aa-d), the F-actin targeting phalloidin (Ae-h), or the microtubule-associated protein 2 (MAP2; Ai-l). The synaptic marker fluorescence (Aa,e,i), GFP-probe staining (Ab,f,j), overlay of the GFP-probe and synaptic marker signals (Ac,g,k), and the extent of overlapping signals between the GFP-probe and synaptic markers (Ad,h,l) are shown. Overlapping signals between GFP-RyR2 and synaptophysin, phalloidin or MAP2 were quantified in panel B. Data shown are mean ± SEM (n = 6 from 3 brains). (unpublished manuscript).

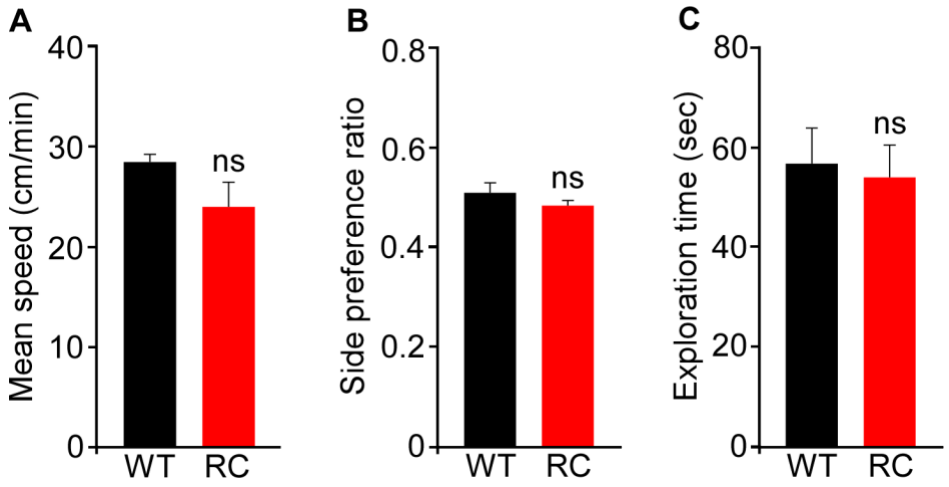

Figure 39 Effect of the CPVT RyR2 R4496C mutation on swimming speed, side preference, and exploration time

The mean swimming speed in Morris water maze test (A), and the side preference (B) and exploration time (C) in novel objective recognition test of WT and RyR2-R4496C mutant mice are shown. Note that there are no significant differences in these parameters between the WT and R4996C mutant mice. Data shown are mean ± SEM (n = 8 for WT, and 8 for R4496C) (ns, non-significant). (unpublished manuscript).

4.4 DISCUSSION AND CONCLUSION

Ryanodine receptor type 2 (RyR2) is predominantly expressed in the heart and brain (23). Given this tissue distribution, defective RyR2 function is expected to cause diseases in both the heart and brain. Indeed, enhanced RyR2 function as a result of naturally occurring mutations in RyR2 can lead to lethal cardiac arrhythmias, such as catecholaminergic polymorphic ventricular tachycardia (CPVT) (86). A number of CPVT RyR2 mutations have also been associated with intellectual disability and cognitive deficits (278–280). While the arrhythmogenic mechanisms of CPVT RyR2 mutations have been well understood, the mechanism by which CPVT RyR2 mutations cause cognitive dysfunction is unknown.

It is well known that $Ca2+$ signaling in neurons occurs locally in spatially segregated compartments with different functional roles (281, 282). Depending on their subcellular localization (presynaptic terminals, dendritic spines, dendritic shafts, or soma), RyRs could play a role in synaptic transmission, postsynaptic signaling, synaptic plasticity, or gene expression (285, 293, 295–301). Therefore, knowing the precise subcellular localization of RyRs is fundamental to the understanding of the functional roles of RyR-mediated local $Ca2+$ signaling in neurons.

Given its pivotal importance, the cellular and subcellular distributions of RyRs have been extensively investigated. RyRs have been shown to be expressed in different compartments, including presynaptic terminals, dendritic spines, dendritic shafts, and the soma in hippocampal neurons (286, 288, 290, 293, 294). However, despite these efforts, little is known about the precise subcellular distribution of the RyR2 protein in these neurons. Although anti-RyR2 antibodies have been used to localize RyR2 in the brain (286, 294), it is unclear whether these anti-RyR2 antibodies also recognize other proteins in the context of whole brain tissue. Hence,

the presence of different RyR isoforms in hippocampal neurons and the uncertain specificity of the antibodies used made the precise subcellular localization of the RyR2 protein difficult. To avoid these potential problems, we developed a novel platform to definitively localize RyR2 in brain tissue. We employed a knock-in mouse model that expresses a GFP-tagged RyR2 (333). The in-frame insertion of GFP into RyR2 allows us to distinguish RyR2 from the other RyR isoforms. Furthermore, we generated a novel AF647-conjugated, GFP-specific probe, which is composed of a GFP-binding protein (or anti-GFP nanobody) (239, 356) fused to the C-terminus of the maltose-binding protein. This novel fluorescent GFP-probe is highly specific for GFP, as it shows strong specific staining in GFP-RyR2 expressed heart and brain tissues, but little detectable signals in WT heart and brain tissues without the expression of GFP-RyR2. Using this novel platform and high resolution confocal and SIM super-resolution imaging, we unambiguously localized RyR2 in dendrites and the soma, but not in presynaptic terminals or dendritic spines, in pyramidal neurons in the hippocampal CA1 region and in granule cells of the dentate gyrus. Our unique GFP-RyR2 platform, therefore, uncovers a previously unappreciated pattern of subcellular distribution of RyR2.

This novel subcellular distribution of RyR2 has important implications for the role of RyR2 in neurons. Although a large number of studies have indicated the involvement of RyRs in presynaptic transmission in hippocampal Schaffer collaterals (295, 299, 300, 357–359), the specific role of RyR2 in this process is unclear. The absence of RyR2 in presynaptic terminals observed in our study would argue against a major role of RyR2 in presynaptic short-term plasticity. In support of this view, we found that genetically enhancing RyR2 function did not significantly alter presynaptic short-term facilitation. Similarly, the failure to detect RyR2 in dendritic spines also argues against a significant role that RyR2 may play in $Ca2+$ signaling in

dendritic spines. The RyR-mediated Ca2+ signalling in presynaptic terminals or dendritic spines of CA1 pyramidal neurons observed in previous studies may be attributable to other RyR isoforms (RyR1 and/or RyR3) (285, 295, 298, 300, 357, 358). However, direct comparison of isoform-specific functions has remained challenging due to methodologically restrains.

In the brain, RyR2 is most abundantly expressed in the hippocampal region as shown before (287–292). Consistent with its hippocampal expression, RyR2 has been shown to play a critical role in hippocampal LTP, learning, and memory (303–306, 360). Altered RyR2 function can lead to impaired LTP and cognitive deficits (314, 315). However, the impact of CPVT RyR2 mutations on hippocampal LTP induction, learning, and memory is completely unknown. To assess the effect of CPVT mutations on cognitive dysfunction, we employed a knock-in mouse model harboring a CPVT RyR2 R4496C mutation. We found that the CPVT RyR2 R4496C mutation exerted no significant effect on presynaptic short-term facilitation, but significantly impaired hippocampal long-term potentiation (LTP), learning, and memory. These observations are consistent with the intellectual disability observed in CPVT patients with RyR2 mutations. Furthermore, we found that this RyR2 R4496C mutation markedly increased the excitability of hippocampal neurons. Since neuronal excitability is thought to be a critical determinant of LTP, learning, and memory (2, 347, 348), our data suggest that CPVT RyR2 mutations may cause intellectual disability by impairing hippocampal LTP, learning, and memory as a result of enhanced neuronal excitability. Hence, our findings provide important new insights into the mechanism of cognitive dysfunction associated with CPVT RyR2 mutations.

In summary, in the present study, we established a novel platform for defining the subcellular expression and distribution of RyR2 in the brain. We demonstrated that RyR2 is specifically localized to the dendritic shafts and soma, but not the presynaptic terminals or

dendritic spines of hippocampal CA1 pyramidal and dentate gyrus granule neurons. We also showed that a CPVT-causing RyR2 mutation R4496C enhances neuronal excitability and impairs LTP, learning, and memory. Our data shed new insights into the mechanism of intellectual disability associated with CPVT RyR2 mutations. These results also have important implications for other neurological disorders associated with RyR2 dysfunction.

CHAPTER 5 DISCUSSION AND FUTURE DIRECTIONS

5.1 The distribution of functional RyR2 Ca2+ release units in the ventricular myocytes

ECC is one of the most fundamental processes in muscle physiology. In the heart, it describes the sophisticated mechanism underlying the coupling of plasma membrane depolarization to intracellular Ca2+ release that ultimately leads to cardiac contraction (3, 320). Extensive research over the past decade provided evidence to advance our understanding of the signaling pathway during ECC. CICR has been identified as a key element in this process allowing the amplification of Ca2+ influx via RyR2-mediated Ca2+ release from the SR. In normal heart cells CICR is graded and tightly controlled (128, 143, 144, 148, 203, 321, 322). How cardiomyocytes are able to maintain graduation and stability of CICR via this positive feedback mechanism is not completely understood. The "local control" theory by Stern has provided a compelling model to explain this phenomenon (143, 144, 323, 361). Therein, isolated groups of voltage-gated L-type Ca2+ channels in the plasma membrane are functionally coupled exclusively to RyR2 clusters that act as CRUs (53, 129, 143–145, 321, 323, 324). Activation of an individual functional RyR2 cluster produces an elementary Ca2+ release event, known as Ca2+ spark (128–131, 146). The spatiotemporal summation of Ca2+ sparks is believed to underlie global Ca2+ transients (131). Thus, graded SR Ca2+ release in response to Ca2+ influx could then be achieved by recruiting various numbers of Ca2+ release units (128–130, 146, 325). In consequence, the distribution of functional RyR2 clusters is believed to be a critical determinant for CICR, hence cardiac contraction.

5.1.1 The distribution of RyR2 clusters is similar in live and fixed cells

The distribution of RyR2s in cardiomyocytes has been extensively investigated using

antibodies in fixed and permeabilized cardiomyocytes (58, 153, 211, 214, 326). However, little is known about in situ distribution of RyR2 clusters ventricular myocytes.

5.1.2 Our novel mouse model expressing GFP-tagged RyR2

We recently generated mice expressing GFP-tagged RyR2. The genetic basis underlying this mouse model has been explored in a previous study. Insertion of GFP-encoding cDNA into the DR2 of the cDNA of RyR2, specifically after residue Thr1366 (RyR2Thr1366-GFP), was achieved via homologous recombination. HEK293 cells that expressed RyR2-Thr1366-GFP showed WT-like Ca2+ release with typical caffeine - and ryanodine sensitivity. Furthermore, cells that expressed the construct emitted GFP fluorescence signals upon excitation at 488 nm. 3D reconstruction of purified RyR2T1366-GFP from cryo-EM data showed structurally intact channels with one GFP molecule per subunit. Taken together, these results demonstrate that the expression of the cDNA of RyR2T1366-GFP leads to the formation of WT-like functional Ca2+ release channels with GFP tags (40).

In the present study, we showed for the first time that genetic knock-in of RyR2Thr13366-GFP into mice provide a reliable tool to study in situ RyR2 distribution. No gross structural, nor functional abnormalities of the heart were observed in these mice. At a cellular level, RyR2s are expected to cluster in the terminal cisternae of the SR juxta-positioning the t-tubular invaginations of the sarcolemma along the z-lines. Indeed, GFP-RyR2 fluorescence signals was detected in highly organized arrays co-localizing with markers for the z-line and sarcolemma invaginations in the interior of isolated cardiomyocytes. The single transverse rows of this arrangement were spaced with inter-row distances of approximately 1.85 μm. This distance is in the range that has been reported to describe the extent of a sarcomere, the

elementary structural unit of muscle fibres, in healthy non-contracted cardiomyocytes (362). This makes one confident that the observed results truly represent in situ distribution of RyR2.

5.1.3 Distribution of GFP-RyR2 in fixed ventricular myocytes

Most localization studies of RyR2 have relied on the use of antibodies. Thus, they required sample preparation, such as fixation. Therewith, biochemical reactions are terminated to prevent decay. However, one might be concerned since long term exposure of chemicals that are required for this process might alter, or even damage, cellular structures.

In the present study, we showed, for the first time, the distribution of GFP-RyR2 clusters in live cardiomyocytes. Furthermore, we re-evaluated previous localization studies that used chemical fixation. We demonstrated that exposure of isolated cardiomyocytes to 4% paraformaldehyde for 5-10 minutes showed similar distribution of GFP-RyR2 clusters as observed in the interior of live ventricular myocytes. Thus, the correct use of fixatives allows the study of `in situ`-like distribution of RyR2 clusters.

5.1.4 RyR2s located between z-lines in the interior of ventricular myocytes

Indirect functional studies suggested the existence of SR-associated RyR2 clusters that are located between z-lines (206). RyR2 clusters at these sites have been proposed to harbor a key role in the propagation of Ca2+ release along the myofilaments (207). To directly evaluate this proposal, we directly determined the distribution of RyR2 clusters in relation to the z-line. We co-localized GFP-RyR2 signals and z-line zone marker, α-actinin, in ventricular myocytes isolated from our KI mice. Signals from both elements occurred in close proximity, even in areas of the cell which appeared disordered at first sight. In conclusion, we could not detect GFP-

RyR2 clusters in between z-line zones. However, the resolution of our confocal microscope is limited. Potentially, small clusters or individual channels of RyR2 do not emit enough light to be detected in our setting. Nevertheless, these units might still allow RyR2 mediated Ca2+ release from the SR. This concern makes the need for synchronous localization of GFP-RyR2 and elementary Ca2+ release, Ca2+ sparks evident.

5.1.5 RyR2 clusters are the origin of Ca2+ sparks

Lukyanenko *et al.* (206) reported that a significant portion of Ca2+ sparks (~20%) were detected at sites away from z-lines. In this study, they used permeabilized cells that were treated with Fluor3 and BODIPY TR-X ryanodine to map Ca2+ sparks in relative spatial correlation to the marker. Importantly, these authors have stated that they originally developed BODIPY TR-X ryanodine to visualize RyR2 directly. However, instead of binding to RyR2 they found this probe to sequester in mitochondria. As such they used it to define the z-line as BODIPY TR-X ryanodine void space. Authors also acknowledged that the ryanodine - based dye might interfere with the activity of RyR2, however they neglected it due to the concentration in which they applied it in (0.1µM). Altogether, such indirect spatial correlation for Ca2+ release site mapping raises concerns.

We could not detect GFP-RyR2 clusters in between z-lines in live ventricular myocytes. Nevertheless, RyR2 CRUs that may have functional relevance could have been potentially missed by our localization technique due to our detection limitation. To evaluate whether physiologically relevant Ca2+ release events occur at sites other than GFP-RyR2 clusters, we determined the origin of Ca2+ sparks in correlation to the center of GFP-RyR2 signals. To this end, we loaded ventricular cardiomyocytes that were isolated from our GFP-RyR2 mice with

Rhod-2 AM, a Ca2+ indicator with a Kd for Ca2+ of ~570 nM, to monitor physiologically relevant Ca2+ release events. Thus, our study did not require permeabilization and cell membrane integrity and interactions with voltage-gated L-type channels remained intact. Spontaneous Ca2+ sparks were triggered via SR Ca2+ overload through application of high external Ca2+ concentrations (> 2 mM). Our analysis of Ca2+ sparks revealed that highly ordered GFP-RyR2 clusters at the z-line zone are the origin of Ca2+ release sites. Thus, we conclude that graded and stable CICR during ECC relies on these sites.

5.1.6 Ca2+ sparks did not lead to detectable changes in mitochondrial Ca2+ levels

The question of whether mitochondrial Ca2+ transport affects the cytosolic Ca2+ concentration during ECC on beat-to-beat basis remains unclear (243). Most studies that addressed this uncertainty used Ca2+-specific fluorescence indicators that predominantly accumulate in mitochondria (Rhod 2-AM; indo 1-AM; or Fluro3-AM). Therewith, mitochondrial Ca2+ levels can be monitored to understand uptake kinetics and store capacity of the mitochondrial matrix.

Fluorescence probes that remained in the cytosol have to be efficiently removed to specifically detect mitochondrial Ca2+ dynamics and avoid signal `contamination`. Quenching of cytosolic probes with Mn2+ (363–366), high temperature treatment (327, 329) and dye wash out after permeabilization (245, 246, 331, 367) have been applied to eliminate residue dyes in the cytosol.

Concerns have been raised in applications of Mn2+. Potential interference with Ca2+ transport and quenching of mitochondrial signals by manganese has been described by Gavin et al. (368). However, these observations have been challenged by a subsequent study, showing that

Mn2+ did affect mitochondrial Ca2+ (364). Nevertheless, Mn2+ should be used with caution during measurements of mitochondrial Ca2+ levels.

Alternatively, extrusion of cytosolic indo 1-AM dye through plasma membrane anion pumps was promoted in rat ventricular myocytes via incubation at 37 °C after loading at RT (327, 329). However, the efficiency of this protocol for indo-1 removal from the cytosol might not be optimal. Trollinger et al. (328) developed an adaptation of this technique that incorporated the concept in rabbit cardiomyocytes. Loading of the cell with Rhod2-AM at 4 °C, hence cold loading, allows the membrane-permeable compound to equilibrate throughout the cell before esterases trap the dye mainly in mitochondria. Therewith, the selectivity of mitochondrial staining is supposedly significantly improved.

Lastly, permeabilization of the sarcolemma via application of detergents has been used to allow cytosolic dye to exit. However, cell permeabilization causes the loss of membrane integrity, regulatory coupling of L-type Ca2+ channels and RyR2 units and structural stress. Thus, permeabilized cells might not reflect healthy Ca2+ homeostasis and signaling. Previous studies in permeabilized cardiomyocytes (245, 246, 331, 367) supported direct coupling of elementary RyR2-mediated Ca2+ release and fast mitochondrial Ca2+ elevation, via the observation of marks (mitochondrial Ca2+ sparks). However, little is known about the influences of Ca2+ sparks on mitochondrial Ca2+ levels in intact cardiomyocytes (without the use of Mn2+).

With our KI mouse models expressing GFP-RyR2, we found ourselves in the unique position to determine whether elementary RyR2-mediated Ca2+ release directly affects mitochondrial Ca2+ levels. In our study, we did not see GFP-RyR2 co-localization with

mitochondria-specific indicator Mitotracker-Red. Nevertheless, we have to acknowledge that confocal imaging does not allow one to resolve the interface of GFP-RyR2 clusters and mitochondria. Thus, functional assessments are required to determine whether elementary SR-Ca2+release influences mitochondrial Ca2+ levels.

To specifically monitor mitochondrial Ca2+ concentrations in direct response to spontaneous Ca2+ sparks, we used cold loading of mitochondria with Rhod2-AM, as described by Trollinger et al.(328). We then applied heat treatment to efficiently eliminate cytosolic dye that remained. The resulting Rhod 2 fluorescence was detected in patterns of fibers with block-like elements (Figure 15), resembling the localization of mitochondria-specific marker, Mitotracker-Red, in the interior of ventricular myocytes (Figure 12). Signal voids between individual segments indicated effective elimination of cytosolic dye, thus selective staining of mitochondria. The cells followed pacing, verifying their viability. Intra luminal Ca2+ build-up in the SR was achieved via application of extracellular Ca2+ (> 2-3 mM) in combination with electric stimulation. Abrupt stopping of pacing in these cells led to SOICR.

We did not detect any marks in live ventricular myocytes, however, we clearly detected Ca2+ sparks in the same cell in subsequent monitoring of the cytosolic Ca2+ concentration. Thus, we conclude that elementary RyR2-mediated Ca2+ release does not affect mitochondrial Ca2+ levels.

One might argue that subsequent measurements of cytosolic and mitochondrial Ca2+ does not allow a direct correlation of Ca2+sparks and instant changes in mitochondrial Ca2+. However, we demonstrated that in cells that readily produce Ca2+sparks, mitochondrial Ca2+ remained unaffected throughout the cell. It is possible that no Ca2+sparks occurred during the

assessment of mitochondrial Ca2+ levels. Nevertheless, the large number of Ca2+ release events observed with cytosolic probes renders this scenario unlikely.

Simultaneous detection via light microscopy of two fluorescence Ca2+ indicators in cytosol and mitochondria has been criticised to be particularly prone to misinterpretation. The risk of channel bleeding and insufficient spatial resolution to separate signals potentially lead to signal 'contamination'.

Rapid SR-mitochondrial Ca2+ transport during ECC has been indicated to be a species – selective characteristic (329). Interestingly, observations that were made in rodent cardiomyocyte (guinea pig vs rats) showed distinct results. In our study, we have shown that in mouse cells, elementary Ca2+ release from the SR did not lead to detectable changes of mitochondrial Ca2+ levels. This novel finding might help to understand in the future whether this phenomenon is the result of distinct intrinsic mechanisms of mitochondrial Ca2+ uptake, or the presence of different regulatory elements.

However, it should be noted that different Ca2+ indicators (indo-1-AM vs rhod2-AM), were used to monitor Ca2+ levels in the mitochondrial matrix. Both dyes have been used in various studies to monitor physiologically relevant Ca2+ levels in cardiac cells. Nevertheless, their difference in Kd values for Ca2+ (indo-1 ~ 250 nM vs Rhod-2 ~570 nM) should be of consideration. Their concentration range over which Ca2+ binding leads to changes in fluorescence intensity (~ between 0.1- and 10-fold the Kd value) is different.

5.2 Dynamic and irregular distribution of RyR2 clusters at the periphery of Ventricular myocytes

In agreement with previous studies (53, 56–59, 153, 154, 205, 208, 214, 215, 326, 334),

highly-organized arrays of RyR2 clusters were found in the interior of live ventricular myocytes that act as CRUs to facilitate stable and graded CICR during ECC. However, distribution of RyR2 clusters at the periphery of live cells remains unknown.

5.2.1 Three layers with different distribution patterns of RyR2 clusters

In our study, confocal, TIRF, HILO and EPI fluorescence imaging revealed three distinct patterns of distribution of RyR2 clusters within the same live ventricular myocytes. Irregular/disordered arrangements were found closest to the sarcolemmal membrane. Tightly-ordered arrays were confirmed in the interior and a double row feature was found in between. These results support previous 3D confocal imaging studies that showed irregular distribution of RyR2 clusters in the outermost optical confocal z-planes of fixed and permeabilized cardiomyocytes (57, 58, 214). However, our findings contrast former TIRF and dSTORM studies that reported `double row` arrangements of RyR2 clusters near the sarcolemmal membrane (56, 215, 227).

This discrepancy has potentially been caused by distinct cell placement for imaging. Our live cardiomyocytes naturally adhered to the glass interface when transferred in free suspension onto a coverslip. However, former studies required cell fixation and permeabilization for antibody-based localization of RyR2. Thus, they had to resort to `gentle sandwiching` between two coverslips to force cardiomyocytes in proximity to the glass interface to facilitate TIRF and STORM imaging. Such mechanical force might have shifted the `double-row` layer into focus.

The novel finding of diverse patterns of distribution of RyR2 revealed the complexity in the periphery of cardiomyocytes. It shows the need for subcellular layer-specific definition of structures in the periphery of cardiomyocytes. Generalized interpretation of `peripheral` patterns

of molecular components should be re-evaluated since it might not allow to resolve the complexity of elements in the periphery of cardiomyocytes. For example, it might help to understand interactions of junctophilin-2 (JPH2) with RyR2 in cardiomyocytes.

JPH2, has been identified as a key structural element of dyadic clefts with interactions with both plasma membrane and SR. They are believed to maintain microdomains in the interior of cardiomyocytes that are essential for CICR, and in turn for ECC (41). The skeletal isoform of this protein has been shown to directly connect with RyR1 and L-type Ca2+ channels (369). However, a recent study reported association of JPH2 with RyR2 clusters with different distribution from dyad to dyad in the `periphery` of fixed and permeabilized cardiomyocytes (57). Their observations were made in a peripheral layer with `double row` distribution of RyR2. However, the relationship of JPH2 and irregularly distributed RyR2 clusters nearest to the sarcolemma remains unknown. Our GFP-RyR2 mouse model may provide a useful tool to evaluate JPH2-RyR2 interactions at the outmost peripheral layer in the future.

5.2.2 Cell area

One might have concerns that long-range orders are difficult to determine in small areas that are provided by adhesion points of a rod-shaped cardiomyocyte. We addressed this issue in two ways. On one hand, we coated the glass surface with laminin, an extracellular matrix protein, to increase cell adhesion. Therewith, we increased the area of cardiomyocytes that could be imaged in TIRF mode. We confirmed that the laminin-use did not affect GFP-RyR2 distribution. TIRF images and Fourier transforms acquired with and without laminin pre-treatment of coverslips were indistinguishable.

On the other hand, we evaluated whether small areas, relative to the area of the cell,

harbor sufficient information to compare relative orderliness of the distribution of RyR2 clusters located in different regions of the cell. We provided compelling evidence that areas as small as 5.5 x 3.5 µm are sufficient to gain reliable and reproducible results.

5.2.3 Implications of the movements of RyR2 clusters

A previous report showed tight association of junctophilin-2 with RyR2 clusters (~90%) in `double rows` of cardiomyocytes (57). However, little is known about structural elements that potentially maintain micro-arrangements in the layer nearest to the sarcolemma.

Our study revealed RyR2-modulator sensitive movements of RyR2 clusters near the sarcolemma in live cells. We found various dynamics of GFP-RyR2 signals, such as separation and fusion, xy – and z-translocation. This was an unexpected and exciting finding. Although the majority of clusters maintained their position within the recorded time span, a significant number of irregularly distributed GFP-RyR2 signals displayed movement. This leads one to speculate that a complex subcellular system is specifically present near to sarcolemma. One the one hand, it stabilizes the positioned irregularly distributed RyR2 clusters. On the other hand, it has to facilitate fast re-arrangements of transmembrane channels in a fashion that depends on the activity of RyR2s. Micro-structures, similar to those in the interior, could account for the stabilizing element. Additionally, Ca2+ dependent vesicular transport could provide a mechanism that allows RyR2 cluster movements.

In favour of this model is the fact that multiple vesicle fusion apparatus, such as secretory vesicle-associated proteins, mediate membrane fusion or vesicle separation in response to Ca2+ binding (370). Opposing this hypothesis, former localization studies of RyR2 (e.g. EM data) have not reported the presence of RyR2 in vesicles near the sarcolemma. However, there is an

argument that potentially explains this phenomenon. Most localization studies have required on cell fixation and permeabilization to localize RyR2 via antibodies. Thus, studies applied agents that dissolve phospholipids, such as vesicle membranes. Thus, these techniques might not have detected RyR2 cluster containing vesicles. However, this remains speculative at this point.

In future prospective, the molecular apparatus that underlies stabilization and dynamic movement of irregularly distributed RyR2 clusters near the plasma membrane needs to be further investigated. As a potential next step, co-localization of RyR2 clusters and markers for vesicles, or JPH2, in live cardiomyocytes could provide evidence for the suggested models.

5.2.4 Functionality of irregular distributed RyR2 clusters

Convincing evidence has been provided that voltage gated L-type Ca2+ channel-mediated Ca2+ influx leads to Ca2+ release via RyR2 in the periphery of cardiomyocytes.

Co-localization studies have been indirectly shown the presence of both molecular components in peripheral couplings of atrial and ventricular myocytes (211, 334). Additionally, ryanodine sensitive Ca2+ sparks were reported in the periphery of detubulated cardiomyocytes(210). In a more direct approach, a study that applied whole cell patch clamp measurements in tandem with confocal line scan imaging of Ca2+ sensitive fluorescence probes characterized peripheral Ca2+ spark generation (209). They detected peripheral Ca2+ sparks with short (~ 4.5ms) and long (~ 41ms) rise times. The authors argued that dynamic recruitment of small, non-uniform cohorts of RyR2 channels accounted for this finding. Our finding of dynamic distribution of RyR2 clusters supports this notion. Nevertheless, their imaging might not have been able to distinguish between different layers of RyR2 clusters in the periphery of cardiomyocytes.

Our discovery of three layers of RyR2 cluster distribution raises the question: Are all types of RyR2 clusters in the periphery, with distinct arrangements, activated by Ca2+ entry through the L-type Ca channels during membrane depolarization, or only particular layers? Furthermore, do all peripheral RyR2 clusters possess similar Ca2+ release properties to those of RyR2 clusters located in the cell interior?

Our simultaneous assessment of Ca2+ sparks and the locations of GFP-RyR2 demonstrated that irregular distributed CRUs possess properties similar to those in the interior. Therewith, cells have the potential to rapidly generate distinct spatiotemporal Ca2+ release events. However, functional implications remain to be determined.

5.2.5 Possible implication of peripheral RyR2 clusters in vesicle transport

Ca2+ release from dynamic irregularly distributed RyR2 clusters could be involved in various Ca2+ dependent mechanisms and pathways in the periphery of cardiomyocytes. Our observation of RyR2-modulator sensitive movements may lead one to speculate that peripheral CRUs are involved in vesicular transport. In support of this hypothesis, partial co-localization of RyR2 and caveolin-3 (~28%) was reported at the periphery of fixed cardiomyocytes (215). Caveolin-3 is a constituent of the caveolae plasma membrane and has been used to mark t-tubules. Their oligomerization can facilitate clathrin-independent raft-dependent vesicle formation and endocytosis (371). This hypothesis was strengthened by the recent discovery of a protein that binds directly to caveolin and the cytosolic region of RyR2. Therewith, heart LIM protein mediates protein-protein interactions and forms a complex with RyR2 and caveolin-3 in heart cells (372). Nevertheless, direct evidence for this theory is still lacking. Monitoring RyR2-modulator dependent formation of caveolin-3 oligomers at CRU near

the plasma membrane of live cells would provide such confirmation. However, most caveolin-3 localizations relied on antibodies. A genetic visualization approach might will overcome this issue in the future.

5.2.6 Fine-structure and size of RyR2 clusters in ventricular myocytes

The exact nature, arrangement and number of RyR2 channels within a CRU in cardiomyocytes remains debated. A number of localization studies with different approaches suggested estimates of single digits to hundreds of RyR2 channels per functional unit (41, 53, 56–60, 334, 373). The resolution in experimental design is not high enough to address this issue, but provides novel insights that have important implications. Our discovery of diverse distribution patterns in distinct layers of the cell, potentially aids the understanding of the large variance in numbers that were suggested to form CRUs. Additionally, complexity might be explained since we demonstrated that the shape and size of peripheral RyR2 clusters is a dynamic feature. Therefore, it might be beneficial if future studies of CRU are carried out in a subcellular-specific manner.

5.3 Unambiguous RyR2 cluster distribution in hippocampal Neurons

It has remained a challenge to specifically localize the RyR2 protein in the brain, since all RyR isoforms are present. Previous studies of RyR2s in brain tissue relied on targeting of messenger RNA (mRNA), or the use of conventional anti-RyR2 antibodies (374, 375). Unfortunately, these approaches have limitations, which might not allow to definitively and unambiguously determine the neuronal distribution of RyR2 in hippocampal neurons.

The distribution of RyR2 mRNA has been extensively studied in brain tissue via in situ hybridization (30, 294, 302). However, mRNA locations might not reflect the position of RyR2 protein. Post-translational modifications, such as phosphorylation, oxidation and nitrosylation of RyR2 have been found to significantly alter RyR2 activity and distribution (30, 314, 315, 374). Furthermore, the expression of RyR2 mRNA has been shown to undergo dynamic changes during brain development (embryo to adulthood) in various species, including humans (30).

Alternatively, RyR2 antibodies have been used to localize RyR2 in intact hippocampal tissue (286, 292, 294). However, the specimen thickness, the range of neuronal cell types, and the complexity of arborization networks, may lead one to be concerned about the specificity of antibodies and accessibility of targets, under some experimental conditions. Hence, subcellular distribution of RyR2 requires verification in intact preparations of adult brain.

In consensus with previous mRNA and conventional antibody-mediated localization studies, we found most extensive GFP-RyR2 expression in the hippocampus of intact brain preparations from our KI mice (Figure 25). Using high resolution confocal and SIM superresolution imaging, we further unambiguously localized RyR2 in dendritic shafts and soma, but not at presynaptic terminals and dendritic spines, of pyramidal shaped cells in the CA1 region (Figure 25; Figure 26; Figure 27; and Figure 37), and in the dendrites of granule cells in the dentate gyrus (Figure 35; Figure 36; Figure 37 and Figure 38). These results have significant implication. On the one hand, they call former suggestions that RyR2 are present in presynaptic terminals of mossy fibers of the CA3 pyramidal neurons (359) and dentate gyrus granule neurons (294) into question. Furthermore, our findings finally clarify that RyR2s are expressed throughout the dendritic shaft (Figure 26 and Figure 27) and not preferentially at dendritic branching points of

pyramidal CA1 neurons as suggested by functional studies (297, 317, 319). Furthermore, our subcellular localization study renders the observation of RyR antagonist/agonists-sensitive release of Ca2+ from internal stores in dendritic spines of hippocampal CA1 neurons (281, 285) unlikely to be mediated by RyR2. Somatic localization of RyR2s may also help to understand their potential implication in complex Ca2+ signals, such as specialized Ca2+ waves that were particularly effective in activating gene expression and protein synthesis in hippocampal CA1 neurons (319).

5.4 Neuronal functions of RyR2 clusters in dendritic shafts and soma of hippocampal neurons

Functional studies have indicated that RyRs play pivotal roles in Ca2+ handling in hippocampal neurons. However, the involvement of RyRs in distinct neuronal processes remains controversial.

Presynaptic functional implications of RyRs in axonal terminals of hippocampal CA3 neurons were supported by pharmacological (299, 300, 357, 376, 377) and shRNA knockdown (359) studies. However, these findings were opposed by an observation of unaffected neurotransmitter release after application of RyR antagonists (378). Similarly, postsynaptic activities of RyRs have been vigorously examined. Analysis of neuronal localized Ca2+ release event appearance in hippocampal slices suggested RyRs to be located preferentially at branch points of dendrites of pyramidal cells (297, 317, 318). In contrast, RyR-antibody signals were localized throughout the dendritic shafts of cultured hippocampal sections (379). Additionally, Watanabe S. et al. reported RyR-mediated Ca2+ release events just under the plasma membrane of the cell body of hippocampal neurons in intact brain slices (319).

These discrepancies may be explained by the fact that former studies suffer from two major problems. On the one hand, most functional assessments were made in developing systems (294). On the other hand, there are no isoform-specific reagents available to study neuronal RyR2 functions. Direct evidence for isoform-specific functions of RyRs is lacking. A number of pharmacological studies have indicated that different RyRs are critically involved in the induction of LTP, a major component of synaptic plasticity, underlying learning and memory (306, 307, 309–311). However, these studies did not distinguish the specific roles of each RyR isoform. In general, extracellular drugs, such as i) ryanodine; ii) caffeine; and iii) dantrolene, have been employed to investigate neuronal functions of RyRs. Ryanodine acts on all three isoforms. It locks the channels in a semiconducting open state at low concentrations, whereas high concentrations of ryanodine ($\geq$ 10 μM) completely block RyR mediated Ca2+ release (110). Caffeine, and agonist of RyRs, has been shown to have multiple other molecular targets that are involved in cellular Ca2+ signaling, including phosphodiesterases, $GABA_A$ receptors, adenosine A_{2A} receptors and possibly A_1Rs (117). Also, whether RyRs antagonist dantrolene affects specific RyR isoforms remains uncertain. In vitro studies and ligand binding assays with native and recombinant RyRs indicated that the Ca2+ channel blocker, dantrolene, act specifically on RyR1, but not on RyR2 (118–120). Furthermore, RyR1 and RyR3, but not the RyR2 isoform, were reported to provide in vivo targets for dantrolene inhibition (121). However, this matter has been put into question. Dantrolene rescued RyR2-mediated arrhythmogenic delayed after-depolarizations in a patient-specific stem cell model (380). Furthermore, dantrolene has been found to directly interact with RyR2 that were incorporated in artificial bilayer membranes (381). Thus no isoform-specific pharmacological reagents to determine isoform-specific neuronal functions of RyR2.

Alternatively, antisense oligonucleotides have been used to selectively knockdown the expression of RyR isoforms (292), but the effectiveness of this knockdown approach in intact animals is not clear. Genetic knockout of RyR3 has been shown to affect learning and memory (312), but this knockout approach is not feasible for RyR1 and RyR2, as RyR1 or RyR2 deficient mice die early during embryonic development (28, 313). Hence, the development of novel models is required to assess the functional roles of a specific RyR isoform.

5.5 Perspective and future directions

Aside from experiments that could evaluate aforementioned theories and models, I will use the following section to propose other directions and interest fields in which our novel research tools may provide aid to localize GFP-tagged proteins and understand their functional roles in the future.

5.5.1 Superresolution imaging of anti-GFP nanobody–tagged GFP-RyR2

In our study, we demonstrated selective and specific targeting of GFP-RyR2 in tissue and cells from our KI mice using the AF-647 conjugated anti-GFP nanobody. Therewith, we developed a novel platform to unambiguously define the location of this intracellular RyR2 channel. However, this approach has not been taken advantage of to its full potential yet. AF-647 is a photoactive dye that has been shown to facilitate STORM imaging. Experiments were performed in which this superresolution technique was employed for image acquisition in the interior of anti-GFP nanobody stained ventricular myocytes. Preliminary data, showed clear reconstruction of highly-ordered arrays of GFP-RyR2 in the interior. However, the quantum yield of blinking events has to be increased before reliable conclusions can be made about the

fine structure and number of RyR2 channels of individual clusters. Therefore, several factors have to be optimized, such as sample preparation and anti-GFP nanobody binding, acquisition redox conditions and handling.

After establishing an optimal approach to perform STORM in single cells, similar set ups may be usable to determine the location of GFP-RyR2 in tissue specimens with nanometric resolution.

5.5.1.1 Application of anti-GFP nanobody to other studies

Our anti-GFP nanobody probe itself may also provide a useful tool for various other studies that use GFP fusion proteins. It is simple to handle, requires no permeabilization by detergents, nor secondary antibodies and is highly specific. Selective binding was detected in specimens treated for only 30 min at RT with GFP probe dilutions. On one hand, it provides a secondary verification of green GFP fluorescence in red (Ex/Em 650/668 nm). On the other hand, it can be used to perform STORM superresolution.

5.5.2 Subcellular RyR2 cluster distribution in other neurons

In our study, we defined the subcellular distribution of RyR2 in hippocampal neurons with a focus on CA1 and DG. Aside from these, other neurons are present in this complex brain region that potentially express RyR2. For instance, conventional antibody-based RyR2-localization by Shimizu et al. (286) indicated that RyR2 is present in the axons, but not at the terminal of mossy fiber-CA3 synapses. This was supported by additional functional studies that reported caffeine- and nicotine- sensitive transmitter release (382) (310). However, little is known about RyR2s in the postsynaptic side of these connections.

In addition, cells in other brain regions have been indicated to express RyR2. Purkinje cells in the cerebellum were among the first sites that were reported to harbor RyRs (383). Although most studies have shown that RyR1 is the predominant isoform in these cells, the presence of RyR2 has been also demonstrated by mRNA studies (384) with antisense oligonucleotide mediated KO (385) and antibody localization in the avian brain (386, 387). Functional studies showed RyR modulator-sensitive neurotransmitter release from basket cells onto Purkinje cells (388, 389). However, which RyR isoform mediates intracellular Ca2+ release to generate inhibitory GABAergic signals in the presynaptic side of this interneuron connections remains unclear. Our novel platform to unambigously localize GFP-RyR2 on a subcellular level in brain tissue might allow are to adress this issue.

Also, a previous Ca2+ imaging study found Ca2+ spark like events in dendrites of L2/3 pyramidal neurons of the somatosensory neocortex (317). In agreement, preliminary images that we acquired from GFP-probe stained intact brain slices derived from our GFP-tagged RyR2 mice showed extensive staining in the cortex (data not shown). This exciting finding should be explored in further detail. Defining the subcellular distribution of RyR2 in these cells may lead to novel insight into the functional involvement of RyR2 in these neurons.

5.5.3 RyR2 as a pharmacological target for improving cognitive function

Carvedilol is a clinically used beta-blocker that has been used to prevent cardiac arrhythmias in human CPVT-patients and SOICR in models that express CPVT-linked RyR2 mutations (89, 90, 269). Compelling evidence has been provided that this drug directly suppresses the activity of RyR2. However, whether this drug has beneficial effects on cognitive

functions in people that carry CPVT-associated RyR2 mutations remains unknown. With our RyR2-R4496C mice, we are in the unique position to directly address this important question in the near future.

5.5.4 Abnormal RyR2-mediated Ca2+ release underlying other brain diseases

Various studies have shown that abnormal expression and function of RyR has been linked to Alzheimer disease (AD). RyRs have been indicated in multiple aspects of the pathogenic mechanism, including i) amyloid plaque generation, ii) neuronal death; iii) synaptic dysfunction; and iv) memory and learning impairment. These observations were made in systems, such as cell cultures, transgenic mouse models and human AD-affected brains (374).

Most recently, abnormal activity of RyR2 has been linked to cognitive dysfunction and Alzheimer`s disease (AD) by Marks and colleagues (314, 315). They reported that mice which expressed a RyR2 mutation, that mimics constitutive PKA phosphorylation of residue S2808D, led to impaired cognitive behaviour. In contrast, mice that harbored RyR2-S2808A, a mutation that prevents PKA phosphorylation at this site, rescued stress-induced dysfunction. In addition, they showed that an AD mouse model that expresses RyR2-S2808A had improved cognition.

Marks group attributed abnormal brain function to altered activity of RyR2 to dissociation of FKBP12.6. However, the regulation of RyR2 activity by FKPB12.6 is highly controversial. Two independent groups showed that FKBP12.6 does not affect gating of RyR2 (101, 265). In addition, the importance of the phosphorylation site S2808 in RyR2 has been put into question since this residue mainly occurs in its phosphorylated state at basal conditions (102). In our study, it was demonstrated that altered sensitivity of RyR2 to luminal Ca2+ is linked to learning and memory defects. It might be beneficial to re-evaluate former findings in

this context.

5.6 SUMMARY

The present studies have demonstrated the subcellular distribution and function of cardiac ryanodine receptor in ventricular myocytes and hippocampal neurons.

Effective, graded and stable excitation-contraction coupling critically depends not only on the expression of RyR2, but also on its distribution. Despite its importance, little is known about the distribution and organization of RyR2 in living cells. To study the distribution of RyR2 in living cardiomyocytes, we generated a knock-in mouse model expressing a GFP-tagged RyR2 (GFP-RyR2). Confocal imaging of live ventricular myocytes isolated from the GFP-RyR2 mouse heart revealed clusters of GFP-RyR2 organized in rows with a striated pattern. Similar organization of GFP-RyR2 clusters was observed in fixed ventricular myocytes. Immunofluorescence staining with the anti-α-actinin antibody (a z-line marker) showed that nearly all GFP-RyR2 clusters were localized in the z-line zone. There were small regions with dislocated GFP-RyR2 clusters. Interestingly, these same regions also displayed dislocated z-lines. Staining with di-8-ANEPPS revealed that nearly all GFP-RyR2 clusters were co-localized with transverse but not longitudinal tubules, whereas staining with MitoTracker Red showed that GFP-RyR2 clusters were not co-localized with mitochondria in live ventricular myocytes. We also found GFP-RyR2 clusters interspersed between z-lines only at the periphery of live ventricular myocytes. Simultaneous detection of GFP-RyR2 clusters and Ca2+ sparks showed that Ca2+ sparks originated exclusively from RyR2 clusters. Ca2+ sparks from RyR2 clusters induced no detectable changes in mitochondrial Ca2+ level. These results reveal, for the first time, the distribution of RyR2 clusters and its functional correlation in living ventricular

myocytes.

RyR2 clusters located in the interior of cardiomyocytes are arranged in highly-ordered arrays. However, little is known about the distribution and function of RyR2 clusters in the periphery of cardiomyocytes. A knock-in mouse model expressing a green fluorescence protein (GFP)-tagged RyR2 was used to localize RyR2 clusters in live ventricular myocytes by virtue of their GFP fluorescence. Confocal imaging and total internal reflection fluorescence (TIRF) microscopy were employed to determine and compare the distribution of GFP-RyR2 in the interior and periphery of isolated live ventricular myocytes and in intact hearts. We found tightly-ordered arrays of GFP-RyR2 clusters in the interior, as previously described. In contrast, irregular distribution of GFP-RyR2 clusters was observed in the periphery. Time-lapse TIRF imaging revealed dynamic movements of GFP-RyR2 clusters in the periphery, which were affected by external Ca2+ and RyR2 activator (caffeine) and inhibitor (tetracaine), but little detectable movement of GFP-RyR2 clusters in the interior. Furthermore, simultaneous Ca2+- and GFP-imaging demonstrated that peripheral RyR2 clusters with an irregular distribution pattern are functional with a Ca2+ release profile similar to those in the interior. These results indicate that the distribution of RyR2 clusters in the periphery of live ventricular myocytes is irregular and dynamic, which is different from that of RyR2 clusters in the interior.

RyR2 is abundantly expressed in the heart and brain. Not surprisingly, naturally occurring mutations in RyR2 have been associated with both cardiac arrhythmias (e.g. catecholaminergic polymorphic ventricular tachycardia, CVPT) and intellectual disability. While the mechanisms underlying RyR2-linked CPVT have been well characterized, little is known about the mechanism of intellectual disability associated with CPVT RyR2 mutations. To better understand the role of RyR2 in cognitive function, we generated a knock-in mouse model

harboring a green fluorescent protein (GFP)-tagged RyR2 and a highly specific GFP probe to define the subcellular localization of RyR2 in hippocampus. Using this novel platform, we unambiguously localized RyR2 to the dendrites and soma, but not presynaptic terminals or dendritic spines of hippocampal CA1 pyramidal and dentate gyrus granule neurons. Furthermore, we assessed the impact of a CPVT RyR2 mutation R4496C on presynaptic and postsynaptic function of hippocampal CA1 neurons in brain slices from the RyR2 R4496C mutant mice. We found that the CPVT RyR2 R4496C mutation had little effect on presynaptic short-term facilitation. On the other hand, the CPVT R4496C mutation markedly enhanced the excitability of hippocampal CA1 neurons, diminished hippocampal long-term potentiation, and impaired learning and memory in mice. Collectively, our data reveal, for the first time, the precise subcellular distribution of RyR2 in hippocampus and the postsynaptic action of a CPVT RyR2 mutation in neuronal excitability, long-term potentiation, learning, and memory. These data provide novel insights into the mechanisms of intellectual disability associated with RyR2 dysfunction.

REFERENCES

1. Carafoli, E. 2003. The calcium-signalling saga: tap water and protein crystals. Nat. Rev. Mol. Cell Biol. 4: 326–332.
2. Berridge, M.J. 1998. Neuronal calcium signaling. Neuron. 21: 13–26.
3. Bers, D.M. 2002. Cardiac excitation-contraction coupling. Nature. 415: 198–205.
4. Carafoli, E. 2007. The unusual history and unique properties of the calcium signal. In: Krebs J, M Michalak, editors. Calcium : A Matter of Life or Death. Amsterdam: Elsevier Science. pp. 3–23.
5. Stutzmann, G.E., and M.P. Mattson. 2011. Endoplasmic reticulum Ca(2+) handling in excitable cells in health and disease. Pharmacol. Rev. 63: 700–27.
6. Stathopulos, P.B., M.-D. Seo, M. Enomoto, F.J. Amador, N. Ishiyama, and M. Ikura. 2012. Themes and Variations in ER/SR Calcium Release Channels: Structure and Function. Physiol Rev. 27: 331–342.
7. Bunney, T.D., and M. Katan. 2011. PLC regulation: emerging pictures for molecular mechanisms. Trends Biochem. Sci. 36: 88–96.
8. Parys, J.B., and H. De Smedt. 2012. Inositol 1,4,5-trisphosphate and its receptors. Adv. Exp. Med. Biol. 740: 255–79.
9. Verkhratsky, A. 2002. The endoplasmic reticulum and neuronal calcium signalling. Cell Calcium. 32: 6–393.
10. Narayanan, D., A. Adebiyi, and J.H. Jaggar. 2012. Inositol trisphosphate receptors in smooth muscle cells. Am J Physiol Hear. Circ Physiol. 302: 2190–2210.
11. Lencesova, L., and O. Krizanova. 2012. IP(3) receptors, stress and apoptosis. Gen. Physiol. Biophys. 31: 119–30.
12. Ter Keurs, H.E.D.J. 2012. The interaction of Ca2+ with sarcomeric proteins: role in function and dysfunction of the heart. Am. J. Physiol. Heart Circ. Physiol. 302: 38–50.
13. Cannell, M.B., R.D. Vaughan-Jones, and W.J. Lederer. 1985. Ryanodine block of calcium oscillations in heart muscle and the sodium-tension relationship. Fed. Proc. 44: 2964–9.
14. Procita, L. 1956. The action of ryanodine on mammalian skeletal muscle in situ. J.

Pharmacol. Exp. Ther. 117: 363–73.

15. Inui, M., A. Saito, and S. Fleischer. 1987. Purification of the ryanodine receptor and identity with feet structures of junctional terminal cisternae of sarcoplasmic reticulum from fast skeletal muscle. J. Biol. Chem. 262: 1740–7.
16. Campbell, K.P., C. Franzini-Armstrong, and A.E. Shamoo. 1980. Further characterization of light and heavy sarcoplasmic reticulum vesicles. Identification of the "sarcoplasmic reticulum feet" associated with heavy sarcoplasmic reticulum vesicles. Biochim. Biophys. Acta - Biomembr. 602: 97–116.
17. Bonilla, E. 1977. Staining of transverse tubular system of skeletal muscle by tannic acid-glutaraldehyde fixation. J. Ultrastruct. Res. : 162–5.
18. Van Petegem, F. 2012. Ryanodine receptors: structure and function. J. Biol. Chem. 287: 31624–32.
19. Serysheva, I.I., S.J. Ludtke, M.L. Baker, Y. Cong, M. Topf, D. Eramian, A. Sali, S.L. Hamilton, W. Chiu, and C. Franzini-Armstrong. 2008. Subnanometer-resolution electron cryomicroscopy-based domain models for the cytoplasmic region of skeletal muscle RyR channel. Proc. Natl. Acad. Sci. 105: 9610–9615.
20. Samsó, M., T. Wagenknecht, and P. Allen. 2005. Internal structure and visualization of transmembrane domains of the RyR1 calcium release channel by cryo-EM. Nat. Struct. Mol. Biol. 12: 539–544.
21. Hakamata, Y., J. Nakai, H. Takeshima, and K. Imoto. 1992. Primary structure and distribution of a novel ryanodine receptor/calcium release channel from rabbit brain. FEBS Lett. 312: 229–235.
22. Zissimopoulos, S., and A.F. Lai. 2007. Ryanodine receptor structure, function and pathophysiology. In: Krebs J, M Michalak, editors. Calcium: A Matter of Life and Death. Amsterdam: Elsevier. pp. 287–342.
23. Nakai, J., T. Imagawa, Y. Hakamat, M. Shigekawa, H. Takeshima, and S. Numa. 1990. Primary structure and functional expression from cDNA of the cardiac ryanodine receptor/calcium release channel. FEBS Lett. 271: 169–77.
24. Zucchi, R., and S. Ronca-Testoni. 1997. The Sarcoplasmic Reticulum Ca2+ Channel/Ryanodine Receptor: Modulation by Endogenous Effectors, Drugs and Disease

States. Pharmacol. Rev. 49: 1–52.

25. Rossi, D., and V. Sorrentino. 2004. The Ryanodine Receptors Gene Family: Expression and Functional Meaning. Basic Appl Myol. 14: 323–343.
26. Löhn, M., W. Jessner, M. Fürstenau, M. Wellner, V. Sorrentino, H. Haller, F.C. Luft, and M. Gollasch. 2001. Regulation of calcium sparks and spontaneous transient outward currents by RyR3 in arterial vascular smooth muscle cells. Circ. Res. 89: 1051–1057.
27. Takeshima, H., M. Iino, H. Takekura, M. Nishi, J. Kuno, O. Minowa, H. Takano, and T. Noda. 1994. Excitation-contraction uncoupling and muscular degeneration in mice lacking functional skeletal muscle ryan-done receptor gene. Nature. : 556–559.
28. Takeshima, H., S. Komazaki, K. Hirose, M. Nishi, T. Noda, and M. Iino. 1998. Embryonic lethality and abnormal cardiac myocytes in mice lacking ryanodine receptor type 2. EMBO J. 17: 3309–16.
29. Mori, F., M. Fukaya, H. Abe, K. Wakabayashi, and M. Watanabe. 2000. Developmental changes in expression of the three ryanodine receptor mRNAs in the mouse brain. Neurosci. Lett. 285: 57–60.
30. Abu-Omar, N., J. Das, V. Szeto, and Z.-P. Feng. 2017. Neuronal Ryanodine Receptors in Development and Aging. Mol. Neurobiol. : 1–10.
31. Fill, M., and J.A. Copello. 2002. Ryanodine receptor calcium release channels. Physiol. Rev. 82: 893–922.
32. Chens, S.R.W., L. Zhang, and D.H. Maclennang. 1993. Antibodies as Probes for Ca2+ Activation Sites in the Ca2+ Release Channel (Ryanodine Receptor) of Rabbit Skeletal Muscle Sarcoplasmic Reticulum*. J. Biol. Chem. 268: 13414–13421.
33. Du, G.G., V.K. Khanna, and D.H. Maclennan. 2000. Mutation of Divergent Region 1 Alters Caffeine and Ca 2+ Sensitivity of the Skeletal Muscle Ca 2+ Release Channel (Ryanodine Receptor). J. Biol. Chem. 275: 11778–11783.
34. Hayek, S.M., X. Zhu, M.B. Bhat, J. Zhao, H. Takeshima, H.H. Valdivia, and J. Ma. 2000. Characterization of a calcium-regulation domain of the skeletal-muscle ryanodine receptor. Biochem. J. 351: 57–65.
35. Bhat, M.B., J. Zhao, S. Hayek, E.C. Freeman, H. Takeshima, and J. Ma. 1997. Deletion of Amino Acids 1641-2437 from the Foot Region of Skeletal Muscle Ryanodine Receptor

Alters the Conduction Properties of the Ca Release Channel. Biophys. Joumal. 73: 1320–1328.

36. Proenza, C., J. O ’brien, J. Nakai, S. Mukherjee, P.D. Allen, K.G. Beam, and K. Beam. 2002. Identification of a region of RyR1 that participates in allosteric coupling with the α 1S (Ca V 1.1) II-III loop. J. Biol. Chem. 277: 6530–6535.
37. Sorrentino, V., and P. Volpe. 1993. Ryanodine receptors: how many, where and why? Trends Pharmacol. Sci. 14: 98–103.
38. Perez, C.F., S. Mukherjee, and P.D. Allen. 2003. Amino Acids 1–1,680 of Ryanodine Receptor Type 1 Hold Critical Determinants of Skeletal Type for Excitation-Contraction Coupling ROLE OF DIVERGENCE DOMAIN D2*. J. Biol. Chem. 278: 39644–39652.
39. Yamazawa, T., H. Takeshima, M. Shimuta, and M. Iino. 1997. A region of the ryanodine receptor critical for excitation-contraction coupling in skeletal muscle. J. Biol. Chem. 272: 8161–4.
40. Liu, Z., J. Zhang, R. Wang, S.R.R. Wayne Chen, and T. Wagenknecht. 2004. Location of Divergent Region 2 on the Three-dimensional Structure of Cardiac Muscle Ryanodine Receptor/Calcium Release Channel. J. Mol. Biol. 338: 533–545.
41. Scriven, D.R.L., P. Asghari, and E.D.W. Moore. 2013. Microarchitecture of the dyad. Cardiovasc. Res. 98: 169–76.
42. Samsó, M., W. Feng, I.N. Pessah, and P.D. Allen. 2009. Coordinated movement of cytoplasmic and transmembrane domains of RyR1 upon gating. PLoS Biol. 7: e85.
43. Ludtke, S.J., I.I. Serysheva, S.L. Hamilton, and W. Chiu. 2005. The pore structure of the closed RyR1 channel. Structure. 13: 1203–11.
44. Sharma, M.R., L.H. Jeyakumar, S. Fleischer, and T. Wagenknecht. 2000. Three-dimensional structure of ryanodine receptor isoform three in two conformational states as visualized by cryo-electron microscopy. J. Biol. Chem. 275: 9485–91.
45. Sharma, M.R., P. Penczek, R. Grassucci, H.B. Xin, S. Fleischer, and T. Wagenknecht. 1998. Cryoelectron microscopy and image analysis of the cardiac ryanodine receptor. J. Biol. Chem. 273: 18429–34.
46. Du, G.G., B. Sandhu, V.K. Khanna, X.H. Guo, and D.H. Maclennan. 2002. Topology of the Ca 2+ release channel of skeletal muscle sarcoplasmic reticulum (RyR1). Proc. Natl.

Acad. Sci. 99: 16725–16730.

47. Yan, Z., X. Bai, C. Yan, J. Wu, Z. Li, T. Xie, W. Peng, C. Yin, X. Li, S.H. Scheres, Y. Shi, and N. Yan. 2015. Structure of the rabbit ryanodine receptor RyR1 at near-atomic resolution. Nature. 517: 50–55.
48. Peng, W., H. Shen, J. Wu, W. Guo, X. Pan, R. Wang, S.R.W. Chen, and N. Yan. 2016. Structural basis for the gating mechanism of the type 2 ryanodine receptor RyR2. Science. 354: aah5324.
49. Bai, X.-C., Z. Yan, J. Wu, Z. Li, and N. Yan. 2016. The Central domain of RyR1 is the transducer for long-range allosteric gating of channel opening. Nat. Publ. Gr. 26.
50. Yin, C.-C., H. Han, R. Wei, and F.A. Lai. 2005. Two-dimensional crystallization of the ryanodine receptor Ca2+ release channel on lipid membranes. J. Struct. Biol. 149: 219–24.
51. Yin, C.-C., L.M. Blayney, and F.A. Lai. 2005. Physical Coupling between Ryanodine Receptor–Calcium Release Channels. J. Mol. Biol. 349: 538–546.
52. Marx, S.O., J. Gaburjakova, M. Gaburjakova, C. Henrikson, K. Ondrias, and A.R. Marks. 2001. Coupled Gating Between Cardiac Calcium Release Channels (Ryanodine Receptors). Circ. Res. 88: 1151–1158.
53. Franzini-Armstrong, C., F. Protasi, and V. Ramesh. 1999. Shape, size, and distribution of Ca(2+) release units and couplons in skeletal and cardiac muscles. Biophys. J. 77: 1528–39.
54. Cheng Yin, C., and F. Anthony Lai. 2000. Intrinsic lattice formation by the ryanodine receptor calcium-release channel. Nat. Cell Biol. 2.
55. Asghari, P., D.R.L. Scriven, S. Sanatani, S.K. Gandhi, A.I.M. Campbell, and E.D.W. Moore. 2014. Nonuniform and variable arrangements of ryanodine receptors within Mammalian ventricular couplons. Circ. Res. 115: 252–62.
56. Baddeley, D., I.D. Jayasinghe, L. Lam, S. Rossberger, M.B. Cannell, and C. Soeller. 2009. Optical single-channel resolution imaging of the ryanodine receptor distribution in rat cardiac myocytes. Proc. Natl. Acad. Sci. U. S. A. 106: 22275–80.
57. Jayasinghe, I.D., D. Baddeley, C.H.T. Kong, X.H.T. Wehrens, M.B. Cannell, and C. Soeller. 2012. Nanoscale organization of junctophilin-2 and ryanodine receptors within peripheral couplings of rat ventricular cardiomyocytes. Biophys. J. 102: L19-21.

58. Chen-Izu, Y., S.L. McCulle, C.W. Ward, C. Soeller, B.M. Allen, C. Rabang, M.B. Cannell, C.W. Balke, and L.T. Izu. 2006. Three-dimensional distribution of ryanodine receptor clusters in cardiac myocytes. Biophys. J. 91: 1–13.
59. Soeller, C., D. Crossman, R. Gilbert, and M.B. Cannell. 2007. Analysis of ryanodine receptor clusters in rat and human cardiac myocytes. Proc. Natl. Acad. Sci. U. S. A. 104: 14958–63.
60. Hayashi, T., M.E. Martone, Z. Yu, A. Thor, M. Doi, M.J. Holst, M.H. Ellisman, and M. Hoshijima. 2009. Three-dimensional electron microscopy reveals new details of membrane systems for Ca2+ signaling in the heart. J. Cell Sci. 122: 1005–13.
61. Nakai, J., R.T. Dirksen, H.T. Nguyen, I.N. Pessah, K.G. Beam, and P.D. Allen. 1996. Enhanced dihydropyridine receptor channel activity in the presence of ryanodine receptor. Nature. 380: 72–75.
62. Baylor, S.M., W.K. Chandler, and M.W. Marshall. 1990. Effects of caffeine on calcium release from the sarcoplasmic reticulum in frog skeletal muscle fibres. J. Physiol. 425: 599–626.
63. Lacampagne, A., M.G. Klein, C.W. Ward, and M.F. Schneider. 2000. Two mechanisms for termination of individual Ca2+ sparks in skeletal muscle. Proc. Natl. Acad. Sci. 97: 7823–7828.
64. Buss, W.C., and G.B. Frank. 1969. Calcium and excitation-contraction coupling in mammalian skeletal muscle. Arch. Int. Pharmacodyn. Ther. 181: 15–26.
65. Kawata, H. 1985. Excitation-contraction coupling in the skeletal muscle and the role of external calcium. Nihon seirigaku zasshi J. Physiol. Soc. Japan. 47: 658–672.
66. Bers, D.M. 2004. Macromolecular complexes regulating cardiac ryanodine receptor function. J. Mol. Cell. Cardiol. 37: 417–429.
67. Gomez, A.C., and N. Yamaguchi. 2014. Two regions of the ryanodine receptor calcium channel are involved in Ca(2+)-dependent inactivation. Biochemistry. 53: 1373–9.
68. Laver, D.R., V.J. Owen, P.R. Junankar, N.L. Taske, A.F. Dulhunty, and G.D. Lamb. 1997. Reduced inhibitory effect of Mg2+ on ryanodine receptor-Ca2+ release channels in malignant hyperthermia. Biophys. J. 73: 1913–1924.
69. Meissner, G. 1986. Ryanodine activation and inhibition of the Ca2+ release channel of

sarcoplasmic reticulum. J. Biol. Chem. 261: 6300–6.

70. Li, P., and S.R.W. Chen. 2001. Molecular Basis of Ca 2+ Activation of the Mouse Cardiac Ca 2+ Release Channel (Ryanodine Receptor). J. Gen. Physiol. 7331200: 33–44.
71. Hymel, L., H. Schindler, M. Inui, and S. Fleischer. 1988. Reconstitution of purified cardiac muscle calcium release channel (ryanodine receptor) in planar bilayers. Biochem. Biophys. Res. Commun. 152: 308–314.
72. Chen, S.R., K. Ebisawa, X. Li, and L. Zhang. 1998. Molecular identification of the ryanodine receptor Ca2+ sensor. J. Biol. Chem. 273: 14675–8.
73. Du, G.G., and D.H. MacLennan. 1998. Functional consequences of mutations of conserved, polar amino acids in transmembrane sequences of the Ca2+ release channel (ryanodine receptor) of rabbit skeletal muscle sarcoplasmic reticulum. J. Biol. Chem. 273: 31867–72.
74. Fearnley, C.J., H.L. Roderick, and M.D. Bootman. 2011. Calcium signaling in cardiac myocytes. Cold Spring Harb. Perspect. Biol. 3: a004242.
75. Ching, L.L., A.J. Williams, and R. Sitsapesan. 2000. Evidence for Ca(2+) activation and inactivation sites on the luminal side of the cardiac ryanodine receptor complex. Circ. Res. 87: 201–6.
76. Györke, I., and S. Györke. 1998. Regulation of the cardiac ryanodine receptor channel by luminal Ca2+ involves luminal Ca2+ sensing sites. Biophys. J. 75: 2801–10.
77. Lukyanenko, V., I. Györke, and S. Györke. 1996. Regulation of calcium release by calcium inside the sarcoplasmic reticulum in ventricular myocytes. Pflugers Arch. 432: 1047–54.
78. Stevens, S.C.W., D. Terentyev, A. Kalyanasundaram, M. Periasamy, and S. Györke. 2009. Intra-sarcoplasmic reticulum Ca2+ oscillations are driven by dynamic regulation of ryanodine receptor function by luminal Ca2+ in cardiomyocytes. J. Physiol. 587: 4863–4872.
79. Györke, S., I. Györke, V. Lukyanenko, D. Terentyev, S. Viatchenko-Karpinski, and T.F. Wiesner. 2002. Regulation of sarcoplasmic reticulum calcium release by luminal calcium in cardiac muscle. Front. Biosci. 7: d1454-63.
80. Sitsapesan, R., and A.J. Williams. 1995. The gating of the sheep skeletal sarcoplasmic

reticulum Ca(2+)-release channel is regulated by luminal Ca2+. J. Membr. Biol. 146: 133–44.

81. Kass, R.S., and R.W. Tsien. 1982. Fluctuations in membrane current driven by intracellular calcium in cardiac Purkinje fibers. Biophys. J. 38: 259–69.

82. Stern, M.D., A.A. Kort, G.M. Bhatnagar, and E.G. Lakatta. 1983. Scattered-light intensity fluctuations in diastolic rat cardiac muscle caused by spontaneous Ca++-dependent cellular mechanical oscillations. J. Gen. Physiol. 82: 119–53.

83. Jiang, D., B. Xiao, D. Yang, R. Wang, P. Choi, L. Zhang, H. Cheng, and S.R.W. Chen. 2004. RyR2 mutations linked to ventricular tachycardia and sudden death reduce the threshold for store-overload-induced Ca2+ release (SOICR). Proc. Natl. Acad. Sci. U. S. A. 101: 13062–7.

84. Bers, D.M. 2002. Calcium and cardiac rhythms: physiological and pathophysiological. Circ. Res. 90: 14–7.

85. Lakatta, E.G. 1992. Functional implications of spontaneous sarcoplasmic reticulum Ca2+ release in the heart. Cardiovasc. Res. 26: 193–214.

86. Priori, S.G., C. Napolitano, N. Tiso, M. Memmi, G. Vignati, R. Bloise, V. Sorrentino, and G.A. Danieli. 2001. Mutations in the Cardiac Ryanodine Receptor Gene (hRyR2) Underlie Catecholaminergic Polymorphic Ventricular Tachycardia. Circulation. 103: 196–200.

87. Jiang, D., B. Xiao, L. Zhang, and S.R.W. Chen. 2002. Enhanced basal activity of a cardiac Ca2+ release channel (ryanodine receptor) mutant associated with ventricular tachycardia and sudden death. Circ. Res. 91: 218–25.

88. Bai, Y., P.P. Jones, J. Guo, X. Zhong, R.B. Clark, Q. Zhou, R. Wang, A. Vallmitjana, R. Benitez, L. Hove-Madsen, L. Semeniuk, A. Guo, L.-S. Song, H.J. Duff, and S.R.W. Chen. 2013. Phospholamban knockout breaks arrhythmogenic Ca^{2+} waves and suppresses catecholaminergic polymorphic ventricular tachycardia in mice. Circ. Res. 113: 517–26.

89. Chen, B., A. Guo, Z. Gao, S. Wei, Y.-P. Xie, S.R.W. Chen, M.E. Anderson, and L.-S. Song. 2012. In situ confocal imaging in intact heart reveals stress-induced Ca(2+) release variability in a murine catecholaminergic polymorphic ventricular tachycardia model of type 2 ryanodine receptor(R4496C+/-) mutation. Circ. Arrhythm. Electrophysiol. 5: 841–

9.

90. Jiang, D., W. Chen, R. Wang, L. Zhang, and S.R.W. Chen. 2007. Loss of luminal Ca2+ activation in the cardiac ryanodine receptor is associated with ventricular fibrillation and sudden death. Proc. Natl. Acad. Sci. U. S. A. 104: 18309–14.
91. Xu, L., and G. Meissner. 1998. Regulation of cardiac muscle Ca2+ release channel by sarcoplasmic reticulum lumenal Ca2+. Biophys. J. 75: 2302–12.
92. Tripathy, A., and G. Meissner. 1996. Sarcoplasmic reticulum lumenal Ca2+ has access to cytosolic activation and inactivation sites of skeletal muscle Ca2+ release channel. Biophys. J. 70: 2600–15.
93. Chen, W., R. Wang, B. Chen, X. Zhong, H. Kong, Y. Bai, Q. Zhou, C. Xie, J.J.J.J. Zhang, A. Guo, X. Tian, P.P. Jones, M.L. O ’mara, Y. Liu, T. Mi, L. Zhang, J. Bolstad, L. Semeniuk, H. Cheng, J.J.J.J. Zhang, J. Chen, D.P. Tieleman, A.M. Gillis, H.J. Duff, M. Fill, L.-S. Song, S.R.W. Chen, M.L. O’Mara, Y. Liu, T. Mi, L. Zhang, J. Bolstad, L. Semeniuk, H. Cheng, J.J.J.J. Zhang, J. Chen, D.P. Tieleman, A.M. Gillis, H.J. Duff, M. Fill, L.-S. Song, and S.R.W. Chen. 2014. The ryanodine receptor store-sensing gate controls Ca2+ waves and Ca2+-triggered arrhythmias. Nat. Med. 20: 184–92.
94. Zhang, J., B. Chen, X. Zhong, T. Mi, A. Guo, Q. Zhou, Z. Tan, G. Wu, A.W. Chen, M. Fill, L.-S. Song, and S.R.W. Chen. 2014. The cardiac ryanodine receptor luminal Ca2+ sensor governs Ca2+ waves, ventricular tachyarrhythmias and cardiac hypertrophy in calsequestrin-null mice. Biochem. J. 461: 99–106.
95. Saucerman, J.J., and D.M. Bers. 2012. Calmodulin binding proteins provide domains of local Ca2+ signaling in cardiac myocytes. J. Mol. Cell. Cardiol. 52: 312–6.
96. Lau, K., M.M.Y. Chan, and F. Van Petegem. 2014. Lobe-Specific Calmodulin Binding to Different Ryanodine Receptor Isoforms. Biochemistry. 53: 932–946.
97. Yamaguchi, N., L. Xu, D.A. Pasek, K.E. Evans, and G. Meissner. 2003. Molecular basis of calmodulin binding to cardiac muscle Ca(2+) release channel (ryanodine receptor). J. Biol. Chem. 278: 23480–6.
98. Xiong, L.-W., R.A. Newman, G.G. Rodney, O. Thomas, J.-Z. Zhang, A. Persechini, M.A. Shea, and S.L. Hamilton. 2002. Lobe-dependent regulation of ryanodine receptor type 1 by calmodulin. J. Biol. Chem. 277: 40862–70.

99. Balshaw, D.M., N. Yamaguchi, and G. Meissner. 2002. Modulation of Intracellular Calcium-Release Channels by Calmodulin. J. Membr. Biol. 185: 1–8.

100. Yoshida, A., M. Takahashi, T. Imagawa, M. Shigekawa, H. Takisawa, and T. Nakamura. 1992. Phosphorylation of ryanodine receptors in rat myocytes during beta-adrenergic stimulation. J. Biochem. 111: 186–90.

101. Xiao, B., X. Tian, W. Xie, P.P. Jones, S. Cai, X. Wang, D. Jiang, H. Kong, L. Zhang, K. Chen, M.P. Walsh, H. Cheng, and S.R.W. Chen. 2007. Functional consequence of protein kinase A-dependent phosphorylation of the cardiac ryanodine receptor: sensitization of store overload-induced Ca2+ release. J. Biol. Chem. 282: 30256–64.

102. Witcher, rick R., R.J. KovacsS, H. Schulmans, D.C. Cefali, and L.R. Jones. 1991. Unique Phosphorylation Site on the Cardiac Ryanodine Receptor Regulates Calcium Channel Activity*. J. Biol. Chem. 266: 11144–11152.

103. Tessier, S., P. Karczewski, E.-G. Krause, Y. Pansard, C. Acar, M. Lang-Lazdunski, J.-J. Mercadier, and S.N. Hatem. 1999. Regulation of the Transient Outward K+ Current by Ca2+/Calmodulin-Dependent Protein Kinases II in Human Atrial Myocytes. Circ. Res. 85: 810–819.

104. Wagner, S., N. Dybkova, E.C.L. Rasenack, C. Jacobshagen, L. Fabritz, P. Kirchhof, S.K.G. Maier, T. Zhang, G. Hasenfuss, J.H. Brown, D.M. Bers, and L.S. Maier. 2006. Ca2+/calmodulin-dependent protein kinase II regulates cardiac Na+ channels. J. Clin. Invest. 116: 3127–38.

105. van Oort, R.J., M.D. McCauley, S.S. Dixit, L. Pereira, Y. Yang, J.L. Respress, Q. Wang, A.C. De Almeida, D.G. Skapura, M.E. Anderson, D.M. Bers, and X.H.T. Wehrens. 2010. Ryanodine receptor phosphorylation by calcium/calmodulin-dependent protein kinase II promotes life-threatening ventricular arrhythmias in mice with heart failure. Circulation. 122: 2669–79.

106. Yang, D., W.-Z. Zhu, B. Xiao, D.X.P. Brochet, S.R.W. Chen, E.G. Lakatta, R.-P. Xiao, and H. Cheng. 2007. Ca2+/calmodulin kinase II-dependent phosphorylation of ryanodine receptors suppresses Ca2+ sparks and Ca2+ waves in cardiac myocytes. Circ. Res. 100: 399–407.

107. Lokuta, A.J., T.B. Rogers, W.J. Lederer, and H.H. Valdivia. 1995. Modulation of cardiac

ryanodine receptors of swine and rabbit by a phosphorylation-dephosphorylation mechanism. J. Physiol. 487 (Pt 3): 609–22.

108. Pessah, I.N., and I. Zimanyi. 1991. Characterization of multiple [3H]ryanodine binding sites on the Ca2+ release channel of sarcoplasmic reticulum from skeletal and cardiac muscle: evidence for a sequential mechanism in ryanodine action. Mol. Pharmacol. 39: 679–89.
109. Lai, F.A., M. Misra, L. Xu, H.A. Smith, and G. Meissner. 1989. The ryanodine receptor-Ca2+ release channel complex of skeletal muscle sarcoplasmic reticulum. Evidence for a cooperatively coupled, negatively charged homotetramer. J. Biol. Chem. 264: 16776–85.
110. Reticulum, S., and G. Meissner. 1986. Ryanodine Activation and Inhibition of the Ca2+ Release Channel of Sarcoplasmic Reticulum. J. Biol. Chem. 261: 6300–6306.
111. Coronado, R., J. Morrissette, M. Sukhareva, D.M. Vaughan, and R. Coronado. 1994. Structure and function of ryanodine receptors. Am. J. Physiol. 266: C1485-504.
112. Rousseau, E., and G. Meissner. 1989. Single cardiac sarcoplasmic reticulum Ca2+-release channel: activation by caffeine. Am. J. Physiol. 256: H328-33.
113. Maier, L.S., T. Zhang, L. Chen, J. DeSantiago, J.H. Brown, and D.M. Bers. 2003. Transgenic CaMKIIdeltaC Overexpression Uniquely Alters Cardiac Myocyte Ca2+ Handling: Reduced SR Ca2+ Load and Activated SR Ca2+ Release. Circ. Res. 92: 904–911.
114. Gaburjakova, J., and M. Gaburjakova. 2006. Comparison of the Effects Exerted by Luminal Ca2+ on the Sensitivity of the Cardiac Ryanodine Receptor to Caffeine and Cytosolic Ca2+. J. Membr. Biol. 212: 17–28.
115. Cheek, T.R., R.B. Moreton, M.J. Berridge, K.A. Stauderman, M.M. Murawsky, and M.D. Bootman. 1993. Quantal Ca2+ release from caffeine-sensitive stores in adrenal chromaffin cells. J. Biol. Chem. 268: 27076–83.
116. Kong, H., P.P. Jones, A. Koop, L. Zhang, H.J. Duff, and S.R.W. Chen. 2008. Caffeine induces Ca2+ release by reducing the threshold for luminal Ca2+ activation of the ryanodine receptor. Biochem. J. 414: 441–52.
117. Yu, L., J.E. Coelho, X. Zhang, Y. Fu, A. Tillman, U. Karaoz, B.B. Fredholm, Z. Weng, and J.-F. Chen. 2009. Uncovering multiple molecular targets for caffeine using a drug

target validation strategy combining A 2A receptor knockout mice with microarray profiling. Physiol. Genomics. 37: 199–210.

118. Paul-Pletzer, K., T. Yamamoto, N. Ikemoto, L.S. Jimenez, H. Morimoto, P.G. Williams, J. Ma, and J. Parness. 2005. Probing a putative dantrolene-binding site on the cardiac ryanodine receptor. Biochem. J. 387: 905–9.
119. Chamberlain, B.K., P. Volpeq, and S. Fleischer. 1984. Inhibition of Calcium-induced Calcium Release from Purified Cardiac Sarcoplasmic Reticulum Vesicles*. J. Biol. Chem. 259: 7547–7553.
120. Fratea, S., O. Langeron, Y. Lecarpentier, P. Coriat, and B. Riou. 1997. In vitro effects of dantrolene on rat myocardium. Anesthesiology. 86: 205–15.
121. Zhao, F., P. Li, S.R.W. Chen, C.F. Louis, and B.R. Fruen. 2001. Dantrolene Inhibition of Ryanodine Receptor Ca 2+ Release Channels. J. Biol. Chem. 276: 13810–13816.
122. Jerome, P. Molecular Characterization of Dantrolene Binding Site. .
123. Radermacher, M., V. Rao, R. Grassucci, J. Frank, A.P. Timerman, S. Fleischer, and T. Wagenknecht. 1994. Cryo-electron microscopy and three-dimensional reconstruction of the calcium release channel/ryanodine receptor from skeletal muscle. J. Cell Biol. 127: 411–23.
124. Serysheva, I.I., E. V Orlova, W. Chiu, M.B. Sherman, S.L. Hamilton, and M. van Heel. 1995. Electron cryomicroscopy and angular reconstitution used to visualize the skeletal muscle calcium release channel. Nat. Struct. Biol. 2: 18–24.
125. Saito, A., M. Inui, M. Radermacher, J. Frank, and S. Fleischer. 1988. Ultrastructure of the calcium release channel of sarcoplasmic reticulum. J. Cell Biol. 107: 211–219.
126. Franzini-Armstrong, C., and A.O. Jorgensen. 1994. Structure and development of E-C coupling units in skeletal muscle. Annu. Rev. Physiol. 56: 509–34.
127. Shkryl, V.M., and L.A. Blatter. 2013. Ca(2+) release events in cardiac myocytes up close: insights from fast confocal imaging. PLoS One. 8: e61525.
128. Cannell, M.B., H. Cheng, and W.J. Lederer. 1995. The control of calcium release in heart muscle. Science. 268: 1045–9.
129. López-López, J.R., P.S. Shacklock, C.W. Balke, and W.G. Wier. 1995. Local calcium transients triggered by single L-type calcium channel currents in cardiac cells. Science.

268: 1042–5.

130. Cheng, H., and W.J. Lederer. 2008. Calcium sparks. Physiol. Rev. 88: 1491–545.
131. Cheng, H., W.J. Lederer, and M.B. Cannell. 1993. Calcium sparks: elementary events underlying excitation-contraction coupling in heart muscle. Science. 262: 740–4.
132. Izu, L.T., Y. Xie, D. Sato, T. Bányász, and Y. Chen-Izu. 2013. Ca^{2+} waves in the heart. J. Mol. Cell. Cardiol. 58: 118–24.
133. Katz, A.M. 2011. Physiology of the heart. 5th ed. Philadelphia: Lippincott Williams & Wilkins, a Wolters Kluwer business.
134. Stenger, R.J., and D. Spiro. 1961. The ultrastructure of mammalien cardiac muscle. J. Biophys. Biochem. Cytol. 9: 325–51.
135. Sandow, A. 1952. Excitation-contraction coupling in muscular response. Yale J. Biol. Med. 25: 176–201l.
136. Fabiato, A. 1983. Calcium-induced release of calcium from the cardiac sarcoplasmic reticulum. Am. J. Physiol. 245: C1-14.
137. Postma, A. V, I. Denjoy, J. Kamblock, M. Alders, J.-M. Lupoglazoff, G. Vaksmann, L. Dubosq-Bidot, P. Sebillon, M.M.A.M. Mannens, P. Guicheney, and A.A.M. Wilde. 2005. Catecholaminergic polymorphic ventricular tachycardia: RYR2 mutations, bradycardia, and follow up of the patients. J. Med. Genet. 42: 863–70.
138. Maier, S.K.G., R.E. Westenbroek, K.A. Schenkman, E.O. Feigl, T. Scheuer, and W.A. Catterall. 2001. An unexpected role for brain-type sodium channels in coupling of cell surface depolarization to contraction in the heart. Proc. Natl. Acad. Sci. : 4073–4078.
139. Fabiato, A., and F. Fabiato. 1977. Calcium release from the sarcoplasmic reticulum. Circ. Res. 40: 119–29.
140. Fabiato, A., and F. Fabiato. 1979. Calcium and cardiac excitation-contraction coupling. Annu. Rev. Physiol. 41: 473–84.
141. Stern, M.D., and H. Cheng. 2004. Putting out the fire: what terminates calcium-induced calcium release in cardiac muscle? Cell Calcium. 35: 591–601.
142. Marx, S.O., K. Ondrias, and A.R. Marks. 1998. Coupled gating between individual skeletal muscle Ca2+ release channels (ryanodine receptors). Science. 281: 818–21.
143. Stern, M.D. 1992. Theory of excitation-contraction coupling in cardiac muscle. Biophys.

J. 63: 497–517.

144. Stern, M.D., and E.G. Lakatta. 1992. Excitation-contraction coupling in the heart: the state of the question. FASEB J. 6: 3092–100.

145. López-López, J.R., P.S. Shacklock, C.W. Balke, W.G. Wier, J.R. Lopez-Lopez, P.S. Shacklock, C.W. Balke, and W.G. Wier. 1994. Local, stochastic release of Ca2+ in voltage-clamped rat heart cells: visualization with confocal microscopy. J. Physiol. 480 (Pt 1: 21–29.

146. Cheng, H., M.R. Lederer, R.P. Xiao, A.M. Gómez, Y.Y. Zhou, B. Ziman, H. Spurgeon, E.G. Lakatta, and W.J. Lederer. 1996. Excitation-contraction coupling in heart: new insights from Ca2+ sparks. Cell Calcium. 20: 129–40.

147. Cheng, H., M.R. Lederer, W.J. Lederer, and M.B. Cannell. 1996. Calcium sparks and [Ca2+]i waves in cardiac myocytes. Am. J. Physiol. 270: C148-59.

148. Cannell, M.B., and C. Soeller. 1997. Numerical analysis of ryanodine receptor activation by L-type channel activity in the cardiac muscle diad. Biophys. J. 73: 112–122.

149. Bers, D.M. 2008. Calcium Cycling and Signaling in Cardiac Myocytes. Annu. Rev. Physiol. 70: 23–49.

150. Izu, L.T., S.A. Means, J.N. Shadid, Y. Chen-Izu, and C.W. Balke. 2006. Interplay of ryanodine receptor distribution and calcium dynamics. Biophys. J. 91: 95–112.

151. Huang, J., and W. Honda. 2006. CED: a conformational epitope database. BMC Immunol. 7: 7.

152. Tokunaga, M., N. Imamoto, and K. Sakata-Sogawa. 2008. Highly inclined thin illumination enables clear single-molecule imaging in cells. Nat. Methods. 5: 159–161.

153. Carl, S.L., K. Felix, A.H. Caswell, N.R. Brandt, W.J. Ball, P.L. Vaghy, G. Meissner, and D.G. Ferguson. 1995. Immunolocalization of sarcolemmal dihydropyridine receptor and sarcoplasmic reticular triadin and ryanodine receptor in rabbit ventricle and atrium. J. Cell Biol. 129: 673–82.

154. Asghari, P., M. Schulson, D.R.L. Scriven, G. Martens, and E.D.W. Moore. 2009. Axial tubules of rat ventricular myocytes form multiple junctions with the sarcoplasmic reticulum. Biophys. J. 96: 4651–60.

155. Soeller, C., I.D. Jayasinghe, P. Li, A. V Holden, and M.B. Cannell. 2009. Three-

dimensional high-resolution imaging of cardiac proteins to construct models of intracellular Ca2+ signalling in rat ventricular myocytes. Exp. Physiol. 94: 496–508.

156. Xu, L., and G. Meissner. 2004. Mechanism of Calmodulin Inhibition of Cardiac Sarcoplasmic Reticulum Ca 21 Release Channel (Ryanodine Receptor). Biophys. J. 86: 797–804.

157. Srinivasan, M., D. Sedmak, and S. Jewell. 2002. Effect of fixatives and tissue processing on the content and integrity of nucleic acids. Am. J. Pathol. 161: 1961–71.

158. Thavarajah, R., V.K. Mudimbaimannar, J. Elizabeth, U.K. Rao, and K. Ranganathan. 2012. Chemical and physical basics of routine formaldehyde fixation. J. Oral Maxillofac. Pathol. 16: 400–5.

159. Buchwalow, I., V. Samoilova, W. Boecker, and M. Tiemann. 2011. Non-specific binding of antibodies in immunohistochemistry: fallacies and facts. Sci. Rep. 1: 28.

160. Soboleski, M.R., J. Oaks, and W.P. Halford. 2005. Green fluorescent protein is a quantitative reporter of gene expression in individual eukaryotic cells. FASEB J. 19: 440–2.

161. Bronstein, I., J. Fortin, P.E. Stanley, G.S. Stewart, and L.J. Kricka. 1994. Chemiluminescent and bioluminescent reporter gene assays. Anal. Biochem. 219: 169–81.

162. Otsu, K., H.F. Willard, V.K. Khanna, F. Zorzato, N.M. Green, and D.H. MacLennan. 1990. Molecular cloning of cDNA encoding the Ca2+ release channel (ryanodine receptor) of rabbit cardiac muscle sarcoplasmic reticulum. J. Biol. Chem. 265: 13472–83.

163. Otsu, K., J. Fujii, M. Periasamy, M. Difilippantonio, M. Uppender, D.C. Ward, and D.H. MacLennan. 1993. Chromosome Mapping of Five Human Cardiac and Skeletal Muscle Sarcoplasmic Reticulum Protein Genes. Genomics. 17: 507–509.

164. Baulcombe, D.C., S. Chapman, and S. Santa Cruz. 1995. Jellyfish green fluorescent protein as a reporter for virus infections. Plant J. 7: 1045–53.

165. Remington, S.J. 2011. Green fluorescent protein: a perspective. Protein Sci. 20: 1509–19.

166. Zimmer, M. 2002. Green fluorescent protein (GFP): applications, structure, and related photophysical behavior. Chem. Rev. 102: 759–81.

167. Chalfie, M., Y. Tu, G. Euskirchen, W.W. Ward, and D.C. Prasher. 1994. Green fluorescent protein as a marker for gene expression. Science. 263: 802–5.

168. Ormö, M., A.B. Cubitt, K. Kallio, L.A. Gross, R.Y. Tsien, and S.J. Remington. 1996. Crystal structure of the Aequorea victoria green fluorescent protein. Science. 273: 1392–5.
169. Ormö, M., A.B. Cubitt, K. Kallio, L.A. Gross, R.Y. Tsien, and S.J. Remington. 1996. Crystal structure of the Aequorea victoria green fluorescent protein. Science. 273: 1392–5.
170. Rizzuto, R., M. Brini, P. Pizzo, M. Murgia, and T. Pozzan. 1995. Chimeric green fluorescent protein as a tool for visualizing subcellular organelles in living cells. Curr. Biol. 5: 635–42.
171. Elliott, G., and P. O'Hare. 1999. Live-cell analysis of a green fluorescent protein-tagged herpes simplex virus infection. J. Virol. 73: 4110–9.
172. Boes, M., J. Cerny, R. Massol, M. Op den Brouw, T. Kirchhausen, J. Chen, and H.L. Ploegh. 2002. T-cell engagement of dendritic cells rapidly rearranges MHC class II transport. Nature. 418: 983–8.
173. Gibson, G. 2009. A Primer of Genome Science. Third Edit. Sunderland, Massachusetts: Sinauer.
174. Doyle, A., M.P. McGarry, N.A. Lee, and J.J. Lee. 2012. The construction of transgenic and gene knockout/knockin mouse models of human disease. Transgenic Res. 21: 327–49.
175. Rust, M.J., M. Bates, and X. Zhuang. 2006. Sub-diffraction-limit imaging by stochastic optical reconstruction microscopy (STORM). Nat. Methods. 3: 793–5.
176. Betzig, E., G.H. Patterson, R. Sougrat, O.W. Lindwasser, S. Olenych, J.S. Bonifacino, M.W. Davidson, J. Lippincott-Schwartz, and H.F. Hess. 2006. Imaging intracellular fluorescent proteins at nanometer resolution. Science. 313: 1642–5.
177. Patterson, G., M. Davidson, S. Manley, and J. Lippincott-Schwartz. 2010. Superresolution imaging using single-molecule localization. Annu. Rev. Phys. Chem. 61: 345–67.
178. Kohl, T., V. Westphal, S.W. Hell, and S.E. Lehnart. 2013. Superresolution microscopy in heart — Cardiac nanoscopy. J. Mol. Cell. Cardiol. 58: 13–21.
179. Hayat M.A. 1986. Glutaraldehyde: Role in electron microscopy. Micron Microsc. Acta. 17: 115–135.
180. Gray, E.G. 1959. Electron microscopy of synaptic contacts on dendrite spines of the cerebral cortex. Nature. 183: 1592–3.
181. Watson, M.L. 1958. Staining of tissue sections for electron microscopy with heavy metals.

II. Application of solutions containing lead and barium. J. Biophys. Biochem. Cytol. 4: 727–30.

182. Angermüller, S., and H.D. Fahimi. 1982. Imidazole-buffered osmium tetroxide: an excellent stain for visualization of lipids in transmission electron microscopy. Histochem. J. 14: 823–35.

183. Franzini-Armstrong, C. 1970. Studies of the Triad: I. Structure of the Junction in Frog Twitch Fibers. J. Cell Biol. 47: 488–99.

184. Campbell, K.P., C.M. Knudson, T. Imagawa, A.T. Leung, J.L. Sutko, S.D. Kahl, C.R. Raab, and L. Madson. 1987. Identification and characterization of the high affinity [3H]ryanodine receptor of the junctional sarcoplasmic reticulum Ca2+ release channel. J. Biol. Chem. 262: 6460–3.

185. Kawamoto, R.M., J.P. Brunschwig, K.C. Kim, and A.H. Caswell. 1986. Isolation, characterization, and localization of the spanning protein from skeletal muscle triads. J. Cell Biol. 103: 1405–14.

186. Jorgensen, A.O., A.C. Shen, W. Arnold, A.T. Leung, and K.P. Campbell. 1989. Subcellular distribution of the 1,4-dihydropyridine receptor in rabbit skeletal muscle in situ: an immunofluorescence and immunocolloidal gold-labeling study. J. Cell Biol. 109: 135–47.

187. Yuan, S.H., W. Arnold, and A.O. Jorgensen. 1991. Biogenesis of transverse tubules and triads: immunolocalization of the 1,4-dihydropyridine receptor, TS28, and the ryanodine receptor in rabbit skeletal muscle developing in situ. J. Cell Biol. 112: 289–301.

188. Carl, S.L., K. Felix, A.H. Caswell, N.R. Brandt, J.-P. Brunschwig, G. Meissner, and D.G. Ferguson. 1995. Immunolocalization of triadin, DHP receptors, and ryanodine receptors in adult and developing skeletal muscle of rats. Muscle Nerve. 18: 1232–1243.

189. Protasi, F., C. Franzini-Armstrong, and B.E. Flucher. 1997. Coordinated incorporation of skeletal muscle dihydropyridine receptors and ryanodine receptors in peripheral couplings of BC3H1 cells. J. Cell Biol. 137: 859–70.

190. Franzini-Armstrong, C., and G. Nunzi. 1983. Junctional feet and particles in the triads of a fast-twitch muscle fibre. J. Muscle Res. Cell Motil. 4: 233–52.

191. Schneider, M.F. 1981. Membrane Charge Movement and Depolarization-Contraction

Coupling. Annu. Rev. Physiol. 43: 507–517.

192. Sun, X.H., F. Protasi, M. Takahashi, H. Takeshima, D.G. Ferguson, and C. Franzini-Armstrong. 1995. Molecular architecture of membranes involved in excitation-contraction coupling of cardiac muscle. J. Cell Biol. 129: 659–71.

193. Protasi, F., X.-H. Sun, and C. Franzini-Armstrong. 1996. Formation and Maturation of the Calcium Release Apparatus in Developing and Adult Avian Myocardium. Dev. Biol. 173: 265–278.

194. Burnette, D.T., P. Sengupta, Y. Dai, J. Lippincott-Schwartz, and B. Kachar. 2011. Bleaching/blinking assisted localization microscopy for superresolution imaging using standard fluorescent molecules. Proc. Natl. Acad. Sci. U. S. A. 108: 21081–6.

195. Paredes, R.M., J.C. Etzler, L.T. Watts, W. Zheng, and J.D. Lechleiter. 2008. Chemical calcium indicators. Methods. 46: 143–51.

196. Xiao, R.-P., H.H. Valdivia, K. Bogdanov, C. Valdivia, E.G. Lakatta, and H. Cheng. 1997. The immunophilin FK506-binding protein modulates CaO release channel closure in rat heart. J. Physiol. 500: 343–354.

197. Bray, M.-A., N.A. Geisse, and K.K. Parker. 2007. Multidimensional Detection and Analysis of Ca 2+ Sparks in Cardiac Myocytes. Biophys. J. 92: 4433–4443.

198. Bridge, J.H., P.R. Ershler, and M.B. Cannell. 1999. Properties of Ca2+ sparks evoked by action potentials in mouse ventricular myocytes. J. Physiol. 518 (Pt 2): 469–78.

199. Shen, J.-X., S. Wang, L.-S. Song, T. Han, and H. Cheng. 2004. Polymorphism of Ca 2+ Sparks Evoked from In-Focus Ca 2+ Release Units in Cardiac Myocytes. Biophys. J. 86: 182–190.

200. Shirokova, N., A. González, W.G. Kirsch, E. Ríos, G. Pizarro, M.D. Stern, and H. Cheng. 1999. Calcium sparks: release packets of uncertain origin and fundamental role. J. Gen. Physiol. 113: 377–84.

201. Lipp, P., and E. Niggli. 1994. Modulation of Ca2+ release in cultured neonatal rat cardiac myocytes. Insight from subcellular release patterns revealed by confocal microscopy. Circ. Res. 74: 979–90.

202. Wang, S.-Q., L.-S. Song, E.G. Lakatta, and H. Cheng. 2001. Ca2+ signalling between single L-type Ca2+ channels and ryanodine receptors in heart cells. Nature. 410: 592–596.

203. Sobie, E.A., K.W. Dilly, J. dos Santos Cruz, W.J. Lederer, and M.S. Jafri. 2002. Termination of cardiac Ca(2+) sparks: an investigative mathematical model of calcium-induced calcium release. Biophys. J. 83: 59–78.
204. Bers, D.M., and M. Fill. 1998. Coordinated feet and the dance of ryanodine receptors. Science. 281: 790–1.
205. Parker, I., W.J. Zang, and W.G. Wier. 1996. Ca2+ sparks involving multiple Ca2+ release sites along Z-lines in rat heart cells. J. Physiol. 497 (Pt 1: 31–8.
206. Lukyanenko, V., A. Ziman, A. Lukyanenko, V. Salnikov, and W.J. Lederer. 2007. Functional groups of ryanodine receptors in rat ventricular cells. J. Physiol. 583: 251–69.
207. Subramanian, S., S. Viatchenko-Karpinski, V. Lukyanenko, S. Györke, and T.F. Wiesner. 2001. Underlying mechanisms of symmetric calcium wave propagation in rat ventricular myocytes. Biophys. J. 80: 1–11.
208. Jayasinghe, I.D., D.J. Crossman, C. Soeller, and M.B. Cannell. 2010. A new twist in cardiac muscle: dislocated and helicoid arrangements of myofibrillar z-disks in mammalian ventricular myocytes. J. Mol. Cell. Cardiol. 48: 964–971.
209. Wang, S.Q., M.D. Stern, E. Ríos, H. Cheng, and C. Franzini-Armstrong. 2004. The quantal nature of Ca2+ sparks and in situ operation of the ryanodine receptor array in cardiac cells. Proc. Natl. Acad. Sci. 101: 3979–3984.
210. Brette, F., L. Sallé, and C.H. Orchard. 2004. Differential Modulation of L-type Ca2+ Current by SR Ca2+ Release at the T-Tubules and Surface Membrane of Rat Ventricular Myocytes. Circ. Res. 95: e1–e7.
211. Scriven, D.R.L., P. Dan, and E.D.W. Moore. 2000. Distribution of Proteins Implicated in Excitation-Contraction Coupling in Rat Ventricular Myocytes. Biophys. J. 79: 2682–2691.
212. Tsien, R.Y. 1998. The green fluorescent protein. Annu. Rev. Biochem. 67: 509–44.
213. Hell, S.W., and J. Wichmann. 1994. Breaking the diffraction resolution limit by stimulated emission: stimulated-emission-depletion fluorescence microscopy. Opt. Lett. 19: 780–2.
214. Dan, P., E. Lin, J. Huang, P. Biln, and G.F. Tibbits. 2007. Three-dimensional distribution of cardiac Na+-Ca2+ exchanger and ryanodine receptor during development. Biophys. J. 93: 2504–18.

215. Jayasinghe, I.D., M.B. Cannell, and C. Soeller. 2009. Organization of ryanodine receptors, transverse tubules, and sodium-calcium exchanger in rat myocytes. Biophys. J. 97: 2664–73.
216. Morgan, C.G., and A.C. Mitchell. 2006. Total internal reflection fluorescence imaging using an upconverting cover slip for multicolour evanescent excitation. J. Microsc. 222: 48–57.
217. Fish, K.N. 2009. Total internal reflection fluorescence (TIRF) microscopy. Curr. Protoc. Cytom. Chapter 12: Unit12.18.
218. Sanderson, M.J., I. Smith, I. Parker, and M.D. Bootman. 2014. Fluorescence microscopy. Cold Spring Harb. Protoc. 2014: pdb.top071795.
219. MacDonald, L., G. Baldini, and B. Storrie. 2015. Does super-resolution fluorescence microscopy obsolete previous microscopic approaches to protein co-localization? Methods Mol. Biol. 1270: 255–75.
220. Göröcs, Z., E. McLeod, and A. Ozcan. 2015. Enhanced light collection in fluorescence microscopy using self-assembled micro-reflectors. Sci. Rep. 5: 10999.
221. Hell, S.W. 2007. Far-field optical nanoscopy. Science. 316: 1153–8.
222. Gustafsson, M.G.L. 2005. Nonlinear structured-illumination microscopy: wide-field fluorescence imaging with theoretically unlimited resolution. Proc. Natl. Acad. Sci. U. S. A. 102: 13081–6.
223. Heintzmann, R., T.M. Jovin, and C. Cremer. 2002. Saturated patterned excitation microscopy—a concept for optical resolution improvement. J. Opt. Soc. Am. A. 19: 1599.
224. Schmidt, R., C.A. Wurm, A. Punge, A. Egner, S. Jakobs, and S.W. Hell. 2009. Mitochondrial cristae revealed with focused light. Nano Lett. 9: 2508–10.
225. Shim, S.-H., C. Xia, G. Zhong, H.P. Babcock, J.C. Vaughan, B. Huang, X. Wang, C. Xu, G.-Q. Bi, and X. Zhuang. 2012. Super-resolution fluorescence imaging of organelles in live cells with photoswitchable membrane probes. Proc. Natl. Acad. Sci. U. S. A. 109: 13978–83.
226. Baddeley, D., M.B. Cannell, and C. Soeller. 2011. Three-dimensional sub-100 nm super-resolution imaging of biological samples using a phase ramp in the objective pupil. Nano Res. 4: 589–598.

227. Baddeley, D., D. Crossman, S. Rossberger, J.E. Cheyne, J.M. Montgomery, I.D. Jayasinghe, C. Cremer, M.B. Cannell, and C. Soeller. 2011. 4D Super-Resolution Microscopy with Conventional Fluorophores and Single Wavelength Excitation in Optically Thick Cells and Tissues. PLoS One. 6: e20645.
228. Heilemann, M., S. van de Linde, M. Schüttpelz, R. Kasper, B. Seefeldt, A. Mukherjee, P. Tinnefeld, and M. Sauer. 2008. Subdiffraction-Resolution Fluorescence Imaging with Conventional Fluorescent Probes. Angew. Chemie Int. Ed. 47: 6172–6176.
229. van de Linde, S., M. Sauer, and M. Heilemann. 2008. Subdiffraction-resolution fluorescence imaging of proteins in the mitochondrial inner membrane with photoswitchable fluorophores. J. Struct. Biol. 164: 250–254.
230. Hess, S.T., T.P.K. Girirajan, and M.D. Mason. 2006. Ultra-high resolution imaging by fluorescence photoactivation localization microscopy. Biophys. J. 91: 4258–72.
231. Gustafsson, Agard, and Sedat. 1999. I5M: 3D widefield light microscopy with better than 100 nm axial resolution. J. Microsc. 195: 10–16.
232. Hell, S.W., S.J. Sahl, M. Bates, X. Zhuang, and R. Heintzmann. 2015. The 2015 super-resolution microscopy roadmap Topical Review. J. Phys. 48: 443001.
233. Wagner, E., M.A. Lauterbach, T. Kohl, V. Westphal, G.S.B. Williams, J.H. Steinbrecher, J.-H. Streich, B. Korff, H.-T.M. Tuan, B. Hagen, S. Luther, G. Hasenfuss, U. Parlitz, M.S. Jafri, S.W. Hell, W.J. Lederer, and S.E. Lehnart. 2012. Stimulated emission depletion live-cell super-resolution imaging shows proliferative remodeling of T-tubule membrane structures after myocardial infarction. Circ. Res. 111: 402–14.
234. Harmsen, M.M., and H.J. De Haard. 2007. Properties, production, and applications of camelid single-domain antibody fragments. Appl. Microbiol. Biotechnol. 77: 13–22.
235. Muyldermans, S. 2013. Nanobodies: natural single-domain antibodies. Annu. Rev. Biochem. 82: 775–97.
236. Wesolowski, J., V. Alzogaray, J. Reyelt, M. Unger, K. Juarez, M. Urrutia, A. Cauerhff, W. Danquah, B. Rissiek, F. Scheuplein, N. Schwarz, S. Adriouch, O. Boyer, M. Seman, A. Licea, D. V Serreze, F.A. Goldbaum, F. Haag, and F. Koch-Nolte. 2009. Single domain antibodies: promising experimental and therapeutic tools in infection and immunity. Med. Microbiol. Immunol. 198: 157–74.

237. Kubala, M.H., O. Kovtun, K. Alexandrov, and B.M. Collins. 2010. Structural and thermodynamic analysis of the GFP:GFP-nanobody complex. Protein Sci. 19: 2389–401.
238. Rothbauer, U., K. Zolghadr, S. Muyldermans, A. Schepers, M.C. Cardoso, and H. Leonhardt. 2008. A versatile nanotrap for biochemical and functional studies with fluorescent fusion proteins. Mol. Cell. Proteomics. 7: 282–9.
239. Ries, J., C. Kaplan, E. Platonova, H. Eghlidi, and H. Ewers. 2012. A simple, versatile method for GFP-based super-resolution microscopy via nanobodies. Nat. Methods. 9: 582–584.
240. Rissiek, B., F. Koch-Nolte, and T. Magnus. 2014. Nanobodies as modulators of inflammation: potential applications for acute brain injury. Front. Cell. Neurosci. 8: 344.
241. Kirichok, Y., G. Krapivinsky, and D.E. Clapham. 2004. The mitochondrial calcium uniporter is a highly selective ion channel. Nature. 427: 360–364.
242. Rizzuto, R., P. Pinton, W. Carrington, F.S. Fay, K.E. Fogarty, L.M. Lifshitz, R.A. Tuft, and T. Pozzan. 1998. Close contacts with the endoplasmic reticulum as determinants of mitochondrial Ca2+ responses. Science. 280: 1763–6.
243. O 'rourke, B., and L.A. Blatter. 2009. Mitochondrial Ca 2+ uptake: tortoise or hare? J Mol Cell Cardiol. 46: 767–774.
244. Marchi, S., and P. Pinton. 2014. The mitochondrial calcium uniporter complex: molecular components, structure and physiopathological implications. J Physiol J. Physiol. T. 5925: 829–839.
245. Pacher, P., A.P. Thomas, and G. Hajnóczky. 2002. Ca2+ marks: miniature calcium signals in single mitochondria driven by ryanodine receptors. Proc. Natl. Acad. Sci. U. S. A. 99: 2380–5.
246. Belmonte, S., and M. Morad. 2008. "Pressure–flow"-triggered intracellular Ca 2+ transients in rat cardiac myocytes: possible mechanisms and role of mitochondria. J Physiol. 5865: 1379–1397.
247. Roston, T.M., J.M. Vinocur, K.R. Maginot, S. Mohammed, J.C. Salerno, S.P. Etheridge, M. Cohen, R.M. Hamilton, A. Pflaumer, R.J. Kanter, J.E. Potts, M.J. LaPage, K.K. Collins, R.A. Gebauer, J.D. Temple, A.S. Batra, C. Erickson, M. Miszczak-Knecht, P. Kubuš, Y. Bar-Cohen, M. Kantoch, V.C. Thomas, G. Hessling, C. Anderson, M.-L.

Young, M. Cabrera Ortega, Y.R. Lau, C.L. Johnsrude, A. Fournier, P.J. Kannankeril, and S. Sanatani. 2015. Catecholaminergic polymorphic ventricular tachycardia in children: analysis of therapeutic strategies and outcomes from an international multicenter registry. Circ. Arrhythm. Electrophysiol. 8: 633–42.

248. Sy, R.W., M.H. Gollob, G.J. Klein, R. Yee, A.C. Skanes, L.J. Gula, P. Leong-Sit, R.M. Gow, M.S. Green, D.H. Birnie, and A.D. Krahn. 2011. Arrhythmia characterization and long-term outcomes in catecholaminergic polymorphic ventricular tachycardia. Hear. Rhythm. 8: 864–871.

249. Leenhardt, A., V. Lucet, I. Denjoy, F. Grau, D.D. Ngoc, and P. Coumel. 1995. Catecholaminergic polymorphic ventricular tachycardia in children. A 7-year follow-up of 21 patients. Circulation. 91: 1512–9.

250. Lehnart, S.E., X.H.T. Wehrens, P.J. Laitinen, S.R. Reiken, S.-X. Deng, Z. Cheng, D.W. Landry, K. Kontula, H. Swan, and A.R. Marks. 2004. Sudden Death in Familial Polymorphic Ventricular Tachycardia Associated With Calcium Release Channel (Ryanodine Receptor) Leak. Circulation. 109: 3208–3214.

251. Wilders, R. 2012. Cardiac ion channelopathies and the sudden infant death syndrome. ISRN Cardiol. 2012: 846171.

252. Tester, D.J., A. Medeiros-Domingo, M.L. Will, C.M. Haglund, and M.J. Ackerman. 2012. Cardiac channel molecular autopsy: insights from 173 consecutive cases of autopsy-negative sudden unexplained death referred for postmortem genetic testing. Mayo Clin. Proc. 87: 524–39.

253. Sumitomo, N., K. Harada, M. Nagashima, T. Yasuda, Y. Nakamura, Y. Aragaki, A. Saito, K. Kurosaki, K. Jouo, M. Koujiro, S. Konishi, S. Matsuoka, T. Oono, S. Hayakawa, M. Miura, H. Ushinohama, T. Shibata, and I. Niimura. 2003. Catecholaminergic polymorphic ventricular tachycardia: electrocardiographic characteristics and optimal therapeutic strategies to prevent sudden death. Heart. 89: 66–70.

254. Laitinen, P.J., K.M. Brown, K. Piippo, H. Swan, J.M. Devaney, B. Brahmbhatt, E.A. Donarum, M. Marino, N. Tiso, M. Viitasalo, L. Toivonen, D.A. Stephan, and K. Kontula. 2001. Mutations of the cardiac ryanodine receptor (RyR2) gene in familial polymorphic ventricular tachycardia. Circulation. 103: 485–90.

255. Priori, S.G., C. Napolitano, M. Memmi, B. Colombi, F. Drago, M. Gasparini, L. DeSimone, F. Coltorti, R. Bloise, R. Keegan, F.E.S. Cruz Filho, G. Vignati, A. Benatar, and A. DeLogu. 2002. Clinical and molecular characterization of patients with catecholaminergic polymorphic ventricular tachycardia. Circulation. 106: 69–74.
256. Hayashi, M., I. Denjoy, F. Extramiana, A. Maltret, N.R. Buisson, J.-M. Lupoglazoff, D. Klug, M. Hayashi, S. Takatsuki, E. Villain, J. Kamblock, A. Messali, P. Guicheney, J. Lunardi, and A. Leenhardt. 2009. Incidence and Risk Factors of Arrhythmic Events in Catecholaminergic Polymorphic Ventricular Tachycardia. Circulation. 119: 2426–2434.
257. Swan, H., K. Piippo, M. Viitasalo, P. Heikkilä, T. Paavonen, K. Kainulainen, J. Kere, P. Keto, K. Kontula, and L. Toivonen. 1999. Arrhythmic Disorder Mapped to Chromosome 1q42– q43 Causes Malignant Polymorphic Ventricular Tachycardia in Structurally Normal Hearts. J. Am. Coll. Cardiol. 34: 2035–42.
258. Sumitomo, N. 2016. Current topics in catecholaminergic polymorphic ventricular tachycardia. J. Arrhythmia. 32: 344–351.
259. Medeiros-Domingo, A., Z.A. Bhuiyan, D.J. Tester, N. Hofman, H. Bikker, J.P. van Tintelen, M.M.A.M. Mannens, A.A.M. Wilde, and M.J. Ackerman. 2009. The RYR2-encoded ryanodine receptor/calcium release channel in patients diagnosed previously with either catecholaminergic polymorphic ventricular tachycardia or genotype negative, exercise-induced long QT syndrome: a comprehensive open reading frame mutational analysis. J. Am. Coll. Cardiol. 54: 2065–74.
260. van der Werf, C., and A.A.M. Wilde. 2013. Catecholaminergic polymorphic ventricular tachycardia: from bench to bedside. Heart. 99: 497–504.
261. Wehrens, X.H.T., S.E. Lehnart, F. Huang, J.A. Vest, S.R. Reiken, P.J. Mohler, J. Sun, S. Guatimosim, L.S. Song, N. Rosemblit, J.M. D'Armiento, C. Napolitano, M. Memmi, S.G. Priori, W.J. Lederer, and A.R. Marks. 2003. FKBP12.6 deficiency and defective calcium release channel (ryanodine receptor) function linked to exercise-induced sudden cardiac death. Cell. 113: 829–40.
262. Wehrens, X.H.T., S.E. Lehnart, S.R. Reiken, S.-X. Deng, J.A. Vest, D. Cervantes, J. Coromilas, D.W. Landry, and A.R. Marks. 2004. Protection from Cardiac Arrhythmia Through Ryanodine Receptor-Stabilizing Protein Calstabin2. Science (80-.). 304: 292–

296.

263. Lehnart, S.E., M. Mongillo, A. Bellinger, N. Lindegger, B.X. Chen, W. Hsueh, S. Reiken, A. Wronska, L.J. Drew, C.W. Ward, W.J. Lederer, R.S. Kass, G. Morley, and A.R. Marks. 2008. Leaky Ca2+ release channel/ryanodine receptor 2 causes seizures and sudden cardiac death in mice. J. Clin. Invest. 118: 2230–45.

264. Jiang, D., R. Wang, B. Xiao, H. Kong, D.J. Hunt, P. Choi, L. Zhang, and S.R.W. Chen. 2005. Enhanced store overload-induced Ca2+ release and channel sensitivity to luminal Ca2+ activation are common defects of RyR2 mutations linked to ventricular tachycardia and sudden death. Circ. Res. 97: 1173–81.

265. George, C.H., G. V Higgs, and F.A. Lai. 2003. Ryanodine receptor mutations associated with stress-induced ventricular tachycardia mediate increased calcium release in stimulated cardiomyocytes. Circ. Res. 93: 531–40.

266. Hunt, D.J., P.P. Jones, R. Wang, W. Chen, J. Bolstad, K. Chen, Y. Shimoni, and S.R.W. Chen. 2007. K201 (JTV519) suppresses spontaneous Ca2+ release and [3H]ryanodine binding to RyR2 irrespective of FKBP12.6 association. Biochem. J. 404: 431–8.

267. Liu, N., B. Colombi, M. Memmi, S. Zissimopoulos, N. Rizzi, S. Negri, M. Imbriani, C. Napolitano, F.A. Lai, and S.G. Priori. 2006. Arrhythmogenesis in catecholaminergic polymorphic ventricular tachycardia: Insights from a RyR2 R4496C knock-in mouse model. Circ. Res. 99: 292–298.

268. Liu, N., N. Rizzi, L. Boveri, and S.G. Priori. 2009. Ryanodine receptor and calsequestrin in arrhythmogenesis: what we have learnt from genetic diseases and transgenic mice. J. Mol. Cell. Cardiol. 46: 149–59.

269. Zhou, Q., J. Xiao, D. Jiang, R. Wang, K. Vembaiyan, A. Wang, C.D. Smith, C. Xie, W. Chen, J. Zhang, X. Tian, P.P. Jones, X. Zhong, A. Guo, H. Chen, L. Zhang, W. Zhu, D. Yang, X. Li, J. Chen, A.M. Gillis, H.J. Duff, H. Cheng, A.M. Feldman, L.-S. Song, M. Fill, T.G. Back, and S.R.W. Chen. 2011. Carvedilol and its new analogs suppress arrhythmogenic store overload-induced Ca2+ release. Nat. Med. 17: 1003–9.

270. Thomas, N.L., C.H. George, and F.A. Lai. 2004. Functional heterogeneity of ryanodine receptor mutations associated with sudden cardiac death. Cardiovasc. Res. 64: 52–60.

271. Eisner, D.A., A.W. Trafford, M.E. Díaz, C.L. Overend, and S.C. O'Neill. 1998. The

control of Ca release from the cardiac sarcoplasmic reticulum: regulation versus autoregulation. Cardiovasc. Res. 38: 589–604.

272. Ikemoto, N., and T. Yamamoto. 2002. Regulation of calcium release by interdomain interaction within ryanodine receptors. Front. Biosci. 7: d671-83.

273. Oda, T., M. Yano, T. Yamamoto, T. Tokuhisa, S. Okuda, M. Doi, T. Ohkusa, Y. Ikeda, S. Kobayashi, N. Ikemoto, and M. Matsuzaki. 2005. Defective Regulation of Interdomain Interactions Within the Ryanodine Receptor Plays a Key Role in the Pathogenesis of Heart Failure. Circulation. 111: 3400–3410.

274. Tateishi, H., M. Yano, M. Ohno, X. Xu, H. Uchinoumi, S. Kobayashi, T. Yamamoto, Y. Ikeda, and M. Matsuzaki. 2007. Potential Treatment Of Mutation-linked Lethal Arrhythmia By Correcting Defective Inter-domain Interaction Within The Cardiac Ryanodine Recepter. Circulation. 116.

275. George, C.H., H. Jundi, N. Walters, N.L. Thomas, R.R. West, and F.A. Lai. 2005. Arrhythmogenic Mutation-Linked Defects in Ryanodine Receptor Autoregulation Reveal a Novel Mechanism of Ca2+ Release Channel Dysfunction. Circ. Res. 98: 88–97.

276. Cerrone, M., B. Colombi, M. Santoro, M.R. di Barletta, M. Scelsi, L. Villani, C. Napolitano, and S.G. Priori. 2005. Bidirectional Ventricular Tachycardia and Fibrillation Elicited in a Knock-In Mouse Model Carrier of a Mutation in the Cardiac Ryanodine Receptor. Circ. Res. 96: e77–e82.

277. Kobayashi, S., M. Yano, H. Uchinoumi, T. Suetomi, T. Susa, M. Ono, X. Xu, H. Tateishi, T. Oda, S. Okuda, M. Doi, T. Yamamoto, and M. Matsuzaki. 2010. Dantrolene, a therapeutic agent for malignant hyperthermia, inhibits catecholaminergic polymorphic ventricular tachycardia in a RyR2(R2474S/+) knock-in mouse model. Circ. J. 74: 2579–84.

278. Lieve, K.V.V., J.M.A. Verhagen, J.M. Bos, C. Van Der Werf, I.M.E. Frohn-Mulder, T. Aiba, H.J.G. Crijns, A.C. Blank, A.C.P. Wiesfeld, N. Sumitomo, S.R.W. Chen, J. Till, M.J. Ackerman, I.M.B. Van Der Laar, and A.A.M. Wilde. 2017. Neurodevelopmental disorders in patients with RYR2-associated catecholaminergic polymorphic ventricular tachycardia. Eur. Heart J. 38.

279. Hamdan, F.F., M. Srour, J.-M. Capo-Chichi, H. Daoud, C. Nassif, L. Patry, C. Massicotte,

A. Ambalavanan, D. Spiegelman, O. Diallo, E. Henrion, A. Dionne-Laporte, A. Fougerat, A. V Pshezhetsky, S. Venkateswaran, G.A. Rouleau, and J.L. Michaud. 2014. De Novo Mutations in Moderate or Severe Intellectual Disability. PLoS Genet. 10: e1004772.

280. LaPage, M.J., M.W. Russell, D.J. Bradley, and M. Dick. 2012. Novel Ryanodine Receptor 2 Mutation Associated with a Severe Phenotype of Catecholaminergic Polymorphic Ventricular Tachycardia. J. Pediatr. 161: 362–364.
281. Raymond, C.R., and S.J. Redman. 2006. Spatial segregation of neuronal calcium signals encodes different forms of LTP in rat hippocampus. J. Physiol. 570: 97–111.
282. Pozzo-Miller, L.D., J.A. Connor, and S.B. Andrews. 2000. Microheterogeneity of calcium signalling in dendrites. J. Physiol. 525 Pt 1: 53–61.
283. Baker, K.D., T.M. Edwards, and N.S. Rickard. 2013. The role of intracellular calcium stores in synaptic plasticity and memory consolidation. Neurosci. Biobehav. Rev. 37: 1211–39.
284. Fitzjohn, S.M., and G.L. Collingridge. 2002. Calcium stores and synaptic plasticity. Cell Calcium. 32: 405–11.
285. Emptage, N., T.V.P.P. Bliss, and A. Fine. 1999. Single Synaptic Events Evoke NMDA Receptor–Mediated Release of Calcium from Internal Stores in Hippocampal Dendritic Spines. Neuron. 22: 115–124.
286. Shimizu, H., M. Fukaya, M. Yamasaki, M. Watanabe, T. Manabe, and H. Kamiya. 2008. Use-dependent amplification of presynaptic Ca2+ signaling by axonal ryanodine receptors at the hippocampal mossy fiber synapse. Proc. Natl. Acad. Sci. U. S. A. 105: 11998–2003.
287. McPherson, P.S., and K.P. Campbell. 1990. Solubilization and Biochemical Characterization of the High Affinity [3H]Ryanodine Receptor from Rabbit Brain Membranes. J. Biol. Chem. 265: 18454–160.
288. Nakanishi, S., G. Kuwajima, and K. Mikoshiba. 1992. Immunohistochemical localization of ryanodine receptors in mouse central nervous system. Neurosci. Res. 15: 130–142.
289. Padua, R.A.A., T. Yamamoto, D. Fyda, M.A.A. Sawchuk, J.D. Geiger, and J.I.L. Nagy. 1992. Autoradiographic analysis of [3H]ryanodine binding sites in rat brain: Regional distribution and the effects of lesions on sites in the hippocampus. J. Chem. Neuroanat. 5: 63–73.

290. Sharp, A.H., P.S. McPherson, T.M. Dawson, C. Aoki, K.P. Campbell, and S.H. Snyder. 1993. Differential immunohistochemical localization of inositol 1,4,5-trisphosphate- and ryanodine-sensitive Ca2+ release channels in rat brain. J. Neurosci. 13: 3051–63.
291. Lai, F.A., M. Dent, C. Wickenden, L. Xu, G. Kumari, M. Misra, H.B. Lee, M. Sar, and G. Meissner. 1992. Expression of a cardiac Ca(2+)-release channel isoform in mammalian brain. Biochem. J. 288 Pt 2: 553–64.
292. Galeotti, N., A. Quattrone, E. Vivoli, M. Norcini, A. Bartolini, and C. Ghelardini. 2008. Different involvement of type 1, 2, and 3 ryanodine receptors in memory processes. Learn. Mem. 15: 315–23.
293. Seymour-Laurent, K.J., and M.E. Barish. 1995. lnositol 1,4,5-Trisphosphate and Ryanodine Receptor Distributions and Patterns of Acetylcholine- and Caffeine-Induced Calcium Release in Cultured Mouse Hippocampal Neurons. J. Neurosci. 15: 2592–2608.
294. Hertle, D.N., and M.F. Yeckel. 2007. Distribution of inositol-1,4,5-trisphosphate receptor isotypes and ryanodine receptor isotypes during maturation of the rat hippocampus. Neuroscience. 150: 625–38.
295. Reyes, M., and P.K. Stanton. 1996. Induction of Hippocampal Long-Term Depression Requires Release of Ca 2+ from Separate Presynaptic and Postsynaptic Intracellular Stores. J. Neurosci. 16: 5951–59060.
296. Reyes-Harde, M., R. Empson, B.V.L. Potter, A. Galione, and P.K. Stanton. 1999. Evidence of a role for cyclic ADP-ribose in long-term synaptic depression in hippocampus. Proc. Natl. Acad. Sci. U. S. A. 96: 4061–4066.
297. Nakamura, T., N. Lasser-Ross, K. Nakamura, and W.N. Ross. 2002. Spatial Segregation and Interaction of Calcium Signalling Mechanisms in Rat Hippocampal CA1 Pyramidal Neurons. J. Physiol. 543: 465–80.
298. Korkotian, E., and M. Segal. 1999. Release of calcium from stores alters the morphology of dendritic spines in cultured hippocampal neurons. Proc. Natl. Acad. Sci. U. S. A. 96: 12068–72.
299. Martínez-Serrano, A., and J. Satrústegui. 1989. Caffeine-sensitive calcium stores in presynaptic nerve endings: a physiological role? Biochem. Biophys. Res. Commun. 161: 965–71.

300. Emptage, N.J., C.A. Reid, and A. Fine. 2001. Calcium stores in hippocampal synaptic boutons mediate short-term plasticity, store-operated Ca2+ entry, and spontaneous transmitter release. Neuron. 29: 197–208.
301. Ziviani, E., G. Lippi, D. Bano, E. Munarriz, S. Guiducci, M. Zoli, K.W. Young, and P. Nicotera. 2011. Ryanodine receptor-2 upregulation and nicotine-mediated plasticity. EMBO J. 30: 194–204.
302. Zhao, W.Q., N. Meiri, H. Xu, S. Cavallaro, A. Quattrone, L. Zhang, and D.L. Alkon. 2000. Spatial learning induced changes in expression of the ryanodine type II receptor in the rat hippocampus. FASEB J. 14: 290–300.
303. Adasme, T., P. Haeger, A.C. Paula-Lima, I. Espinoza, M.M. Casas-Alarcón, M.A. Carrasco, and C. Hidalgo. 2011. Involvement of ryanodine receptors in neurotrophin-induced hippocampal synaptic plasticity and spatial memory formation. Proc. Natl. Acad. Sci. U. S. A. 108: 3029–34.
304. Cavallaro, S., N. Meiri, C.L. Yi, S. Musco, W. Ma, J. Goldberg, and D.L. Alkon. 1997. Late memory-related genes in the hippocampus revealed by RNA fingerprinting. Proc. Natl. Acad. Sci. U. S. A. 94: 9669–73.
305. Alkon, D.L., T.J. Nelson, W. Zhao, and S. Cavallaro. 1998. Time domains of neuronal Ca2+ signaling and associative memory: steps through a calexcitin, ryanodine receptor, K+ channel cascade. Trends Neurosci. 21: 529–37.
306. Mellentin, C., H. Jahnsen, and W.C. Abraham. 2007. Priming of long-term potentiation mediated by ryanodine receptor activation in rat hippocampal slices. Neuropharmacology. 52: 118–25.
307. Welsby, P., M. Rowan, and R. Anwyl. 2006. Nicotinic receptor-mediated enhancement of long-term potentiation involves activation of metabotropic glutamate receptors and ryanodine-sensitive calcium stores in the dentate gyrus. Eur. J. Neurosci. 24: 3109–18.
308. Bliss, T.V.P., and G.L. Collingridge. 1993. A synaptic model of memory: long-term potentiation in the hippocampus. Nature. 361: 31–39.
309. Wang, Y., J. Wu, M.J. Rowan, and R. Anwyl. 1996. Ryanodine produces a low frequency stimulation-induced NMDA receptor-independent long-term potentiation in the rat dentate gyrus in vitro. J. Physiol. 495 Pt 3: 755–67.

310. Sharma, G., and S. Vijayaraghavan. 2003. Modulation of presynaptic store calcium induces release of glutamate and postsynaptic firing. Neuron. 38: 929–39.
311. Lauri, S. 2003. A Role for Ca2+ Stores in Kainate Receptor-Dependent Synaptic Facilitation and LTP at Mossy Fiber Synapses in the Hippocampus. Neuron. 39: 327–341.
312. Shimuta, M., M. Yoshikawa, M. Fukaya, M. Watanabe, H. Takeshima, and T. Manabe. 2001. Postsynaptic modulation of AMPA receptor-mediated synaptic responses and LTP by the type 3 ryanodine receptor. Mol. Cell. Neurosci. 17: 921–30.
313. Takeshima, H., T. Yamazawa, T. Ikemoto, H. Takekura, M. Nishi, T. Noda, and M. Iino. 1995. Ca(2+)-induced Ca2+ release in myocytes from dyspedic mice lacking the type-1 ryanodine receptor. EMBO J. 14: 2999–3006.
314. Liu, X., M.J. Betzenhauser, S. Reiken, A.C. Meli, W. Xie, B.-X. Chen, O. Arancio, and A.R. Marks. 2012. Role of leaky neuronal ryanodine receptors in stress-induced cognitive dysfunction. Cell. 150: 1055–67.
315. Lacampagne, A., X. Liu, S. Reiken, R. Bussiere, · Albano, C. Meli, I. Lauritzen, A.F. Teich, R. Zalk, N. Saint, O. Arancio, C. Bauer, F. Duprat, C.A. Briggs, S. Chakroborty, G.E. Stutzmann, M.L. Shelanski, F. Checler, M. Chami, and A.R. Marks. 2017. Post-translational remodeling of ryanodine receptor induces calcium leak leading to Alzheimer's disease-like pathologies and cognitive deficits. Acta Neuropathol. .
316. Jaffe, D.B., and T.H. Brown. 1994. Metabotropic glutamate receptor activation induces calcium waves within hippocampal dendrites. J. Neurophysiol. 72: 471–4.
317. Manita, S., and W.N. Ross. 2009. Synaptic activation and membrane potential changes modulate the frequency of spontaneous elementary Ca2+ release events in the dendrites of pyramidal neurons. J. Neurosci. 29: 7833–45.
318. Miyazaki, K., and W.N. Ross. 2013. Ca2+ sparks and puffs are generated and interact in rat hippocampal CA1 pyramidal neuron dendrites. J. Neurosci. 33: 17777–88.
319. Watanabe, S., M. Hong, N. Lasser-Ross, and W.N. Ross. 2006. Modulation of calcium wave propagation in the dendrites and to the soma of rat hippocampal pyramidal neurons. J. Physiol. 575: 455–468.
320. Bers, D.M. 2001. Excitation-Contraction Coupling and Cardiac Contractile Force. 2nd ed. Dordrecht, The Netherlands: Kluwer Academic Publishers,Springer.

321. Niggli, E., and W.J. Lederer. 1990. Voltage-independent calcium release in heart muscle. Science. 250: 565–8.
322. Bassani, J.W., W. Yuan, and D.M. Bers. 1995. Fractional SR Ca release is regulated by trigger Ca and SR Ca content in cardiac myocytes. Am. J. Physiol. 268: C1313-9.
323. Stern, M.D., G. Pizarro, and E. Ríos. 1997. Local control model of excitation-contraction coupling in skeletal muscle. J. Gen. Physiol. 110: 415–40.
324. Wier, W.G., T.M. Egan, J.R. López-López, and C.W. Balke. 1994. Local control of excitation-contraction coupling in rat heart cells. J. Physiol. 474: 463–71.
325. Smith, G.D., J.E. Keizer, M.D. Stern, W.J. Lederer, and H. Cheng. 1998. A simple numerical model of calcium spark formation and detection in cardiac myocytes. Biophys. J. 75: 15–32.
326. Sedarat, F., L. Xu, E.D. Moore, and G.F. Tibbits. 2000. Colocalization of dihydropyridine and ryanodine receptors in neonate rabbit heart using confocal microscopy. Am. J. Physiol. Heart Circ. Physiol. 279: H202-9.
327. Griffiths, E.J., M.D. Stern, and H.S. Silverman. 1997. Measurement of mitochondrial calcium in single living cardiomyocytes by selective removal of cytosolic indo 1. Am. J. Physiol. 273: C37-44.
328. Trollinger, D.R., W.E. Cascio, and J.J. Lemasters. 1997. Selective Loading of Rhod 2 into Mitochondria Shows Mitochondrial Ca 2+ Transients during the Contractile Cycle in Adult Rabbit Cardiac Myocytes. Biochem. Biophys. Res. Commun. 236: 738–742.
329. Griffiths, E.J. 1999. Species Dependence of Mitochondrial Calcium Transients during Excitation–Contraction Coupling in Isolated Cardiomyocytes. Biochem. Biophys. Res. Commun. 263: 554–559 (1999).
330. Cordeiro, J.M., K.W. Spitzer, W.R. Giles, P.E. Ershler, M.B. Cannell, and J.H.B. Bridge. 2001. Location of the initiation site of calcium transients and sparks in rabbit heart Purkinje cells. J. Physiol. 531: 301–314.
331. Szalai, G., G. Csordás, B.M. Hantash, A.P. Thomas, and G. Hajnóczky. 2000. Calcium signal transmission between ryanodine receptors and mitochondria. J. Biol. Chem. 275: 15305–13.
332. Cleemann, L., W. Wang, and M. Morad. 1998. Two-dimensional confocal images of

organization, density, and gating of focal Ca 2% release sites in rat cardiac myocytes. Proc. Natl. Acad. Sci. 95: 10984–10989.

333. Hiess, F., A. Vallmitjana, R. Wang, H. Cheng, H.E.D.J. ter Keurs, J. Chen, L. Hove-Madsen, R. Benitez, and S.R.W. Chen. 2015. Distribution and Function of Cardiac Ryanodine Receptor Clusters in Live Ventricular Myocytes. J. Biol. Chem. 290: 20477–87.
334. Scriven, D.R.L.L., P. Asghari, M.N. Schulson, and E.D.W.W. Moore. 2010. Analysis of Cav1.2 and ryanodine receptor clusters in rat ventricular myocytes. Biophys. J. 99: 3923–3929.
335. Tinevez, J.-Y., N. Perry, J. Schindelin, G.M. Hoopes, G.D. Reynolds, E. Laplantine, S.Y. Bednarek, S.L. Shorte, and K.W. Eliceiri. 2017. TrackMate: An open and extensible platform for single-particle tracking. Methods. 115: 80–90.
336. Yu, J.-G., and B. Russell. 2005. Cardiomyocyte Remodeling and Sarcomere Addition after Uniaxial Static Strain In Vitro. J. Histochem. Cytochem. 53: 839–844.
337. Song, L.-S., E.A. Sobie, S. McCulle, W.J. Lederer, C.W. Balke, and H. Cheng. 2006. Orphaned ryanodine receptors in the failing heart. Proc. Natl. Acad. Sci. U. S. A. 103: 4305–10.
338. Squire, L.R. 2009. The legacy of patient H.M. for neuroscience. Neuron. 61: 6–9.
339. Korte, M., and D. Schmitz. 2016. Cellular and system biology of memory: timing, molecules, and beyond. Physiol Rev. 96: 647–693.
340. Saerens, D., M. Pellis, R. Loris, E. Pardon, M. Dumoulin, A. Matagne, L. Wyns, S. Muyldermans, and K. Conrath. 2005. Identification of a universal VHH framework to graft non-canonical antigen-binding loops of camel single-domain antibodies. J. Mol. Biol. 352: 597–607.
341. Yao, J.-J., Q.-R. Zhao, D.-D. Liu, C.-W. Chow, and Y.-A. Mei. 2016. Neuritin Up-regulates Kv4.2 α-Subunit of Potassium Channel Expression and Affects Neuronal Excitability by Regulating the Calcium-Calcineurin-NFATc4 Signaling Pathway. J. Biol. Chem. 291: 17369–81.
342. Low, W.C., S.L. Bement, and D. Whitehorn. Field-Potential Evidence for Extrasynaptic Alterations in the Hippocampal CA1 Pyramidal Cell Population during Paired-Pulse

Potentiation. .

343. Turner, R.W., D.E.R. Meyers, and J.L. Barker. 1989. Localization of Tetrodotoxin-Sensitive Field Potentials of CA1 Pyramidal Cells in the Rat Hippocampus. J. Neurophysiol. 62: 1375–1387.
344. Morris, R. 1984. Developments of a water-maze procedure for studying spatial learning in the rat. J. Neurosci. Methods. 11: 47–60.
345. Micu, I., A. Ridsdale, L. Zhang, J. Woulfe, J. Mcclintock, C.A. Brantner, B. Andrews, and P.K. Stys. 2007. Real-time measurement of free Ca 2+ changes in CNS myelin by two-photon microscopy. Nat. Med. 13: 874–879.
346. Schulz, P.E., E.P. Cook, and D. Johnston. 1994. Changes in Paired-Pulse Facilitation Suggest Presynaptic Involvement in Long-Term Potentiation. J. Neurosci. 14.
347. Disterhoft, J.F., L.T. Thompson, J.R. Moyer, and D.J. Mogu. 1996. Calcium-dependent afterhyperpolarization and learning in young and aging hippocampus. Life Sci. 59: 413420–19.
348. Kawai, T., and M. Watanabe. 1989. Effects of ryanodine on the spike after-hyperpolarization in sympathetic neurones of the rat superior cervical ganglion. Pfluegers Arch. Eur. J. Physiol. 413: 470–475.
349. Chen, T.-W., T.J. Wardill, Y. Sun, S.R. Pulver, S.L. Renninger, A. Baohan, E.R. Schreiter, R.A. Kerr, M.B. Orger, V. Jayaraman, L.L. Looger, K. Svoboda, and D.S. Kim. 2013. Ultra-sensitive fluorescent proteins for imaging neuronal activity. July. 18: 295–300.
350. Chen, Q., J. Cichon, W. Wang, L. Qiu, S.-J.R. Lee, N.R. Campbell, N. Destefino, M.J. Goard, Z. Fu, R. Yasuda, L.L. Looger, B.R. Arenkiel, W.-B. Gan, and G. Feng. 2012. Imaging Neural Activity Using Thy1-GCaMP Transgenic mice. Neuron. 76: 297–308.
351. Peron, S.P., J. Freeman, V. Iyer, C. Guo, and K. Svoboda. 2015. A Cellular Resolution Map of Barrel Cortex Activity during Tactile Behavior. Neuron. 86: 783–799.
352. Dana, H., T.-W. Chen, A. Hu, B.C. Shields, C. Guo, L.L. Looger, D.S. Kim, and K. Svoboda. 2014. Thy1-GCaMP6 Transgenic Mice for Neuronal Population Imaging In Vivo. PLoS One. 9: e108697.
353. Busche, M.A., G. Eichhoff, H. Adelsberger, D. Abramowski, K.-H. Wiederhold, C. Haass,

M. Staufenbiel, A. Konnerth, and O. Garaschuk. 2008. Clusters of hyperactive neurons near amyloid plaques in a mouse model of Alzheimer's disease. Science (80-.). 321: 1686–1690.

354. Sato, T.R., N.W. Gray, Z.F. Mainen, and K. Svoboda. 2007. The Functional Microarchitecture of the Mouse Barrel Cortex. PLoS Biol. 5.

355. Kerr, J.N.D., D. Greenberg, and F. Helmchen. 2005. Imaging input and output of neocortical networks in vivo. Proc. Natl. Acad. Sci. 102: 14063–14068.

356. Kirchhofer, A., J. Helma, K. Schmidthals, C. Frauer, S. Cui, A. Karcher, M. Pellis, S. Muyldermans, C.S. Casas-Delucchi, M.C. Cardoso, H. Leonhardt, K.-P. Hopfner, and U. Rothbauer. 2010. Modulation of protein properties in living cells using nanobodies. Nat. Struct. Mol. Biol. 17: 133–8.

357. Martín, E.D., W.B. No, and W. Buño. 2003. Caffeine-mediated presynaptic long-term potentiation in hippocampal CA1 pyramidal neurons. J. Neurophysiol. 89: 3029–38.

358. Chakroborty, S., I. Goussakov, M.B. Miller, and G.E. Stutzmann. 2009. Neurobiology of Disease Deviant Ryanodine Receptor-Mediated Calcium Release Resets Synaptic Homeostasis in Presymptomatic 3xTg-AD Mice. J. Neurosci. 29: 9458–9470.

359. Wu, B., H. Yamaguchi, F.A. Lai, and J. Shen. 2013. Presenilins regulate calcium homeostasis and presynaptic function via ryanodine receptors in hippocampal neurons. Proc. Natl. Acad. Sci. U. S. A. 110: 15091–6.

360. Arias-Cavieres, A., T. Adasme, G. Sánchez, P. Muñoz, and C. Hidalgo. 2017. Aging Impairs Hippocampal- Dependent Recognition Memory and LTP and Prevents the Associated RyR Up-regulation. Front. Aging Neurosci. 9: 111.

361. Stern, M.D., L.S. Song, H. Cheng, J.S. Sham, H.T. Yang, K.R. Boheler, and E. Ríos. 1999. Local control models of cardiac excitation-contraction coupling. A possible role for allosteric interactions between ryanodine receptors. J. Gen. Physiol. 113: 469–89.

362. Brady, A.J. 1991. Mechanical Properties of Isolated Cardiac Myocytes. Physiol. Rev. 71.

363. Schreur, J.H., V.M. Figueredo, M. Miyamae, D.M. Shames, A.J. Baker, and S.A. Camacho. 1996. Cytosolic and mitochondrial [Ca2+] in whole hearts using indo-1 acetoxymethyl ester: effects of high extracellular Ca2+. Biophys. J. 70: 2571–80.

364. Miyata, H., H.S. Silverman, S.J. Sollott, E.G. Lakatta, M.D. Stern, and R.G. Hansford.

1991. Measurement of mitochondrial free Ca2+ concentration in living single rat cardiac myocytes. Am. J. Physiol. 261: H1123-34.

365. Di Lisa, F., G. Gambassi, H. Spurgeon, and R.G. Hansford. 1993. Intramitochondrial free calcium in cardiac myocytes in relation to dehydrogenase activation. Cardiovasc. Res. 27: 1840–4.

366. Zhou, Z., M.A. Matlib, and D.M. Bers. 1998. Cytosolic and mitochondrial Ca2+ signals in patch clamped mammalian ventricular myocytes. J. Physiol. 507 (Pt 2): 379–403.

367. Sharma, V.K., V. Ramesh, C. Franzini-Armstrong, and S.S. Sheu. 2000. Transport of Ca2+ from sarcoplasmic reticulum to mitochondria in rat ventricular myocytes. J. Bioenerg. Biomembr. 32: 97–104.

368. Gavin, C.E., K.K. Gunter, and T.E. Gunter. 1990. Manganese and calcium efflux kinetics in brain mitochondria. Relevance to manganese toxicity. Biochem. J. 266: 329.

369. Golini, L., C. Chouabe, C. Berthier, V. Cusimano, M. Fornaro, R. Bonvallet, L. Formoso, E. Giacomello, V. Jacquemond, and V. Sorrentino. 2011. Junctophilin 1 and 2 proteins interact with the L-type Ca2+ channel dihydropyridine receptors (DHPRs) in skeletal muscle. J. Biol. Chem. 286: 43717–25.

370. Jena, B.P. 2009. Membrane fusion: role of SNAREs and calcium. Protein Pept. Lett. 16: 712–7.

371. Parton, R.G., and K. Simons. 2007. The multiple faces of caveolae. Nat. Rev. Mol. Cell Biol. 8: 185–194.

372. Song, D.W., K.-E. Lee, J.Y. Ryu, H. Jeon, D.H. Kim, and H. Kim. 2015. The molecular interaction of heart LIM protein (HLP) with RyR2 and caveolin-3 is essential for Ca2+-induced Ca2+ release in the heart. Biochem. Biophys. Res. Commun. 463: 975–981.

373. Brochet, D.X.P., D. Yang, A. Di Maio, W.J. Lederer, C. Franzini-Armstrong, and H. Cheng. 2005. Ca2+ blinks: rapid nanoscopic store calcium signaling. Proc. Natl. Acad. Sci. U. S. A. 102: 3099–104.

374. Del Prete, D., F. Checler, and M. Chami. 2014. Ryanodine receptors: physiological function and deregulation in Alzheimer disease. Mol. Neurodegener. 9: 21.

375. Bouchard, R., R. Pattarini, and J.D. Geiger. 2003. Presence and functional significance of presynaptic ryanodine receptors. Prog. Neurobiol. 69: 391–418.

376. Chakroborty, S., J. Kim, C. Schneider, C. Jacobson, J. Molgó, and G.E. Stutzmann. 2012. Presynaptic and Postsynaptic Calcium Signaling Abnormalities Mask Underlying Synaptic Depression in Presymptomatic Alzheimer's Disease Mice. J. Neurosci. 32: 8341–8353.
377. Le Magueresse, C., and E. Cherubini. 2007. Presynaptic Calcium Stores Contribute to Nicotine-Elicited Potentiation of Evoked Synaptic Transmission at CA3-CA1 Connections in the Neonatal Rat Hippocampus. Hippocampus. 17: 316–325.
378. Carter, A.G., K.E. Vogt, K.A. Foster, and W.G. Regehr. 2002. Assessing the role of calcium-induced calcium release in short-term presynaptic plasticity at excitatory central synapses. J. Neurosci. 22: 21–8.
379. Wayman, G.A., D. Yang, D.D. Bose, A. Lesiak, V. Ledoux, D. Bruun, I.N. Pessah, and P.J. Lein. 2012. PCB-95 Promotes Dendritic Growth via Ryanodine Receptor–Dependent Mechanisms. Environ. Health Perspect. 120: 997–1002.
380. Jung, C.B., A. Moretti, M. Mederos y Schnitzler, L. Iop, U. Storch, M. Bellin, T. Dorn, S. Ruppenthal, S. Pfeiffer, A. Goedel, R.J. Dirschinger, M. Seyfarth, J.T. Lam, D. Sinnecker, T. Gudermann, P. Lipp, and K.-L. Laugwitz. 2012. Dantrolene rescues arrhythmogenic RYR2 defect in a patient-specific stem cell model of catecholaminergic polymorphic ventricular tachycardia. EMBO Mol. Med. 4: 180–91.
381. Oo, Y.W., N. Gomez-Hurtado, K. Walweel, D.F. van Helden, M.S. Imtiaz, B.C. Knollmann, and D.R. Laver. 2015. Essential Role of Calmodulin in RyR Inhibition by Dantrolene. Mol. Pharmacol. 88: 57–63.
382. Liang, Y., L.-L. Yuan, D. Johnston, and R. Gray. 2002. Calcium signaling at single mossy fiber presynaptic terminals in the rat hippocampus. J. Neurophysiol. 87: 1132–7.
383. Mignery, G.A., T.C. Südhof, K. Takei, and P. De Camilli. 1989. Putative receptor for inositol 1,4,5-trisphosphate similar to ryanodine receptor. Nature. 342: 192–5.
384. Furuichi, T., D. Furutama, Y. Hakamata, J. Nakai, H. Takeshima, and K. Mikoshiba. 1994. Multiple types of ryanodine receptor/Ca2+ release channels are differentially expressed in rabbit brain. J. Neurosci. 14: 4794–805.
385. Galeotti, N., E. Vivoli, A. Bartolini, and C. Ghelardini. 2008. A gene-specific cerebral types 1, 2, and 3 RyR protein knockdown induces an antidepressant-like effect in mice. J.

Neurochem. 106: 2385–94.

386. Ouyang, Y., M.E. Martone, T.J. Deerinck, J.A. Airey, J.L. Sutko, and M.H. Ellisman. 1997. Differential distribution and subcellular localization of ryanodine receptor isoforms in the chicken cerebellum during development. Brain Res. 775: 52–62.

387. Walton, P.D., J.A. Airey, J.L. Sutko, C.F. Beck, G.A. Mignery, T.C. Südhof, T.J. Deerinck, and M.H. Ellisman. 1991. Ryanodine and inositol trisphosphate receptors coexist in avian cerebellar Purkinje neurons. J. Cell Biol. 113: 1145–57.

388. Llano, I., J. González, C. Caputo, F.A. Lai, L.M. Blayney, Y.P. Tan, and A. Marty. 2000. Presynaptic calcium stores underlie large-amplitude miniature IPSCs and spontaneous calcium transients. Nat. Neurosci. 3: 1256–65.

389. Galante, M., and A. Marty. 2003. Presynaptic Ryanodine-Sensitive Calcium Stores Contribute to Evoked Neurotransmitter Release at the Basket Cell–Purkinje Cell Synapse. J. Neurosci. 23: 11229–11234.

APPENDIX: COPYRIGHT PERMISSIONS

WOLTERS KLUWER HEALTH LICENSE TERMS AND CONDITIONS

Jan 23, 2018

This Agreement between University of Calgary -- Florian HIESS ("You") and Wolters Kluwer Health ("Wolters Kluwer Health") consists of your license details and the terms and conditions provided by Wolters Kluwer Health and Copyright Clearance Center.

License Number	4274590873579
License date	Jan 23, 2018
Licensed Content Publisher	Wolters Kluwer Health
Licensed Content Publication	WK Health Book
Licensed Content Title	Physiology of the Heart
Licensed Content Author	Arnold M. Katz MD
Licensed Content Date	Jan 1, 2010
Type of Use	Dissertation/Thesis
Requestor type	academic/educational
Format	print and electronic
Portion	figures/tables/illustrations
Number of figures/tables/illustrations	1
The ID numbers of the figures/tables/illustrations are...	FIG. 1-15: Ultrastructure of a working cardiac myocyte.
Will you be translating?	no
Reusing current or a previous edition	current edition
Circulation/distribution	100
Title of your thesis / dissertation	Subcellular Distribution and Function of Cardiac Ryanodine Receptor i Ventricular Myocytes and Hippocampal Neurons

SPRINGER NATURE LICENSE
TERMS AND CONDITIONS

Jan 23, 2018

This Agreement between University of Calgary -- Florian HIESS ("You") and Springer Nature ("Springer Nature") consists of your license details and the terms and conditions provided by Springer Nature and Copyright Clearance Center.

License Number	4274351473780
License date	Jan 22, 2018
Licensed Content Publisher	Springer Nature
Licensed Content Publication	Nature
Licensed Content Title	Cardiac excitation–contraction coupling
Licensed Content Author	Donald M. Bers
Licensed Content Date	Jan 10, 2002
Licensed Content Volume	415
Licensed Content Issue	6868
Type of Use	Thesis/Dissertation
Requestor type	non-commercial (non-profit)
Format	print and electronic
Portion	figures/tables/illustrations
Number of figures/tables/illustrations	1
High-res required	no
Will you be translating?	no
Circulation/distribution	<501
Author of this Springer Nature content	no
Title	Subcellular Distribution and Function of Cardiac Ryanodine Receptor in Ventricular Myocytes and Hippocampal Neurons
Instructor name	S.R. Wayne Chen
Institution name	University of Calgary
Expected presentation date	Jan 2020
Portions	Figure 1: Ca2+ transport in ventricular myocytes.

THE AMERICAN ASSOCIATION FOR THE ADVANCEMENT OF SCIENCE LICENSE TERMS AND CONDITIONS

Jan 23, 2018

This Agreement between University of Calgary -- Florian HIESS ("You") and The American Association for the Advancement of Science ("The American Association for the Advancement of Science") consists of your license details and the terms and conditions provided by The American Association for the Advancement of Science and Copyright Clearance Center.

License Number	4274421056522
License date	Jan 22, 2018
Licensed Content Publisher	The American Association for the Advancement of Science
Licensed Content Publication	Science
Licensed Content Title	Crystal Structure of the ***Aequorea victoria*** Green Fluorescent Protein
Licensed Content Author	Mats Ormö, Andrew B. Cubitt, Karen Kallio, Larry A. Gross, Roger Y. Tsien, S. James Remington
Licensed Content Date	Sep 6, 1996
Licensed Content Volume	273
Licensed Content Issue	5280
Volume number	273
Issue number	5280
Type of Use	Thesis / Dissertation
Requestor type	Scientist/individual at a research institution
Format	Print and electronic
Portion	Figure
Number of figures/tables	1
Order reference number	
Title of your thesis / dissertation	Subcellular Distribution and Function of Cardiac Ryanodine Receptor in Ventricular Myocytes and Hippocampal Neurons
Expected completion date	Jan 2020

Copyright Permission Policy| Frontiers in Cellular Neuroscience - https://www.frontiersin.org/articles/10.3389/fncel.2014.00344/full - accessed Jan 2018

Copyright © 2014 Rissiek, Koch-Nolte and Magnus. This is an open-access article distributed under the terms of the Creative Commons Attribution License (CC BY). The use, distribution and reproduction in other forums is permitted, provided the original author(s) or licensor are credited and that the original publication in this journal is cited, in accordance with accepted academic practice. No use, distribution or reproduction is permitted which does not comply with these terms.

ELSEVIER LICENSE
TERMS AND CONDITIONS

Jan 23, 2018

This Agreement between University of Calgary -- Florian HIESS ("You") and Elsevier ("Elsevier") consists of your license details and the terms and conditions provided by Elsevier and Copyright Clearance Center.

License Number	4274420725855
License date	Jan 22, 2018
Licensed Content Publisher	Elsevier
Licensed Content Publication	Neuron
Licensed Content Title	Neuronal Calcium Signaling
Licensed Content Author	Michael J Berridge
Licensed Content Date	Jul 1, 1998
Licensed Content Volume	21
Licensed Content Issue	1
Licensed Content Pages	14
Start Page	13
End Page	26
Type of Use	reuse in a thesis/dissertation
Intended publisher of new work	other

Portion	figures/tables/illustrations
Number of figures/tables/illustrations	1
Format	both print and electronic
Are you the author of this Elsevier article?	No
Will you be translating?	No
Original figure numbers	Figure 3. Binary Membrane System of Neural Calcium Signaling As
Title of your thesis/dissertation	Subcellular Distribution and Function of Cardiac Ryanodine Receptor in Ventricular Myocytes and Hippocampal Neurons
Publisher of new work	University of Calgary
Author of new work	S.R. Wayne Chen
Expected completion date	Jan 2020

Copyright Permission Policy| Journal of Biological Chemistry

These guidelines apply to the reuse of articles, figures, charts and photos in the ***Journal of Biological Chemistry***, *Molecular & Cellular Proteomics* and the *Journal of Lipid Research*. http://www.jbc.org/site/misc/edpolicy.xhtml#copyright - accessed Nov 2017

For authors reusing their own material:

Authors need **NOT** contact the journal to obtain rights to reuse their own material. They are automatically granted permission to do the following: Reuse the article in print collections of their own writing; Present a work orally in its entirety; **Use an article in a thesis and/or dissertation**; Reproduce an article for use in the author's courses. (If the author is employed by an academic institution, that institution also may reproduce the article for teaching purposes.); Reuse a figure, photo and/or table in future commercial and non-commercial works; Post a copy of the paper in PDF that you submitted via BenchPress. Link to the journal site containing the final edited PDFs created by the publisher. Authors who published their papers under the "Author's Choice" option may post the final edited PDFs created by the publisher to their own/departmental/university Web sites immediately upon publication. All other authors may do so 12 months after publication.

Permission from the Biophysical Journal

From: Biophysical Journal
Mon 2018-01-22 1:38 PM

To whom it may concern,

This is to confirm that the Biophysical Journal gives Florian Hiess permission to use all figures from the paper “Dynamic and Irregular Distribution of Cardiac Ryanodine Receptor Clusters in the Periphery of Live Ventricular Myocytes” in his dissertation.

Regards,

Catie Curry
Publications Coordinator
Biophysical Journal